Model Studies of Ziegler-Natta Olefin Polymerization Using Group 3 and Group 4 Metallocenes

Thesis by

Jeffrey C. Yoder

In Partial Fulfillment of the Requirements

For the Degree of

Doctor of Philosophy

California Institute of Technology

Pasadena, California

2001

(Defended June 8, 2000)

For Shelly and Jordan

Acknowledgments

Although acknowledging the assistance I have received while in graduate school is very important, the writing of this section was unfortunately rushed, and thus I apologize and thank here anyone who was inadvertently forgotten. I want to thank Shelly for her encouragement and patience with long hours in lab. I really could not have done this without her support. In addition, Jordan always provided me with something to occupy my time while not in lab. My parents and sisters as well as my in-laws have also been very encouraging and only asked a few times "what exactly are you doing out there in California?" I must acknowledge John Bercaw for his incredible wealth of knowledge and teaching skills. His hands-off management style was something that I greatly appreciated and was of tremendous help in allowing me to become an independent scientist.

Prof. Colleen Kelley first introduced me to inorganic chemistry at Walter Reed and I am grateful to her for pointing me in the right direction. Matt Holtcamp was a great friend both at Texas A&M and in the Bercaw group, and I'm glad to have had the chance to work with him. He truly is one of the best chemists and teachers I have ever met and was an example that I wish to emulate. Tim Herzog, despite not getting me a job at Union Carbide, was instrumental in getting me started on the vacuum line in the infamous "213". I also must thank Susan Brookhart who was very kind in teaching me how to use the beloved AM 500 NMR. Jim Gilchrist, when he could be found, was an amazing reference on NMR and the use of notecards to record every piece of information. Andy Kiely was one of the smartest people in the group as well as a surly addition to poker night. Mike Abrams demonstrated to me the finer points of allyl rotation and also the correct formula for the Screaming Weasel. Cory Nelson was a fine Hogs coach before cursing me with that responsibility. I don't think Dario Veghini ever really understood my sarcasm but I thank him for trying. Shannon Stahl was always either on the NMR or sleeping in the nook or the "ladies lounge". Chris Levy was a good friend and a better cook, and I thank him for his hospitality. John Scollard ruled the computer room with an iron fist and was always willing to go see the worst movie that was playing in theaters at the time. Lars provided us with a new car for a sweet deal and also had an epic going away party which I think I'm glad I had to miss. Seva Rostovtsev was an eager student of American culture and I'm happy to have introduced him to the fine art of watching baseball and eating chili-cheese fries.

In return he introduced me to Russian vodka, and repeatedly called me a honkey. His hallway screaming matches with Koert Liekelema were also quite memorable. Ola Wendt made me an eager student of Swedish culture (the bun game, bppp, and amorous roosters) and also revolutionized the practice of kinetics in the Bercaw group: "linear fits suck". I will miss his knowledge and sense of humor. I learned a lot talking chemistry with Theory in the computer room, even though he insisted on looking at the golf and basketball pages on ESPN. His choice of sports teams was unfortunate, but I wish him the best of luck with the "Krypton Factor". Joseph was one of the few who actually appreciated the bitter side of my humor and I will miss him sitting on my right in the computer room. Alex Muci was always willing for a run to Lucky Baldwin's or a round of golf, and was an excellent resource for organic chemistry questions. Sara Klamo will soon be a kinetics stud and also did a good deed by keeping the Mustang in the group. Susan Schofer has a large responsibility as the new Hogs coach, and the only surviving group 3 chemist in the Bercaw group. I hope that Lily Ackerman keeps up the Bay of Pigs tradition, and enjoys the occasional Dr. Pepper. I will consume large quantities of Pho in Seattle in her honor. Annita was a great lab-mate who was able to ask difficult questions of me and also to answer mine. Her TA-ing skills (*i.e.*, screaming at students) I could never hope to equal, although I will always try. She also introduced me to the wonders of North China Noodle. Antek Wong-Foy was also an excellent lab-mate. He introduced me to shooting craps in Vegas and I was also able to learn about his culture by visiting Chinese restaurants. I thank him for helping me with chemistry problems as well as being a great friend to me, Shelly, and Jordan. Melanie Sanford was also a good friend whose gambling luck should be legendary.

Larry Henling solved several of the crystal structures in my thesis and was a great, although foul tempered Hog teammate. Mike Day provided the remaining crystal structure data. Peter Green and Nathan Daleska carried out the GC-MS measurements in Chapter 3. Finally, Dr. Lee never ceased to confound me when using the NMR.

Abstract

Evidence for the stereochemical isomerization of a variety of *ansa* metallocene compounds is presented. For the scandocene allyl derivatives described here, we have established that the process is promoted by a variety of salts in both ether and hydrocarbon solvents and is not accelerated by light. A plausible mechanism based on an earlier proposal by Marks, *et al.*, is offered as an explanation of this process. It involves coordination of anions and/or donor solvents to the metal center with cation assistance to encourage metal-cyclopentadienyl bond heterolysis, rotation about the Si-Cp bond of the detached cyclopentadienide and recoordination of the opposite face. Our observations in some cases of thermodynamic racemic:meso ratios under the reaction conditions commonly used for the synthesis of the metallocene chlorides suggests that the interchange is faster than metallation, such that the composition of the reaction mixture is determined by thermodynamic, not kinetic, control in these cases.

Two new *ansa*-scandocene alkenyl compounds react with olefins resulting in the formation of η^3-allyl complexes. Kinetics and labeling experiments indicate a tuck-in intermediate on the reaction pathway; in this intermediate the metal is bound to the carbon adjacent to the silyl linker in the rear of the metallocene wedge. In contrast, reaction of permethylscandocene alkenyl compounds with olefins results, almost exclusively, in vinylic C-H bond activation. It is proposed that relieving transition state steric interactions between the cyclopentadienyl rings and the olefin by either linking the rings together or using a larger lanthanide metal may allow for olefin coordination, stabilizing the transition state for allylic σ-bond metathesis.

A selectively isotopically labeled propylene, $CH_2CD(^{13}CH_3)$, was synthesized and its polymerization was carried out at low concentration in toluene solution using isospecific metallocene catalysts. Analysis of the NMR spectra (^{13}C, ^{1}H, and ^{2}H) of the resultant polymers revealed that the production of stereoerrors through chain epimerization proceeds exclusively by the tertiary-alkyl mechanism. Additionally, enantiofacial inversion of the terminally unsaturated polymer chain occurs by a non-dissociative process. The implications of these results on the mechanism of olefin polymerization with these catalysts is discussed.

Table of Contents

Dedication iii

Acknowledgments iv

Abstract vi

Table of Contents vii

List of Figures viii

List of Schemes xi

List of Tables xii

Introduction 1

Chapter 1 3

Racemic-Meso Interconversion for *ansa*-Scandocene and *ansa*-Yttrocene Derivatives, and a Study of the Fluxional Processes for *ansa*-Scandocene η^3-Allyl Ligands

Chapter 2 54

A Study of the Mechanism of Conversion of Scandocene Alkenyl Compounds to Scandocene η^3-Allyl Compounds and a Comparison of σ-Bond Metathesis Reactivity Between $(C_5Me_5)_2$- and $Me_2Si(C_5Me_4)_2$- Ligated Scandocenes

Chapter 3 89

A Study of the Mechanism of Chain Epimerization Using a Doubly Labeled Propylene

Appendices 115

Appendix 1 116

Numbering Scheme for Compounds Referred to in the Text

Appendix 2 120

List of Figures

Chapter 1

Figure 1. Drawing of the two diastereomers of ethylene*bis*(4,5,6,7-tetrahydro-1-indenyl)zirconium dichloride. 5

Figure 2. Representations of *rac*- and *meso*-BpYCl. 8

Figure 3. Drawing of the structure of $IpLi_2$. 8

Figure 4. ORTEP representation of the molecular structure of **1**. 10

Figure 5. ORTEP representation of the molecular structure of **4**. 12

Figure 6. ORTEP representation of the molecular structure of **5**. 14

Figure 7. ORTEP representation of the molecular structure of **8**. 16

Figure 8. Drawing of the two limiting structures for crotyl bonding in **8**. 18

Figure 9. ORTEP representation of the molecular structure of **9**. 19

Figure 10. Assignment of the allyl resonances in the ^1H NMR of **5** and **6**. 22

Figure 11. Allyl and isopropyl methine resonances of the variable-temperature 500 MHz ^1H NMR spectra for **6** in toluene-d_8. 23

Figure 12. Allyl and isopropyl methine resonances of the variable-temperature 500 MHz ^1H NMR spectra for **5** in toluene-d_8. 25

Figure 13. Illustration of processes proposed to account for the fluxional behavior of **5** and **6**. 26

Figure 14. Stack plot of ^{1}H NMR spectra showing the progression of the reaction which interconverts **1** and **2** at room temperature in THF-d_8. 28

Figure 15. Stack plot of ^{1}H NMR spectra showing the progression of the reaction which interconverts **5** and **6** at 80 °C in THF-d_8. 30

Chapter 2

Figure 1. Representations of both normal and β-agostic alkenyl ligands. 60

Figure 2. ORTEP representation of the molecular structure of **10**. 61

Figure 3. Representative kinetics trace for the conversion of **12** to **15**. 69

Figure 4. Eyring plot of observed rate constants for the conversion of **12** to **15**. 70

Figure 5. Stack plot of ^{1}H NMR spectra detailing the assignment of resonances for **12**. 73

Figure 6. ORTEP representation of the molecular structure of **15**. 78

Figure 7. Representations of the transition states for olefinic σ-bond metathesis both including and excluding olefin π-bonding. 81

Chapter 3

Figure 1. Metal-bound products of chain epimerization for the doubly-labeled propylene. 96

Figure 2. ^{1}H NMR spectrum of the doubly labeled propylene monomer in 1,1,2,2-tetrachloroethane-d_2. 98

Figure 3. ^{13}C NMR spectrum of poly-[2-D-3-^{13}C]propylene made using *rac*-(EBTHI)$ZrCl_2$ with 1 atm monomer in toluene solution at 50 °C. 100

Figure 4. Structures expected for both the products of the tertiary alkyl mechanism of chain epimerization and stereoerrors due to enantiofacial misinsertion and their assignments in the ^{13}C NMR. 102

Appendix 2

Figure 1. ORTEP representation of the molecular structure of **1** showing the complete atom labeling scheme. 120

Figure 2. ORTEP representation of the molecular structure of **4** showing the complete atom labeling scheme. 130

Figure 3. ORTEP representation of the molecular structure of **5** showing the complete atom labeling scheme. 138

Figure 4. ORTEP representation of the molecular structure of the allyl ligand of **5** showing the disorder. 139

Figure 5. ORTEP representation of the molecular structure of **8** showing the complete atom labeling scheme. 149

Figure 6. ORTEP representation of the molecular structure of **9** showing the complete atom labeling scheme. 157

Figure 7. ORTEP representation of the molecular structure of **10** showing the complete atom labeling scheme. 164

Figure 8. ORTEP representation of the molecular structure of the isobutenyl ligand of **10** showing the disorder. 165

Figure 9. ORTEP representation of the molecular structure of **15** showing the complete atom labeling scheme. 171

Figure 10. ORTEP representation of the molecular structure of the crotyl ligand of **15** showing the disorder. 172

List of Schemes

Chapter 1

Scheme 1. Racemic-meso interconversion during ansa-metallocene synthesis using the amine elimination route. 7

Scheme 2. Synthesis of IpMCl derivatives. 10

Scheme 3. Synthesis of IpSc(η^3-allyl) complexes. 13

Scheme 4. Mechanism proposed for racemic-meso isomerization of ansa-metallocenes. 35

Chapter 2

Scheme 1. Proposed mechanisms for reaction of $Cp^*_2M(CH_2CHMe_2)$ with olefins. 57

Scheme 2. Mechanism proposed for formation of OpSc(η^3-$CH_2C(CH_2)_3CH$) from $OpScH(PMe_3)$. 57

Scheme 3. Products resulting from thermolysis of **10** and **11**. 65

Scheme 4. Mechanism proposed for isotope exchange into the α-methyl groups of $OpScH(PMe_3)$. 74

Scheme 5. Proposed mechanism for olefin isomerization catalyzed by **15**. 77

Chapter 3

Scheme 1. Competition between insertion and chain epimerization for metallocene catalysts. 91

Scheme 2. Illustration of the chain epimerization process following the tertiary-alkyl mechanism. 93

Scheme 3. Illustration of the mechanisms proposed to account for *gem*-olefin enantiofacial inversion during chain epimerization. 94

Scheme 4. Illustration of the chain epimerization process following the allyl mechanism. 94

Scheme 5. Synthesis of the doubly labeled propylene monomer. 97

Scheme 6. Branching between chain epimerization and production of internal unsaturation in metallocene catalyzed polymerization. 107

Appendix.

Scheme 1. Summary of proposed steps for chain epimerization using the tertiary-alkyl mechanism. 113

Scheme 2. Summary of proposed steps for chain epimerization using the allyl mechanism. 114

List of Tables

Chapter 1

Table 1. Selected Bond Distances and Bond Angles Obtained from the X-Ray Structure Determination of **1** and **4** 11

Table 2. Selected Bond Distances and Bond Angles Obtained from the X-Ray Structure Determination of **5** 15

Table 3. Selected Bond Distances and Bond Angles Obtained from the X-Ray Structure Determination of **8** 17

Table 4. Selected Bond Distances and Bond Angles Obtained from the X-Ray Structure Determination of **9** 20

Table 5. Summary of Rates and Activation Free Energies for η^3-η^1 Allyl Conversion (k_1, $\Delta G_1^{\ddagger}$) and for η^3-Allyl Rotation (k_2, $\Delta G_2^{\ddagger}$) for Allyl Complexes **5** and **6** 27

Table 6. Results of Epimerization Experiments Carried out on Allyl Derivatives **5** - **8** 31

Chapter 2

Table 1. Selected Bond Distances and Bond Angles Obtained from the X-Ray Structure Determination of **10** 62

Table 2. Rate Constants for Alkenyl M-C Bond Rotation for **12** and **13** as Determined by Dynamic ^{1}H NMR Spectroscopy 65

Table 3. Observed Rate Constants for the Reactions of **12** and **13** with Olefins 68

Table 4. Conditions Used and products Observed for Reactions of **12** with Olefins 71

Table 5. Selected Bond Distances and Bond Angles Obtained from the X-Ray Structure Determination of **15** 79

Chapter 3

Table 1. Assignment of the Resonances in the ^{13}C NMR Spectrum of Poly-[2-D-3-^{13}C]Propylene as Shown in Figure 3 101

Table 2. Intensity of Resonances in the ^{13}C NMR Spectra for Poly-[2-D-3-^{13}C]Propylene 103

Table 3. Estimated Amounts of Structures **A** – **D** and **H** 104

Appendix 2

Table 1. X-ray Diffraction Data Collection Parameters for **1** 121

Table 2. Special Refinement Details for **1** 121

Table 3. Atomic Coordinates and Equivalent Isotropic Displacement Parameters for **1** 122

Table 4. Complete List of Bond Lengths and Angles for **1** 123

Table 5. Anisotropic Displacement Parameters for **1** 127

Table 6. Hydrogen Coordinates and Isotropic Displacement Parameters for **1** 128

Table 7. X-ray Diffraction Data Collection Parameters for **4** 131

Table 8. Special Refinement Details for **4** 131

Table 9. Atomic Coordinates and Equivalent Isotropic Displacement Parameters for **1** 132

Table 10. Complete List of Bond Lengths and Angles for **4** 133

Table 11. Anisotropic Displacement Parameters for **4** 134

Table 12. Hydrogen Coordinates and Isotropic Displacement Parameters for **4** 135

Table 13. X-ray Diffraction Data Collection Parameters for **5** 140

Table 14. Special Refinement Details for **5** 140

Table 15. Atomic Coordinates and Equivalent Isotropic Displacement Parameters for **5** 141

Table 16. Complete List of Bond Lengths and Angles for **5** 142

Table 17. Anisotropic Displacement Parameters for **5** 147

Table 18. Hydrogen Coordinates and Isotropic Displacement Parameters for **5** 148

Table 19. X-ray Diffraction Data Collection Parameters for **8** 150

Table 20. Special Refinement Details for **8** 150

Table 21. Atomic Coordinates and Equivalent Isotropic Displacement Parameters for **8** 151

Table 22. Complete List of Bond Lengths and Angles for **8** 152

Table 23. Anisotropic Displacement Parameters for **8** 155

Table 24. Hydrogen Coordinates and Isotropic Displacement Parameters for **8** 156

Table 25. X-ray Diffraction Data Collection Parameters for **9** 158

Table 26. Special Refinement Details for **9** 158

Table 27. Atomic Coordinates and Equivalent Isotropic Displacement Parameters for **9** 159

Table 28. Complete List of Bond Lengths and Angles for **9** 160

Table 29. Anisotropic Displacement Parameters for **9** 162

Table 30. Hydrogen Coordinates and Isotropic Displacement Parameters for **9** 163

Table 31. X-ray Diffraction Data Collection Parameters for **10** 166

Table 32. Special Refinement Details for **10** 166

Table 33. Atomic Coordinates and Equivalent Isotropic Displacement Parameters for **10** 167

Table 34. Complete List of Bond Lengths and Angles for **10** 168

Table 35. Anisotropic Displacement Parameters for **10** 170

Table 36. Hydrogen Coordinates and Isotropic Displacement Parameters for **10** 171

Table 37. X-ray Diffraction Data Collection Parameters for **15** 174

Table 38. Special Refinement Details for **15** 174

Table 39. Atomic Coordinates and Equivalent Isotropic Displacement Parameters for **15** 176

Table 40. Complete List of Bond Lengths and Angles for **15** 177

Table 41. Anisotropic Displacement Parameters for **15** 180

Table 42. Hydrogen Coordinates and Isotropic Displacement Parameters for **15** 181

Introduction

This thesis contains the majority of the work I performed during my five years at Caltech. Although the three chapters are separate studies, they are unified under the heading of mechanistic studies of metallocene catalyzed Ziegler-Natta olefin polymerization. This is a subject in which many groups are interested, but despite the enormous effort directed toward the study of this process, there are still many important unsolved problems, and still much exciting research in the area. I hope this will be obvious from the studies described herein.

The chemistry discussed in Chapter 1 grew out of an effort, ongoing in the group at the time I arrived, to design ligands which would selectively bind group 3 and group 4 transition metals in a chiral fashion. It was hoped that a minor change in architecture from a ligand successfully demonstrated to do this, would not affect the diastereoselectivity for binding but would result in a more active olefin polymerization catalyst. This goal was not realized, but the study took a new course in examining the mechanism of interconversion between the chiral and achiral metallocene diastereomers. This interconversion reaction was found to be a general phenomenon, and one which must be considered when carrying out reactions involving a chiral metallocene and any sort of salt or alkylating reagent. Metallocene trihapto allyl complexes proved to be most useful for mechanistic studies of this process and the work described in Chapter 2 expounds on the mechanism of their formation.

A potential side reaction in the metallocene catalyzed polymerization of olefins involves allylic C–H bond activation of the terminally unsaturated polymer chain following β-H elimination. This side reaction results in the liberation of H_2, a potential chain transfer agent, and also results in internal unsaturation in the polymer which is produced. Although these effects had been noted in metallocene catalyzed olefin polymerizations, the mechanism of allyl formation had not been previously uncovered. The work described in Chapter 2 is a study of the mechanism of conversion of scandocene alkenyl compounds to scandocene η^3-allyl compounds, a model of the transformation proposed to occur during polymerization. Discovered during the course of these investigations is that the selectivity observed for σ-bond metathesis reactions

with olefins is altogether different between Cp^*_2Sc and $Me_2Si(C_5Me_4)_2Sc$ ligated metal fragments.

A more subtle possible consequence of the allylic activation reaction discussed above is that the metallocene η^3-allyl complexes so formed can catalyze the epimerization of the stereochemistry at the β-carbon of the growing polymer chain. This process is known as chain epimerization and is especially observed for polymerizations carried out with low monomer concentration. Although the intermediacy of allylic species was proposed for this process, another valid mechanism had also been proposed, and both of these were consistent with all evidence gathered to date. Thus, an experiment was designed and carried out that allowed differentiation between these two mechanisms. The results of these studies are not consistent with the intermediacy of allylic compounds for chain epimerization, and the implications of these results for the mechanism of olefin polymerization are discussed.

Chapter 1

Racemic-Meso Interconversion for *ansa*-Scandocene and *ansa*-Yttrocene Derivatives, and a Study of the Fluxional Processes for *ansa*-Scandocene η^3-Allyl Ligands[a]

Abstract

Dilithio *bis*(cyclopentadienide) $Li_2\{Me_2Si[C_5H_2\text{-}2,4\text{-}(CHMe_2)_2]_2\}$, Li_2Ip, reacts with $ScCl_3(THF)_3$ to afford *rac*-$IpScCl{\cdot}LiCl(THF)_2$ (**1**) and [*meso*-$IpSc(\mu_2\text{-}Cl)]_2$ (**2**), and with $YCl_3(THF)_{3.5}$ to afford *rac*-$IpYCl{\cdot}LiCl(THF)_2$ (**3**) and [*meso*-$IpY(\mu_2\text{-}Cl)]_2$ (**4**). Metallation with both scandium and yttrium chlorides yields the metallocene chlorides in an approximately 3:1 racemic:meso ratio. Reaction of IpH_2 with $Zr(NMe_2)_4$ yields exclusively *meso*-$IpZr(NMe_2)_2$ (**9**). Treatment of **1** or **2** with allylmagnesium bromide affords the allyl complexes *rac*-$IpSc(\eta^3\text{-}C_3H_5)$ (**5**) and *meso*-$IpSc(\eta^3\text{-}C_3H_5)$ (**6**) and with crotylmagnesium chloride affords *rac*-$IpSc(\eta^3\text{-}1\text{-}Me\text{-}C_3H_4)$ (**7**) and *meso*-$IpSc(\eta^3\text{-}1\text{-}Me\text{-}C_3H_4)$ (**8**). The fluxional behavior of the allyl ligands in **5** and **6** has been studied by dynamic ^1H NMR allowing for extraction of rate constants. Diastereomerically pure *rac* dichloro-metallate compounds (**1** or **3**) or pure *meso* chloro dimers (**2** or **4**) undergo spontaneous isomerization upon dissolution in THF-d_8 with reversion back to a 3:1 racemic:meso ratio. Isomerization of **5** and **6** is observed in THF-d_8, above 55 °C, affording an equilibrium ratio of ~2:1 racemic:meso isomers. While spontaneous isomerization of **5**, **6**, **7** or **8** is very slow at room temperature, various salts and Grignard reagents promote isomerization even at room temperature; the isomerizations are not accelerated by light. The proposed mechanism for racemic-meso isomerization involves heterolytic dissociation of one cyclopentadienide ligand from the metal, rotation around that Si-Cp^- bond and recoordination on the opposite face, effecting net epimerization. X-ray diffraction studies have been performed on *rac*-$IpScCl{\cdot}LiCl(THF)_2$ (**1**), [*meso*-$IpY(\mu_2\text{-}Cl)]_2$ (**4**), *rac*-$IpSc(\eta^3\text{-}C_3H_5)$ (**5**), *meso*-$IpSc(\eta^3\text{-}1\text{-}Me\text{-}C_3H_4)$ (**8**), and *meso*-$IpZr(NMe_2)_2$ (**9**).

[a]The bulk of this chapter has been excerpted from two publications.[1]

Table of Contents, Chapter 1

I. Introduction 5

II. Results and Discussion 8

A. Synthesis and Characterization of Ip-Ligated Scandocene and Yttrocene Compounds 8

B. Variable Temperature ^{1}H NMR Spectra for Allyl Complexes 21

C. Racemic-Meso Interconversions for IpScCl and IpYCl Complexes 27

D. Racemic-Meso Isomerizations for IpSc(η^3-allyl) Complexes 29

E. Studies of the Kinetics of Metallation and Attempts to Determine the Generality of *ansa*-Metallocene Ligand Isomerization 35

III. Conclusions 37

IV. Experimental Section 38

V. References and Notes 50

Introduction

The active species in the new metallocene-based polymerizations of α-olefins are 14-electron group 4 metallocenium-alkyl cations, $[Cp_2M\text{-}R]^+$ (Cp = variously substituted cyclopentadienyl and M = a group 4 transition metal), with a very weakly coordinating counter-anion.[2] The polymerization performance of these catalysts and the less active, isoelectronic neutral group 3 and lanthanide metallocene-alkyls $Cp_2M\text{-}R$ have been extensively investigated.[3]

Stereo-random enchainment to afford atactic poly-α-olefins is effected by achiral metallocene catalyst precursors, while stereospecific polymerization yielding isotactic polymers[4,5] is best effected using C_2-symmetric *ansa*-metallocenes.[6] In Brintzinger's original reports,[7] ethylenebis(1-indenyl) (EBI) and ethylenebis(4,5,6,7-tetrahydro-1-indenyl) (EBTHI) derivatives of titanium and zirconium are described. Linking the indenyl ligands results in two possible isomers on metallation: a C_2-symmetric racemic isomer (consisting of the (*R*,*R*) and (*S*,*S*) enantiomeric pairs) and a C_s-symmetric meso (achiral) isomer (Figure 1).

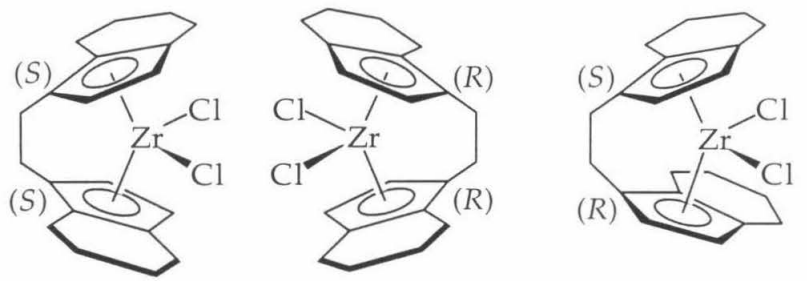

rac-(EBTHI)$ZrCl_2$ *meso*-(EBTHI)$ZrCl_2$

Figure 1. Drawing of the two diastereomers of ethylenebis(4,5,6,7-tetrahydro-1-indenyl)zirconium dichloride.

When combined with methylaluminoxane (MAO) chiral *rac*-(EBTHI)$ZrCl_2$, and *rac*-(EBI)$TiCl_2$ polymerize α-olefins to isotactic polymers. The achiral *meso*-(EBTHI) ligated metallocenes produce atactic polymer. These differences in polymer microstructure obtained with racemic *vs.* meso isomers have been shown to be general for a large number of group 3 or group 4 transition metal metallocenes.[2]

The racemic isomer, therefore, normally is the desired product of metallation of the ligand. Unfortunately, in most cases some amount of the achiral meso isomer is also formed, necessitating an often tedious separation process. Brintzinger has suggested that the racemic:meso ratios obtained on metallation may be kinetically controlled by the face selection for the attachment of the second cyclopentadienyl ring to the metal.[8] On the other hand, Marks and coworkers have reported that some lanthanide *ansa*-metallocenes bearing a chiral substituent may undergo epimerization to the more stable diastereomer, a process that requires one of the cyclopentadienyl ligands to dissociate from the metal and recoordinate by the opposite face (Eqn 1).[3b,9] Coordinating solvents

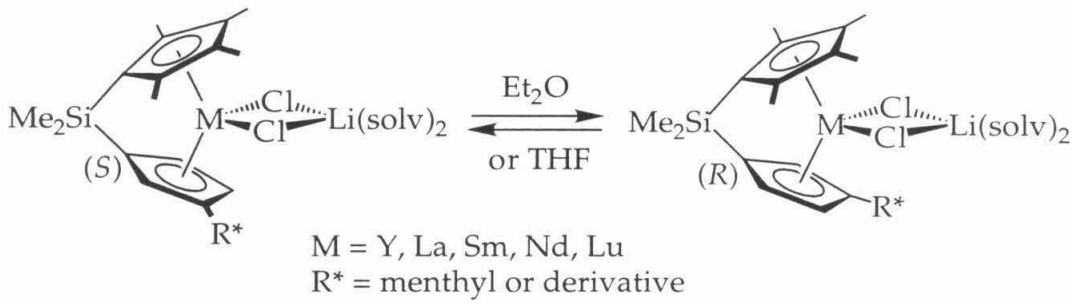

(1)

M = Y, La, Sm, Nd, Lu
R* = menthyl or derivative

(THF-d_8 and Et_2O-d_{10}) were found to promote interchange, as was lithium chloride. Several other recent articles have appeared which attest to the generality of this isomerization reaction for *ansa*-metallocene halide complexes.[10] Since these promoters are commonly present during the preparation of the *ansa*-metallocene halides, we wondered whether during metallation the racemic:meso ratio is thermodynamically, rather than kinetically, controlled.

Jordan, *et al.* have reported that racemic-meso isomerizations take place concurrently with metallations of linked *bis*(cyclopentadiene) ligands utilizing amine elimination reactions for amide complexes (Scheme 1).[11] Equilibrium is thus established between the two metallocene diastereomers, and in metallation reactions of this type a higher yield of the desired racemic isomer can often be achieved.

The studies detailed above, along with earlier investigations of photoisomerization reactions of *ansa*-titanocenes and zirconocenes,[6,12] appear to be the only examples of *ansa*-metallocene racemic-meso interconversion reactions. Numerous examples have been reported, however, of reactions that

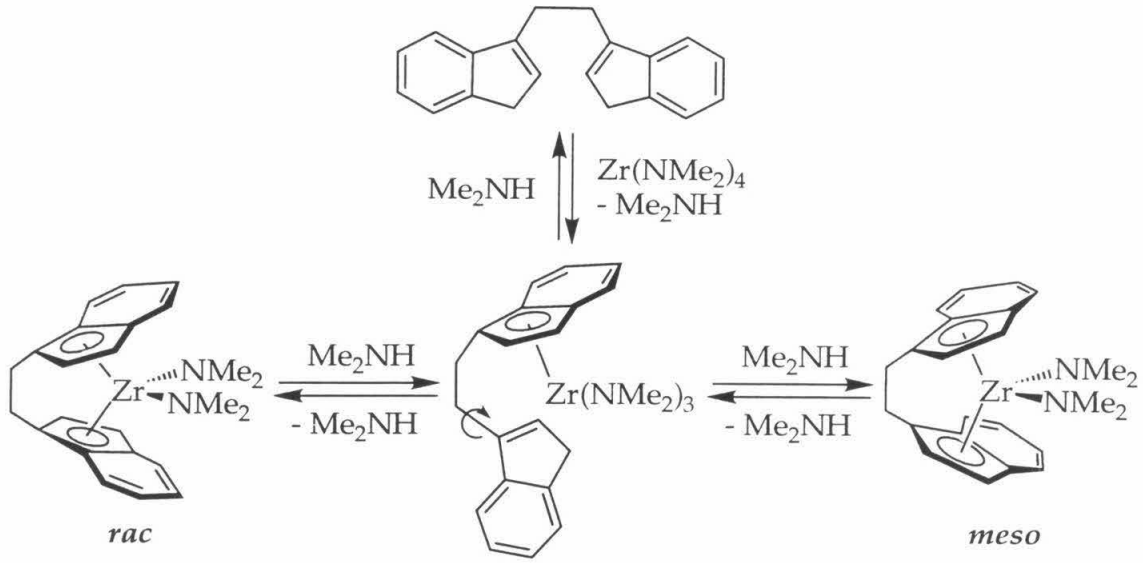

Scheme 1. Racemic-meso interconversion during *ansa*-metallocene synthesis using the amine elimination route.

involve metal-cyclopentadienyl bond rupture. Photochemically induced ring loss from non-bridged titanocenes has been extensively studied.[13] Disproportionation reactions of Cp'_nLnX_{3-n} ($Cp' = \eta^5\text{-}C_5H_5$, $\eta^5\text{-}C_5Me_5$ (Cp*); X = Cl, OR, NR_2, *etc.*) compounds are well known[14] and have been used in the synthesis of Cp'_2LnCl derivatives.[14d] Recently, loss of Cp* has been observed from mixed-ring zirconocenes in ethereal solvents.[15] Also, "flyover dimer" complexes formed by linked *bis*(cyclopentadienyl) ligands when they span two metal centers have been observed to form spontaneously from group 3 *ansa*-metallocene hydride dimers;[16] one example is shown in Eqn 2.[16a] Thus, there appear to be many pathways available for M-Cp bond rupture and reformation.

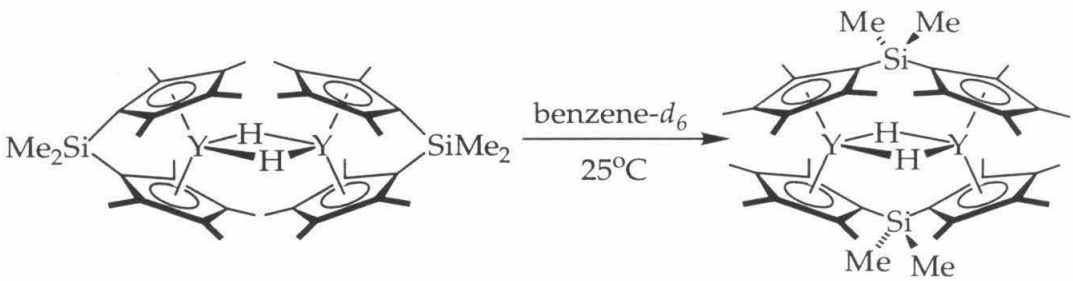

(2)

Bercaw *et al.* have described a ligand system that undergoes metallation with group 3 and 4 transition metals to afford only the desired racemic isomer,

thus obviating the need for isomer separation.[3a,17] The yttrocene hydride so obtained, [*rac*-$Me_2Si(\eta^5\text{-}C_5H_2\text{-}2\text{-}SiMe_3\text{-}4\text{-}CMe_3)_2Y(\mu_2\text{-}H)]_2$ ($[BpY(\mu_2\text{-}H)]_2$), is active for the isospecific polymerization of α-olefins.[3a] The sterically demanding trimethylsilyl substituents α-to the silylene linker atom direct metallation of the Bp ligand exclusively to the racemic isomer, since in the meso isomer the ($SiMe_3$) substituents would be placed next to one another in the narrow portion of the metallocene wedge (Figure 2).

rac-$BpYCl_2Li(THF)_2$ *meso*-$BpYCl_2Li(THF)_2$

Figure 2. Representations of *rac*- and *meso*-BpYCl.

The dimethylsilylene linked $Me_2Si\{[C_5H_2\text{-}2,4\text{-}(CHMe_2)_2]_2\}$ ("Ip") *ansa*-ligand system utilized in the present study was designed by analogy to Bp (Figure 3). Although molecular mechanics calculations[18] predicted that the

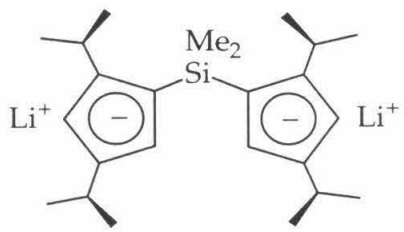

Figure 3. Drawing of the structure of $IpLi_2$.

isopropyl substituents in the 2-positions should direct coordination preferentially to the racemic isomer, we find instead that metallations of Li_2Ip with scandium or yttrium chlorides afford a mixture of racemic and meso isomers. Relatively facile interconversion of these isomers is observed, especially in coordinating solvents such as THF and in the presence of salts such as lithium chloride. We report herein the synthesis and characterization of scandocene and yttrocene

compounds with the Ip ligand system together with the results of an investigation of the racemic-meso interconversion process.

Results and Discussion

Synthesis and Characterization of Ip-Ligated Scandocene and Yttrocene Compounds

The protonated form of the ligand, IpH_2, is conveniently prepared by the reaction between two equivalents of $[C_5H_3\text{-}1,3\text{-}(CHMe_2)_2]Li$ with dichlorodimethylsilane in THF solution. This procedure affords IpH_2 as a light yellow oil after Kugelröhr distillation (Eqn 3). Deprotonation proceeds readily

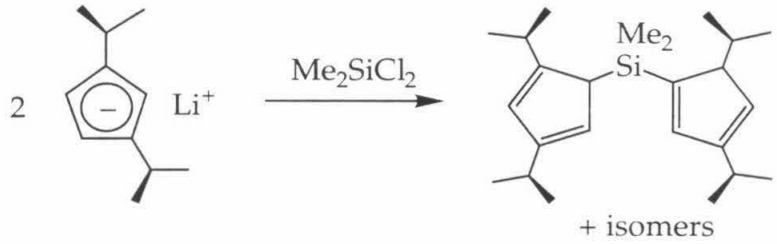

(3)

using *n*-butyllithium in petroleum ether, and a white powder is obtained after workup with THF that consistently analyzes (by ^1H NMR) as $Li_2Ip(THF)_{0.3}$.

Reactions of $Li_2Ip(THF)_{0.3}$ with $ScCl_3(THF)_3$ as well as with $YCl_3(THF)_{3.5}$ in refluxing THF afford mixtures of racemic and meso isomers (Scheme 2). The resulting metallocene chlorides are separated by successive filtration/crystallization cycles. Thus, after a series of heptane washes of the crude product mixture to remove excess THF, separation of the meso from the racemic complexes is accomplished by successive dissolutions of the mixtures in heptane or petroleum ether followed by filtration, isolating the mostly insoluble meso chloride-bridged dimers. After 2-3 iterations of this process, the filtrate is essentially pure *rac*-IpMCl·LiCl(THF)$_2$ (M = Sc, **1**; M = Y, **3**); the racemic species may then be recrystallized from cold (-40 °C) pentane solutions.

Light yellow plates of **1** were obtained from a concentrated petroleum ether/THF solution upon cooling and an X-ray structure determination was carried out. The X-ray structure for **1**, shown in Figure 4, reveals the lithium dichloroscandate formulation given in Scheme 2. This formulation is further supported by the presence of coordinated THF (^1H NMR) for solutions of **1**. The

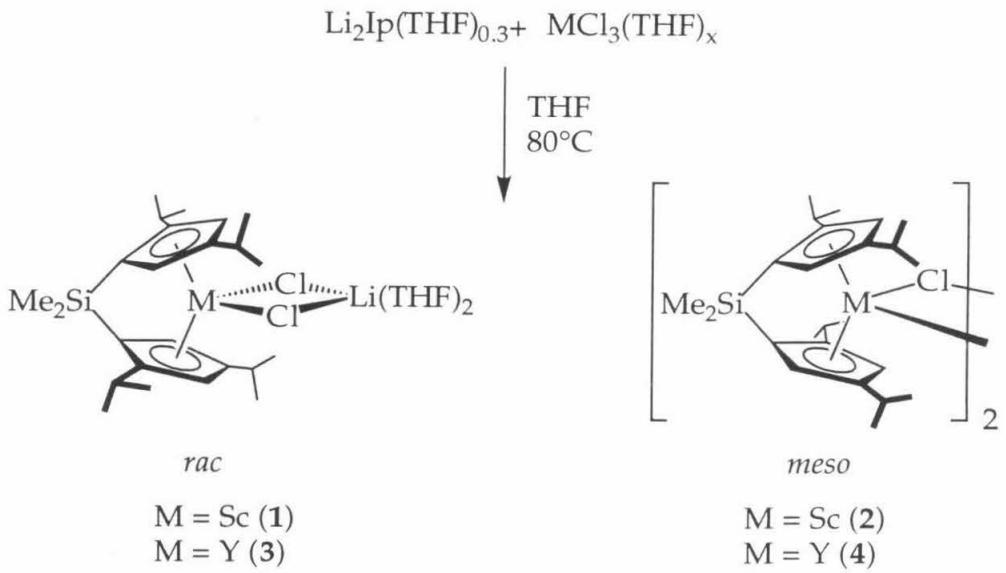

rac

M = Sc (**1**)
M = Y (**3**)

meso

M = Sc (**2**)
M = Y (**4**)

Scheme 2. Synthesis of IpMCl derivatives (M = Sc, Y).

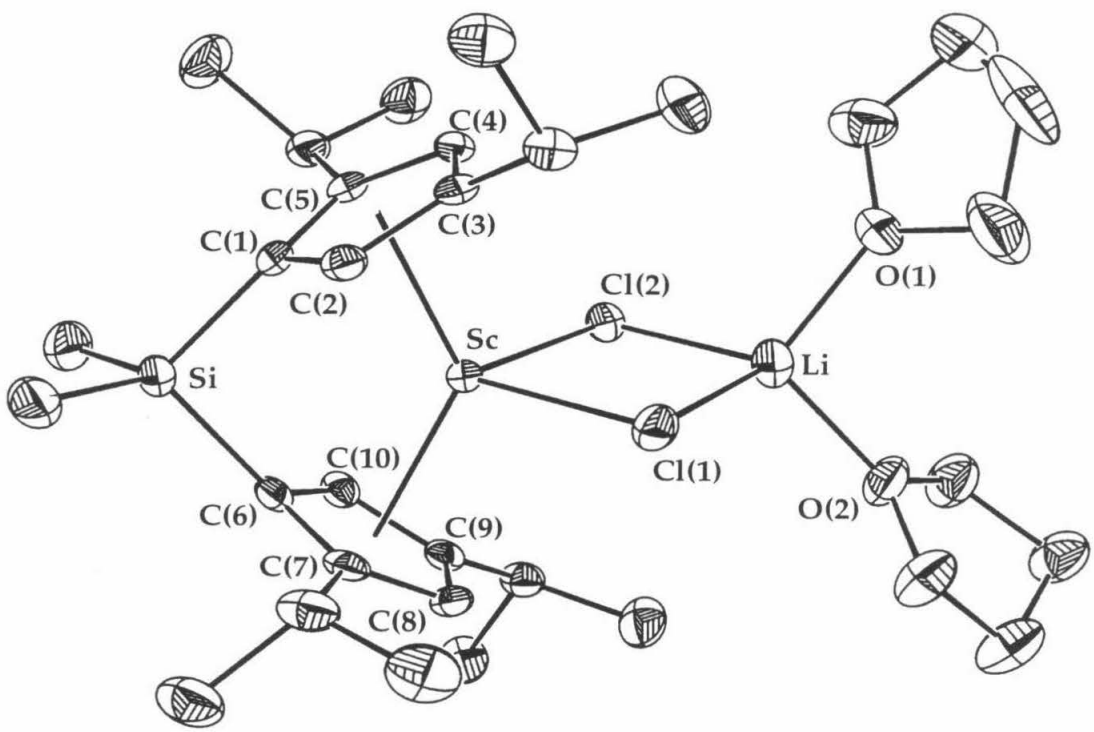

Figure 4. ORTEP representation of the molecular structure of **1** (50% probability ellipsoids, hydrogens omitted for clarity).

Sc-Cp(centroid) distances (2.239 (1) Å and 2.236 (1) Å) are at the long end of those normally encountered in scandocene complexes (2.171 Å - 2.212 Å),[19] and the Cp-M-Cp angle of 127.9 (1)° is within the normal range. Due to the similar solubility properties between **1** and "*rac*-IpYCl" and the presence of coordinated THF (^{1}H NMR) in the yttrium species, the yttrium congener (**3**) is formulated as a {LiCl(THF)$_2$} adduct as well. Selected bond distances and angles for **1** can be found in Table 1. Details of the data collection and solution and refinement of the structure can be found in Appendix 2.

Table 1. Selected Bond Distances (Å) and Bond Angles (°) Obtained from the X-Ray Structure Determination of **1** and **4**

Feature	Distance (Å) or Angle (°) for **1** (M = Sc)	Distance (Å) or Angle (°) for **4** (M = Y)
M-Ct(1)[a]	2.239 (1)	2.344 (1)
M-Ct(2)[b]	2.236 (1)	
M-Cl(1)	2.496 (1)	2.668 (2)
M-Cl(2)	2.509 (1)	
Ct(1)-M-Ct(2)[a, b]	127.91 (2)	123.7 (2)
Ct(1)-M-Cl(1)[a]	108.7 (3)	110.2 (2)
Ct(1)-M-Cl(2)[a]	107.9 (3)	111.6 (2)
Ct(2)-M-Cl(1)[b]	107.9 (3)	
Ct(2)-M-Cl(2)[b]	109.1 (3)	
Cl(1)-M-Cl(2)	88.14 (3)	81.57 (4)

[a]Ct(1) is defined as the centroid of the plane made up of C(1) - C(5); [b]Ct(2) is defined as the centroid of the plane made up of C(6) - C(10).

Colorless prisms of *meso*-[IpY(μ_2-Cl)]$_2$ (**4**) were obtained from a pentane solution cooled to -40 °C and an X-ray structure determination was carried out. The molecule is located on an inversion center, and due to this crystallographically induced symmetry it was only necessary to locate 1/4 of the total atoms in the unit cell. Solution and refinement of the data revealed a dimeric structure, shown in Figure 5. The distance from Y to the centroids of the cyclopentadienyl rings (2.344 (1) Å) is within the range of normal Y-Cp centroid distances (2.279 Å - 2.414 Å).[20] The Y-Cl distance (2.668 (2) Å) is consistent with a bond from yttrium to a bridging chlorine atom (2.614 Å - 2.776 Å), and is

significantly longer than those typically found from yttrium to a terminal chlorine atom (~2.58 Å).[21] The Cp centroid-Y-Cp centroid angle is 123.7 (1)°, in good agreement with the angles typically observed in other *ansa*-yttrocenes. The lack of coordinated THF in the NMR spectrum of "*meso*-IpScCl" (**2**) and the similarity of its solubility properties to those of **4** indicate that the scandium *meso* compound is most likely dimeric also. A list of selected bond lengths and bond angles obtained for **4** can be found in Table 1. Details of the data collection and solution and refinement of the structure can be found in Appendix 2.

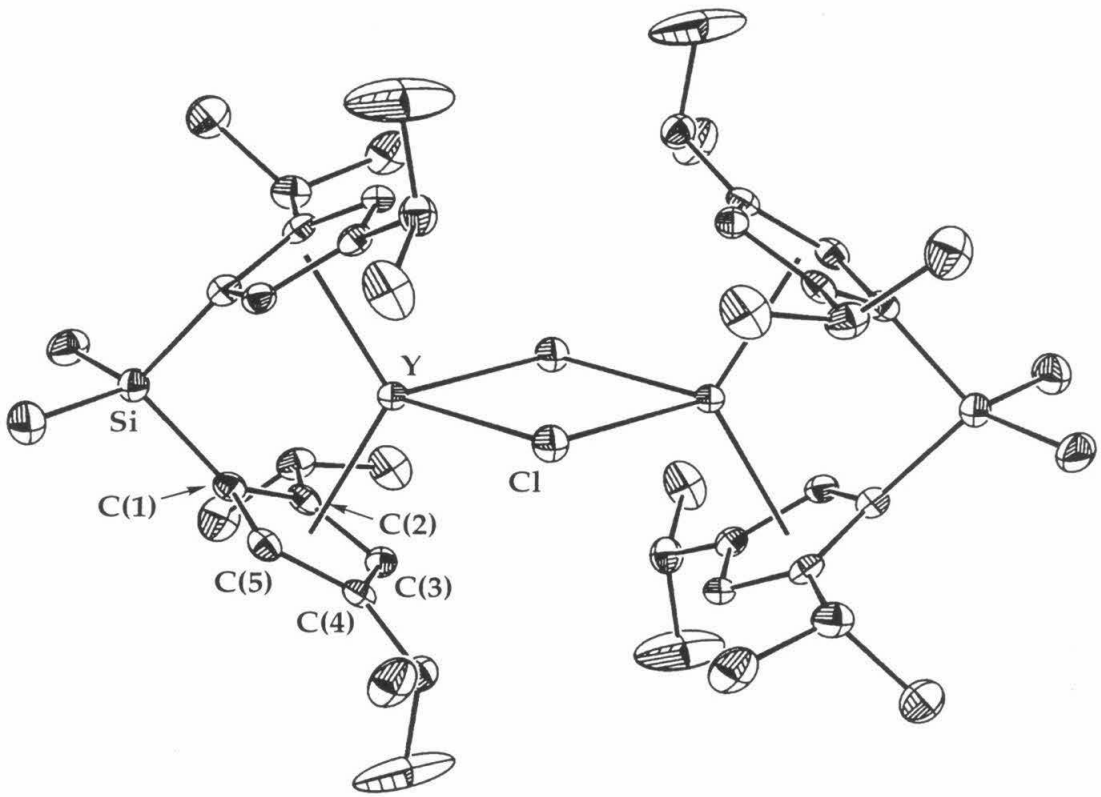

Figure 5. ORTEP representation of the molecular structure of **4** (50% probability ellipsoids, hydrogens omitted for clarity).

Both *rac*-IpSc(η^3-C_3H_5) (**5**) and *meso*-IpSc(η^3-C_3H_5) (**6**) may be synthesized by slowly warming toluene solutions of either **1** or **2**, respectively, from -78 °C to room temperature in the presence of a slight excess of allylmagnesium bromide. Slow warming of these reaction mixtures is necessary because at higher temperatures an excess of the Grignard reagent serves to promote the interconversion of the racemic and meso isomers (*vide infra*). In the same

manner, the crotyl derivatives *rac*-IpSc(η^3-1-Me-C_3H_4) (**7**) and *meso*-IpSc(η^3-1-Me-C_3H_4) (**8**) may be prepared (Scheme 3).

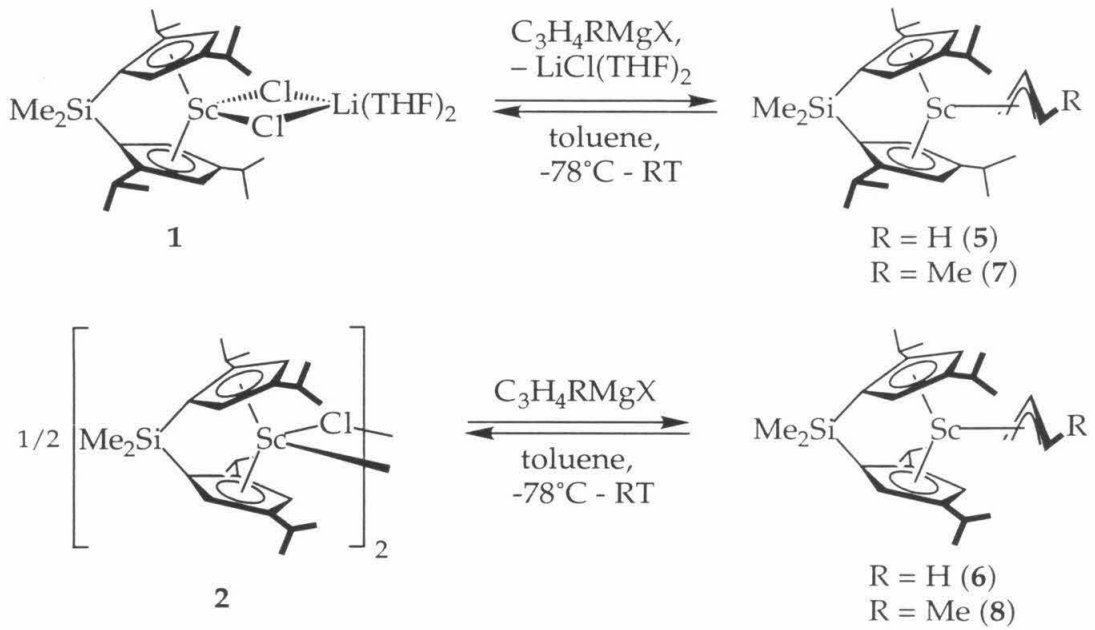

Scheme 3. Synthesis of IpSc(η^3-allyl) complexes.

Upon slow cooling from 80 °C, single crystals of **5** precipitated as orange plates from a saturated toluene solution and an X-ray structure determination was carried out. The allyl ligand was found to be disordered and the disorder was modeled as a 70:30 population of sites, using two separate allyl methine carbons (C(14A) and C(14B)) one directed at each of the cyclopentadienyl rings. The positions of the allyl methylene carbons C(13) and C(15) are identical for each allyl site. The structure of the molecule oriented in the major position is shown in Figure 6; selected bond lengths and angles are given in Table 2. Details of the data collection and solution and refinement of the structure can be found in Appendix 2.

The geometry about scandium is probably best described by considering the bonds from scandium to the centroid of each ligand. It is then evident that the scandium is coordinated in an approximately trigonal planar geometry with a Cp centroid-Sc-Cp centroid angle of 128.5 (2)°, and the two Cp centroid-Sc-allyl centroid angles slightly less than 120°. For each allyl site the sum of the centroid-

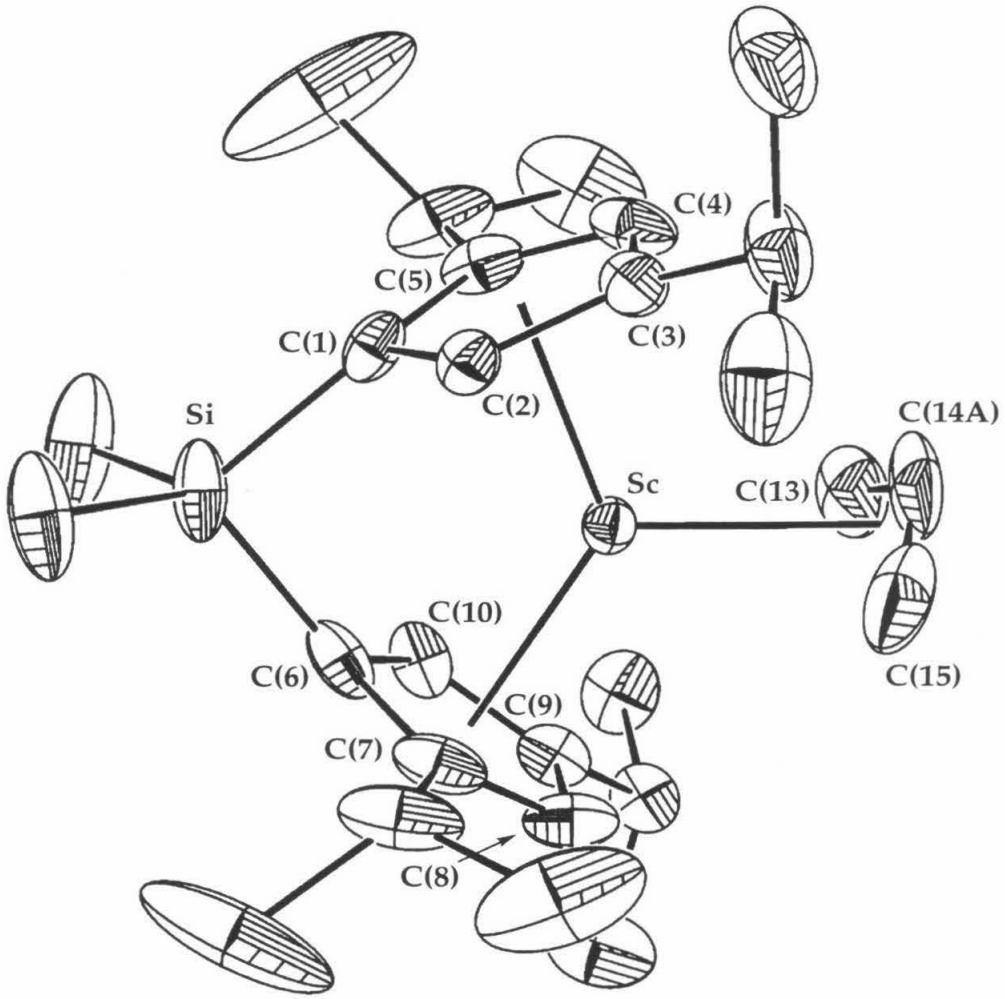

Figure 6. ORTEP representation of the molecular structure of **5** (50% probability ellipsoids, hydrogens omitted for clarity).

Sc-centroid angles is 360°, indicating that the metal center and all four centroids are coplanar. The Sc-Cp centroid bond lengths (2.188 (1) Å and 2.189 (1) Å) are identical within experimental error and are in the normal range for Sc-Cp bond lengths in scandocene alkyls (2.170 Å- 2.212 Å).[19] The centroid-Sc-centroid angle is in excellent agreement with the same angles of the other crystallographically characterized *ansa*-scandocene allyl compounds described in this work (see below and Chapter 2). The allyl ligands in each site appear to be symmetrically bonded η^3-allyl structures. The Sc-C(13) and Sc-C(15) bond lengths of 2.487 (3) Å, and 2.469 (3) Å, respectively, are only slightly greater than 3σ apart, and the C-C bond lengths in each allyl site are equivalent within

standard deviation. Thus, there appears to be no distortion toward an η^1-structure for **5** in the solid state. The bond lengths from scandium to the central allyl methine carbons of each site are slightly shorter than the corresponding scandium-methylene carbon distances; Sc-C(14A) = 2.465 (5) Å, Sc-C(14B) = 2.436 (7) Å.

Table 2. Selected Bond Distances (Å) and Bond Angles (°) Obtained from the X-Ray Structure Determination of **5**

Feature	Distance (Å) or Angle (°)	Feature	Distance (Å) or Angle (°)
Sc-Ct(1)[a]	2.188 (1)	Sc-Ct(2)[b]	2.189 (1)
Sc-Ct(3)[c]	2.245	Sc-Ct(4)[d]	2.237
Sc-C(13)	2.487 (3)	Sc-C(14A)	2.465 (5)
Sc-C(14B)	2.436 (7)	Sc-C(15)	2.469 (3)
C(13)-C (14A)	1.340 (8)	C(13)-C(14B)	1.349 (11)
C(14A)-C(15)	1.381 (9)	C(14B)-C(15)	1.331 (12)
Ct(1)-Sc-Ct(2)[a, b]	128.5 (2)	Ct(1)-Sc-Ct(3)[a, c]	111.4
Ct(1)-Sc-Ct(4)[a, d]	120.2	Ct(2)-Sc-Ct(3)[b, c]	120.1
Ct(2)-Sc-Ct(4)[b, d]	111.3	C(13)-C(14A)-C(15)	128.5 (7)
C(13)-C(14B)-C(15)	132.3 (10)	C(13)-Sc-C(15)	59.28 (14)
C(13)-Sc-C(14A)	31.4 (2)	C(13)-Sc-C(14B)	31.8 (3)
C(14A)-Sc-C(15)	32.5 (2)	C(14B)-Sc-C(15)	31.5 (3)

[a]Ct(1) is defined as the centroid of the ring made up of C(1) - C(5); [b]Ct(2) is defined as the centroid of the ring made up of C(6) - C(10); [c]Ct(3) is defined as the centroid of the allyl ligand in the major rotamer made up of C(13), C(14A), and C(15); [d]Ct(4) is defined as the centroid of the allyl ligand in the minor rotamer made up of C(13), C(14B), and C(15).

Single crystals of **8** were obtained by slow cooling of a saturated heptane solution from 80 °C to room temperature and an X-ray structure determination was carried out. Two perspectives of the molecular structure of **8** are shown in Figure 7; selected bond lengths and bond angles can be found in Table 3. Details of the data collection and solution and refinement of the structure can be found in Appendix 2. Again, if one considers the bonds from scandium to the centroids

of each ligand, the scandium can be described by a slightly distorted trigonal planar geometry. The Cp centroid-Sc-Cp centroid angle is 128.66 (3)° and the two Cp centroid-Sc-crotyl centroid angles are 113.05 (2)° and 118.26 (2)°. The sum of these angles is 359.97° indicating that the Sc atom and all three centroids are coplanar. The Sc-Cp centroid bond lengths (2.192 (2) Å and 2.205 (2) Å) agree well with the same distances in other crystallographically characterized *ansa*-scandocenes.[19]

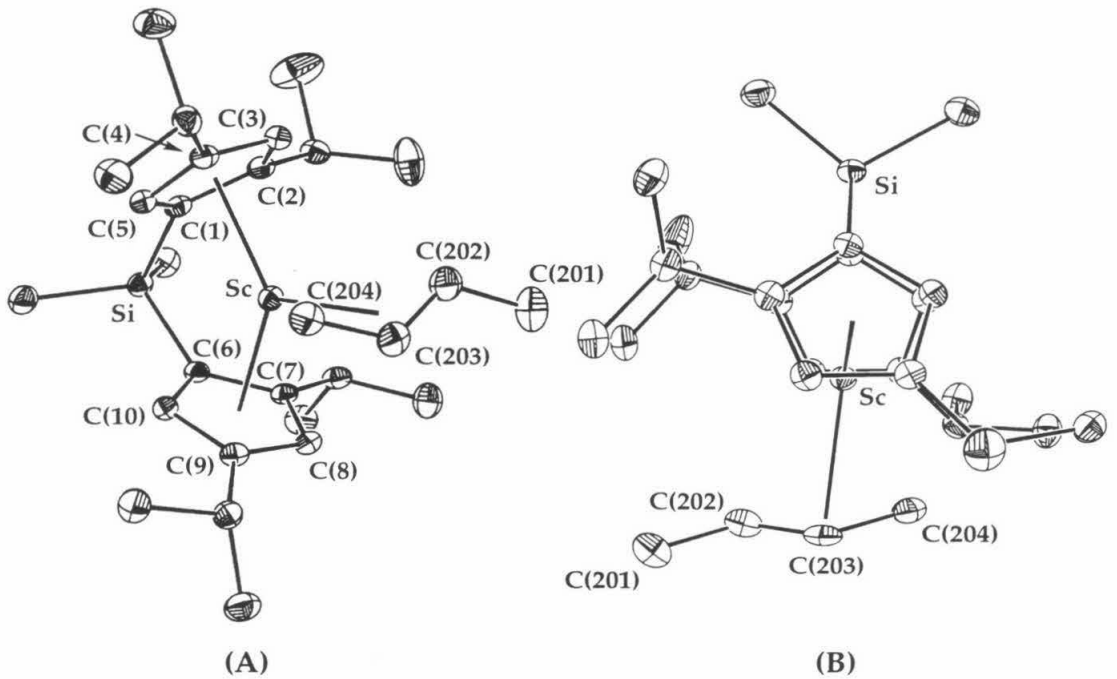

Figure 7. ORTEP representation of the molecular structure of **8** showing a normal view (**A**) and also the distortion toward monohapto binding for the crotyl ligand (**B**) (50% probability ellipsoids, hydrogens omitted for clarity).

The methyl group of the crotyl ligand in this structure is found in a trans-like orientation with the opposite carbon and, as also expected, the methyl group occupies the side of the molecule away from the bulky isopropyl groups in the front of the metallocene wedge. However, the Sc-crotyl centroid bond length (2.300 (2) Å) is considerably longer than the Sc-allyl centroid bond lengths in the two other scandocene η^3-allyl structures described in this work (see above and also Chapter 2). In addition, the bonds from scandium to the three nominally sp^2-hybridized carbons of the crotyl ligand lengthen noticeably as one progresses from C(204), the methylene carbon (Sc-C(204) = 2.317 (2) Å), to

C(202), the carbon possessing the methyl group (Sc-C(202) = 2.748 (3) Å). Furthermore, the crotyl C-C bond lengths show a marked alternation (C(202)-C(203) = 1.361 (3) Å, C(203)-C(204) = 1.422 (3) Å) with the shorter C-C bond length corresponding to the carbons with the longer Sc-C bond lengths. All of the above evidence is characteristic of a distortion toward a monohapto crotyl group for **8** in the solid state (Figure 7, view (B), and Figure 8). It is likely that steric interactions between the crotyl methyl group and the isopropyl groups α-to the linker in the rear of the metallocene wedge are responsible for this behavior.

Table 3. Selected Bond Distances (Å) and Bond Angles (°) Obtained from the X-Ray Structure Determination of **8**

Feature	Distance (Å) or Angle (°)	Feature	Distance (Å) or Angle (°)
Sc-Ct(1)[a]	2.205 (2)	Sc-Ct(2)[b]	2.192 (2)
Sc-Ct(3)[c]	2.300 (2)	Sc-C(202)	2.748 (3)
Sc-C(203)	2.509 (2)	Sc-C(204)	2.317 (2)
C(201)-C(202)	1.501 (3)	C(202)-C(203)	1.361 (3)
C(203)-C(204)	1.422 (3)		
Ct(1)-Sc-Ct(2)[a, b]	128.6 (2)	Ct(1)-Sc-Ct(3)[a, c]	118.3 (2)
Ct(2)-Sc-Ct(3)[b, c]	113.1 (2)	C(201)-C(202)-C(203)	123.7 (2)
C(202)-C(203)-C(204)	126.3 (2)		

[a]Ct(1) is defined as the centroid of the ring made up of C(1) - C(5); [b]Ct(2) is defined as the centroid of the ring made up of C(6) - C(10); [c]Ct(3) is defined as the centroid of the crotyl ligand made up of the three sp^2-hybridized carbons C(202) - C(204).

η^3 η^1

Figure 8. Drawing of the two limiting structures for crotyl bonding in **8**.

Despite the ease with which IpSc(η^3-allyl) complexes can be synthesized, all attempts to prepare the yttrium analogs by reaction of **3** or **4** with allylmagnesium bromide have failed. Reaction of Cp^*_2YCl with allylic Grignard reagents also results in decomposition. Furthermore, reaction of allene with $[Cp^*_2Y(H)]_2$ yielded, as the only organometallic product, $Cp^*_2Y(H)C{=}C{=}CH_2$, derived through σ-bond metathesis. Admittedly this is a small number of synthetic attempts, but it is unknown why yttrium η^3-allyl complexes should be difficult to prepare.

Since initial attempts to synthesize a group 4 metallocene, $IpZrCl_2$, by a metathetical reaction between $IpLi_2$ and $ZrCl_4$ or $ZrCl_4(THF)_2$ were unsuccessful, alternative metallation strategies were sought. Using the amine elimination reaction between a *bis*(cyclopentadiene) ligand and $Zr(NMe_2)_4$, as described by Jordan, *et al.*,[11] reaction of IpH_2 with $Zr(NMe_2)_4$ (Eqn 4) proceeds cleanly during an overnight reflux at 140 °C in xylenes open to a mercury bubbler.

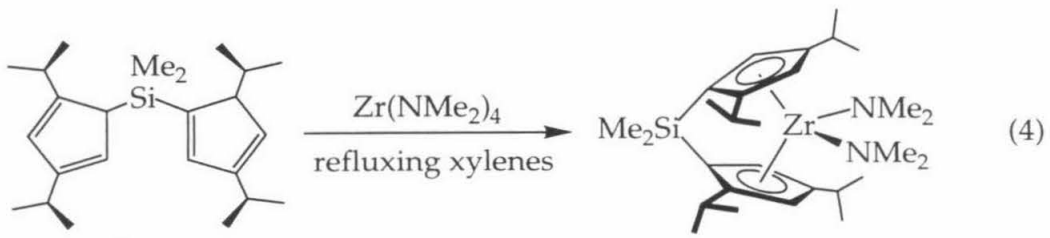

+ isomers **9** (4)

Filtration of the reaction mixture from pentane, and cooling at -80 °C for 1 week yielded bright orange crystals which were suitable for an X-ray diffraction study. The meso structure of **9** is shown in Figure 9; ^1H NMR spectra show no

evidence for formation of the racemic analog of **9**. Selected bond lengths and angles for the structure of **9** can be found in Table 4. Details of the data collection and solution and refinement of the structure can be found in Appendix 2.

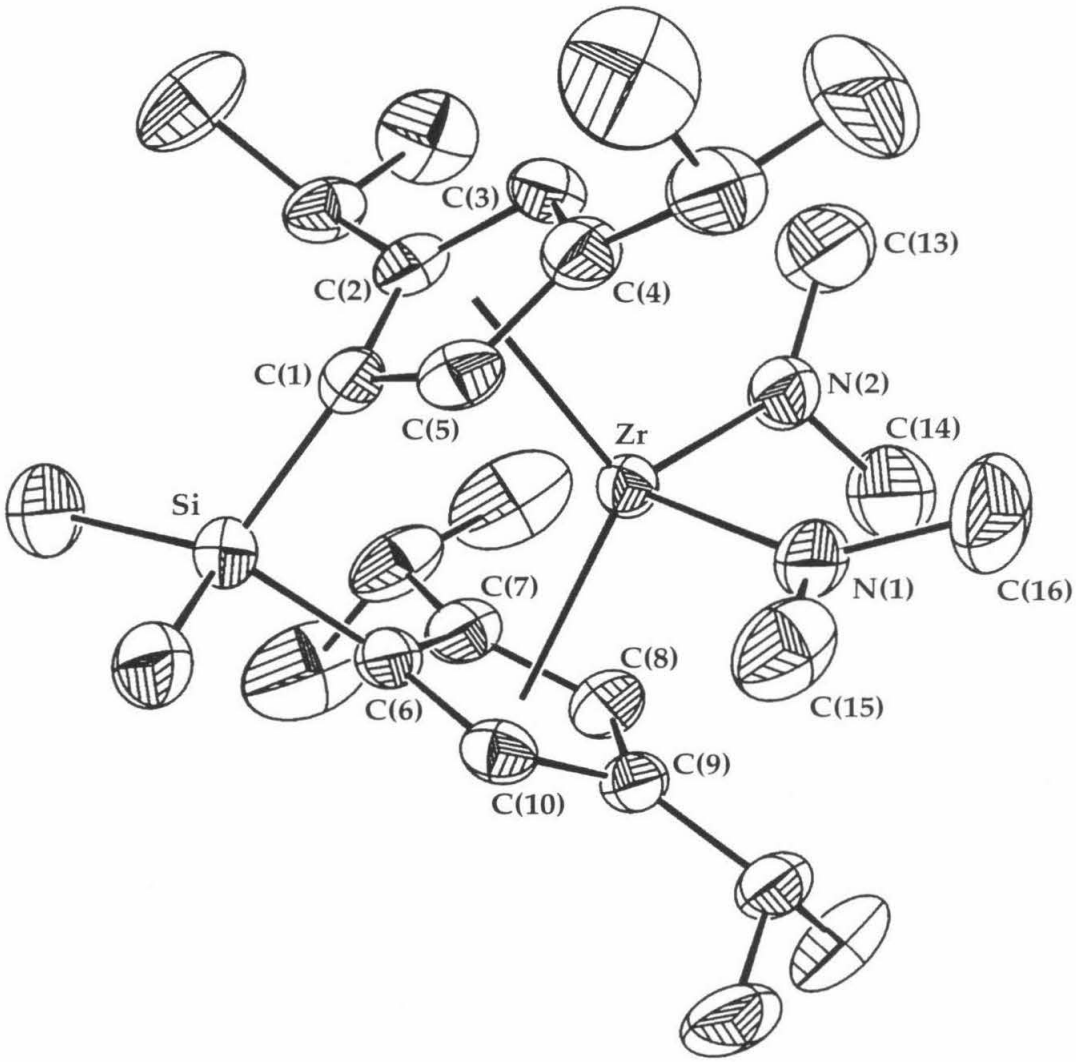

Figure 9. ORTEP representation of the molecular structure of **9** (50% probability ellipsoids, hydrogens omitted for clarity).

Table 4. Selected Bond Distances (Å) and Bond Angles (°) Obtained from the X-Ray Structure Determination of **9**

Feature	Distance (Å) or Angle (°)	Feature	Distance (Å) or Angle (°)
Zr-Ct(1)[a]	2.348 (2)	Zr-Ct(2)[b]	2.312 (2)
Zr-N(1)	2.107 (3)	Zr-N(2)	2.067 (3)
N(1)-C(15)	1.446 (5)	N(1)-C(16)	1.450 (5)
N(2)-C(13)	1.450 (4)	N(2)-C(14)	1.468 (5)
Ct(1)-Zr-Ct(2)[a, b]	122.9 (2)	Ct(1)-Zr-N(1)[a]	106.0 (2)
Ct(1)-Zr-N(2)[a]	110.8 (2)	Ct(2)-Zr-N(1)[b]	108.0 (2)
Ct(2)-Zr-N(2)[b]	110.0 (2)	N(1)-Zr-N(2)	95.38 (14)
Zr-N(1)-C(15)	125.2 (3)	Zr-N(1)-C(16)	125.0 (3)
Zr-N(2)-C(13)	137.6 (3)	Zr-N(2)-C(14)	116.8 (3)
C(15)-N(1)-C(16)	109.3 (4)	C(13)-N(2)-C(14)	105.4 (3)

[a]Ct(1) is defined as the centroid of the ring made up of C(1) - C(5); [b]Ct(2) is defined as the centroid of the ring made up of C(6) - C(10).

The distances from zirconium to the centroids of the cyclopentadienyl rings (2.348 (4) Å, 2.312 (4) Å) are longer than those typically observed in zirconocene chloride compounds, which average 2.2 Å - 2.3 Å. However, these values are in excellent agreement with the Zr-Cp bond distances in *rac*-$Me_2Si(\eta^5$-C_5H_2-2-Me-4-$CMe_3)_2Zr(NC_4H_8)_2$ (**A**) (2.357 Å, 2.348 Å), one of the only other structurally characterized *ansa*-zirconocene amides.[11d] Slightly longer M-Cp distances for amido-ligated zirconocenes may be attributable to the larger size of the amide functionality, as well as to possible N-to-Zr lone electron pair donation that should serve to lower the electrophilicity of zirconium. The Cp centroid-Zr-Cp centroid angle in **9** (122.9 (2)°) agrees well with the corresponding angle in **A** (122.5°), at the low end of those typically observed in *ansa*-zirconocene compounds. Both nitrogen atoms adopt essentially planar geometries. The orientations of the two NMe_2 ligands, one with the C-N-C plane essentially coincident with the zirconocene equatorial plane (dihedral angle = 7.8 (3)°), the other with the C-N-C plane close to perpendicular (dihedral angle = 66.3 (4)°), is as expected for the former amide ligand serving as a one-electron donor, the latter as a three-electron donor, completing the 18-electron count at zirconium. A similar arrangement of phosphide ligands was reported by Baker and

coworkers for $(\eta^5\text{-}C_5H_5)_2Hf(PEt_2)_2$.[22] The Zr-N bond lengths in the structure for **9** reveal a difference of only 0.04 Å for the two Zr-N bond lengths (Zr-N(1) = 2.107 (3) Å, and Zr-N(2) = 2.067 (3) Å). Although the shorter Zr-N bond is that for the amide ligand oriented properly for N to Zr π donation, the small difference in bond lengths suggests that this bonding is relatively weak. The two amide ligands appear to adopt an arrangement which minimizes unfavorable steric interactions.

The ^{1}H NMR spectrum of **9** in benzene-d_6 at room temperature reveals that one of the two $N(CH_3)_2$ resonances is considerably broadened, presumably due to restricted rotation about the Zr-N bond. Consideration of the (limiting) static solid state structure leads to a prediction of three N*Me* signals in a 2:1:1 relative intensity ratio. The broadened signal suggests that the two methyl groups of N(1) are at intermediate exchange, reminiscent of the temperature dependent ^{1}H NMR spectrum for $(\eta^5\text{-}C_5Me_5)_2Hf(H)NMe_2$, which reveals a (steric) rotational barrier for the Hf-N bond of 13.5 (10) kcal·mol^{-1}.[23] Variable temperature ^{1}H NMR data were recorded on **9** which revealed a barrier to rotation of 12.7 (5) kcal·mol^{-1} at 270 K. A Hf-N bond distance of 2.027 (8) Å was determined for $(\eta^5\text{-}C_5Me_5)_2Hf(H)NH(Me)$, where the magnitude of the Hf-N π bonding was shown to be less than *ca.* 10 kcal·mol^{-1}.[23] In view of the close similarity of hafnium and zirconium covalent radii, we may conclude from the longer Zr-N(2) distance in **9** (2.067 (3) Å) that the Zr-N(2) π bonding is even weaker for **9**.

Variable temperature ^{1}H NMR spectra for allyl complexes

It was discovered during the course of these syntheses that all of the η^3-allylic compounds (**5** - **8**) are fluxional and a mechanistic investigation was carried out on the parent η^3-allyl derivatives (**5**, **6**). A short synopsis of the conclusions reached in these studies is presented herein; more detailed analyses can be found elsewhere.[1b,24] Rate constants for allyl ligand fluxionality were obtained by line broadening techniques using dynamic ^{1}H NMR. All of the temperature dependent changes are reversible; cooling the samples after recording higher temperature spectra results in regeneration of the previously observed lower temperature spectra, although prolonged heating at temperatures above 60 °C does lead to decomposition. In addition, for the studies carried out in THF-d_8, higher temperatures lead to interchange of the racemic and meso diastereomers (*vide infra*). As the analysis of the obtained data is simpler for the meso

derivative, its behavior is discussed first. The assignment of the resonances discussed in the following section is shown in Figure 10.

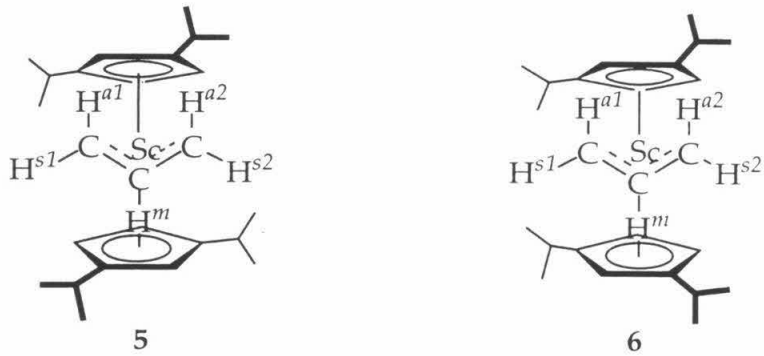

Figure 10. Assignment of the allyl resonances in the ^{1}H NMR of **5** and **6**.

At low temperatures, in toluene-d_8 solution, the meso compound **6** exhibits the expected AGMPX splitting pattern for the allyl ligand, resulting from the inequivalence of the two sides of the metallocene wedge. At the lowest temperature available (*ca.* 177 K) the molecule exhibits C_1-symmetry with four cyclopentadienyl resonances, four isopropyl methine resonances, and four broad and unresolved isopropyl methyl resonances. In addition, all five hydrogens of the allyl ligand are inequivalent. As the probe temperature is raised (244 K), the resonances for H^{a1} and H^{a2} broaden and coalesce, as do the resonances for H^{s1} and H^{s2} (which are obscured by solvent until higher temperatures). Continuing to raise the temperature results in the appearance of two new allyl resonances, one located approximately midway between the previous signals for H^{s1} and H^{s2}, and the other resonance midway between those of H^{a1} and H^{a2} (306 K), corresponding to an averaging of the two types of *syn* and two types of *anti* methylene protons of the allyl ligand. Accompanying these changes at higher temperatures are averaging of the protons of the two different cyclopentadienyl ligands and the isopropyl substituents. As the temperature of the sample is raised further, the averaged *syn* and averaged *anti* methylene protons in the AM_2X_2 spectra broaden, coalesce, and a new signal begins to grow in, located approximately equidistant from those of the previously averaged H^s and H^a resonances. A rate sufficient to produce an AX_4 pattern with a sharp singlet for all four allyl methylene hydrogens is not reached even at the highest temperature examined (~ 393 K). Shown in Figure 11 are the allyl and isopropyl

methine resonances of the variable temperature ^{1}H NMR spectra for **6** in toluene-d_8.

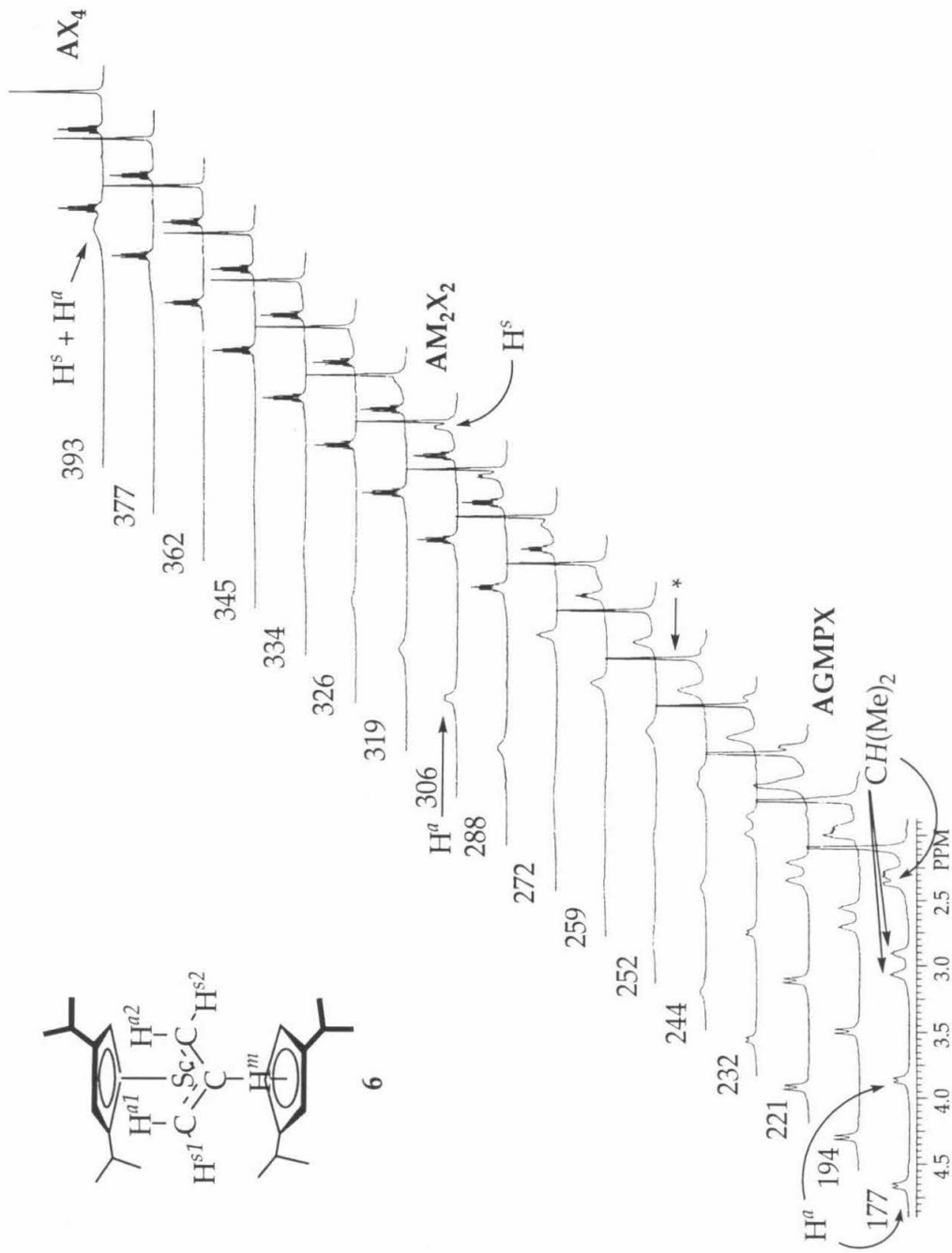

Figure 11. Allyl and isopropyl methine resonances of the variable-temperature 500 MHz ^{1}H NMR spectra for **6** (the * label indicates toluene-d_8 solvent).

The variable temperature behavior of the racemic complex **5** is distinct from that of the meso compound **6**. At low temperatures the complex exhibits C_1-symmetry with an AGMPX allyl splitting pattern and inequivalent cyclopentadienyl resonances, attributable to a static η^3-C_3H_5 structure. As the probe temperature is raised the isopropyl methine hydrogens become equivalent (252 K), and at higher temperatures there is simultaneous broadening of all four signals for the allyl methylene protons (301 K). These signals remain broadened into the baseline over a large temperature range, until at the highest temperatures a single resonance begins to appear at approximately the average of the signals for the four methylene protons. Thus, the AGMPX pattern is replaced by an AX_4, with no intermediate AM_2X_2 pattern, as was observed for **6**. Again, a sharp singlet is not observed for the allyl methylene protons even at the highest temperature available (404 K). Shown in Figure 12 are the allyl and isopropyl methine resonances of the variable temperature ^{1}H NMR spectra for **5** in toluene-d_8.

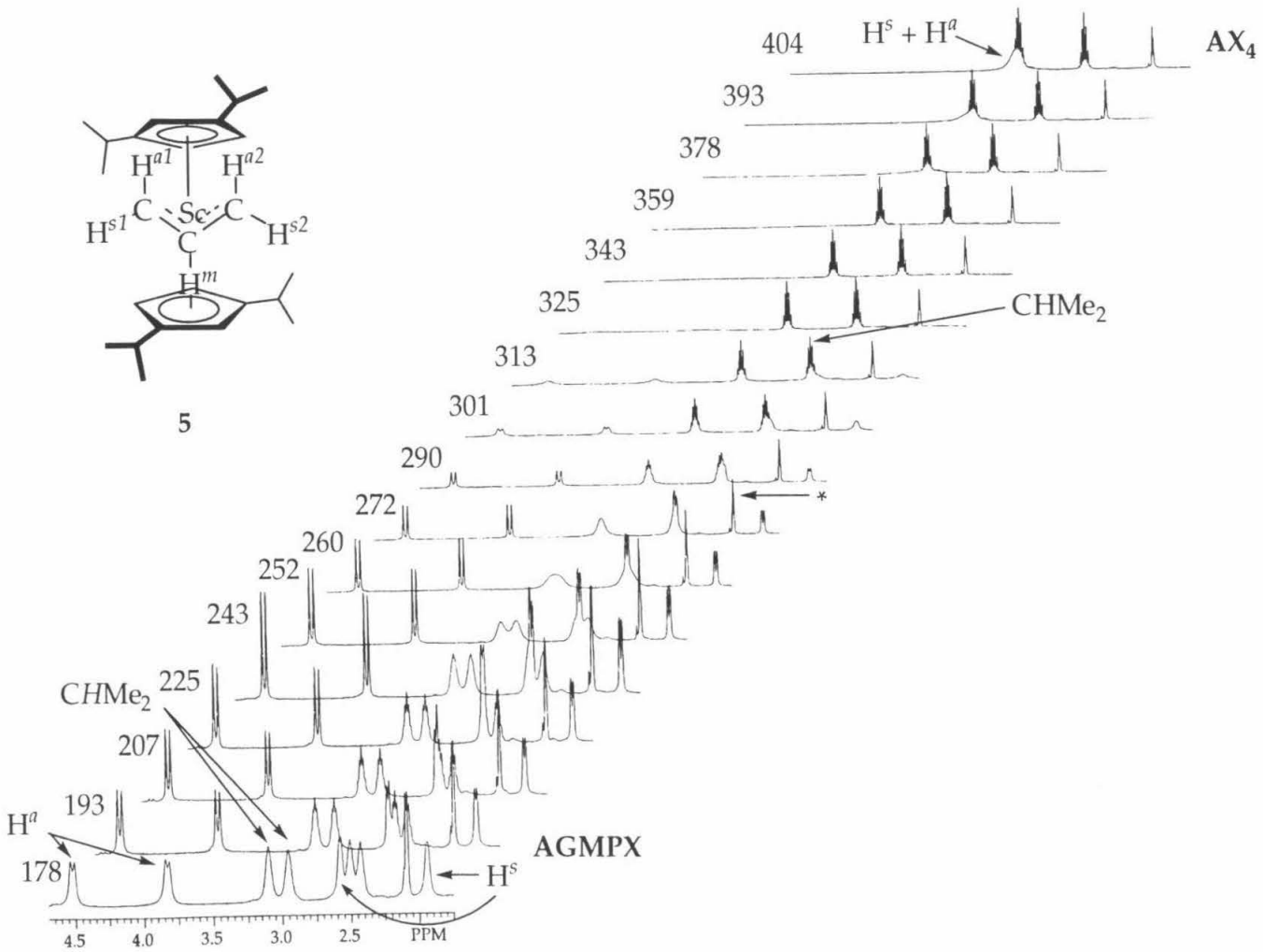

Figure 12. Allyl and isopropyl methine resonances of the variable-temperature 500 MHz ^{1}H NMR spectra for **5** (the * label indicates toluene-d_8 solvent).

The spectral simulation program gNMR was used to model the variable temperature behavior of both **5** and **6**. Two processes were found to occur: (a) a reversible change in hapticity for the allyl ligand followed by rotation around the allyl C-C single bond and (b) in-place η^3-rotation of the allyl group. These processes are shown graphically in Figure 13. For the meso complex **6** (and other meso allyl complexes),[1b,24] η^3-rotation was found to be occurring *ca.* 1 - 2 orders of magnitude faster than the η^3-η^1 process. For the racemic complex **5** (and other racemic allyl complexes)[1b,24] satisfactory fits to the observed data were observed upon simulating only an η^3-η^1 process. However, since the allyl hydrogens are broadened into the baseline over such a wide temperature range, these simulations are rather imprecise. The obtained data indicate that the upper limit of the strength of the metal-olefin interactions for complexes of this type is on the order of 11 - 16 kcal·mol^{-1}. The observed rate constants for allyl hydrogen exchange can be found in Table 5.

(a) Interconversion by $\eta^3 \rightarrow \eta^1$ / C- C 180° bond rotation / $\eta^1 \rightarrow \eta^3$:

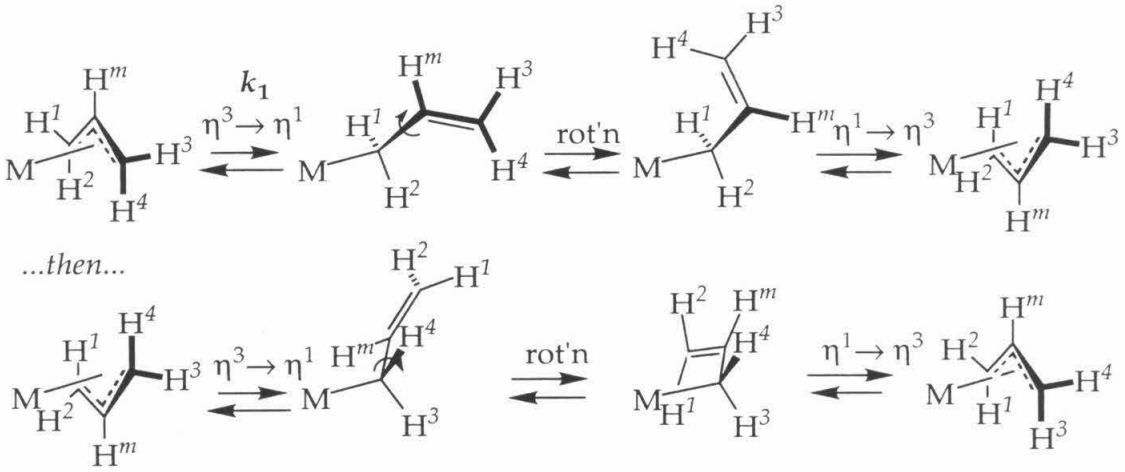

(b) Allyl 180° rotation while η^3-coordinated:

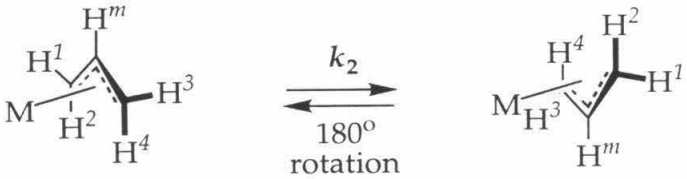

Figure 13. Illustration of processes proposed to account for the fluxional behavior of **5** and **6**.

Table 5. Summary of Rates and Activation Free Energies for η^3-η^1 Allyl Conversion (k_1, $\Delta G_1^{\ddagger}$) and for η^3-Allyl Rotation (k_2, $\Delta G_2^{\ddagger}$) for Allyl Complexes **5** and **6**[a]

Compd	Solvent	T (K)	k_1 (s^{-1})	k_2 (s^{-1})	$\Delta G_1^{\ddagger}$ (kcal·mol^{-1})	$\Delta G_2^{\ddagger}$ (kcal·mol^{-1})
5	toluene-d_8	359	8400		14.7	
5	THF-d_8	359	5200		14.6	
6	toluene-d_8	259		490		11.9
6	toluene-d_8	362	7600		14.9	

[a]Uncertainties in the free energies of activation are estimated to be approximately 1.0 kcal·mol^{-1}.

Racemic-Meso Interconversions for IpScCl and IpYCl Complexes

As described above, metallation by reaction of $Li_2Ip(THF)_{0.3}$ in THF solvent with either $ScCl_3(THF)_3$, or $YCl_3(THF)_{3.5}$ invariably yields a 3:1 ratio of the racemic and meso metallocene chlorides. Presumably due to the difference in preferred solid state structures (*vide supra*), separation of the group 3 compounds is possible in non-coordinating solvents.

When dissolved in THF, diastereomerically pure *rac*-IpScCl·LiCl(THF)$_2$ (**1**) or *rac*-IpYCl·LiCl(THF)$_2$ (**3**) each spontaneously revert back to the 3:1 racemic:meso ratios obtained on metallation. The mechanism operating here is assumed to be analogous to that proposed earlier, *i.e.*, LiCl assisted heterolysis of the M-Cp bond followed by Si-Cp$^-$Li$^+$ bond rotation and recoordination to the opposite face of the cyclopentadienyl ring.[3b,9] A stack plot showing the course of this isomerization starting from **1** in THF-d_8 solution is shown in Figure 14. The resonances for **3** including the characteristic inequivalent silyl methyl resonances of a meso metallocene grow in over time until the equilibrium concentration is reached.

Considering the proposed mechanism for the isomerization of chiral *ansa*-metallocenes, it is perhaps not surprising that the LiCl adducts **1** and **3** undergo spontaneous isomerization in THF-d_8. Not expected, however, was the facile interconversion that is also observed, upon dissolution in THF-d_8, of *meso*-[IpM(μ_2-Cl)]$_2$ derivatives **2** or **4**, with reversion back to a 3:1 racemic:meso ratio observed for each. These compounds have no obvious source of lithium ion to assist isomerization and to generate the lithium chloride adducts. Moreover, the

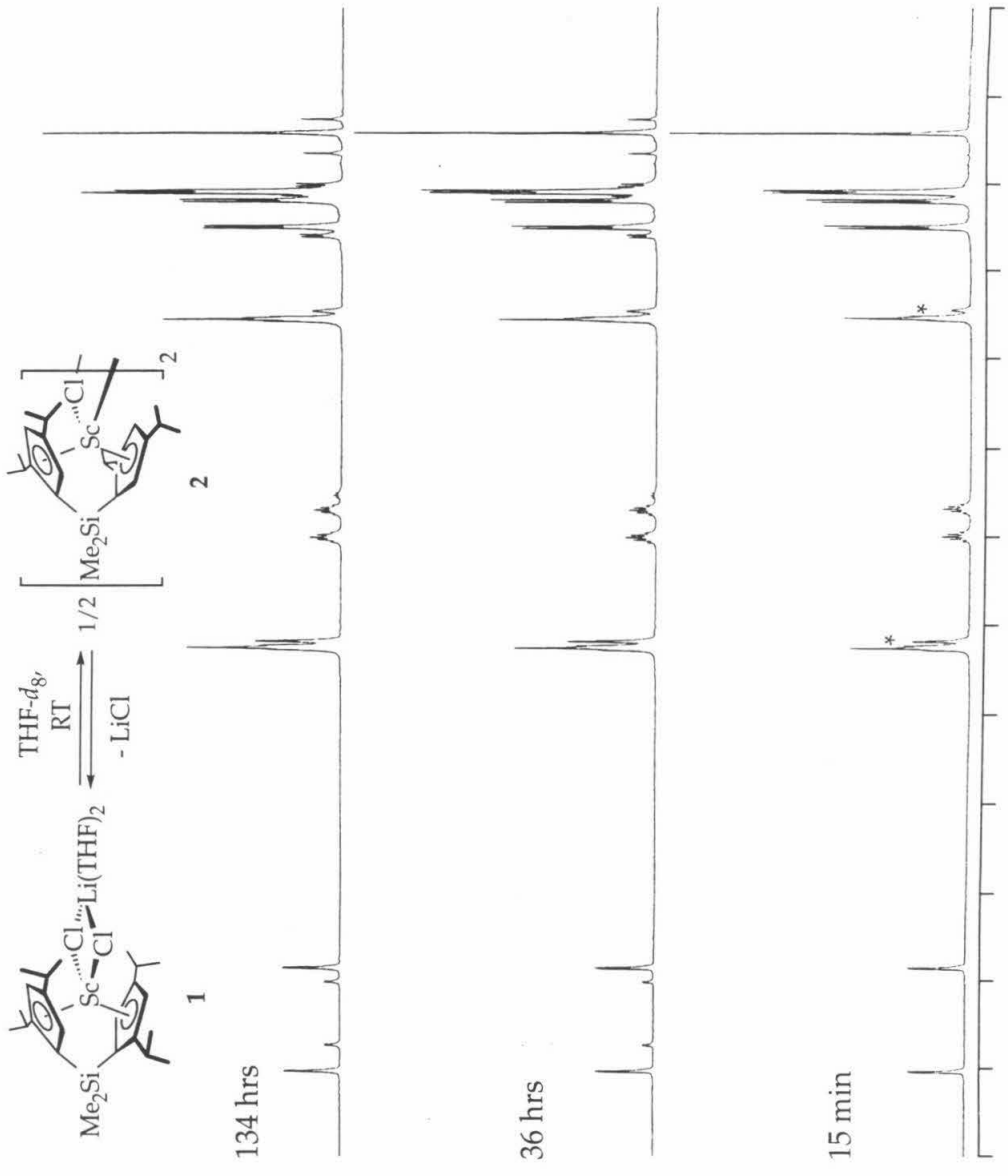

Figure 14. Stack plot of ^{1}H NMR spectra showing the progression of the reaction which interconverts **1** and **2** at room temperature (the * label indicates THF-d_8 solvent).

racemic-meso interconversion for these Ip derivatives does not occur in diethyl ether, unlike the system examined by Marks, *et al.*[3b,9] Further, the addition of 1-2 equivalents of 12-crown-4 to THF-d_8 solutions of **1**, **2**, or **4** does not slow the rate of interchange. Moreover, while addition of 35 equivalents of 12-crown-4 to a solution of **4** in THF-d_8 does slow the process, it does not prevent racemic-meso interchange. Consistent with previous observations, no isomerization is observed for **1**, **2**, or **4** in toluene-d_8 solution.

If the mechanism previously proposed is assumed to be operative for these Ip complexes, then it must be assumed that the meso compounds **2** and **4** are contaminated with LiCl and that the crystal structure obtained for **4** is not representative of the isolated bulk solid. Elemental analyses for chlorine, carbon and hydrogen in **4** are not mutually consistent, and thus do not rule out some lithium chloride contamination.

A THF solution of **2** was stirred for 8 days, and the resulting product mixture was examined by ^{1}H NMR spectroscopy. Heptane washings permitted **2** to be separated from the new product. The heptane-soluble component does indeed prove to be a racemic metallocene derivative, but its ^{1}H NMR spectrum is different from that of **1**, and coordinated THF is not evident. Significantly, when this new product was dissolved in THF, no isomerization to **2** was observed even after one week at ambient temperature. Addition of lithium chloride to the THF solution caused an immediate shift in the ^{1}H NMR signals to those of **1**, and isomerization to **2** was then rapid. We tentatively conclude that the heptane-soluble species is [*rac*-IpSc(μ_2-Cl)]$_2$, but all attempts to verify this assignment by independent synthesis have been unsuccessful. The heptane-insoluble species proved to be a (*ca.* 3:1) mixture of **1** and **2**. The results of these experiments indicate that, of the meso complexes, at least **2** is contaminated with LiCl. In THF solution the racemic and meso isomers are equilibrating, but the equilibrium process is complicated by the presence of dichloro-bridged dimers and lithium chloride adducts for both, the relative amounts of each depending upon the amount of lithium chloride present.

Racemic-Meso Isomerizations for IpSc(η^3-allyl) Complexes

While performing the variable temperature ^{1}H NMR experiments with allyl compounds **5** and **6**, it was discovered that these are also configurationally unstable, although the isomerization reactions are slower and occur only at higher temperatures. In THF-d_8 at 80 °C, both **5** and **6** isomerize to a 2:1 racemic:meso ratio as they decompose. Slower isomerization is observed at 55 °C, whereas no reaction is observed at room temperature after 7 weeks. Addition of 4 equivalents of 12-crown-4 to a sample of **6** in THF-d_8 with subsequent heating to 80 °C showed no change in the rate of racemic-meso interchange. In Et_2O-d_{10} no isomerization is observed at temperatures at or below 55 °C, and only decomposition is observed after heating to 110 °C in

toluene-d_8. A stack plot of ^{1}H NMR spectra showing the progress of the isomerization reaction starting from **5** at 80 °C is shown in Figure 15.

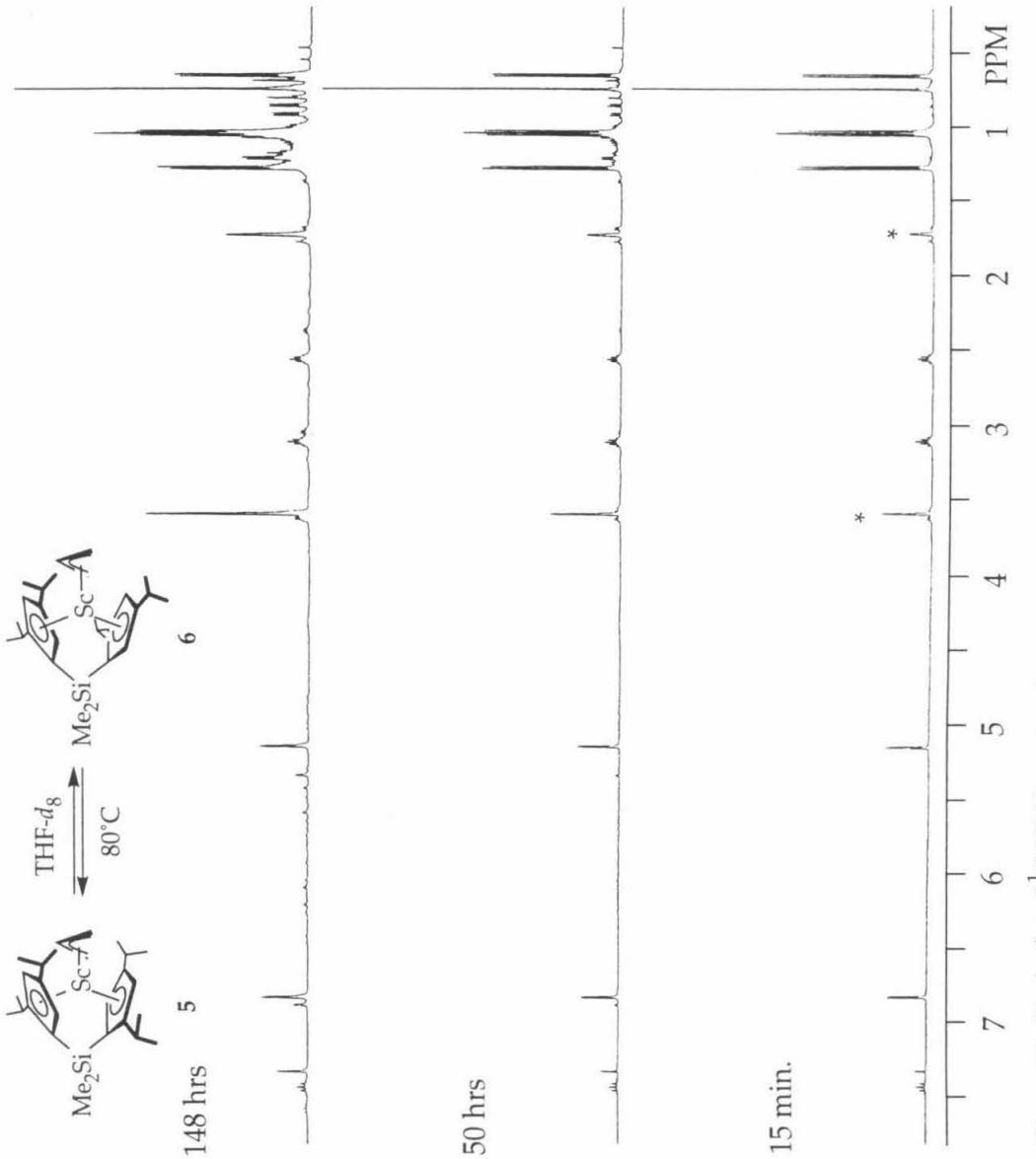

Figure 15. Stack plot of ^{1}H NMR spectra showing the progression of the reaction which interconverts **5** and **6** at 80 °C (the * label indicates THF-d_8 solvent).

The allyl derivatives **5** and **6** provide a system much better suited to mechanistic studies than the chloride compounds (*vide supra*), since lithium chloride is not added or lost during the interconversion. Moreover, since no

isomerization occurs for **5** or **6** at room temperature in any of the solvents examined, any promoting effects of added salts in various solvents could be systematically studied (Eqn 5).

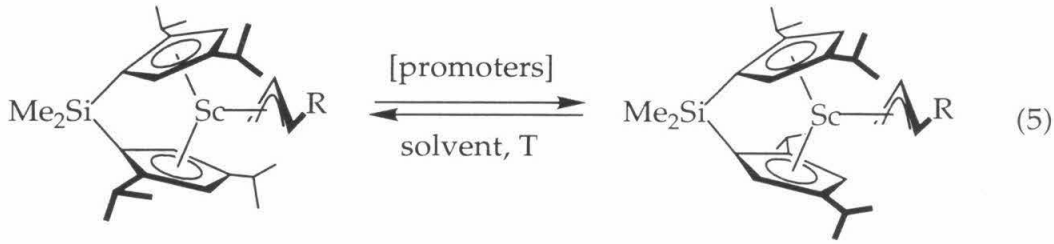

(5)

R = H (**5**)
R = Me (**7**)
racemo

R = H (**6**)
R = Me (**8**)
meso

In order to determine their effects on the rate of approach to equilibrium, various reagents were used as promoters to effect isomerization of **5** and **6**. The results of the equilibration experiments are summarized in Table 6.

Table 6. Results of Epimerization Experiments Carried out on Allyl Derivatives **5** - **8**[a]

Compd	Solvent	Additive	Final *rac*:*meso* Ratio	Reaction Time
5 or **6**[b]	THF-d_8	—	2:1[c]	10 days
6[d]	THF-d_8	—	(1:6)[c, e]	7 days
5 or **6**[d]	Et_2O-d_{10}	—	no reaction	5 months
5[f]	toluene-d_8	—	dec.	7 days
7 or **8**[g]	toluene-d_8	—	2:1[c]	1 day
6	THF-d_8	16 mol% allylMgBr	1.5:1	~ 3 weeks
5 or **6**	THF-d_8	10 mol% $allyl_2Mg$	1.7:1	~6 weeks
7	THF-d_8	50 mol% $allyl_2Br$	2:1 allyls and 1.3:1 crotyls	7 days
7	Et_2O-d_{10}	$allyl_2Mg$[h]	no reaction	5 weeks
5 or **6**	THF-d_8	2 equiv. LiCl	2:1	1 day
7	THF-d_8	2 equiv. LiCl	2.8:1	3 days
5 or **6**	THF-d_8	KCl[h]	2:1	10 days
5	toluene-d_8	30 mol% (n-$C_7H_{15})_4NCl$	2:1	6 h

Table 6. (Cont.)

5	*c*-C_6D_{12}	35 mol% (*n*-$C_7H_{15})_4NCl$	2:1	3 days
5	THF-d_8	35 mol% (*n*-$C_7H_{15})_4NCl$	1.5:1	7 days
5	Et_2O-d_{10}	60 mol% (*n*-$C_7H_{15})_4NCl$	(1.6:1)[i]	1 day
5	toluene-d_8	27 mol% (*n*-$C_7H_{15})_4NBr$	2:1[c]	1 day
5	*c*-C_6D_{12}	24 mol% (*n*-$C_7H_{15})_4NBr$	2:1[c]	2 days
5	THF-d_8	1.1 equiv. $LiB(C_6F_5)_4$	2:1	1 day
5	THF-d_8	20 mol% $LiB(C_6F_5)_4$	1.9:1	~ 6 weeks
5	THF-d_8	1.5 equiv. $NaB(C_6H_3(CF_3)_2)_4$	2.5:1	1 day
5	THF-d_8	20 mol% $NaB(C_6H_3(CF_3)_2)_4$	2:1	~ 6 weeks
5	Et_2O-d_{10}	$LiB(C_6F_5)_4$[h]	(8:1)[e]	2 weeks
5	Et_2O-d_{10}	25 mol% $NaB(C_6H_3(CF_3)_2)_4$	no reaction	7 days
5	THF-d_8	1.3 equiv. (*n*-$C_7H_{15})_4NB(C_6H_3(CF_3)_2)_4$	2:1	~ 4 weeks
5	Et_2O-d_{10}	1.1 equiv. (*n*-$C_7H_{15})_4NB(C_6H_3(CF_3)_2)_4$	no reaction	3 weeks
5	toluene-d_8	(*n*-$C_7H_{15})_4NB(C_6H_3(CF_3)_2)_4$[h]	dec.	2 weeks

[a]Reactions were carried out at 22 °C unless otherwise specified; [b]80 °C; [c]reaction was accompanied by partial decomposition; [d]55 °C; [e]reaction was stopped before equilibrium was established; [f]110 °C; [g]120 °C; [h]additive is only partially soluble; [i]additive reacts with allyl species to make an unidentified compound which is the major component of the reaction mixture.

When *rac*-IpSc(η^3-C_3H_5) (**5**) was dissolved together with an excess of *LiCl* in THF-d_8, a variety of species was observed, none of which corresponded to **5** or **6** (^{1}H NMR). Replacing THF-d_8 with toluene-d_8 after 14 hours resulted in precipitation of LiCl, and from the ^{1}H NMR spectrum of the soluble complexes it was then evident that epimerization to a 2:1 ratio of **5** and **6** had taken place with little or no decomposition. Although addition of solid potassium chloride to either **5** or **6** in THF-d_8 results in no detectable dissolution, ^{1}H NMR spectra reveal that isomerization takes place over a period of 3 to 4 weeks yielding the same ~2:1 ratio of **5** and **6**.

Grignard reagents also promote racemic-meso isomerization. Thus, addition of 16 mol% allylmagnesium bromide to a THF-d_8 solution of **6** afforded isomerization to a racemic:meso ratio of 1.5:1 after 2 weeks. Also, addition of 10 mol% diallylmagnesium to individual THF-d_8 solutions of **5** and **6** yielded the

same result, a 1.7:1 racemic:meso ratio after 4 weeks. A qualitative test (silver ion) for the presence of halide was negative on a sample of $(C_3H_5)_2Mg$, indicating that halide is not required for isomerization of **5** and **6**.

A ^1H NMR spectrum taken immediately after mixing diallylmagnesium and a THF-d_8 solution of the crotyl compound *rac*-IpSc(η^3-C_3H_4Me) (**7**) revealed the presence of both racemic allyl complex **5** and racemic crotyl complex **7**, suggesting fast and reversible formation of *bis*(allyl) scandate intermediates. After a period of approximately 3 hours, both meso compounds **6** and **8** were also observed.

The effects of other added salts to solutions of the allyl complexes in less polar solvents were also examined (Table 6). Addition of 30 mol% (*n*-heptyl)$_4$NCl to a toluene-d_8 solution of **5** results in immediate initiation of isomerization to the meso isomer. After about 6 hours a 2:1 equilibrium mixture of **5** and **6** is observed. Following the same procedure, but in the absence of light, resulted in isomerization at qualitatively the same rate. Addition of 35 mol% (*n*-heptyl)$_4$NCl to **5** in cyclohexane-d_{12} also initiates isomerization, but at a slower rate; equilibrium is established after ~3 days. Tetraheptylammonium bromide also promotes racemic-meso isomerizations at about the same rates. These isomerizations promoted by tetraheptylammonium halide salts in hydrocarbon solvents are qualitatively faster than those promoted by allyl magnesium salts in tetrahydrofuran, indicating that halides are more effective in promoting Sc-Cp heterolysis.

When (*n*-heptyl)$_4$NCl is added to THF-d_8 or Et_2O-d_{10} solutions of **5**, the ^1H NMR signals for **5** broaden somewhat and/or new signals are present suggestive of a dynamic equilibrium with a chloroscandate complex. When **5** is titrated with LiCl at –56 °C in THF-d_8, clean conversion to a LiCl adduct with an η^1-C_3H_5 splitting pattern was observed. Formation of the LiCl adduct is complete upon addition of 1 equivalent of LiCl, and no further changes are observed in the ^1H NMR spectrum after addition of a second equivalent. Raising the temperature to 25 °C results in the same complex spectrum observed previously. Addition of an excess of LiBr to either **1**, **2**, or **4** results in isomerization, qualitatively at the same rate as when no promoter is added, but compounds other than the respective racemic and meso chloride complexes do not build up in detectable levels.

Addition of salts having a small cation and large, weakly coordinating counter-anion were also tested as possible promoters. Addition of $LiB(C_6F_5)_4$ to

a solution of **5** in THF-d_8 resulted in isomerization to the same 2:1 ratio of **5** and **6**. The analogous isomerization reaction carried out in Et_2O-d_{10} was very slow, either due to the lower basicity of Et_2O as compared to THF or to the lower solubility of $LiB(C_6F_5)_4$ in diethyl ether. The related sodium salt $NaB\{3,5\text{-}C_6H_3(CF_3)_2\}_4$ promotes isomerization in THF-d_8 at approximately the same rate as that for $LiB(C_6F_5)_4$. On the other hand, addition of 25 mol% $NaB\{3,5\text{-}C_6H_3(CF_3)_2\}_4$ to solutions of **5** in Et_2O-d_{10} (in which the salt is completely soluble) fails to promote isomerization to **6**, even after a week at room temperature.

Since salts containing either a large cation with halide or a small cation with a large, weakly coordinating anion promoted racemic-meso isomerization, a salt having a large cation with weakly coordinating anion was also tested. The addition of $(n\text{-heptyl})_4NB(C_6H_3(CF_3)_2)_4$ to samples of **5** was carried out in THF-d_8, Et_2O-d_{10}, and toluene-d_8 (Table 6). Although no reaction was observed in either toluene-d_8 (in which the salt is insoluble) or Et_2O-d_{10}, slow isomerization *was observed* in THF-d_8.

These results suggest that in tetrahydrofuran merely increasing the ionic strength of the solution is adequate to induce interconversion of racemic and meso isomers. In less polar solvents such as diethyl ether, toluene or cyclohexane, it appears that the assistance of a coordinating anion or a small cation is a further requirement for promotion of isomerization. Based on these considerations, we propose the general mechanism for racemic:meso interchange shown in Scheme 4.

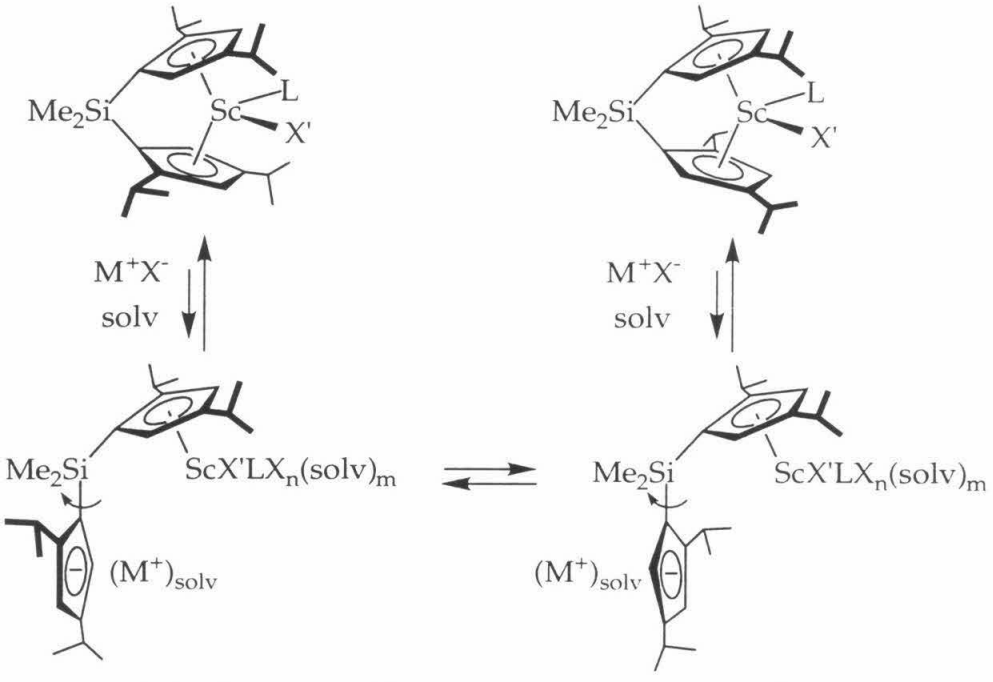

Scheme 4. Mechanism proposed for racemic-meso isomerization of *ansa*-metallocenes.

Studies of the Kinetics of Metallation and Attempts to Determine the Generality of *ansa*-Metallocene Ligand Isomerization

Following the metallation reactions of $IpLi_2(THF)_{0.3}$ with both $ScCl_3(THF)_3$ and $YCl_3(THF)_{3.5}$ by ^1H NMR revealed that the meso isomers initially are formed in greater than the thermodynamic concentrations. Thus, after 15 minutes at 71 °C in THF-d_8, a 1.7:1 racemic:meso ratio of **1** to **2** is observed. Racemic isomer **1** grows to approach the thermodynamic 3:1 racemic:meso ratio within 1 hour. Similarly, after 15 minutes at room temperature, $IpLi_2$ metallates to a 1.5:1 racemic:meso ratio of yttrocenes, which converts to the 3:1 thermodynamic ratio immediately upon heating to 71 °C.

The kinetics of metallation of another *ansa*-metallocene were also examined. The ligand $[Me_2Si(\eta^5\text{-}3\text{-}CMe_3\text{-}C_5H_3)_2]Li_2$ ($DpLi_2$) has been shown to coordinate yttrium in THF to yield a 1:1 racemic:meso mixture (Eqn 6).[25] Upon mixing $DpLi_2$ and $YCl_3(THF)_{3.5}$ in THF-d_8 at room temperature, a 1:1 racemic:meso ratio had already been established. When the reaction was carried out under more controlled conditions, however, a kinetic product mixture was observed. Dissolution of the reagents in THF-d_8 at -78 °C, followed by insertion

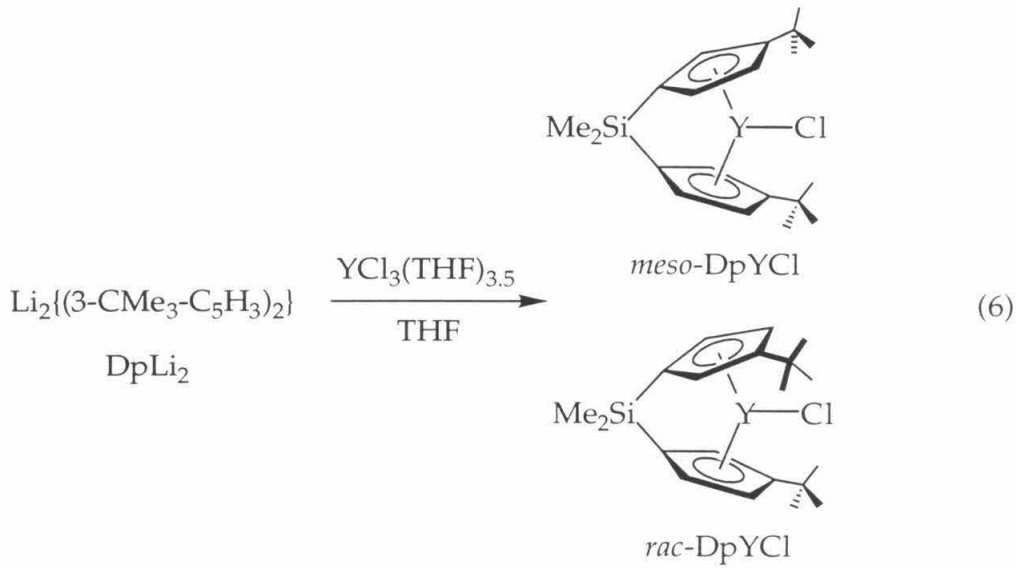

(6)

of the NMR tube into the probe which had been precooled to 227 K, resulted in the observation of a 2:1 racemic:meso mixture of yttrocenes. After warming to room temperature, the ratio initially remained unchanged, but after 20 hours converted to the 1:1 thermodynamic mixture. Separation of these yttrocenes into diastereomerically pure *rac*- and *meso*-DpYCl has not been accomplished.[26]

Other *ansa*-metallocene complexes were examined briefly to establish whether racemic-meso interconversions could be promoted. Addition of LiCl to THF-d_8 solutions of pure *meso*-DpScCl did not promote formation of detectable amounts of the racemic isomer. Since the meso isomer is formed exclusively on metallation of $ScCl_3(THF)_3$ with LiDp in toluene solution, it is not clear whether the racemic isomer is thermodynamically or kinetically inaccessible, however. Similarly, both $\{(C_5H_2\text{-}2\text{-}SiMe_3\text{-}4\text{-}CMe_3)_2SiMe_2\}Li_2$ ($BpLi_2$)[3a] and *rac*-$\{(C_5H_2\text{-}2\text{-}CMe_3\text{-}4\text{-}SiMe_3)SiO_2C_{20}H_{12}\}K_2$ (*rac*-$BnBpK_2$)[27] metallate exclusively to the racemic isomer, and perhaps not surprising is the failure of LiCl in THF-d_8 to promote formation of any new isomers.

Using amine elimination followed by treatment with $SiMe_3Cl$, as described by Jordan and coworkers,[11d] a 1:5 racemic:meso mixture of $DpZrCl_2$ isomers may be obtained. A different ratio (racemic:meso = 1.3:1) is obtained by reaction of $DpLi_2$ with $ZrCl_4(THF)_2$ in THF-d_8. Addition of LiCl to either of these mixtures of $DpZrCl_2$ isomers in THF-d_8 does not result in racemic:meso interconversion at room temperature or at 80 °C. Thus, it appears that racemic-meso isomerization for $DpZrCl_2$ is unfavorable in THF-d_8.

Addition of LiCl to diastereomerically pure *rac*-(EBI)$ZrCl_2$ in THF-d_8 does result in isomerization to a 1:1 racemic:meso mixture after 6 days, the same ratio of products obtained when (EBI)Li_2 and $ZrCl_4$ are allowed to react for 10 days at room temperature in THF-d_8. There is no doubt in this case, therefore, that thermodynamic control is operating.

Thus, it appears that for group 4 *ansa*-metallocenes, racemic-meso interchange does not occur in some cases. In general, the 16-electron group 4 metallocenes are expected to be less disposed to coordinate salts or donor solvents as compared with their 14-electron group 3 analogs. Also, being less electropositive than the group 3 metals, cyclopentadienyl bonds to group 4 metals are less ionic and thus less readily heterolyzed. These two factors stabilize the M-Cp bonds and discourage isomerization for group 4 metallocenes.

Conclusions

Evidence for the stereochemical isomerization of a variety of *ansa* metallocene compounds has been observed. Racemic-meso interchange has been established now for scandium and yttrium complexes with the Ip ligand system, for DpYCl, $DpZrMe_2$ and (EBI)$ZrCl_2$. Moreover, isomerizations have been reported by several groups for lanthanide derivatives.[3b,9,10] In addition Brintzinger, Kaminsky, and Bosnich have found that racemic:meso interchange may be promoted photochemically.[7,12] For the allyl derivatives described here, we have established that the process is promoted by a variety of salts in both ether and hydrocarbon solvents and is not accelerated by light.

A plausible mechanism based on an earlier proposal by Marks, *et al.*,[3b] is offered as an explanation of this process (Scheme 4). It involves coordination of anions and/or donor solvents to the metal center with cation assistance to encourage metal-cyclopentadienyl bond heterolysis, rotation about the Si-Cp bond of the detached cyclopentadienide and recoordination of the opposite face. The facility of the process in toluene and even cyclohexane solution indicates that a donor solvent is not required. The highly ionic nature of the M-Cp bonds in group 3 metallocenes permits metal-cyclopentadienyl bond heterolysis merely by raising the ionic strength of a THF-d_8 solution of **5** or **6** with (n-$C_7H_{15})_4NB(C_6H_3(CF_3)_2)_4$. Both coordinating anions or small cations also appear to promote racemic-meso interchange. Our observations in some cases of

thermodynamic racemic:meso ratios under the reaction conditions commonly used for the synthesis of the metallocene chlorides suggests that the interchange is faster than metallation, such that the composition of the reaction mixture is determined by thermodynamic, not kinetic control in these cases.

Experimental Section

All air and/or moisture sensitive compounds were manipulated using standard high-vacuum line, Schlenk, or cannula techniques, or in a glove box under a nitrogen atmosphere, as described previously.[28] Argon gas was purified and dried by passage through columns of MnO on vermiculite and activated 4 Å molecular sieves. All solvents were stored under vacuum over titanocene[29] or sodium benzophenone ketyl. The preparations of crotylMgCl,[30] $ScCl_3(THF)_3$,[31] and 1,3-$(CHMe_2)_2C_5H_3Li$[32] were carried out as previously reported. The preparation of $YCl_3(YHF)_{3.5}$ was carried out as reported for the scandium derivative.[31] *Rac*-(EBI)$ZrCl_2$ was prepared by the amine elimination route as reported by Jordan[11a] with subsequent substitution with TMSCl.[11b] *Rac*-$[BpYCl]_2$,[3a] *meso*-$[DpScCl]_2$,[25] $LiB(C_6F_5)_4$,[33] $NaB(C_6H_3(CF_3)_2)_4$,[34] $TlB(C_6H_3(CF_3)_2)_4$,[35] (EBI)Li_2,[6] and (*R*,*S*)-$BnBpK_2$[27] were prepared according to previous procedures. *n*-Butyllithium and allylmagnesium bromide were purchased (Aldrich) and used as received. Lithium chloride, potassium chloride, and lithium bromide were purchased from Aldrich and dried *in vacuo* at ≥ 150 °C for ≥ 36 hours. (*n*-Heptyl)$_4$NCl was purchased from Aldrich and was dried *in vacuo* at 120 °C for 6 hours. (*n*-Heptyl)$_4$NBr was purchased from Fluka and dried *in vacuo* at room temperature for 3 hours.

NMR spectra were recorded on General Electric QE300 (300 MHz for ^1H) and Bruker AM500 (500.13 MHz for ^1H) spectrometers. Elemental analyses were carried out at the Caltech Elemental Analysis Facility by Fenton Harvey. Many of the compounds failed to give satisfactory carbon/hydrogen analyses, even when combusted with added V_2O_5 oxidant. Moreover, in many cases the results were inconsistent from run to run.

Preparation of $Me_2Si[C_5H_3$-2,4-$(CHMe_2)_2]_2$ (IpH_2). In an inert atmosphere dry box, $(CHMe_2)_2C_5H_3Li$ (19.1 g, 0.12 mol) was transferred to a 200 mL Kjeldahl flask, which was then attached to a swivel frit assembly. THF (175 mL) was transferred into the flask via cannula. The resulting yellow solution was evacuated at -78 °C, and dichlorodimethylsilane (7.4 mL, 0.061 mol) was added

by vacuum transfer. The solution was allowed to warm from -78 °C to room temperature over the period of one hour and was stirred overnight at room temperature. The THF was then removed *in vacuo* and petroleum ether (100 mL) was added by vacuum transfer. The resulting yellow slurry was stirred for 2 hours and filtered, resulting in a yellow supernatant and slightly yellow precipitate. The precipitate was washed twice with fresh petroleum ether, and the combined supernatants were evaporated to leave a yellow oil. The product was Kugelröhr distilled at 100 °C under dynamic vacuum, affording 20.0 grams of a light yellow oil (92% yield). ^{1}H NMR (THF-d_8) δ 6.27, 6.10, 6.03, 5.94, 5.87, 5.74 (C_5H_3, s, 2H total), 2.80 (C_5H_3, d, 1.3H), 2.64, 2.54, 2.40 ($CH(CH_3)_2$, m, 2H total), 1.12, 1.11 ($CH(CH_3)_2$, d, 12H total), 0.08, 0.55, 0.49, 0.45, 0.37 ($Si(CH_3)_2$, s, 3H total).

Preparation of $Me_2Si[C_5H_2$-2,4-$(CHMe_2)_2]_2Li_2(THF)_{0.3}$ ($IpLi_2\cdot(THF)_{0.3}$). The Kügelrohr distillate of IpH_2 (20.0 g, 0.056 mol) was weighed into a 200 mL Kjeldahl flask and attached to a swivel frit assembly. The assembly was degassed, and petroleum ether (175 mL) was added via cannula. A 1.6 M solution of *n*-butyllithium (80 mL, 0.13 mol,) was added via syringe at 0 °C affording a light orange solution. After stirring overnight at room temperature the petroleum ether was removed in vacuo to give a viscous orange gel. THF (75 mL) was added by vacuum transfer, and the solution was stirred for 30 minutes. The THF was then removed, yielding an off-white solid. Petroleum ether (150 mL) was added by vacuum transfer and the resulting light orange slurry was stirred for 2 hours. Filtration yielded a white precipitate which was washed twice with fresh petroleum ether and dried *in vacuo* to afford a white solid, $IpLi_2(THF)_{0.3}$ (19.6 g, 89% yield). ^{1}H NMR (THF-d_8) δ 5.67 (s, 1H, C_5H_2), 5.62 (s, 1H, C_5H_2), 3.11 (sep (br), 1H, $CH(CH_3)_2$), 2.79 (sep, 1H, $CH(CH_3)_2$, J = 7 Hz), 1.14 (d, 12H, $CH(CH_3)_2$, J = 7 Hz), 0.35 (s, 3H, $Si(CH_3)_2$).

Preparation of *rac*-$IpScCl\cdot LiCl(THF)_2$ (1) and *meso*-$[IpSc(\mu\text{-}Cl)]_2$ (2). $IpLi_2(THF)_{0.3}$ (4.00 g, 10.2 mmol) and $ScCl_3(THF)_3$ (3.8 g, 10.3 mmol) were weighed into a 200 mL Kjeldahl flask equipped with a stir bar in an inert atmosphere glove box. THF (175 mL) was added, and a reflux condenser and argon inlet adapter were attached to the flask. The resulting slurry was stirred at room temperature until all the ligand had dissolved. The solution was then heated to reflux, resulting in a slightly cloudy, golden-colored solution; after refluxing for three days, the reaction flask containing the clear, light yellow solution was attached to a swivel frit assembly. The THF was evacuated from

the frit assembly and petroleum ether (100 mL) was added by vacuum transfer. The resulting bright yellow slurry was stirred for 1 hour and then filtered, separating the yellow supernatant from a white precipitate. Immediately after filtration, a slightly green microcrystalline solid, subsequently identified as [*meso*-IpSc(μ-Cl)]$_2$, precipitated from the filtrate. This solid was isolated by repeated crystallization/filtration cycles from heptane. Once separated completely from the *meso* compound, hydrocarbon-soluble *racemo*-IpScCl·LiCl(THF)$_2$ was recrystallized by cooling a pentane solution to -40 °C. Yield was 3.31 g (55%) for **1** and 0.96 g (22%) for **2**.

rac-IpScCl·LiCl(THF)$_2$: Anal. Calcd. for $C_{32}H_{54}Cl_2LiO_2ScSi$: C, 61.91%, H, 8.77%. Found: C, 62.18, 61.51%, H, 8.68, 7.19%. ^{1}H NMR (THF-d_8) δ 6.02 (d, C_5H_2, 1H, J = 2 Hz), 5.44 (d, C_5H_2, 1H, J = 2 Hz), 3.01 (sep, $CH(CH_3)_2$, 1H, J = 7 Hz), 2.84 (sep, $CH(CH_3)_2$, 1H, J = 7 Hz), 1.25 (d, $CH(CH_3)_2$, 3H, J = 7 Hz), 1.10 (d, $CH(CH_3)_2$, 3H, J = 7 Hz), 1.05 (d, $CH(CH_3)_2$, 6H, J = 7 Hz), (s, $Si(CH_3)_2$, 3H).

[*meso*-IpSc(μ-Cl)]$_2$: Anal. Calcd. for $C_{24}H_{38}ClScSi$: C, 66.26%, H, 8.80%. Found: C, 72.09, 71.58%, H, 10.09, 9.80%. ^{1}H NMR (THF-d_8) δ 5.87 (s, C_5H_2, 2H), 5.50 (s, C_5H_2, 2H), 3.01 (sep, $CH(CH_3)_2$, 2H, J = 7 Hz), 2.77 (sep, $CH(CH_3)_2$, 2H, J = 7 Hz), 1.30 (d, $CH(CH_3)_2$, 6H, J = 7 Hz), 1.07 (d, $CH(CH_3)_2$, 6H, J = 7 Hz), 1.04 (d, $CH(CH_3)_2$, 6H, J = 7 Hz), 1.01 (d, $CH(CH_3)_2$, 6H, J = 7 Hz), 0.83 (s, $Si(CH_3)_2$, 3H), 0.63 (s, $Si(CH_3)_2$, 3H).

Preparation of *rac*-IpYCl·LiCl(THF)$_2$ (3) and [*meso*-IpY(μ$_2$-Cl)]$_2$ (4). An analogous procedure to that of the scandium compounds (**1** and **2**) was followed using IpLi$_2$(THF)$_{0.3}$ (2.02 g, 5.15 mmol) and YCl$_3$(THF)$_{3.5}$ (2.05 g, 4.58 mmol). All aspects of the separation procedure are also identical for the yttrium congeners. Yield was 1.74 g (58%) for **3** and 0.51 g (23%) for **4**.

rac-IpYCl·LiCl(THF)$_2$: Anal. Calcd. for $C_{32}H_{54}Cl_2LiO_2SiY$: C, 57.81%, H, 8.19%. Found: C, 56.86, 56.83%, H, 8.29, 7.96%. ^{1}H NMR (C_6D_6/THF-d_8) δ 6.57 (s, C_5H_2, 1H), 5.77 (s, C_5H_2, 1H), 3.62, 3.47 (sep, $CH(CH_3)_2$, 1H, J = 7 Hz), 2.94 (sep, $CH(CH_3)_2$, 1H, J = 7 Hz), 1.77, 1.39 (d, $CH(CH_3)_2$, 3H, J = 7 Hz), 1.33 (d, $CH(CH_3)_2$, 3H, J = 7 Hz), 1.25 (d, $CH(CH_3)_2$, 3H, J = 7 Hz), 1.20 (d, $CH(CH_3)_2$, 3H, J = 7 Hz), 0.81 (s, $Si(CH_3)_2$, 3H).

[*meso*-IpY(μ-Cl)]$_2$: Anal. Calcd. for $C_{24}H_{38}ClSiY$: C, 60.18%, H, 8.00%. Found: C, 43.17, 42.85%, H, 6.21, 6.17%. ^{1}H NMR (THF-d_8) δ 5.95 (d, C_5H_2, 2H, J = 2 Hz), 5.39 (d, C_5H_2, 2H, J = 2 Hz), 3.09 (sep, $CH(CH_3)_2$, 2H, J = 7 Hz), 2.99 (sep, $CH(CH_3)_2$, 2H, J=7 Hz), 1.33 (d, $CH(CH_3)_2$, 6H, J=7 Hz), 1.11 (d, $CH(CH_3)_2$, 6H,

J=7 Hz), 1.05 (d, $CH(CH_3)_2$, 6H, J=7 Hz), 1.04 (d, $CH(CH_3)_2$, 6H, J=7 Hz), 0.76 (s, $Si(CH_3)_2$, 3H), 0.52 (s, $Si(CH_3)_2$, 3H).

Preparation of *rac*-IpSc(η^3-C_3H_5) (5). In an inert atmosphere glove box **1** (0.45 g, 0.76 mmol) was weighed into a 50 mL Kjeldahl flask which was subsequently attached to a swivel frit assembly. Toluene (25 mL) was added by vacuum transfer and the contents of the flask were stirred at -78 °C. A 1.0 M solution (Et_2O) of allylmagnesium bromide (1.0 mL, 1.0 mmol) was syringed against a strong argon counterflow into the stirred solution at -78 °C. The solution was allowed to warm slowly to room temperature over a period of 10 hours, providing an orange solution. Toluene was removed *in vacuo* and the resulting solid was washed once with petroleum ether (10 mL) in order to remove residual diethyl ether. Petroleum ether (15 mL) was then added by vacuum transfer and the orange slurry was stirred for 1 hour at room temperature; subsequent filtration separated an off-white precipitate from the orange supernatant. The petroleum ether was then evacuated, leaving 0.24 grams of an orange powder (0.54 mmol, 72% yield). Anal. Calcd. for $C_{27}H_{43}ScSi$: C, 73.59%, H, 9.84%. Found: C, 72.92%, H, 10.09%.

^{1}H NMR (toluene-d_8, 193 K) δ 7.42 (m (br), CH_2CHCH_2, 1H), 6.59 (s, C_5H_2, 1H), 6.42 (s, C_5H_2, 1H), 5.23 (s, C_5H_2, 1H), 5.16 (s, C_5H_2, 1H), 4.52 (d, *anti*-CH_2CHCH_2, 1H, J = 15 Hz), 3.81 (d, *anti*-CH_2CHCH_2, 1H, J = 15 Hz), 3.10 (sep, $CH(CH_3)_2$, 1H, J = 7 Hz), 2.96 (sep, $CH(CH_3)_2$, 1H, J = 7 Hz), 2.57 (d, *syn*-CH_2CHCH_2, 1H, J = 8 Hz), 2.52 (sep, $CH(CH_3)_2$, 1H, J = 7 Hz), 2.43 (sep, $CH(CH_3)_2$, 1H, J = 7 Hz), 1.93 (d, *syn*-CH_2CHCH_2, 1H, J = 8 Hz), 1.32 (s (br), $CH(CH_3)_2$, 6H), 1.16 (m (br), $CH(CH_3)_2$, 6H), 0.95 (m (br), $CH(CH_3)_2$, 6H), 0.75 (s (br), $Si(CH_3)_2$, 6H), 0.61 (s (br), $CH(CH_3)_2$, 6H).

^{1}H NMR (toluene-d_8, 295 K) δ 7.43 (m, CH_2CHCH_2, 1H), 6.67 (d, C_5H_2, 2H, J = 2 Hz), 5.17 (d, C_5H_2, 2H, J = 2 Hz), 4.46 (d (br), *anti*-CH_2CHCH_2, 1H, coupling unresolved), 3.58 (d (br), *anti*-CH_2CHCH_2, 1H, coupling unresolved), 3.04 (sep, $CH(CH_3)_2$, 2H, J = 7 Hz), 2.54 (sep, $CH(CH_3)_2$, 2H, J = 7 Hz), 2.5 (s (br), *syn*-CH_2CHCH_2, 1H), 1.9 (s (br), *syn*-CH_2CHCH_2, 1H), 1.29 (d, $CH(CH_3)_2$, 6H, J = 7 Hz), 1.11 (d, $CH(CH_3)_2$, 6H, J = 7 Hz), 1.05 (d, $CH(CH_3)_2$, 6H, J = 7 Hz), 0.72 (s, $Si(CH_3)_2$, 6H), 0.64 (d, $CH(CH_3)_2$, 6H, J = 7 Hz).

^{1}H NMR (toluene-d_8, 404 K) δ 7.41 (quin, CH_2CHCH_2, 1H, J = 12 Hz), 6.70 (d, C_5H_2, 2H, J = 2 Hz), 5.18 (d, C_5H_2, 2H, J = 2 Hz), ~ 3.1 (s (br) CH_2CHCH_2, 4H (obscured)) 3.04 (sep, $CH(CH_3)_2$, 2H, J = 7 Hz), 2.58 (sep, $CH(CH_3)_2$, 2H, J = 7

Hz), 1.27 (d, $CH(CH_3)_2$, 6H, J = 7 Hz), 1.08 (d, $CH(CH_3)_2$, 6H, J = 7 Hz), 1.05 (d, $CH(CH_3)_2$, 6H, J = 7 Hz), 0.71 (s, $Si(CH_3)_2$, 6H), 0.66 (d, $CH(CH_3)_2$, 6H, J = 7 Hz).

^{1}H NMR (THF-d_8, 190 K) δ 7.46 (m, CH_2CHCH_2, 1H), 6.93 (s, C_5H_2, 1H), 6.85 (s, C_5H_2, 1H), 5.21 (s, C_5H_2, 1H), 5.11 (s, C_5H_2, 1H), 4.32 (d, *anti*-CH_2CHCH_2, 1H, J = 15 Hz), 3.49 (d, *anti*-CH_2CHCH_2, 1H, J = 15 Hz), 3.18 (sep (br), $CH(CH_3)_2$, 1H, J = 7 Hz), 3.06 (sep (br), $CH(CH_3)_2$, 1H, J = 7 Hz), 2.59 (sep, $CH(CH_3)_2$, 1H, J = 7 Hz), 2.46 (sep, $CH(CH_3)_2$, 1H, J = 7 Hz), 2.33 (d, *syn*-CH_2CHCH_2, 1H, J = 9 Hz), 1.58 (d, *syn*-CH_2CHCH_2, 1H, J = 8 Hz), 1.27 (m (br), $CH(CH_3)_2$, 6H), 1.06 (m (br), $CH(CH_3)_2$, 6H), 1.00 (m (br), $CH(CH_3)_2$, 6H), 0.76 (s (br), $Si(CH_3)_2$, 6H), 0.65 (m (br), $CH(CH_3)_2$, 6H).

^{1}H NMR (THF-d_8, 347 K) δ 7.41 (quin, CH_2CHCH_2, 1H, J = 12 Hz), 6.80 (d, C_5H_2, 2H, J = 2 Hz), 5.12 (d, C_5H_2, 2H, J = 2 Hz), 3.10 (sep, $CH(CH_3)_2$, 2H, J = 7 Hz), 2.55 (sep, $CH(CH_3)_2$, 2H, J = 7 Hz), 1.28 (d, $CH(CH_3)_2$, 6H, J = 7 Hz), 1.06 (d, $CH(CH_3)_2$, 6H, J = 7 Hz), 1.04 (d, $CH(CH_3)_2$, 6H, J = 7 Hz), 0.75 (s, $Si(CH_3)_2$, 6H), 0.67 (d, $CH(CH_3)_2$, 6H, J = 7 Hz).

Preparation of *meso*-IpSc(η^3-C_3H_5) (6). In an inert atmosphere dry box, **2** (0.60 g, 1.4 mmol) was weighed into a 50 mL Kjeldahl flask which was then attached to a swivel frit assembly. Toluene (25 mL) was added by vacuum transfer, and the resulting light green slurry was stirred at -78 °C. Allylmagnesium bromide, as a 1.0 M solution in Et_2O (1.7 mL, 1.7 mmol), was added via syringe against a strong argon counterflow. The solution was allowed to come slowly to room temperature over a period of 10 hours at which time the mixture was orange. This slurry was stirred at room temperature for an additional 4 hours. The toluene was removed and petroleum ether (20 mL) was added by vacuum transfer. The orange slurry was stirred for one hour and filtered affording an off-white precipitate and an orange supernatant. After washing the precipitate four times with fresh portions of petroleum ether, the solvent was removed from the filtrate, leaving a bright orange powder (0.46 g, 1.0 mmol, 75% yield). Anal. Calcd. for $C_{27}H_{43}ScSi$: C, 73.59%, H, 9.84%. Found: C, 72.99, 72.52%, H, 10.25, 10.10%.

^{1}H NMR (Et_2O-d_{10}, 295 K) δ 7.53 (m, 1H, CH_2CHCH_2), 6.78 (d, 2H, C_5H_2, J = 2 Hz), 5.27 (d, 2H, C_5H_2, J = 2 Hz), 4.03 (d (br), 2H, *anti*-CH_2CHCH_2, coupling unresolved), 3.04 (sep, 2H, $CH(CH_3)_2$, J = 7 Hz), 2.36 (sep, 2H, $CH(CH_3)_2$, J = 7 Hz), 1.97 (d, 2H, *syn*-CH_2CHCH_2, J = 9 Hz), 1.22 (d, 6H, $CH(CH_3)_2$, J = 7 Hz), 1.07 (d, 6H, $CH(CH_3)_2$, J = 7 Hz), 0.92 (d, 6H, $CH(CH_3)_2$, J = 7 Hz), 0.86 (d, 6H, $CH(CH_3)_2$, J = 7 Hz), 0.81 (s, 3H ($Si(CH_3)_2$), 0.69 (s, 3H, $Si(CH_3)_2$).

^{1}H NMR (toluene-d_8, 194 K) δ 7.53 (m (br), 1H, CH_2CHCH_2), 6.56 (d, 1H, C_5H_2, J = 2 Hz), 6.52 (d, 1H, C_5H_2, J = 2 Hz), 5.49 (d, 1H, C_5H_2, J = 2 Hz), 5.35 (d, 1H, C_5H_2, J = 2 Hz), 4.64 (d (br), 1H, *anti*-CH_2CHCH_2, J = 15Hz), 3.84 (d (br), 1H, *anti*-CH_2CHCH_2, J = 15Hz), 3.05 (sep (br), 1H, $CH(CH_3)_2$), 2.91 (sep (br), 1H, $CH(CH_3)_2$), 2.34 (s (br), 2H, $CH(CH_3)_2$), 2.30 (m, 2H, *syn*-CH_2CHCH_2, obscured), 1.28 (m (br), 6H, $CH(CH_3)_2$), 1.16 (m (br), 6H, $CH(CH_3)_2$), 0.89 (m (br), 6H, $CH(CH_3)_2$, J = 7 Hz), 0.87 (m (br), 6H, $CH(CH_3)_2$), 0.77 (s, 3H, $(Si(CH_3)_2$), 0.76 (s, 3H, $Si(CH_3)_2$).

^{1}H NMR (toluene-d_8, 393 K) δ 7.53 (quin, CH_2CHCH_2, 1H, J = 12 Hz), 6.73 (d, C_5H_2, 2H, J = 2 Hz), 5.40 (d, C_5H_2, 2H, J = 2 Hz), 3.12 (s (br), CH_2CHCH_2, 4H) 2.96 (sep, $CH(CH_3)_2$, 2H, J = 7 Hz), 2.37 (sep, $CH(CH_3)_2$, 2H, J = 7 Hz), 1.20 (d, $CH(CH_3)_2$, 6H, J = 7 Hz), 1.09 (d, $CH(CH_3)_2$, 6H, J = 7 Hz), 0.92 (d, $CH(CH_3)_2$, 6H, J = 7 Hz), 0.88 (d, $CH(CH_3)_2$, 6H, J = 7 Hz), 0.78 (s, $Si(CH_3)_2$, 3H), 0.69 (s, $Si(CH_3)2$, 3H).

Preparation of *rac*-IpSc(η^3-1-Me-C_3H_4) (7). In an inert atmosphere dry box, a 50 mL Kjeldahl flask was charged with **1** (0.43 g, 0.72 mmol) and attached to a swivel frit apparatus. Toluene (~20 mL) was added by vacuum transfer affording a light yellow slurry. The solution was warmed until all *rac*-IpScCl was dissolved at which time the solution was cooled back to -78 °C. A standardized 3.2 M solution of crotylMgCl (0.3 mL, 0.96 mmol) was added by syringe against a strong argon counterflow. The reaction flask was allowed to warm to room temperature over 12 hours at which time the solution was dark red. The solution was stirred for 6 hours at room temperature and the solvent was removed under vacuum giving a dark red oil. The oil was dried by washing 9 times with fresh portions of heptane followed by drying *in vacuo*. Extraction with heptane yielded a deep red supernatant and a light orange precipitate which was washed 3 times with heptane. The supernatant was dried for 2 hours leaving a dark red paste. Anal. Calcd. for $C_{28}H_{45}ScSi$: C, 73.96%, H, 9.98%. Found: C, 79.53, 79.01%, H, 10.19, 11.30%. ^{1}H NMR (THF-d_8, 295 K) δ 6.91 (m, $CH_2CHCH(CH_3)$, 1H), 6.73 (s, C_5H_2, 2H), 5.15 (s, C_5H_2, 2H), 4.6 (s (br), $CH_2CHCH(CH_3)$), 3.11 (sep, $CH(CH_3)_2$, 2H, J = 7 Hz), 2.56 (s (br), $CH(CH_3)_2$, 2H), 1.34 (d, $CH_2CHCH(CH_3)$, 3H, J = 5 Hz), 1.27 (d, $CH(CH_3)_2$, 6H, J = 7 Hz), 1.06 (s (br), $CH(CH_3)_2$, 12H), 0.73 (s, $Si(CH_3)_2$, 6H), 0.69 (d, $CH(CH_3)_2$, 6H, J = 7 Hz). (The $CH_2CHCH(CH_3)$ resonance cannot be located at this temperature.)

Preparation of *meso*-IpSc(η^3-1-Me-C_3H_4) (8). In an inert atmosphere glove box, **2** (0.34 g, 0.78 mmol) was weighed into a 50 mL Kjeldahl flask which

was attached to a swivel frit assembly. Toluene (~20 mL) was added by vacuum transfer affording a bright yellow slurry. At -78 °C, a 3.2 M solution of crotylMgCl (0.3 mL, 0.96 mmol) was added by syringe against an argon counterflow. The reaction mixture was allowed to come to room temperature over a period of 12 hours and then stirred for an additional 24 hours at room temperature at which time the reaction mixture was dark red. The solvent was removed under vacuum and the resulting red sludge was washed 3 times with heptane. Extraction with heptane afforded a dark red supernatant and left a tan precipitate which was washed 3 times with heptane. The supernatant was dried affording red crystals. Anal. Calcd. for $C_{28}H_{45}ScSi$: C, 73.96%, H, 9.98%. Found: C, 73.32, 74.10, 73.37%, H, 10.21, 10.49, 9.94%. ^{1}H NMR (C_6D_6, 295 K) δ 7.08 (m, $CH_2CHCH(CH_3)$, 1H), 6.70 (s, C_5H_2, 2H), 5.31 (s, C_5H_2, 2H), 5.07 (m, $CH_2CHCH(CH_3)$, 1H), 3.08 (sep, $CH(CH_3)_2$, 2H, J = 7 Hz), 2.48 (sep, $CH(CH_3)_2$, 2H, J = 7 Hz), 1.39 (d, $CH_2CHCH(CH_3)$, 3H, J = 6 Hz), 1.30 (d, $CH(CH_3)_2$, 6H, J = 7 Hz), 1.15 (d, $CH(CH_3)_2$, 6H, J = 7 Hz), 0.96 (d, $CH(CH_3)_2$, 6H, J = 7 Hz), 0.83 (d, $CH(CH_3)_2$, 6H, J = 7 Hz), 0.80 (s, $Si(CH_3)_2$, 3H), 0.68 (s, $Si(CH_3)_2$, 3H). (The $CH_2CHCH(CH_3)$ resonance cannot be located at this temperature.)

Preparation of *meso*-IpZr(NMe$_2$)$_2$ (9). A 100 mL Schlenk flask was charged with $Zr(NMe_2)_4$ (0.5 g, 1.9 mmol) in an inert atmosphere dry box and xylenes (~40 mL) was added via pipette. IpH_2 (0.67 g, 1.9 mmol) was then added via pipette affording a light yellow solution. The flask was attached to a reflux condenser and an Ar inlet valve and was brought to reflux open to a mercury bubbler. The solution darkened to orange over 1 hour and after 12 hours was black and opaque. At this point, the reaction was cooled and the flask transferred to a swivel frit apparatus with a 100 mL receiver flask. The xylenes were removed under vacuum and pentane (30 mL) was added to the black residue by vacuum transfer. The resulting black slurry was stirred for 1 hour at which point filtration removed a small amount of jet black ppt from the yellow/brown supernatant. The pentane was evacuated from the supernatant leaving a brown oil which was dried for several hours under vacuum. Redissolution of the brown oil in fresh pentane and cooling for 1 week at -80 °C yielded a crop of yellow/orange needles. Additional cooling of the mother liquor after isolation of the first batch of crystals yielded an additional crop of crystals. Total yield was 0.74 g, 73%. Anal. Calcd. for $C_{28}H_{50}N_2SiZr$: C, 35.92%, H, 9.04%, N, 20.94%. Found: C, 36.17, 36.72%, H, 5.35, 5.94%, N, 20.77, 21.09%. ^{1}H NMR (C_6D_6): δ 6.46 (d, C_5H_2, 2H, J = 2 Hz), 5.67 (d, C_5H_2, 2H, J = 2 Hz), 3.18

(s, N(CH_3)$_2$, 6H), 3.01 (sep, CH(CH$_3$)$_2$, 2H, J = 7 Hz), 2.91 (sep, CH(CH$_3$)$_2$, overlaps with N(CH_3)$_2$), 2.88 (s (br), N(CH_3)$_2$, overlaps with CH(CH$_3$)$_2$), 1.33 (d, CH(CH_3)$_2$, 6H, J = 7 Hz), 1.25 (d, CH(CH_3)$_2$, 6H, J = 7 Hz), 1.23 (d, CH(CH_3)$_2$, 6H, J = 7 Hz), 1.12 (d, CH(CH_3)$_2$, 6H, J = 7 Hz), 0.74 (s, Si(CH_3)$_2$, 3H), 0.54 (s, Si(CH_3)$_2$, 3H).

Generation of *rac*-IpSc(η^1-C_3H_5)·LiCl(THF)$_x$ *in situ*. In an inert atmosphere glove box, **5** (17.5 mg, 0.0397 mmol) was weighed into an NMR tube with a threaded top. THF-d_8 (0.5 mL) was added by pipette and the tube was fitted with a septumed screw cap. The solution of **5** was cooled to -56 °C in the NMR probe and ^{1}H spectrum acquired. The sample was then ejected from the probe and cooled immediately to -78 °C in a dry ice/acetone bath. The solution of **5** was titrated with a standardized solution of LiCl in THF-d_8, (0.4658 M) added 0.2 equivalents at a time through the septum. A ^{1}H NMR spectrum was acquired at each interval of titration from 0 to 2 equivalents and during this process the tube was never allowed to warm above -56 °C. After the addition of 1 equivalent of LiCl, resonances assigned to *rac*-IpSc(η^1-C_3H_5)·LiCl(THF)$_x$ were the only thing visible (besides decomposition product resulting from air leakage into NMR tube) in the ^{1}H NMR spectra acquired. ^{1}H NMR: (THF-d_8, -65 °C) δ 6.23 (s, 1H, C_5H_2), 6.14 (m, 1H, ScCH$_2$CHCH$_2$), 5.93 (s, 1H, C_5H_2), 5.24 (s, 1H, C_5H_2), 5.17 (s, 1H, C_5H_2), 3.84 (d, br, 1H, *anti*-ScCH$_2$CHCH_2, J = 16 Hz), 3.68 (d, br, 1H, *syn*-ScCH$_2$CHCH_2, J = 7 Hz), 3.11 (sep, br, 1H, CH(CH$_3$)$_2$), 2.88 (sep, br, 1H, CH(CH$_3$)$_2$), 2.69 (sep, br, 1H, CH(CH$_3$)$_2$), 2.25 (sep, br, 1H, CH(CH$_3$)$_2$), 1.31 (d, br, 2H, ScCH_2CHCH$_2$, J = 7 Hz), 1.20 - 0.98 (m, br, 24H, CH(CH_3)$_2$), 0.55 (s, 3H, Si(CH_3)$_2$), 0.53 (s, 3H, Si(CH_3)$_2$).

Preparation of (C_3H_5)$_2$Mg. In an inert atmosphere glove box, a 1.0 M solution of allylmagnesium bromide in diethyl ether (5 mL, 5 mmol) was measured into a 100 mL Kjeldahl flask and attached to a swivel frit assembly. The diethyl ether solvent was removed under vacuum and the resulting white paste was dried for 1 hour. Dioxane (10 mL) was added by vacuum transfer affording a slurry with copious amounts of white precipitate. This slurry was stirred for 1 hour and then filtered separating a slightly yellow supernatant from the off white precipitate. The precipitate was washed once with dioxane and the filtrate was then dried affording a sticky yellow powder. Excess dioxane was removed from the product by five cycles of vacuum transfer - evacuation with 5 mL portions of toluene. Subsequently, the product was dried to a free-flowing powder. ^{1}H NMR indicated less than 0.1 equivalents of dioxane present in the

final product. ^{1}H NMR (THF-d_8): δ 6.25 (quin, CH_2CHCH_2, 1H, J = 11 Hz), 2.36 (d, 4H, CH_2CHCH_2, J = 11 Hz). A small sample was quenched with water and tested negative for halide by the absence of precipitate after addition of silver nitrate.

Preparation of $(n\text{-}C_7H_{15})_4NB(C_6H_3(CF_3)_2)_4$. $TlB(C_6H_3(CF_3)_2)_4$ (1.0 g, 0.87 mmol) was dissolved in Et_2O (50 mL) in a 250 mL round bottom flask. In a separate round bottom flask, $(n\text{-}C_7H_{15})_4NCl$ (0.387 g, 0.87 mmol) was dissolved in Et_2O (25 mL). After all species were dissolved, the ammonium salt solution was added to the solution of $TlB(C_6H_3(CF_3)_2)_4$ by pipette, immediately forming a fine, white precipitate in the reaction mixture. After the addition was complete, the reaction was stirred for 24 hours at which time the mixture was filtered through celite and washed three times with Et_2O. The filtrate was a clear, gold colored solution. The Et_2O was removed in vacuo, and the resulting sticky, gold colored solid was dried *in vacuo* at 100 °C for 12 hours. ^{1}H NMR (CD_2Cl_2) δ 7.73 (d, 2H, *o*-$C_6H_3(CF_3)_2$, J = 2 Hz), 7.57 (s, 1H, *p*-$C_6H_3(CF_3)_2$), 3.04 (m, 2H, $NCH_2(C_6H_{13})$), 1.60 (s, br, 2H, $NCH_2CH_2(C_5H_{11})$), 1.54 - 1.27 (m, 8H, $NCH_2CH_2(C_4H_8)CH_3$), 0.88 (t, $N(C_6H_{12})CH_3$, J = 7 Hz).

Isomerization of *rac*-IpScCl·LiCl(THF)$_2$ (1), *meso*-[IpScCl]$_2$ (2), *rac*-IpYCl·LiCl(THF)$_2$ (3), and *meso*-[IpYCl]$_2$ (4). A small sample of the appropriate metallocene (~20 mg) was placed in a J. Young NMR tube in an inert atmosphere glove box. The appropriate solvent (0.4 mL) was added by vacuum transfer at -78 °C and the reactions were followed by ^{1}H NMR until either equilibrium was reached (THF-d_8) or lack of reaction was established (Et_2O-d_{10}, toluene-d_8). Reactions were also carried out in THF-d_8 with added LiBr (~ 5 equiv.).

Preparative Scale Isomerization of *meso*-[IpScCl]$_2$ (2). In an inert atmosphere glove box, **2** (300 mg, 0.069 mmol) was weighed into a 25 mL Kjeldahl flask. This flask was attached to a swivel frit assembly and THF (10 mL) was added by vacuum transfer at -78 °C. The resulting yellow solution was stirred at room temperature for 8 days at which time the THF was removed *in vacuo*. The bright yellow powder was dried and excess THF removed by three successive cycles of vacuum transfer - evacuation with 10 mL portions of heptane followed by filtration yielding a light yellow precipitate and a bright yellow/green filtrate. Both species were dried *in vacuo* and isolated in powder form. ^{1}H NMR of heptane soluble species: (THF-d_8) δ 6.14 (s, br, 1H, C_5H_2), 5.62 (s, 1H, C_5H_2), 2.96 (sep, 1H, $CH(CH_3)_2$, J = 7 Hz), 2.81 (s, br, 1H, $CH(CH_3)_2$), 1.22

(d, 3H, $CH(CH_3)_2$, J = 7 Hz), 1.17 (d, 3H, $CH(CH_3)_2$, J = 7 Hz), 1.06 (d, 3H, $CH(CH_3)_2$, J = 7 Hz), 1.04 (d, 3H, $CH(CH_3)_2$, J = 7 Hz), 0.76 (s, 3H, $Si(CH_3)_2$).

Isomerization of *rac*-IpSc(η^3-C_3H_5) (5), and *meso*-IpSc(η^3-C_3H_5) (6). A small sample of the appropriate metallocene (~20 mg, 0.045 mmol) was placed in a J. Young NMR tube in an inert atmosphere glove box. The appropriate solvent (0.4 mL) was then added by vacuum transfer. In some experiments promoters were also added (Table 3). The NMR tube was either placed in an oil bath at the correct temperature or allowed to sit at room temperature. The reactions were monitored by ^1H NMR until either equilibrium was reached or lack of reaction was established.

Reactions of $ScCl_3(THF)_3$ and $YCl_3(THF)_{3.5}$ with $IpLi_2$. $IpLi_2$ was weighed into a J. Young NMR tube along with one equivalent of either $ScCl_3(THF)_3$ or $YCl_3(THF)_{3.5}$ in an inert atmosphere glove box. In the case of the yttrium complex, THF-d_8 was added by vacuum transfer, and a ^1H NMR spectrum was immediately acquired at room temperature. The reaction mixture was then heated to 71 °C in the NMR probe. The reaction was followed by ^1H NMR for 30 minutes at which point the thermodynamic product mixture had been achieved. In the case of the scandium complex, THF-d_8 was added by vacuum transfer, and reaction mixture was heated to 71 °C in the NMR probe. The reaction was followed by ^1H NMR for 1 hour at which point the thermodynamic product mixture had been achieved.

Reaction of $YCl_3(THF)_{3.5}$ with $DpLi_2$. $DpLi_2$ (14 mg, 0.045 mmol) and $YCl_3(THF)_{3.5}$ (20 mg, 0.045 mmol) were weighed into a J. Young NMR tube in an inert atmosphere glove box. THF-d_8 was added by vacuum transfer at -78 °C followed by immediate warming of the mixture to room temperature. The reaction was followed by ^1H NMR at room temperature for 17 hours. All ligand had metallated after 17 hours, resulting in a 1:1 racemic:meso ratio. The reaction mixture was then heated to 80 °C for 44 hours with no change in the product ratio.

Reaction of $YCl_3(THF)_{3.5}$ with $DpLi_2$ at -46 °C. In an inert atmosphere glove box, $DpLi_2$ (9.8 mg, 0.0313 mmol) and $YCl_3(THF)_{3.5}$ (13.7 mg, 0.0313 mmol) were weighed into a J. Young NMR tube. THF-d_8 (0.5 mL) was added by vacuum transfer at -78 °C. The tube was shaken to dissolve the reagents being careful not to let the contents warm. The NMR probe was cooled to -80 °C and the cold reaction mixture was inserted. The probe was then warmed to -46 °C and a ^1H spectrum was acquired. The sample was warmed to room

temperature in the probe, and another ^1H spectrum was acquired. The sample was allowed to stand for 20 hours at room temperature, and another ^1H spectrum was acquired. Attainment of the thermodynamic 1:1 racemic:meso ratio was complete after that period.

Preparation of (*R,S*)-$Me_2Si\{C_5H_2$-2-$(Si(CH_3)_3$-4-$(C(CH_3)_3\}_2ScCl(THF)$ [(*R,S*)-BnBpScCl(THF)]. In an inert atmosphere glove box, (*R,S*)-$BnBpK_2$ (2.0 g, 2.57 mmol) and $ScCl_3(THF)_3$ (0.946 g, 2.57 mmol) were weighed into a 200 mL Kjeldahl flask. A reflux condenser and 180° needle valve were then attached to the flask and the assembly was evacuated. THF (80 mL) was added by vacuum transfer and the mixture was heated to reflux for 2 days open to an argon bubbler. The THF was evaporated resulting in a dark orange, sticky solid. Petroleum ether (~ 50 mL) was added by vacuum transfer and the resulting thick slurry was stirred for 1 hour at which time the solvent was evaporated. The reaction flask was then attached to a swivel frit assembly and Et_2O (100 mL) was added by vacuum transfer. The orange slurry was stirred for 1 hour and then filtered to remove KCl. The precipitate was washed once with Et_2O followed by evaporation of the solvent. Petroleum ether (75 mL) was then added to the filtrate by vacuum transfer and the resulting mixture was filtered isolating a tan solid. This solid was washed 3 times with hexane and then dried affording 1.12 g of product (51%). Anal. Calcd. for $C_{48}H_{56}ClO_3ScSi_3$: C, 68.18%, H, 6.67%. Found: C, 69.34, 69.83, 69.34%, H, 7.19, 8.21, 7.90%. ^1H NMR (THF-d_8) δ 7.94 ($C_{20}H_{12}$, d, 1H, J = 9 Hz), 7.87 ($C_{20}H_{12}$, d, 1H, J = 8 Hz), 7.66 ($C_{20}H_{12}$, d, 1H, J = 9 Hz), 7.29 ($C_{20}H_{12}$, d, 1H, J = 7 Hz), 7.16 ($C_{20}H_{12}$, m, 2H), 6.54 (C_5H_2, d, 1H, J = 2 Hz), 6.42 (C_5H_2, d, 1H, J = 2 Hz), 1.31 ($C(CH_3)_3$, s, 9H), 0.20 ($Si(CH_3)_3$, s, 9H).

Variable-temperature ^1H NMR experiments. The NMR samples were brought to the lowest temperature available for measurement (ca. –85 °C for toluene-d_8, ca. –105 °C for THF-d_8) and allowed to equilibrate for at least 20 minutes. Spectra were then recorded at intervals of increasing temperature, equilibrating for 5 - 10 minutes at each iteration. Probe temperatures were then calculated using the same procedure with a pure methanol sample at low temperature and an ethylene glycol sample at high temperature.

Attempted Isomerizations of *rac*-$[BpYCl]_2$, (*R,S*)-[BnBpScCl(THF)], *meso*-$[DpScCl]_2$, and *rac*-(EBI)$ZrCl_2$ with LiCl. A small sample of the appropriate metallocene (~25 mg) was placed in a J. Young NMR tube along with LiCl (~5 equiv.) in an inert atmosphere glove box. THF-d_8 was added by vacuum transfer and the corresponding reactions were monitored by ^1H NMR.

After 100 hours at room temperature without reaction, each sample was heated to 80 °C for several days with no reaction evident by ^{1}H NMR.

Metallation of $ZrCl_4$ with (EBI)Li_2. In an inert atmosphere glove box, (EBI)Li_2 (14.0 mg, 0.0338 mmol) and $ZrCl_4$ (8.6 mg, 0.0369 mmol) were weighed into a J. Young NMR tube. THF-d_8 (0.5 mL) was added by vacuum transfer at -78 °C affording a slightly cloudy red/orange solution. The mixture was warmed to room temperature and allowed to react for 10 days at which time the contents were bright yellow. At this point, ^{1}H NMR indicated the formation of metallocenes in a 1:1 racemic:meso ratio.

Metallation of $ZrCl_4$ with $DpLi_2$. $DpLi_2$ (24 mg, 0.077 mmol) and $ZrCl_4$ (18 mg, 0.077 mmol) were weighed into a J. Young NMR tube in an inert atmosphere glove box. THF-d_8 was added by vacuum transfer at -78 °C affording a slightly cloudy light brown solution upon warming. The reaction was monitored by ^{1}H NMR and allowed to proceed at room temperature for 48 hours. After this time, the reaction was heated to 80 °C for 68 hours without change to the racemic:meso ratio (1.3:1).

Structure Determinations for *rac*-IpScCl·LiCl(THF)$_2$ (1), *meso*-[IpYCl]$_2$ (4), and *meso*-IpZr(NMe$_2$)$_2$ (9). A fragment cut from a single crystal under paratone oil for **1** **4**, **5**, and **8** was attached to a glass fiber and centered on an Enraf-Nonius CAD-4 diffractometer under a stream of cold N_2 gas. A single crystal mounted in a glass capillary for **9** was centered on an Enraf-Nonius CAD-4 diffractometer at room temperature. Unit cell parameters and orientation matrices were obtained by least-squares calculations based on the setting angles of 25 reflections with $11.6° < \theta < 12.1°$ for **1**, $12.5° < \theta < 13.1°$ for **4**, $12.5° < \theta < 13.3°$ for **5**, $14.5° < \theta < 15.0°$ for **8**, and $10.5° < \theta < 11.2°$ for **9**. During the data collection for all samples, three reference reflections were measured every hour and showed no significant decay. Two equivalent data sets were collected and no correction was made for decay or absorption for **1**, **5**, **8**, and **9**; absorption corrections by ψ scans were applied to **4**. Lorentz and polarization factors were applied to each, and the two data sets for each were then merged. Structures **1**, **4**, **5**, and **8** were solved by direct methods which for each revealed all non-hydrogen atom positions (SHELXS). Subsequent difference Fourier maps were successful in finding all hydrogens. In the refinements for **1**, **4**, and **8**, all hydrogens were freely refined. In the refinement for **5**, disorder in the allyl ligand was modeled as a 70:30 distribution of populations using identical methylene carbons and two separate methine carbons. The methyl group

angles were restrained and all other hydrogens were refined without restraints. The structure of **9** was solved by the Patterson method which revealed most of the heavy atoms, the remaining heavy atoms being revealed in subsequent difference Fourier maps. The hydrogens of **9** were treated as riding atoms in the refinement. All non-hydrogen atoms were refined anisotropically for each of the structures. Full matrix least squares refinement on F^2 converged at R_F = 0.0464 and GOF (F^2) = 1.514 for **1**, R_F = 0.0951 and GOF (F^2) = 1.615 for **4**, R_F = 0.0643 and GOF (F^2) = 2.153 for **5**, R_F = 0.0621 and GOF (F^2) = 1.579 for **8**, and R_F = 0.0939 and GOF (F^2) = 1.403 for **9**. The final difference Fourier maps for each of the structures did not reveal any significant features. Crystallographic data have been deposited at the CCDC, 12 Union Road, Cambridge CB2 1EZ, UK and copies can be obtained on request, free of charge, by quoting the publication citation. Details of the data collection and solution and refinement of all of the structures can be found in Appendix 2. Also in this Appendix are ORTEP drawings showing the complete atom labeling schemes, tables of atomic coordinates, complete bond distances and angles, anisotropic displacement parameters, and hydrogen atom coordinates for all structures.

References and Notes

1. (a) Yoder, J. C.; Day, M. W.; Bercaw, J. E. *Organometallics* **1998**, *17*, 4946; (b) Abrams, M. B.; Yoder, J. C.; Loeber, C. L.; Day, M. W.; Bercaw, J. E. *Organometallics* **1999**, *18*, 1389.
2. Brintzinger, H. H.; Fischer, D.; Mülhaupt, R.; Rieger, B.; Waymouth, R. N. *Angew. Chem. Int. Ed. Eng.* **1995**, *34*, 1143 and references therein.
3. (a) Coughlin, E. B.; Bercaw, J. E. *J. Am. Chem. Soc* **1992**, *114*, 7606; (b) Giardello, M. A., Conticello, V. P.; Brand, L.; Sabat, M.; Rheingold, A. L.; Stern, C. L.; Marks, T. J. *J. Am. Chem. Soc* **1994**, *116*, 10212; (c) Watson, P. L. *J. Am. Chem. Soc.* **1982**, *104*, 337 ; (d) Den Haan, K. H.; Wielstra, T.; Eshuis, J. J. W.; Teuben, J. H. *J. Organomet. Chem.* **1987**, *323*, 181; (e) Yasuda, H.; Ihara, E. *Tetrahedron* **1995**, *51*, 4563; (f) Evans, W. J.; DeCoster, D. M.; Greaves, J. *Organometallics* **1996**, *15*, 3210.
4. Ewen, J. A. *J. Am. Chem. Soc.* **1984**, *106*, 6355.

5. Kaminsky, W.; Külper, K.; Brintzinger, H. H.; Wild, F. R. W. P. *Angew. Chem. Int. Ed. Engl.* **1985**, *24*, 507.
6. Wild, F. R. W. P.; Zsolnai, L.; Huttner, G.; Brintzinger, H. H. *J. Organomet. Chem.* **1982**, *232*, 233.
7. Wild, F. R. W. P.; Wasiucionek, M.; Huttner, G.; Brintzinger, H. H. *J. Organomet. Chem.* **1985**, *288*, 63.
8. Wiesenfeldt, H.; Reinmuth, A.; Barsties, E.; Evertz, K.; Brintzinger, H. H. *J. Organomet. Chem.* **1989**, *369*, 359.
9. Haar, C. M.; Stern, C. L.; Marks, T. J. *Organometallics* **1996**, *15*, 1765.
10. (a) Wang S. W.; Yang Q. C.; Mak T. C. W.; Xie Z. W. *Organometallics* **2000**, *19*, 334; (b) Lee L. W. M.; Piers W. E.; Parvez M.; Rettig S. J.; Young V. G. *Organometallics* **1999**, *18*, 3904; (c) Miyake S.; Henling L. M.; Bercaw J. E.; *Organometallics* **1998**, *17*, 5528; (d) Hultzsch, K. C.; Spaniol, T. P.; Okuda, J. *Organometallics* **1997**, *16*, 4845.
11. (a) Diamond, G. M.; Rodewald, S.; Jordan, R. F. *Organometallics* **1995**, *14*, 5; (b) Diamond, G. M.; Jordan, R. F.; Petersen, J. L. *Organometallics* **1996**, *15*, 4030; (c) Christopher, J. N.; Diamond, G. M.; Jordan, R. F.; Petersen, J. L. *Organometallics* **1996**, *15*, 4038; (d) Diamond, G. M.; Jordan, R. J.; Petersen, J. L. *Organometallics* **1996**, *15*, 4045.
12. (a) Schmidt, K.; Reinmuth, A.; Rief, U.; Diebold, J.; Brintzinger, H. H. *Organometallics* **1997**, *16*, 1724; (b) Kaminsky, W.; Schauwienold, A.-M., Freidanck, F. *J. Mol. Catal. A* **1996**, *112*, 37; (c) Rheingold, A. L.; Robinson, N. P.; Whelan, J.; Bosnich, B. *Organometallics* **1992**, *11*, 1869.
13. Brindley, P. B.; Davies, A. G.; Hawari, J. A.-A. *J. Organomet. Chem.* **1983**, *250*, 247 and references therein.
14. (a) Hazin, P. N.; Huffman, J. C.; Bruno, J. W. *Organometallics* **1987**, *6*, 23; (b) Heeres, H. J.; Meetsma, A.; Teuben, J. H.; Rogers, R. D. *Organometallics* **1989**, *8*, 2637; (c) Heeres, H. J.; Teuben, J. H. *Recl. Trav. Chim. Pays-Bas* **1990**, *109*, 226; (d) Maginn, R. E.; Manastyrskyj, S.; Dubeck, M. *J. Am. Chem. Soc.* **1962**, *85*, 672.
15. Shafiq, F. A.; Richardson, D. E.; Boncella, J. M. *J. Organomet. Chem.* **1998**, *555*, 1.
16. (a) Coughlin, E. B.; Henling, L. M.; Bercaw, J. E. *Inorg. Chim. Acta* **1996**, *242*, 205; (b) Stern, D.; Sabat, M.; Marks, T. J. *J. Am. Chem. Soc.* **1990**, *112*, 9558;

(c) Desurmont, G.; Li, Y.; Yasuda, H.; Maruo, T.; Kanehisa, N.; Kai, Y. *Organometallics* **2000**, *19*, 1811.

17. Chacon, S. T.; Coughlin, E. B.; Henling, L. M.; Bercaw, J. E. *J. Organomet. Chem.* **1995**, *497*, 171.
18. Hajela, S.; Bercaw, J. E. unpublished results. Structures for *rac*- and *meso*-IpMCl·LiCl(THF)$_2$ and (IpMCl)$_2$ (M = Sc, Y) were minimized using augmented MM2 parameters with the CAChe program. In each case the racemo isomer was found to be more stable than the meso isomer by more than 2 kcal/mol.
19. (a) Campion, B. K.; Heyn, R. H.; Tilley, T. D. *Organometallics* **1993**, *12*, 2584; (b) Schaefer, W. P.; Köhn, R. D.; Bercaw, J. E. *Acta Cryst.* **1992**, *C48*, 251; (c) Hajela, S.; Schaefer, W. P.; Bercaw, J. E. *Acta Cryst.* **1992**, *C48*, 1771; (d) St. Clair, M.; Schaefer, W. P.; Bercaw, J. E. *Organometallics* **1991,** *10*, 525; (e) Lappert, M. F.; Singh, A.; Atwood, J. L.; Hunter, W. E *J. Chem. Soc., Chem. Commun.* **1983**, 206.
20. (a) Evans, W. J.; Sollberger, J. S.; Shreeve, J. L.; Olofson, F. M.; Hain, J. H., Jr.; Ziller, J. W. *Inorg. Chem.* **1992**, *31*, 2492; (b) Marsh, R. E.; Schaefer, W. P.; Coughlin, E. B.; Bercaw, J. E. *Acta Cryst.* **1992**, *C48*, 1773; (c) den Haan, K. H.; de Boer, J. L.; Teuben, J. H.; Spek, A. L.; Kojic-Prodic, B.; Gays, G. R.; Huis, R. *Organometallics* **1986**, *5*, 1726; (d) Evans, W. J.; Dominguez, R.; Levan, K. R.; Doedens, R. J. *Organometallics* **1985**, *4*, 1836; (e) Evans, W. J.; Meadows, J. H.; Wayda, A. L.; Hunter, W. E.; Atwood, J. L. *J. Am. Chem. Soc.* **1982**, *104*, 2008.
21. Evans, W. J.; Peterson,T. T.; Rausch, M. D.; Hunter, W. E.; Zhang, H.; Atwood, J. L. *Organometallics* **1985**, *4*, 554.
22. Baker, R. T.; Whitney, J. F.; Wreford, S. S. *Organometallics* **1983**, *2*, 1049.
23. Hillhouse, G. L.; Bulls, A. R.; Santarsiero, B. D.; Bercaw, J. E. *Organometallics* **1988**, *7*, 1309.
24. Abrams, M. B. Ph.D. Thesis, California Institute of Technology, 1998.
25. Bunel, E. E., Ph.D. Thesis, California Institute of Technology, 1989.
26. It is quite likely that both *rac*- and *meso*-DpYCl are dimeric.
27. Mitchell, J. P.; Hajela, S.; Brookhart, S. K.; Hardcastle, K. I.; Henling, L. M.; Bercaw, J. E. *J. Am. Chem. Soc.* **1996**, *118*, 1045.

28. Wayda, A. L.; Darensbourg, M. Y. "Experimental Organometallic Chemistry," Washington, D.C., 1987.
29. Marvich, R. H.; Brintzinger, H. H. *J. Am. Chem. Soc.* **1971**, *93*, 2046.
30. Zair, T.; Santellirouvier, C.; Sandelli, M. *J. Org. Chem.* **1993**, *58*, 2691.
31. Manzer, L. E. *Inorg. Synth.* **1982**, *21*, 135.
32. Herzog, T. A. Ph.D. Thesis, California Institute of Technology, 1997
33. Massey, A. G.; Park, A. J. *J. Organomet. Chem.* **1964**, *2*, 245.
34. Brookhart, M.; Grant, B.; Volpe, J. A. F. *Organometallics* **1992**, *11*, 3920.
35. Hughes, R. P.; Lindner, D. C.; Rheingold, A. L.; Yap, G. P. A. *Inorg. Chem.* **1997**, *36*, 1726.

Chapter 2

A Study of the Mechanism of Conversion of Scandocene Alkenyl Compounds to Scandocene η^3-Allyl Compounds and a Comparison of σ-Bond Metathesis Reactivity Between $(C_5Me_5)_2$- and $Me_2Si(C_5Me_4)_2$-Ligated Scandocenes

Abstract

Several scandocene alkenyl compounds have been synthesized and their reactions with olefins have been examined. The complexes (*E*)-{$Me_2Si[\eta^5$-$C_5Me_4]_2$}ScC(Me)=CH(R) (R = Me, **12**; R = $CHMe_2$, **13**) ($Me_2Si[\eta^5$-$C_5Me_4]_2$ = Op) react with the allylic C-H bonds of olefins generating η^3-allyl complexes. For both complexes, an intermediate derived from intramolecular σ-bond metathesis (a "tuck-in" complex) was inferred from both kinetics and labeling experiments. Activation parameters for the reaction of OpScC(Me)=CH(Me) with *cis*-2-butene have been determined: $\Delta H^{\ddagger}$ = 22.8 (1.7) kcal·mol^{-1}, $\Delta S^{\ddagger}$ = -17 (2) eu. The η^3-allyl compounds generated in these reactions are catalysts for the isomerization of internal olefins to a mixture of the *cis*-, *trans*-, and terminal isomers. These olefin isomerization reactions also proceed through a tuck-in intermediate. Permethylscandocene alkenyl compounds have been found to react almost exclusively with the vinylic C-H bonds of olefins consistent with earlier studies. The difference in σ-bond metathesis reactivity between the two systems is attributed to steric differences in the transition states in which the $Me_2Si[\eta^5$-$C_5Me_4]_2$Sc (OpSc) ligand array allows for olefin π-coordination while the $(\eta^5$-$C_5Me_5)_2$Sc (Cp^*_2Sc) ligand array does not. X-ray structure determinations for Cp^*_2ScC(H)=CMe_2 (**10**) and OpSc(η^3-1-Me-C_3H_4) (**15**) have been carried out.

Table of Contents, Chapter 2

I. Introduction 56

II. Results and Discussion 59

A. Synthesis of Scandocene Alkenyl Compounds 59

B. X-ray Structure Determination for $Cp^*_2ScC(H)=CMe_2$ (**10**) 61

C. Variable Temperature ^1H NMR Studies of Alkenyl M-C Bond Rotation 64

D. Reactions of Permethylscandocene Alkenyl Compounds with Olefins 65

E. Reactions of OpScC(Me)=CH(R) with Olefins (R = Me, $CHMe_2$) 66

F. Reactions of $OpSc(\eta^3\text{-}C_4H_7)$ with Olefins 75

G. X-ray Structure Determination for $OpSc(\eta^3\text{-}C_4H_7)$ (**15**) 77

III. Conclusions 80

IV. Experimental Section 81

V. References and Notes 86

Introduction

Trihapto-allyl ligands are ubiquitous across the whole series of the transition elements.[1] Their prevalence in early transition metal and *f*-element chemistry stems from the extra stability which a three-electron-donating ligand can confer on otherwise electronically unsaturated d^0-metal centers. The lack of π-backbonding in these complexes, however, often renders the allyl ligands fluxional.[2] Recently, η^3-allyl complexes of early transition metal metallocenes have been proposed as intermediates in a variety of important transformations pertaining to metallocene-catalyzed olefin polymerization. These include dehydrogenation of a growing polymer chain which results in internal unsaturation[3] and polymer chain epimerization in which the chirality at the β-carbon of a growing polymer chain is scrambled.[3c,4] The creation of a metallocene allyl complex from a metallocene alkyl precursor is required for both of these processes, and while this transformation has been often observed,[5] a detailed study of the mechanism(s) of allyl formation has been lacking.

Watson has examined the chemistry of $(\eta^5\text{-}C_5Me_5)_2Lu(CH_2CHMe_2)$, ($C_5Me_5$ = Cp*) which undergoes competitive β-hydrogen and β-methyl elimination at room temperature in C_6D_{12} solution.[5d-f] When this compound is thermolyzed in C_6D_{12}, $Cp^*_2Lu(\eta^3\text{-}C_3H_5)$, $Cp^*_2Lu(\eta^3\text{-}2\text{-}Me\text{-}C_3H_4)$, and isobutane are observed as final products (Scheme 1). Two pathways can be envisioned for this process: intermolecular σ-bond metathesis between $Cp^*_2Lu(CH_2CHMe_2)$ and the olefin (pathway (a), Scheme 1), and intramolecular σ-bond metathesis affording an intermediate "tuck-in" complex which then reacts with olefin (pathway (b), Scheme 1). The decomposition of $Cp^*_2Lu(CH_2CHMe_2)$ was too complicated for a detailed kinetic study, but pathway (b) was favored by Watson based on labeling studies.[5e] In contrast, pathway (a) was proposed by Evans and Marks for related permethylsamarocene chemistry although no kinetics data were reported;[5g-k] transition state olefin-coordination was invoked to explain the preference for reaction with allylic C-H bonds over the normally preferred[6] vinylic σ-bond metathesis.

Previous studies from this group have shown that the *ansa*-scandocene $\{Me_2Si[\eta^5\text{-}C_5Me_4]_2\}ScH(PMe_3)$ ($OpScH(PMe_3)$) reacts with excess methylenecyclopentane to afford one equivalent of methylcyclopentane and an η^3-allyl compound.[7] Based on the ^{13}C NMR observation of two intermediates (δ 54 and 175) when *exo*-^{13}C-labeled methylenecyclopentane was used, vinylic σ-

bond metathesis was proposed to precede reaction with the allylic protons (Scheme 2). Again, no kinetics studies were performed.

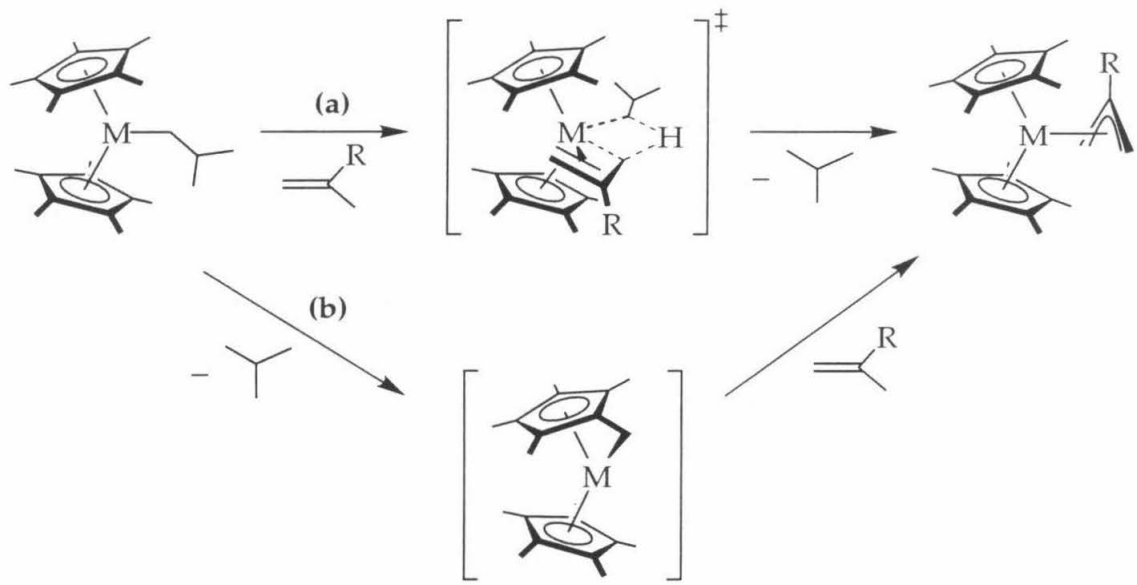

Scheme 1. Proposed mechanisms for reaction of $Cp^*_2M(CH_2CHMe_2)$ with olefins (M = lanthanide, R = H, Me).

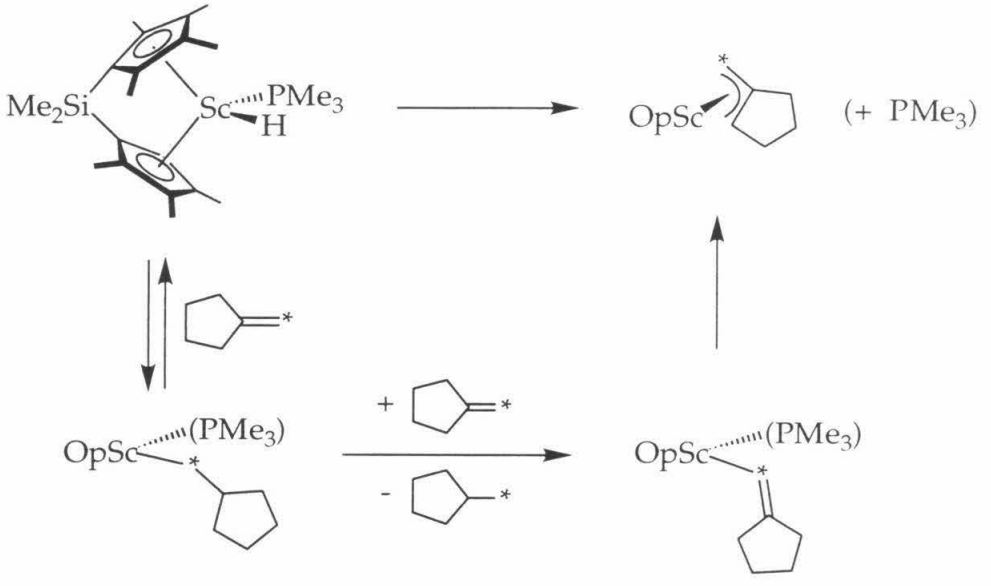

Scheme 2. Mechanism proposed for formation of OpSc(η^3-$CH_2C(CH_2)_3CH$) from OpScH(PMe_3).

In the studies discussed above, the reactions with olefin afforded alkane as a byproduct, but molecular hydrogen is observed upon allylic activation in actual polymerization systems.[3] Activation of olefins by transition metal complexes in the gas phase often results in stable η^3-allyl complexes with loss of H_2,[8] and this has recently been observed during gas-phase olefin oligomerization.[8g] The mechanism proposed for these reactions is identical to that which is typically proposed for the polymerization systems (Eqn 1): insertion of olefin into the metal alkyl bond followed by β-H elimination and allylic σ-bond metathesis.

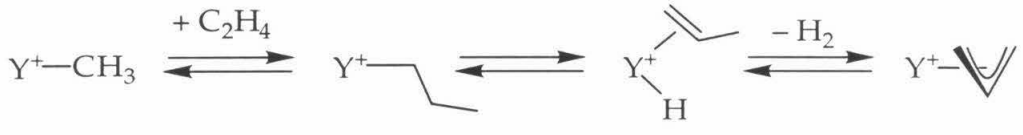

(1)

Brintzinger has recently performed computational studies on the mechanism of allyl formation and has also examined the reaction of $Cp_2ZrMe(\eta^3\text{-}2\text{-}Me\text{-}C_3H_4)$ with propylene;[9] in the presence of $B(C_6F_5)_3$, insertion of propylene occurs exclusively into the methallyl group. When the reaction is carried out with $Cp_2ZrMe(\eta^3\text{-}CH_2CH(Me)CD_2)$, after hydrolysis and separation of the organic products, incorporation of deuterium atoms is observed into all positions of the first inserted propylene unit and what was formerly the

methallyl ligand (Eqn 2). These results indicate that metallocene η^3-allyl

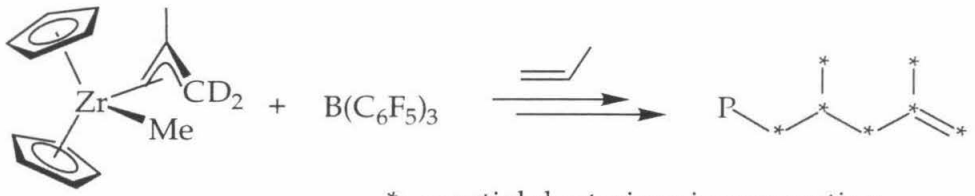

(2)

* = partial deuterium incorporation

complexes can, indeed, insert propylene and can also undergo isomerization processes reminiscent of those proposed to occur during chain epimerization. The computational aspect of these studies revealed olefin coordination in the transition state for allylic σ-bond metathesis. Ziegler has also investigated these issues using density functional methods.[10]

In light of the studies described above, we sought to clarify the mechanistic details of the transformations of metallocene alkyls to the corresponding allyl complexes using scandocenes as models. As scandocene alkyl compounds are notoriously difficult to work with and, especially, to isolate cleanly due to facile β-H elimination,[11] all studies were carried out on scandocene alkenyl compounds which are simpler to prepare and inherently much more stable. Presented herein are attempts to prepare permethylscandocene η^3-allyl complexes by reaction of various Cp^*_2ScR complexes with olefins, and a study of the mechanism of the alkenyl to η^3-allyl rearrangement for (*E*)-OpScC(Me)=CH(R) (R = Me, $CHMe_2$).

Results and Discussion

Synthesis of Scandocene Alkenyl Compounds

The permethylscandocene alkenyl compounds $Cp^*_2ScC(H)=CMe_2$[6] (**10**) and $Cp^*_2ScC(Me)=CMe_2$[12] (**11**) were prepared from Cp^*_2ScMe as previously described. This compound reacts with isobutene by σ-bond metathesis to afford **10** and with 2-butene by insertion to afford **11**.

The *ansa*-scandocene alkenyl compounds (*E*)-OpScC(Me)=CH(R) (R = Me, **12**; R = $CHMe_2$, **13**) were prepared by reaction of the corresponding alkyne with $OpScH(PMe_3)$ (Eqn 3). Complete regioselectivity was observed in the reaction

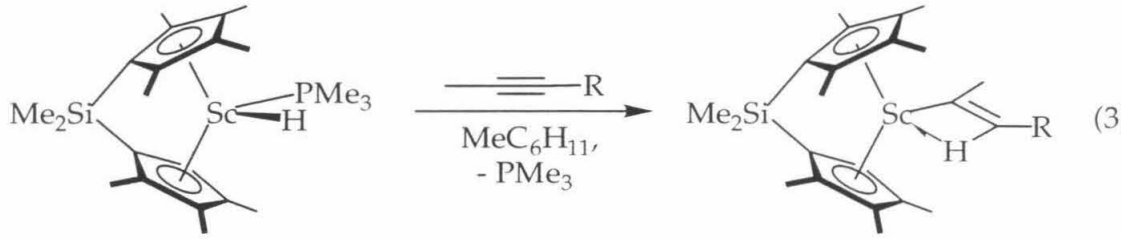

(3)

R = Me: (**12**)
R = $CHMe_2$: (**13**)

with 4-methyl-2-pentyne; the alkyne approaches such that the insertion occurs with the bulky isopropyl group farther from the sterically demanding scandium center. Trimethylphosphine does not bind tightly to either **12** or **13** as it can be easily removed *in vacuo*.

Both the position of the vinyl resonance in the ^1H NMR spectra (δ 3.7 for **12**; δ 3.6 for **13**) and the presence of a low-field C-H stretch (ν_{CH} = 2578 cm^{-1} for **12**; 2568 cm^{-1} for **13**) in the infrared spectra of these compounds (all acquired in C_6D_6 solution) are indicative of β-agostic alkenyl groups. The vinyl resonance for each shifts downfield (δ 4.9 for **12**; δ 4.7 for **13**) upon dissolution in the coordinating solvent THF-d_8, indicating disruption of the agostic C-H interactions. It has been previously observed that (*E*)-$Cp^*_2ScC(Me)=CH(Me)$ shows spectral features consistent with a β-agostic alkenyl ligand while (*E*)-$Cp^*_2ScC(H)=CH(Me)$ does not.[13] It is proposed that alkyl substituents geminal to scandium on an alkenyl ligand produce adverse steric interactions with substituents on the cyclopentadienyl rings thus, in effect, pushing the β-C-H bond into close contact with the metal (Figure 1). Similar effects have been observed for compounds of the form (*E*)-$Cp^*_2M(H)[(R)C=CH(R')]$ or (*E*)-$Cp^*_2M[(R)C=CH(R')]_2$ (M = Zr, Hf; R, R' = H, alkyl).[14]

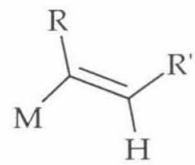

favored for R = H,
R' = alkyl

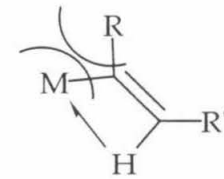

favored for R ≥ Me,
R' = alkyl

Figure 1. Representations of both normal and β-agostic alkenyl ligands.

Previous studies have shown that reaction of Cp^*_2ScH with 2-pentyne yields an approximately 2:1 ratio of regioisomers,[13] the favored isomer having the ethyl group disposed away from the scandium center on the alkenyl β-carbon. Upon reaction of 2-pentyne with $OpScH(PMe_3)$ in petroleum ether solution, two regioisomeric alkenyl compounds are obtained in approximately equal proportion (Eqn 4). Thus, as expected, the Op ligand array exerts a weaker steric influence in the transition state for alkyne insertion than the *bis*-pentamethylcyclopentadienyl ligand array.

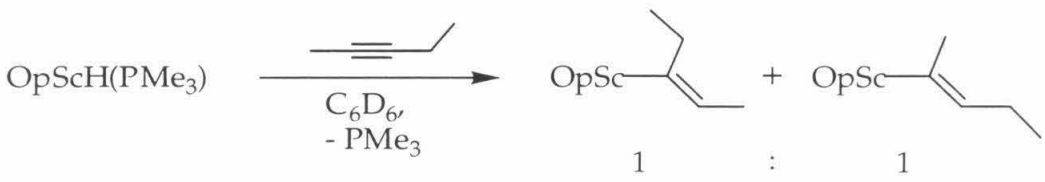

(4)

X-ray Structure Determination for $Cp^*_2ScC(H)=CMe_2$ (10)

Upon cooling a saturated methylcyclohexane solution of **10** from 85 °C to room temperature, single crystals deposited as yellow wedges and an X-ray structure determination was completed. Refinement of the obtained data revealed disorder in the isobutenyl ligand; the disorder was modeled as two separate groups with a 73:27 population of sites. The major isomer (including the hydrogens) was refined anisotropically with no restraints. The minor isomer was refined isotropically with calculated hydrogens. The structure of the molecule oriented in the major position is shown in Figure 2, selected bond lengths and angles are given in Table 1. Details of the data collection and solution and refinement of the structure can be found in Appendix 2.

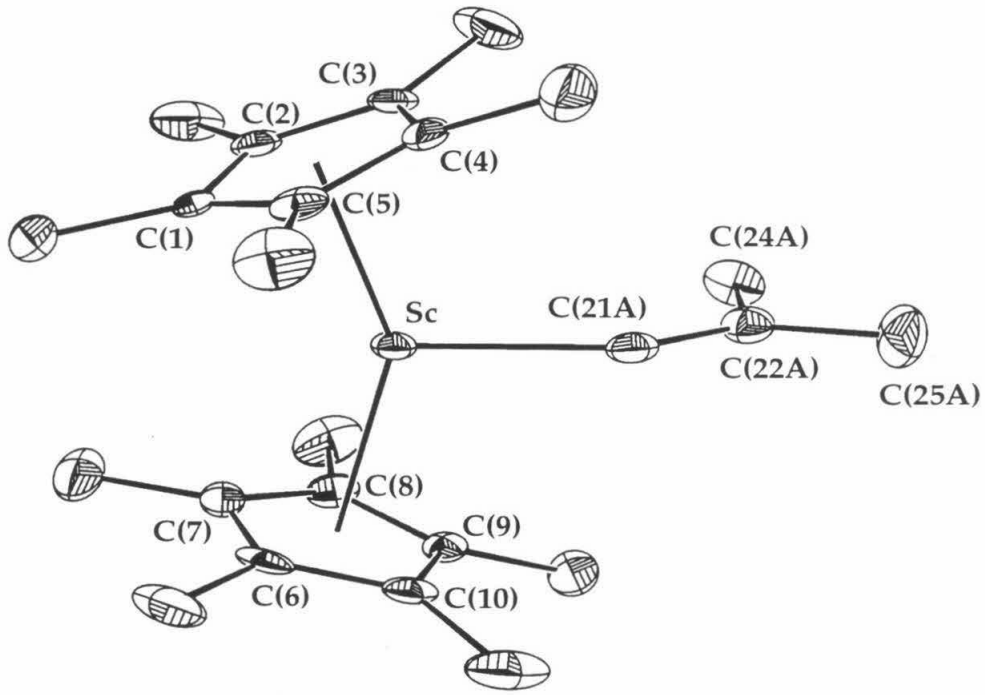

Figure 2. ORTEP representation of the molecular structure of **10** with selected atoms labeled (50% probability ellipsoids, hydrogens omitted for clarity).

Table 1. Selected Bond Distances (Å) and Bond Angles (°) Obtained From the X-Ray Structure Determination of **10**

Feature	Distance (Å) or Angle (°)	Feature	Distance (Å) or Angle (°)
Sc-Ct(1)[a]	2.164 (3)	Sc-Ct(2)[b]	2.167 (3)
Sc-C(21A)	2.282 (4)	Sc-C(21B)	2.202 (10)
C(21A)-C(22A)	1.332 (7)	C(21B)-C(22B)	1.356 (18)
C(22A)-C(23A)	1.505 (8)	C(22B)-C(23B)	1.43 (2)
C(22A)-C(24A)	1.533 (7)	C(22B)-C(24B)	1.506 (18)
Ct(1)-Sc-C(21A)[a]	106.3 (4)	Ct(1)-Sc-C(21B)[a]	107.7 (10)
Ct(2)-Sc-C(21A)[b]	107.9 (4)	Ct(2)-Sc-C(21B)[b]	104.3 (10)
Sc-C(21A)-C(22A)	140.2 (4)	Sc-C(21B)-C(22B)	127.2 (11)
C(21A)-C(22A)-C(23A)	125.1 (5)	C(21B)-C(22B)-C(23B)	124.2 (16)
C(21A)-C(22A)-C(24A)	121.3 (6)	C(21B)-C(22B)-C(24B)	119.1 (16)
Ct(1)-Sc-Ct(2)[a,b]	144.4 (3)		

[a]Ct(1) is defined as the centroid of the ring made up of C(1) - C(5); [b]Ct(2) is defined as the centroid of the ring made up of C(6) - C(10).

The scandium center appears to be bonded in a distorted trigonal planar geometry. The Cp centroid-Sc-Cp centroid angle is 144.4°, and the Cp centroid-Sc-C(21) angles are between 104° and 108°. The Sc-Cp centroid bond lengths (2.164 Å and 2.167 Å) and the Cp centroid-Sc-Cp centroid angle are within the normal ranges expected.[2,6,15] The C-C bond lengths in both the major and minor alkenyl sites are consistent with the expected hybridizations of the carbons involved and both alkenyl groups are planar. The dihedral angle between the planes defined by Sc, Ct(1), and Ct(2) and that defined by C(21A), C(22A), C(23A) and C(24A) is 85.7°. The analogous angle for the minor alkenyl isomer is 93°. The minor alkenyl isomer has a much lower Sc-C(21)-C(22) bond angle (127.2 (11)°) as compared to the major isomer (140.2 (4)°). The C(22B)-C(23B) bond length also seems anomolously short at 1.43 (2) Å (C(22A)-C(23A) = 1.505 (8) Å). However, the large errors for these values and the problems inherent in refining atoms that are only 1/4 occupancy means that these differences should probably not cause alarm.

Variable temperature ^{1}H NMR studies of alkenyl M-C bond rotation

In the ^{1}H NMR spectra for both **12** and **13** at room temperature in C_6D_6, one of the cyclopentadienyl methyl resonances is considerably broader than the second. This phenomenon can be explained for each by invoking hindered rotation about the M-C bond of the alkenyl ligand due to the β-C-H agostic interaction. Dynamic ^{1}H NMR studies of this process in both toluene-d_8 and THF-d_8 solutions were carried out.

At the lowest temperature available in toluene-d_8 (approx. –85 °C) both **12** and **13** are static and exhibit C_s-symmetry, while in the high temperature limit both molecules exhibit C_{2v}-symmetry. Sharp linewidths are observed at room temperature for all signals of **12** and **13** in THF-d_8 solution in which the compounds do not exhibit ground state β-agostic structures. Indeed, there is no evidence for a β-C-H agostic interaction for these compounds in THF-d_8 solution even below –100 °C as the locations of the vinyl resonances for **12** and **13** are identical to those observed at room temperature. However, even in THF-d_8 solution, static NMR structures are observed for both at low temperature. The behavior of **12** is complicated by the appearance of a second species at low temperature precluding the measurement of rate constants.

The rate constants obtained at the coalescence temperatures for **12** and **13** in toluene-d_8 and **13** in THF-d_8 are shown in Table 2. It would be tempting to ascribe these rate constants and the associated barriers to measures of the strengths of the agostic C-H bonds. However, the fact that completely static structures are observed at low temperature for both **12** and **13** in THF-d_8 solution without any evidence for an agostic interaction provokes caution. The exact structure of the compounds in THF solution, whether solvent bound or not, and the associated uncertainties make meaningful analysis of this system difficult. It can, however, be stated that the rates for the fluxional process(es) in THF-d_8 solution are faster than those in toluene-d_8.

Table 2. Rate Constants for Alkenyl M–C Bond Rotation for **12** and **13** as Determined by Dynamic ^{1}H NMR Spectroscopy

Compound	Solvent	k (s^{-1})	Temp. (K)	$\Delta G^{\ddagger}$ (kcal·mol^{-1})
12	toluene-d_8	103[a]	238	11.6
		162[b]	248	11.9
		104[c]	238	11.6
13	toluene-d_8	251[a]	258	12.2
		321[b]	263	12.3
		207[c]	253	12.0
13	THF-d_8	195[a]	205	9.7
		77[b]	198	9.7
		53[c]	196	9.8

[a]rate constant obtained from coalescence of the α-cyclopentadienyl methyl signals; [b]rate constant obtained from coalescence of the β-cyclopentadienyl methyl signals; [c]rate constant obtained from coalescence of the silyl methyl signals.

Reactions of Permethylscandocene Alkenyl Compounds with Olefins

Thermolysis of **10** or **11** at 85 °C in C_6D_{12} results in conversion to the previously characterized[15c] dimeric complex $[Cp^*(C_5Me_4\text{-}\mu\text{-}CH_2)Sc]_2$ (**14**) after ~ 1 week. Carrying out the thermolyses in C_6D_6 produces $Cp^*_2ScC_6D_5$, the reactions reaching completion in approximately 20 hours (Scheme 3). Heating **10**

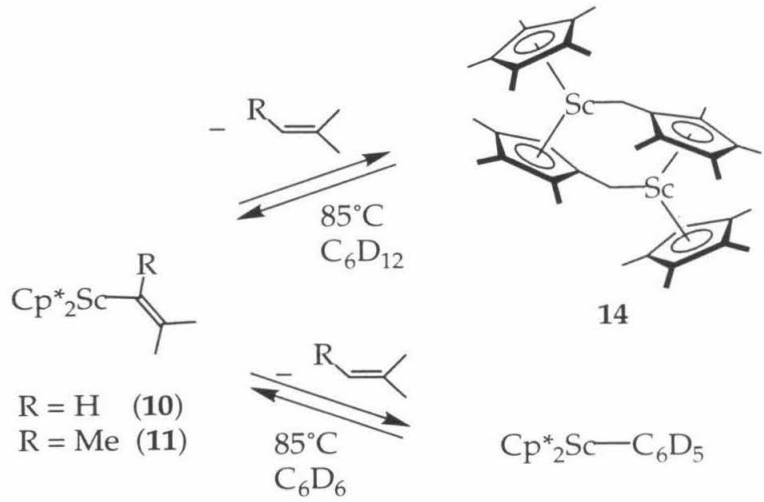

Scheme 3. Products resulting from thermolysis of **10** and **11**.

in the presence of 10 equivalents of isobutene in C_6D_6 greatly slows formation of the phenyl complex, the reaction reaching completion only after about 1 week. Analogously, the presence of 10 or more equivalents of the appropriate olefin precludes formation of **14** at 85 °C in C_6D_{12}, indeed, the ^1H NMR spectra of these reactions are unchanged even after 2 weeks. Thermolysis of isolated samples of **14** in C_6D_{12} in the presence of isobutene results in vinylic σ-bond metathesis to regenerate **10** at 85 °C. Consistent with these observations, isotope exchange at the vinylic position of 2-methyl-2-butene has been previously observed upon thermolysis with Cp^*_2ScD under an atmosphere of D_2.[12]

Reaction of **11** with 10 equivalents of *cis*-2-butene in C_6D_{12} at 85 °C does afford $Cp^*_2Sc(\eta^3\text{-}1\text{-}Me\text{-}C_3H_4)$ in moderate yield but decomposition is also observed. Cp^*_2ScMe also affords the η^3-crotyl complex under these conditions, but it appears that the methyl compound is not directly involved in the σ-bond metathesis reaction as very little methane is observed in the ^1H NMR spectra of the reaction mixture (5 - 25% of the expected value). The identity of the reacting species, perhaps an insertion product, is not readily apparent by inspection of the ^1H NMR spectra.

Addition of 5 equivalents of propylene to either **14** or **11** followed by thermolysis at 85 °C affords only decomposition. $Cp^*_2Sc(\eta^3\text{-}C_3H_5)$ has been previously synthesized[6] by addition of allene to Cp^*_2ScH and is stable at 70 °C.[2] Attempts to synthesize $Cp^*_2Sc(\eta^3\text{-}2\text{-}Me\text{-}C_3H_4)$ by addition of allene to Cp^*_2ScMe resulted in a 3:1 ratio (^1H NMR) of the desired product and $Cp^*_2ScC(H)=C=CH_2$ the product of σ-bond metathesis. Thermolysis of independently prepared samples of $Cp^*_2Sc(\eta^3\text{-}C_3H_5)$ in C_6D_6 solution in the presence of 5 equivalents of isobutene resulted in decomposition and no reaction was observed with 5 equivalents of *cis*-2-butene under the same conditions for 3 days. Thus, allyl compounds do not appear to be viable intermediates in the σ-bond metathesis reactions of Cp^*_2ScR compounds with olefins.

Reactions of $OpScC(Me)=CH(R)$ with Olefins (R = Me, $CHMe_2$)

Samples of **12** or **13** may be thermolyzed in the presence of up to 30 equivalents of the appropriate olefin in either C_6D_6 or C_6D_{12} solution to afford η^3-allyl complexes (**15** or **16**, Eqn 5). A preparative scale reaction was carried out

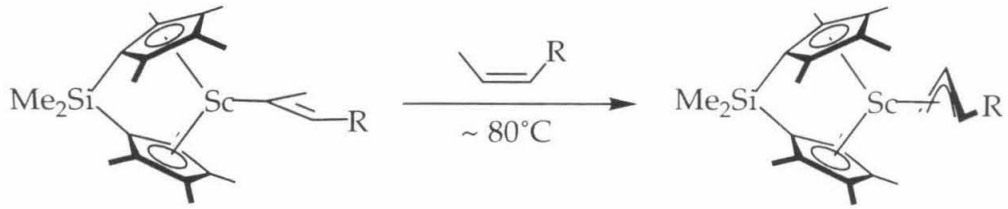

(5)

R = Me (**12**)
R = $CHMe_2$ (**13**)

R = Me (**15**)
R = $CHMe_2$ (**16**)

on a sample of **12** to afford crystals of **15** for X-ray analysis (*vide infra*). The excess olefin in these reactions is isomerized to a mixture of the *cis*-2-, *trans*-2-, and 1-olefin isomers, the latter of which is converted to the head-to-tail dimer under the reaction conditions (Eqn 6). When the thermolyses are carried out in the absence of olefin, a trace amount of free olefin is observed by ^1H NMR, which also isomerizes under the reaction conditions.

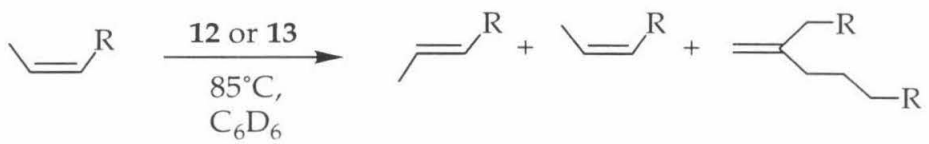

(6)

Under pseudo-first order conditions, clean kinetics are observed for all reactions and the obtained data indicates that the reactions are zero-order in olefin. The rate constants were obtained from the disappearance of the vinyl ^1H NMR resonances of **12** or **13** and can be found in Table 3. For all reactions except those carried out in the absence of added olefin in C_6D_6 (*vide infra*), identical rate constants are obtained from the appearance of the allyl methine ^1H NMR resonances of **15** and **16**. A representative kinetics trace can be found in Figure 3, and an Eyring plot based on the obtained rate data can be found in Figure 4. Activation parameters ($\Delta H^{\ddagger}$ = 22.8 (1.7) kcal·mol^{-1}, $\Delta S^{\ddagger}$ = -17 (2) eu) are consistent with σ-bond metathesis as the rate determining step.

Table 3. Observed Rate Constants for the Reactions of **12** and **13** with Olefins[a]

Compound	Olefin Conc. (M)	Temp. (K)	k_{obs} x 10^6 (s^{-1})[b]
12	0.15	345	6.7 (5)
12	1.04	345	5.9 (6)
12	0.32	355	15.3 (8)
12	0.76	355	13.9 (8)
12	0.38	365	39 (2)
12	0.78	365	33 (2)
12	0.36	375	116 (9)
12	0.59	375	104 (9)
12	0.91	375	88 (5)
12	0.23	385	190 (20)
12	0.38	385	190 (20)
13	0.88[c]	365	64 (4)
13	1.86[c]	365	58 (4)

[a][Sc] ≈ 0.04 M, olefin is *cis*-2-butene unless otherwise noted; [b]values reported are obtained from the disappearance of the vinyl ^{1}H NMR resonance of the starting material; [c]*cis*-4-methyl-2-pentene.

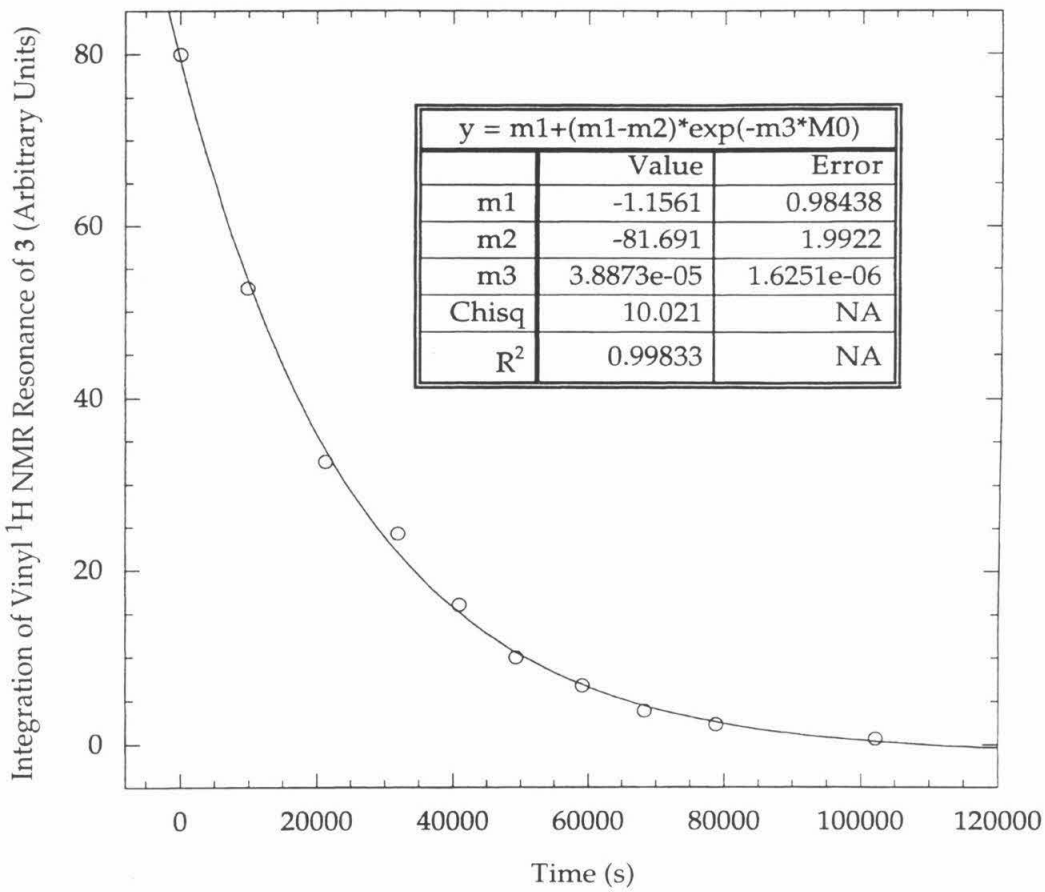

Figure 3. Representative kinetics trace for the conversion of **12** to **15** (cis-2-butene = 0.38 M, Temp = 365 K).

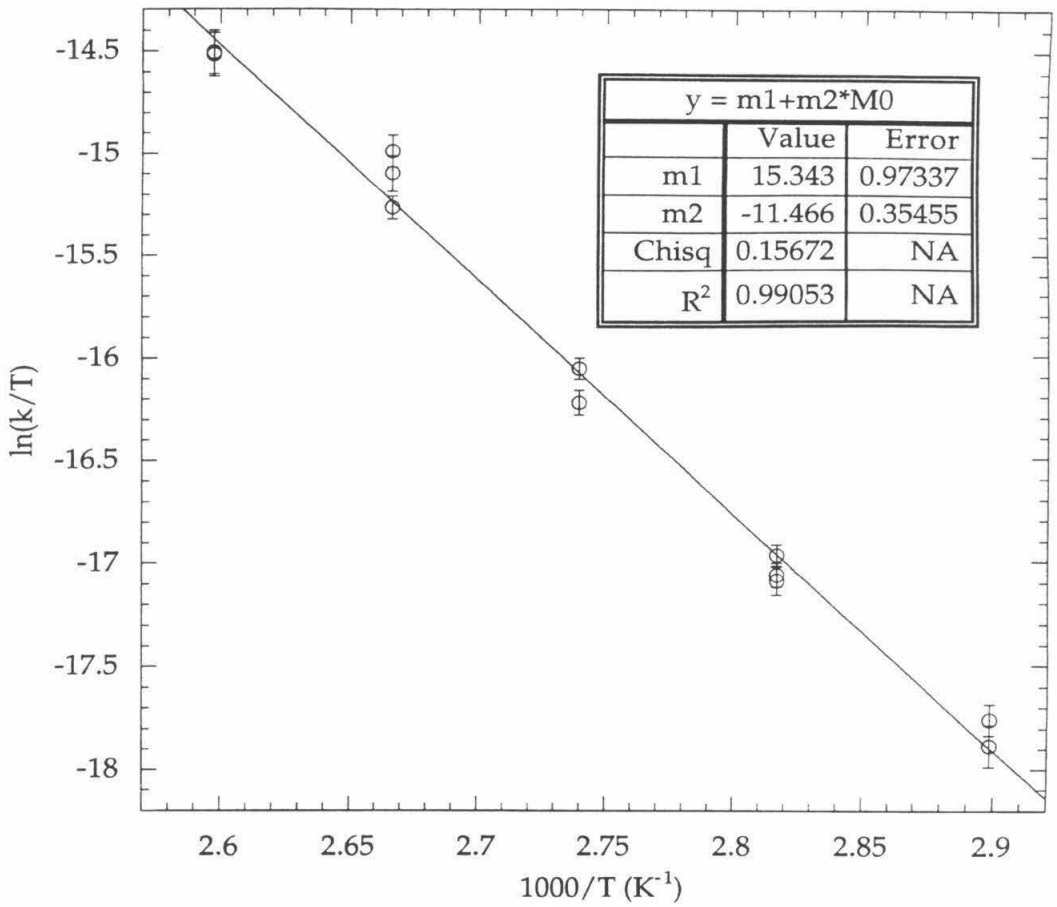

Figure 4. Eyring plot of observed rate constants for the conversion of **12** to **15**.

Thermolysis of **12** in the presence of various olefins results in formation of η^3-allyl scandocene products. A list of reaction conditions and observed products is shown in Table 4. Prior to heating, all of these reactions were allowed to stand for 24 hours at room temperature to test for olefin exchange. During this time propylene was completely converted to the head-to-tail dimer (Table 4, entry 4). However, olefin exchange by vinylic C-H σ-bond metathesis was not observed after the 24-hour induction period in any reaction and, indeed, even at 85 °C no alkenyl compound other than **12** was observed by ^{1}H NMR. The rate constants obtained for these reactions from the disappearance of the vinyl resonance of **12** are identical within experimental error to those measured in the presence of *cis*-2-butene under otherwise identical conditions.

Table 4. Conditions Used and Products Observed for Reactions of **12** with Olefins[a]

Olefin	Conc. (M)	Products	$k_{obs} \times 10^6$ (s^{-1})[b]
cis-2-butene	0.88	**15**	5.9 (2)
isobutene	0.20	**15** + $OpSc(\eta^3\text{-}2\text{-}Me\text{-}C_3H_4)$[c]	not measured
isobutene[d]	1.05	$OpSc(\eta^3\text{-}2\text{-}Me\text{-}C_3H_4)$	not measured
propylene	0.21	**15** + $OpSc(\eta^3\text{-}2\text{-}^n Pr\text{-}C_3H_4)$[e]	not measured
cis-2-pentene	0.45	$OpSc(\eta^3\text{-}1\text{-}^n Pr\text{-}C_3H_4)$	5.3 (4)
cis-4-methyl-2-pentene	0.40	$OpSc(\eta^3\text{-}1\text{-}CHMe_2\text{-}C_3H_4)$	6.0 (3)

[a][Sc] ≈ 0.04 M; all reactions were carried out in C_6D_6; [b]values reported are obtained from the disappearance of the vinyl ^1H NMR resonance of the starting material; [c]*ca.* 1:4 ratio; [d]85 °C; [e]*ca.* 4:1 ratio.

A side product, $OpScC_6D_5$, is observed when **12** is thermolyzed in the absence of olefin in C_6D_6 solution. At intermediate reaction times, this compound accounts for approximately 30% of the total organometallic species in solution but it is eventually completely consumed. Formation of the phenyl compound is greatly suppressed in the presence of a minute excess of olefin, and in the presence of five or more olefin equivalents it is not observed. Heating a solution of $OpScMe(PMe_3)$[16] in benzene for 20 minutes at 85 °C results in clean conversion to $OpScC_6H_5$ (**17**) (Eqn 7). The cyclopentadienyl methyl and silyl methyl ^1H NMR signals for isolated **17** are identical to those observed for $OpScC_6D_5$.

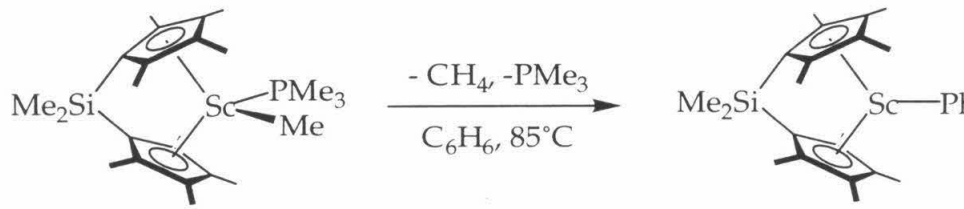

(7)

17

When **17** is thermolyzed at 85 °C in C_6D_6 in the presence of 5 - 30 equivalents of *cis*-2-butene, the ^1H NMR spectrum of the reaction mixture is reduced to a few broad features over the course of 2 days; a small amount of **15**

is also observed (< 10% of total organometallic products). Olefin isomerization also occurs, but at a much slower rate than observed during thermolysis of **12**. Surprisingly, a C_6D_6 solution of **17** shows total decomposition after 1 week even at room temperature. Thus, it appears that **17** is not a viable intermediate on the pathway to formation of **15** or **16**.

Simply allowing a suspension of OpScH(PMe_3) in C_6D_6 to stand for three days at room temperature results in the loss of one of the two cyclopentadienyl methyl ^1H NMR signals. Surprisingly, the rate of this H/D exchange reaction is not accelerated by the addition of D_2, although the product obtained is slightly purer. No deuterium incorporation into the methyl groups is observed upon addition of D_2 to a suspension of OpScH(PMe_3) in either C_6H_6 or toluene. Apparently, reaction with solvent is comparable in energy to reaction with D_2. Addition of 2-butyne to the deuterated sample of OpScD(PMe_3) affords the deuterated analog of **12** (Eqn 8). As the hydride resonance cannot be located in the ^1H NMR spectrum of OpScH(PMe_3), integration of the vinyl resonance of

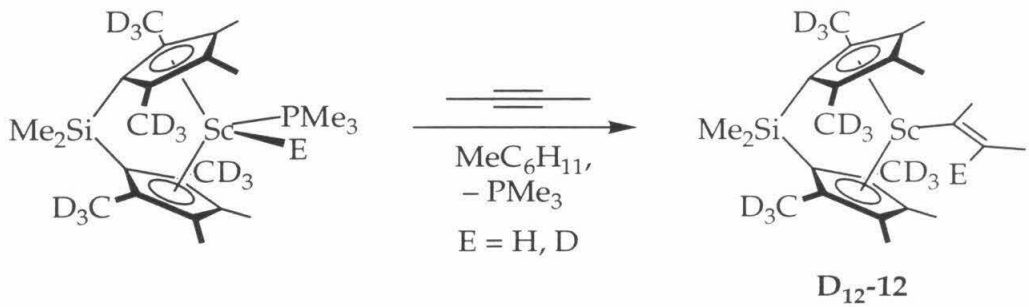

(8)

D_{12}-12

deuterated **12** is the only measure of the amount of deuterium incorporation into the scandium hydride. In this way, it was discovered that isotope exchange into the hydride position occurs at a greater rate than exchange into the cyclopentadienyl methyl positions as the Sc-D can be hydrogenated to Sc-H without exchange into the cyclopentadienyl methyl groups by stirring under an H_2 atmosphere for short periods of time.[17] The isotopomer of **12** with deuterium in the butenyl vinyl position evidences the low-field IR C-D stretch indicative of a β-agostic structure (ν_{CD} = 1943 cm^{-1}; calculated = 1882 cm^{-1}).

A difference NOE experiment was performed to assign the ^1H NMR resonances for **12**. NOE enhancement is observed between the silyl methyl signal (δ 0.98) and the downfield cyclopentadienyl methyl signal (δ 1.91). Upon irradiation of the upfield cyclopentadienyl methyl signal (δ 1.81), NOE

enhancement is not observed in any resonance. The results of this experiment as well as the ^{1}H NMR spectra for **12** and **D_{12}-12** are presented in Figure 5. The ^{1}H NMR resonance that is absent in **D_{12}-12** corresponds to the methyl groups adjacent to the $SiMe_2$ linker in the narrow part of the metallocene wedge.

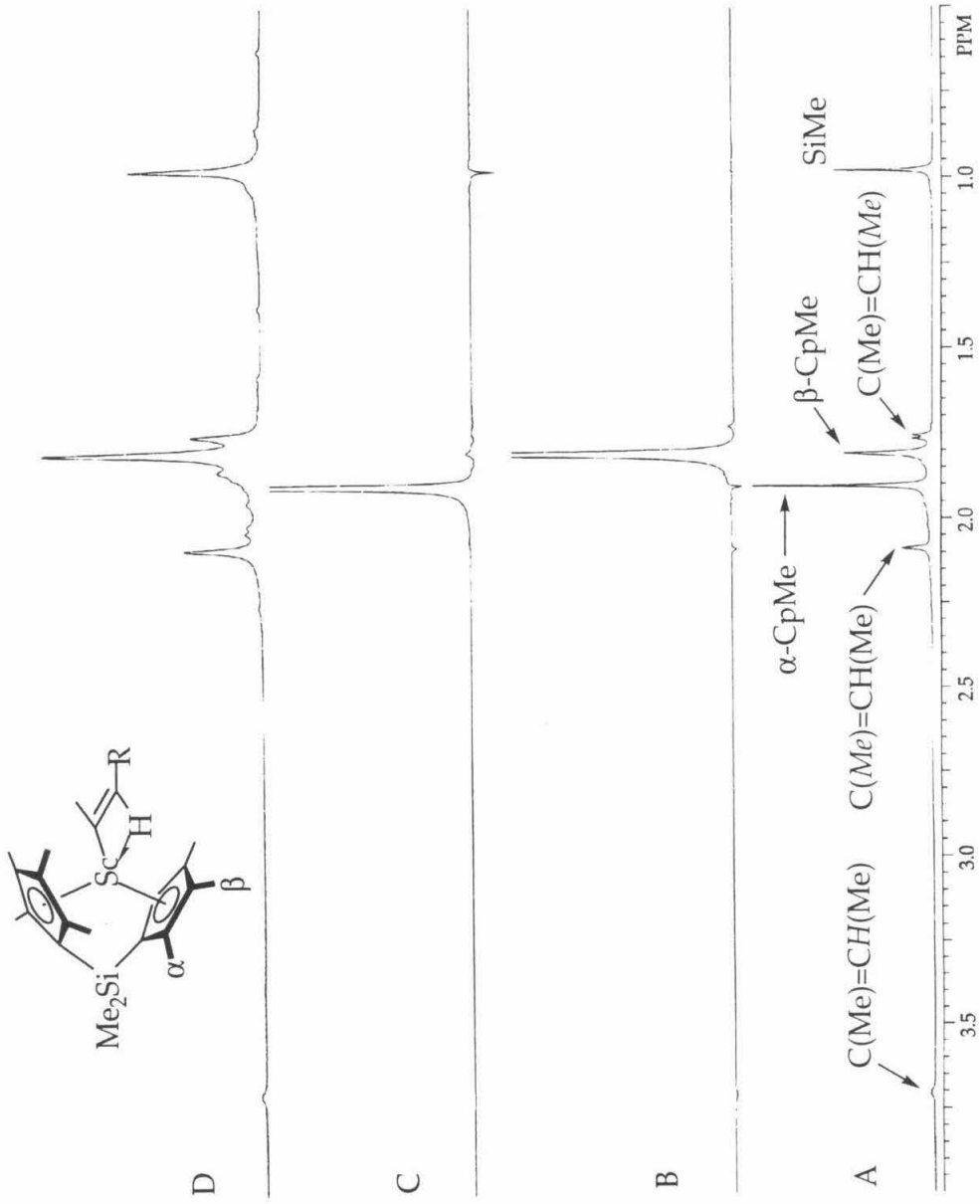

Figure 5. Stack plot of ^{1}H NMR spectra detailing the assignment of resonances for **12**; all spectra were acquired in C_6D_6. **A.** ^{1}H NMR spectrum of **12**. **B**. Difference NOE spectrum obtained from irriadiation of the resonance at δ 1.8. **C**. Difference NOE spectrum obtained from irriadiation of the resonance at δ 1.9. **D**. ^{1}H NMR spectrum of **D_{12}12**.

The mechanism proposed for deuteration of the Op ligand is shown in Scheme 4. For OpScH(PMe)$_3$, intramolecular σ-bond metathesis leads to a tuck-in complex in which the scandium is bound to a carbon atom in the rear of the metallocene wedge (**14**). Reaction of this intermediate with either D_2 or C_6D_6 results in the incorporation of one deuterium atom into the methyl group, and the repetition of these processes results in the complete substitution of deuterium for hydrogen in the α-methyl positions. The frontier molecular orbitals of an *ansa*-metallocene are located in a belt at the front of the wedge,[18] thus it is somewhat surprising to infer a scandium-carbon bond away from this

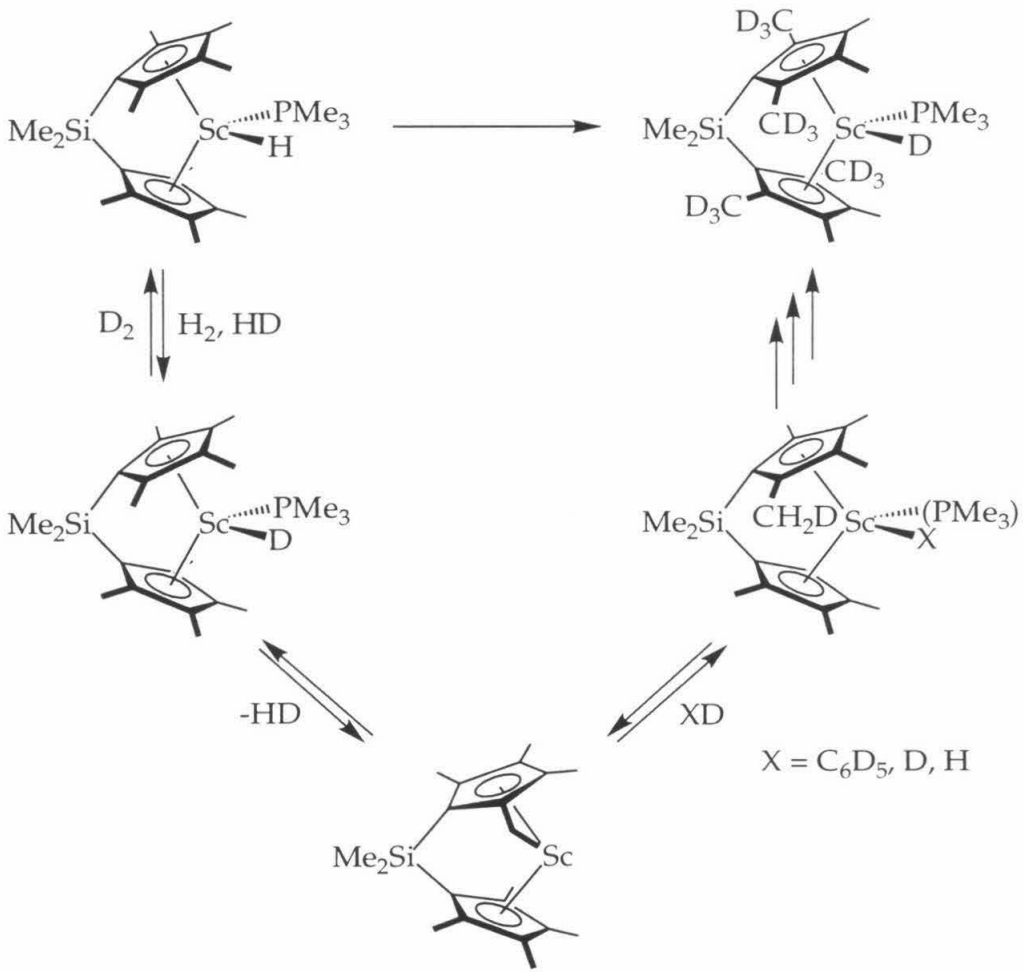

14

Scheme 4. Mechanism proposed for isotope exchange into the α-methyl groups of OpScH(PMe$_3$).

region. It may be that the methyl groups in the front of the wedge simply project out too far from the scandium center to engage in effective orbital overlap. Consistent with this mechanistic proposal, the X-ray structure of {$Me_2Si[(\eta^5\text{-}C_5Me_4)(\eta^5;\eta^1\text{-}C_5Me_4CH_2)]$}TiPh has recently appeared in which the titanium is bound to the carbon α-to the Me_2Si linker.[19]

As expected, thermolysis of **D_{12}-12** at 85 °C in either C_6D_6 or C_6D_{12} solution in the presence of 0 - 15 equivalents of *cis*-2-butene affords an η^3- crotyl compound. A small resonance is observed in the ^1H NMR of the crotyl product which corresponds to the cyclopentadienyl methyl group position that was completely deuterated in the starting material (Eqn 9). This indicates that the

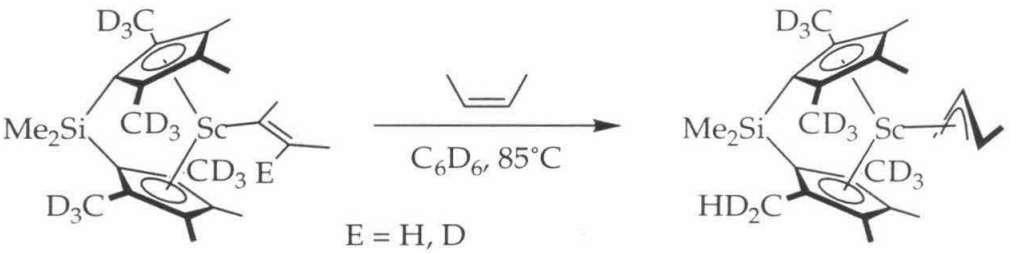

D_{12}-12 **D_{11}-15** (9)

intermediate on the pathway to formation of the allyl complexes is the same as that in the deuteration of $OpScH(PMe_3)$, namely **14**. The measurement of rate constants for the transformation of **D_{12}-12** to **D_n-15** has been problematic, thus the value of the kinetic isotope effect for this reaction has not been established. The rate constants are most conveniently measured by monitoring the disappearance of the butenyl vinyl ^1H NMR resonance of **D_{12}-12** during the reactions, and widely varying measurements are obtained depending on the isotopic composition of this position in the starting material.

Reactions of $OpSc(\eta^3\text{-}C_4H_7)$ with Olefins

Isolated **15** is thermally stable at 85 °C for periods longer than 1 week showing no appreciable decomposition by ^1H NMR. Thermolysis of **15** in C_6D_6 at 85 °C in the presence of 15 equivalents of isobutene, however, results in formation of an equilibrium mixture of **15** and $OpSc(\eta^3\text{-}2\text{-}Me\text{-}C_3H_4)$ (Eqn 10). An exact equilibrium constant for this system has not been determined but the equilibrium is weighted toward the crotyl complex presumably due to unfavorable steric interactions for the 2-methallyl compound.

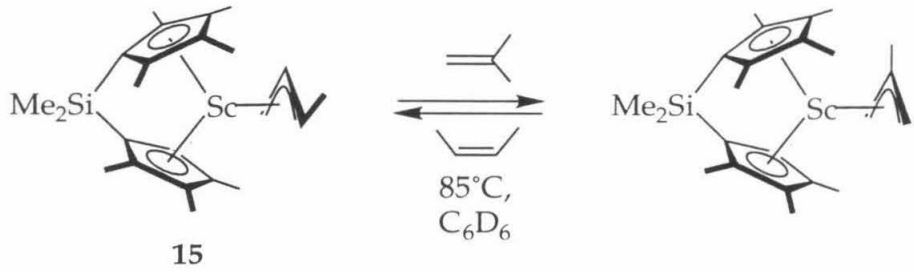

15 (10)

Interestingly, thermolysis of **15** at 85 °C in C_6D_6 in the presence of *cis*-2-butene results in isomerization of the olefin to the same mixture of *cis*-2-butene, *trans*-2-butene, and 1-butene dimer observed during thermolysis of **12** (Eqn 11).

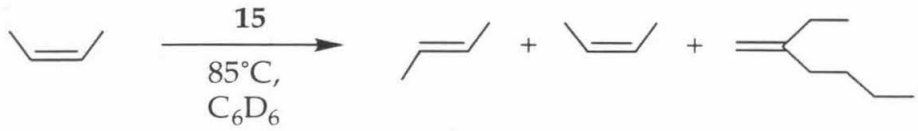

(11)

Based on this result, a mechanism for olefin isomerization is proposed (Scheme 6). Reversible changes in hapticity of the crotyl ligand in **15** are rapid even on the NMR timescale at room temperature as the crotyl methylene resonances are broadened into the baseline. Due to the crotyl ligand's asymmetry, two pathways are available for the hapticity change (Scheme 5, pathways (i) and (ii)). Intramolecular σ-bond metathesis can then occur from either η^1-allyl intermediate generating **14** and an isomer of butene. It should be noted that cis/trans isomerization requires formation of the unfavored stereoisomer of **15** which contains a *cis*-methyl group. It is unknown how 1-butene is dimerized, but evidently such processes are facile in this system as propylene is dimerized in hours at room temperature by **12** (*vide supra*). Consistent with this proposed mechanism, Evans observed three isomeric samarocene carboxylates upon addition of CO_2 to $Cp^*_2Sm(\eta^3\text{-}1\text{-}Me\text{-}C_3H_4)$ corresponding to the three isomers of butene observed herein.[20] Additionally, Horton has reported the generation of a tuck-in compound through intramolecular σ-bond metathesis of a cationic zirconocene η^3-allyl compound, $[Cp^*_2Zr(\eta^3\text{-}1,3\text{-}Me_2\text{-}C_3H_3)]B(C_6F_5)_4$.[21]

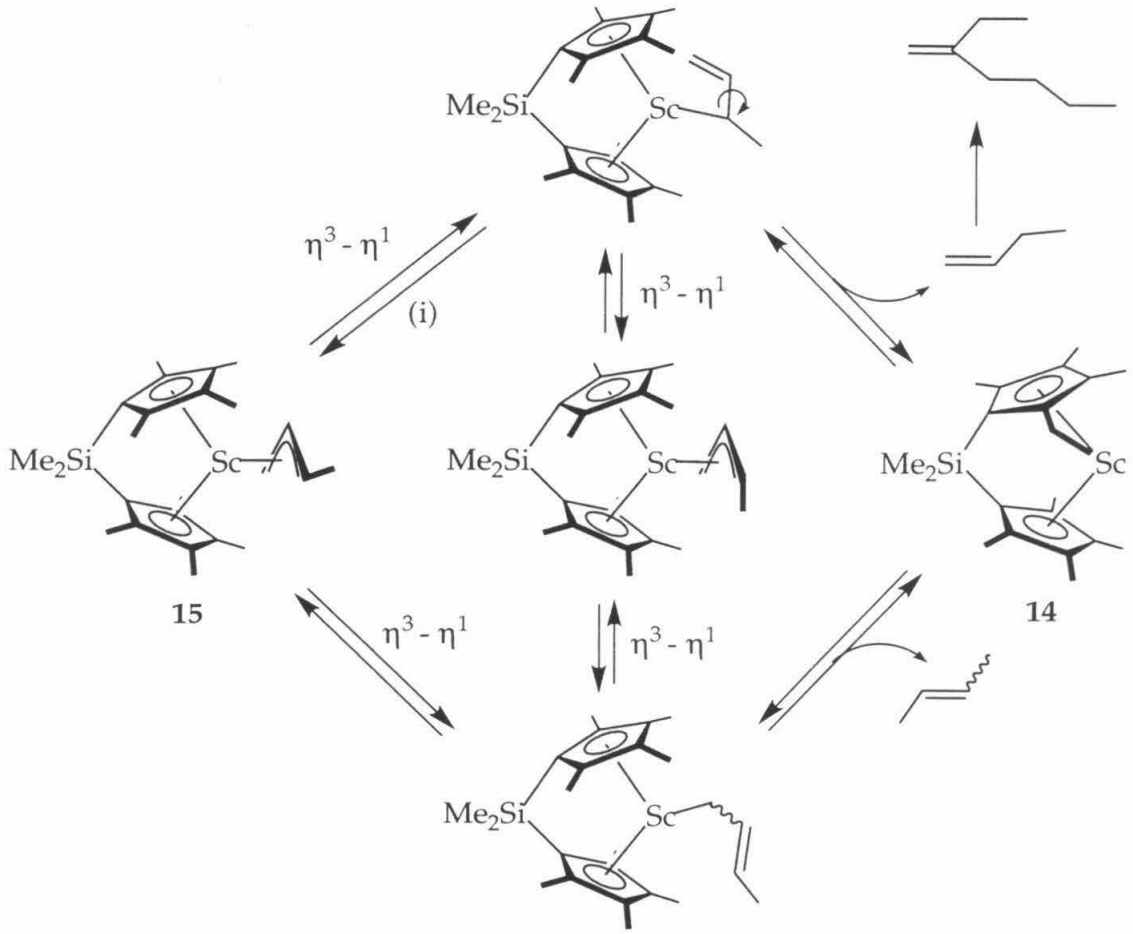

Scheme 5. Proposed mechanism for olefin isomerization catalyzed by **15**.

X-ray Structure Determination for OpSc(η^3-C_4H_7) (15)

Upon slow cooling of a saturated toluene solution of **15** from 80 °C single crystals precipitated as orange plates and an X-ray structure determination was completed. Refinement of the obtained data revealed disorder in the crotyl ligand involving rotation about the C_2-axis defined by the cyclopentadienyl ligand set; the disorder was modeled as a 65:35 population of sites. The major rotamer was refined anisotropically with bond distances restrained to reasonable values and the anisotropic displacement parameters restrained to approximately isotropic behavior. The minor rotamer was then refined isotropically with distances and angles restrained to be similar to those of the major isomer. The structure of the molecule oriented in the major position is shown in Figure 6, and selected bond lengths and angles are given in Table 5. Additional information,

including details of the data collection and solution and refinement of the structure can be found in Appendix 2.

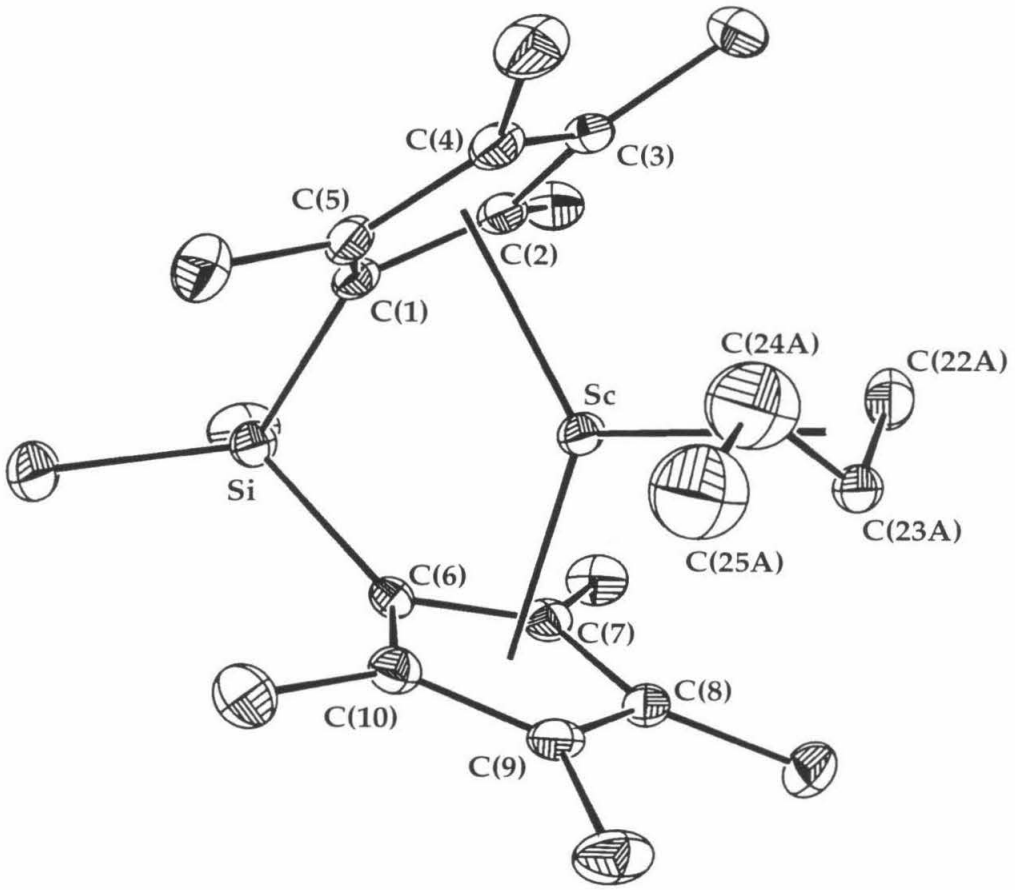

Figure 6. ORTEP representation of the molecular structure of **15** with selected atoms labeled (50% probability ellipsoids, hydrogens omitted for clarity).

If one considers the bonds from scandium to the centroid of each ligand, the scandium can be described by approximately trigonal planar geometry. The Cp centroid-Sc-Cp centroid angle is 130.6 (1)°, and the Cp centroid-Sc-crotyl centroid angles are between 113° and 115°. For each crotyl site the sum of the centroid-Sc-centroid angles is 360°, indicating that the metal center and all four centroids are coplanar. The Sc-Cp centroid bond lengths (2.211 (1) Å and 2.201 (1) Å) are within the normal range for Sc-Cp bond lengths (2.170 Å- 2.212 Å).[2,6,15] The Cp centroid-Sc-Cp centroid angle agrees well with the same angles of other reported crystallographically characterized *ansa*-scandocene allyl

compounds, *rac*-($Me_2Si\{C_5H_2$-2,4-$[CH(Me_2)]_2\}_2$)$Sc(\eta^3$-$C_3H_5)$ and *meso*-($Me_2Si\{C_5H_2$-2,4-$[CH(Me_2)]_2\}_2$)$Sc(\eta^3$-1-Me-$C_3H_4)$[22] (128.5 (2) and 128.7 (2), respectively). The crotyl methyl group is in a trans-like arrangement with the opposite carbon in accordance with sterics. The angle between the Sc-Ct(3) bond vector and the plane defined by C(22A), C(23A), C(24A), and C(25A) is 158.4°, with the central allyl carbon tilted toward the scandium center

Table 5. Selected Bond Distances (Å) and Bond Angles (°) Obtained From the X-Ray Structure Determination of **15**

Feature	Distance (Å) or Angle (°)	Feature	Distance (Å) or Angle (°)
Sc-Ct(1)[a]	2.211 (2)	Sc-Ct(2)[b]	2.201 (2)
Sc-Ct(3)[c]	2.240 (2)	Sc-Ct(4)[d]	2.154 (4)
Sc-C(22A)	2.459 (5)	Sc-C(23A)	2.469 (4)
Sc-C(24A)	2.496 (6)	Sc-C(22B)	2.458 (8)
Sc-C(23B)	2.471 (13)	Sc-C(24B)	2.256 (17)
C(22A)-C(23A)	1.430 (1)	C(23A)-C(24A)	1.426 (1)
C(24A)-C(25A)	1.507 (1)	C(22B)-C(23B)	1.429 (2)
C(23B)-C(24B)	1.425 (2)	C(24B)-C(25B)	1.507 (2)
Ct(1)-Sc-Ct(2)[a,b]	130.6 (1)	Ct(1)-Sc-Ct(3)[a,c]	115.9 (3)
Ct(2)-Sc-Ct(3)[b,c]	113.5 (3)	Ct(1)-Sc-Ct(4)[a,d]	115.7 (5)
Ct(2)-Sc-Ct(4)[b,d]	113.5 (5)	C(22A)-C(23A)-C(24A)	116.6 (3)
C(23A)-C(24A)-C(25A)	122.0 (4)	C(22B)-C(23B)-C(24B)	116.5 (4)
C(23B)-C(24B)-C(25B)	122.1 (5)		

[a]Ct(1) is defined as the centroid of the ring made up of C(1) - C(5); [b]Ct(2) is defined as the centroid of the ring made up of C(6) - C(10); [c]Ct(3) is defined as the centroid of the crotyl ligand in the major isomer made up of C(22A) - C(24A); [d]Ct(4) is defined as the centroid of the crotyl ligand in the minor isomer made up of C(22B) - C(24B)

The crotyl ligands in each site appear to be symmetrically bonded trihapto structures. While one of the Sc-C bond lengths for the minor isomer is very short (Sc-C(24B) = 2.256 (17)), the large error involved in the refinement due to

the disorder means that the value is most likely anomalous. The Sc-C(22A) and Sc-C(24A) bond lengths of 2.459 (5) Å, and 2.496 (6) Å, respectively, are only slightly greater than 3σ apart, and the C-C bond lengths in each allyl site are equivalent within standard deviation. Thus, there appears to be no distortion toward an η^1-structure for **15** in the solid state.

Conclusions

Two new *ansa*-scandocene alkenyl compounds have been synthesized and found to have β-agostic ground state structures. Variable temperature ^{1}H NMR studies establish that the agostic interactions are very weak, on the order of 1 - 3 kcal·mol^{-1}. Reaction of these *ansa*-scandocene alkenyl compounds with olefins results in the formation of η^3-allyl complexes (see Tables 3 and 4). Kinetics and labeling experiments indicate a tuck-in intermediate with the scandium bound to the methyl group carbon adjacent to the silyl linker in the rear of the metallocene wedge.

During reactions of **12** and **13** with various olefins, vinylic σ-bond metathesis was never observed. In contrast to this, reactions of permethylscandocene alkenyl compounds (**10** and **11**) with olefins resulted, almost exclusively, in vinylic C-H bond activation. The selectivity for σ-bond metathesis for permethylscandocene derivatives is dominated by transition state effects.[6] For reactions with olefins, therefore, alkenyl products are observed to the exclusion of η^3-allyl products as the greater *s*-character in a vinylic C-H bond affords much better transition state bonding. This is in contrast to olefin activation with lanthanidocene compounds[5] as well as with Op ligated scandocenes (described above) in which the thermodynamically preferred η^3-allyl products are observed.

Shown below (Figure 7) are representations of the σ-bond metathesis transition states for reaction with olefins both including and excluding olefin π-coordination; it can be seen that adverse steric effects will be much greater when the olefin is allowed to coordinate through its π-system. Thus, the extremely oppressive environment afforded by the *bis*-pentamethylcyclopentadienyl ligand array only allows for vinylic activation. It seems that relieving transition state steric interactions between the cyclopentadienyl rings and the olefin by either linking the rings together or using a larger lanthanide metal may allow for olefin coordination, stabilizing the transition state for allylic σ-bond metathesis. Recent

calculations on the mechanism of allyl formation during polymerizations with metallocene catalysts support this assertion.[9,10]

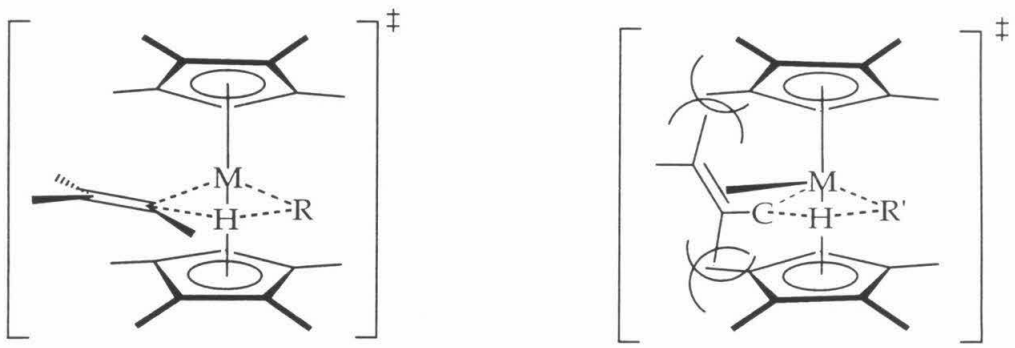

does not allow for olefin π-coordination

includes olefin π-coordination

Figure 7. Representations of the transition states for olefinic σ-bond metathesis both including and excluding olefin π-bonding.

Experimental Section

General Considerations

All air and/or moisture sensitive compounds were manipulated using standard high-vacuum line, Schlenk, or cannula techniques, or in a glove box under a nitrogen atmosphere, as described previously.[23] Argon, hydrogen and deuterium gases were purified and dried by passage through columns of MnO on vermiculite and activated 4 Å molecular sieves. Solvents were stored under vacuum over titanocene[24] or sodium benzophenone ketyl. The syntheses of $Cp^*_2ScC(H)=CMe_2$ (**10**),[6] $Cp^*_2ScC(Me)=CMe_2$ (**11**),[12] $OpScH(PMe_3)$,[7] $OpScMe(PMe_3)$,[16] and $Cp^*_2Sc(\eta^3\text{-}C_3H_5)$[6] were carried out as previously reported. 2-Butyne (Aldrich), *cis*-2-pentene (Aldrich), 4-methyl-2-pentyne (ChemSampCo), and *cis*-4-methyl-2-pentene (Aldrich) were purchased and stored over CaH_2. Isobutene was purchased (Aldrich), dried with Al(*i*-Bu)$_3$ then stored in a thick-walled glass vessel. *Cis*- and *trans*-2-butene were purchased (Matheson) and stored over activated 4 Å molecular sieves in thick-walled glass vessels. Propylene was purchased and stored as a dilute solution in Al^iBu_3 in a thick-walled glass bomb.

NMR spectra were recorded on Bruker AM500 and (500.13 MHz for ^1H) and Varian ^{UNITY}INOVA 500 (499.853 MHz for ^1H) spectrometers. Elemental

analyses were carried out at the Caltech Elemental Analysis Facility by Fenton Harvey. Many of the compounds failed to give satisfactory carbon/hydrogen analyses, even when combusted with added V_2O_5 oxidant. Moreover, in many cases the results were inconsistent from run to run.

Preparation of (*E*)-{$Me_2Si[\eta^5\text{-}C_5Me_4]_2$}ScC(Me)=CH(Me) (12). In an inert atmosphere glove box, a 50 mL Kjeldahl flask was loaded with OpScH(PMe_3) (0.72g, 1.71 mmol) and the flask attached to a 180° needle valve adapter. Methylcyclohexane (15 mL) was added by vacuum transfer at -78 °C. 2-Butyne (0.2 mL, 2.56 mmol) was then added by vacuum transfer at -78 °C. The reaction was stirred for 20 hours at which time the solvent was removed and the flask was transferred to a swivel frit assembly. Petroleum ether (8 mL) was added by vacuum transfer and the bright yellow precipitate was isolated by filtration. The product was washed once with petroleum ether and then dried for 3 hours in vacuo. Yield = 0.48 g (1.20 mmol), 70%. A second crop may also be isolated after drying the filtrate by filtration using 1 mL of petroleum ether. Anal. Calcd for $C_{24}H_{37}ScSi$: C, 72.32; H, 9.36; Found: C, 72.41; H, 10.07. IR (C_6D_6): ν_{CH} (agostic) 2578 cm^{-1}. ^1H NMR (C_6D_6): δ 3.71 (m (br), $Sc(CH_3)C{=}CH(CH_3)$, 1H), 2.09 (s, $Sc(CH_3)C{=}CH(CH_3)$, 3H), 1.91 (s, α-$C_5(CH_3)_4$, 12H), 1.81 (s, β-$C_5(CH_3)_4$, 12H), 1.76 (d, $Sc(CH_3)C{=}CH(CH_3)$, 3H, J = 5 Hz), 0.98 (s, $Si(CH_3)_2$, 6H).

Preparation of (*E*)-{$Me_2Si[\eta^5\text{-}C_5Me_4]_2$}ScC(Me)=CH(CHMe$_2$) (13). In an inert atmosphere glove box a 25 mL Kjeldahl flask was charged with OpScH(PMe_3) (0.305 g, 0.725 mmol) and the flask attached to a calibrated gas measure. Methylcyclohexane (8 mL) was added by vacuum transfer at -78 °C. 4-Methyl-2-pentyne (1.09 mmol) was then measured into the gas bulb and added to the solution at -78 °C. The solution was stirred for 75 min. at which time the solvent was removed and the flask was attached to a 180° needle valve adapter. Petroleum ether (3 mL) was added by vacuum transfer at -78 °C and the solution was warmed to room temperature. The volume of the solvent was reduced until the product began to precipitate (~0.5 mL) and the solution was heated to 80 °C and allowed to slowly cool back to room temperature. The flask assembly was loaded into an inert atmosphere glove box where the light orange crystalline material was washed twice with 0.5 mL portions of petroleum ether. The product was dried in vacuo for 3 hours. Yield = 0.204 g (0.478 mmol), 66%. Anal. Calcd for $C_{26}H_{41}ScSi$: C, 73.19; H, 9.69. Found: C, 71.33; H, 9.97. IR (C_6D_6): ν(CH) (agostic) 2568 cm^{-1}. ^1H NMR (C_6D_6): δ 3.64 (dd, ScC(Me)=C*H*(iPr), 1H, J =

6.2 Hz, 1.6 Hz), 2.82 (oct, ScC(Me)=CH(C*H*(CH_3)$_2$), 1H, J = 6.7 Hz), 2.08 (d, ScC(C*H*$_3$)=CH(iPr), 3H, J = 1.6 Hz), 1.93 (s, C_5(C*H*$_3$)$_4$, 12H), 1.84 (s, C_5(C*H*$_3$)$_4$, 12H), 1.01 (d, ScC(Me)=CH(CH(C*H*$_3$)$_2$), 6H, J = 6.7 Hz), 0.97 (s, Si(C*H*$_3$)$_2$, 6H).

Preparation of {Me$_2$Si[η^5-C$_5$Me$_4$]$_2$}Sc(η^3-C$_4$H$_7$) (15). In an inert atmosphere glove box, a thick walled glass bomb was charged with **12** (0.110 g, 0.276 mmol). Benzene (5 mL) was added by vacuum transfer at -78 °C. *Cis*-2-butene (5.52 mmol, 20 equiv.) was then condensed into the assembly at 77 K from a calibrated gas bulb. When the solution had thawed, the bomb was placed in an 85 °C oil bath behind a protective shield for 7 days. After this time, the product deposited as large red plates which were isolated by pipetting off the solvent along with a grey powdery byproduct in an inert atmosphere glove box. The isolated crystals were dried in vacuo for 3 hours. Yield = 40 mg (0.100 mmol), 36%. Anal. Calcd for $C_{24}H_{37}ScSi$: C, 72.32; H, 9.36; Found: C, 72.69, 72.64; H, 10.29, 10.09. ^{1}H NMR (C_6D_6, 292 K): δ 6.77 (m, $CH_2C\mathit{H}CH(CH_3)$, 1H), 4.43 (m, $CH_2CHC\mathit{H}(CH_3)$, 1H), 2.01 (s, α-C_5(C*H*$_3$)4, 12H), 1.67 (s, β-C_5(C*H*$_3$)$_4$, 12H), 1.13 (d, $CH_2CHCH(C\mathit{H}_3)$, 3H, J = 6 Hz), 0.89 (s, Si(C*H*$_3$)$_2$, 6H). The $C\mathit{H}_2CHCH(CH_3)$ resonance(s) could not be located at this temperature.

Preparation of {Me$_2$Si[η^5-C$_5$Me$_4$]$_2$}ScC$_6$H$_5$ (17). In an inert atmosphere glove box a thick walled glass bomb was loaded with OpScMe(PMe$_3$) (0.12g, 0.276 mmol). Benzene (7 mL) was added by vacuum transfer at -78 °C and the reaction vessel was then placed in an 85 °C oil bath for 20 min. Following this, the solvent was removed in vacuo and the solid was transferred to a 10 mL Kjeldahl flask as a slurry in petroleum ether. The flask was attached to a swivel frit assembly and the slurry concentrated to ~ 2 mL. Filtration isolated a yellow/grey solid which was washed once and dried in vacuo. Yield = 45 mg (0.107 mmol), 39%. Anal. Calcd for $C_{26}H_{35}ScSi$: C, 74.25; H 8.39. Found: C, 72.46, 72.53; H, 8.71, 8.80. ^{1}H NMR (C_6D_6): δ 7.35 (t, *m*-C_6H_5, 2H, J = 7 Hz), 7.26 (t, *p*-C_6H_5, 1H, J = 7 Hz), 6.93 (d, *o*-C_6H_5, 2H, J = 7 Hz), 1.82 (s, C_5(C*H*$_3$)$_4$, 12H), 1.59 (s, C_5(C*H*$_3$)$_4$, 12H), 1.02 (s, Si(C*H*$_3$)$_2$, 6H).

Preparation of D$_{12}$-{Me$_2$Si[η^5-C$_5$Me$_4$]$_2$}ScE(PMe$_3$) (E = H, D). In an inert atmosphere glove box, a thick walled glass bomb was charged with OpScH(PMe$_3$) (0.22 g, 0.52 mmol). Benzene-d$_6$ (~ 20 mL) was added by vacuum transfer at -78 °C followed by addition of 1 atm of D_2 at 77 K. The vessel was attached to an agitater and the reaction allowed to proceed for 6 days. The solvent was then removed in vacuo and the solid was transferred to a 25 mL Kjeldahl flask as a slurry in pet. ether. The flask was attached to a swivel frit

assembly, the volume of solvent was reduced to ~ 8 mL and the off-white solid was isolated by filtration. Yield = 0.135 g (0.312 mmol) = 61%. Following the above procedure results in isolation of a compound which is ~90% deuterated in the scandium hydride position.

Preparation of (*E*)-D_{12}-{$Me_2Si[\eta^5$-$C_5Me_4]_2$}ScC(H)=CE(Me) (E = H, D) (D_{12}-12). In an inert atmosphere glove box a 25 mL Kjeldahl flask was loaded with D_{12}-OpScH(PMe_3) (0.13 g, 0.30 mmol) and attached to a calibrated gas measure. Methylcyclohexane (15 mL) was added by vacuum transfer followed by addition of 2-butyne (0.361 mmol) at –78 °C. The reaction was stirred for 10 hours and the solvent was then removed in vacuo. The reaction flask was attached to a swivel frit assembly and petroleum ether (1 mL) was added by vacuum transfer. The bright yellow solid was isolated by filtration. Yield = 0.075g (0.18 mmol), 51%. IR (C_6D_6): ν_{CD} (agostic) 1943 cm^{-1} (calculated, 1882 cm^{-1}). The ^1H NMR for this compound is identical to that for **12** except the ligand methyl resonance at δ 1.91 is absent.

Thermolysis reactions of alkenyl compounds (10 - 13). In an inert atmosphere glove box, the appropriate compound (~ 10 mg) was loaded into a J. Young NMR tube. For reactions where kinetics measurements were made, a small amount of sublimed ferrocene was also added to the tube as internal standard. Deuterated solvent (~ 0.5 mL) was added by vacuum transfer at –78 °C followed by addition of olefin, if necessary, using a calibrated gas measure at 77 K. The solution was thawed in a room temperature water bath and the tube was then placed in an oil bath at the appropriate temperature. NMR spectra were recorded at room temperature.

Variable-temperature ^1H NMR experiments. The NMR samples were brought to the lowest temperature available for measurement (~ –85 °C for toluene-d_8, ~ –105 °C for THF-d_8) and allowed to equilibrate for ~ 20 minutes. Spectra were then recorded at intervals of increasing temperature, equilibrating for 5 - 10 minutes at each iteration. Probe temperatures were then calculated using the same procedure with a pure methanol sample.

Structure determination for (η^5-$C_5Me_5)_2ScC(H)=CMe_2$ (10) and {$Me_2Si[\eta^5$-$C_5Me_4]_2$}Sc(η^3-1-Me-C_3H_4) (15). Fragments cut from single crystals of **10** and **15** under paratone oil were attached to glass fibers and centered on an Enraf-Nonius CAD-4 diffractometer under a stream of cold N_2 gas. Unit cell parameters and an orientation matrix were obtained by a least-squares calculation based on the setting angles of 25 reflections with $12.5° < \theta < 13.3°$ for

10 and $12.0° < \theta < 14.0°$ for **15**. During the data collections, three reference reflections were measured every hour and showed no significant decay. Two equivalent data sets were collected for each. Absorption correction was done by Ψ-scans for **10** with an absorption coefficient of 0.336 mm^{-1}. No correction was made for decay or absorption for **15**. Lorentz and polarization factors were applied for each molecule, and the two data sets for each were then merged. The structures for both were solved by direct methods which revealed all non-hydrogen atom positions (SHELXS). Subsequent difference Fourier maps were successful in finding all hydrogens except those for the minor alkenyl isomer for **10** and all hydrogens except those on the crotyl ligand for **15**. In the refinement of **10**, disorder in the isobutenyl ligand was modeled as separate groups with a 75:25 population of sites. The major component was refined anisotropically with isotropic hydrogens. The minor component was refined isotropically with hydrogens in calculated positions. All other non-hydrogen atoms were refined anisotropically and all other hydrogens were refined with displacement parameters fixed at 1.2 times the U_{eq} of the attached carbon. In the refinement of **15**, disorder in the crotyl ligand was modeled as separate groups with a 65:35 population of sites. The major component was refined anisotropically with bond distances restrained to reasonable values and the anisotropic displacement parameters restrained to approximate isotropic behavior. The minor component was refined isotropically with distances and angles restrained to be similar to those of the major component. The hydrogens for both of the crotyl ligand components were constrained to calculated geometries with displacement parameters set equal to 1.2 times the U_{eq} of the attached carbon. All other non-hydrogen atoms were refined anisotropically and all other hydrogens were refined without restraints. Full matrix least squares refinement of all data on F^2 converged at $R_F = 0.0875$ and GOF (F^2) = 1.562 for **10** and $R_F = 0.0475$ and GOF (F^2) = 2.153 for **15**. The final difference Fourier maps for each did not reveal any significant features. Crystallographic data have been deposited at the CCDC, 12 Union Road, Cambridge CB2 1EZ, UK, and copies can be obtained on request, free of charge, by quoting the publication citation. Details of the data collection and solution and refinement of the structures can be found in Appendix 2. Also in this Appendix are ORTEP drawings showing the complete atom labeling schemes, tables of atomic coordinates, complete bond distances and angles, anisotropic displacement parameters, and hydrogen atom coordinates for all structures.

References and Notes

1. Collman, J. P.; Hegedus, L. S.; Norton, J. R.; Finke, R. G., *Principles and Applications of Organotransition Metal Chemistry*, University Science Books, Mill Valley, 1987.
2. Abrams, M. B.; Yoder, J. C.; Loeber, C.; Day, M. W. *Organometallics* **1999**, *18*, 1389 and references therein.
3. (a) Karol, F.; Dao, S.-C.; Wasserman, E. P.; Brady, R. C. *New J. Chem.* **1997**, *21*, 797; (b) Wasserman, E.; Hsi, E.; Young, W.-T. *Polymer Preprints* **1998**, *39* (2), 425; (c) Resconi, L. J. *Mol Catal. A* **1999**, *146*, 167.
4. For leading references on chain epimerization see: (b) Leclerc, M. K.; Brintzinger, H. H. *J. Am. Chem. Soc.* **1996**, *118*, 9024 and references therein; (c) Busico, V.; Cipullo, C. R.; Landriani, L.; Angelini, G.; Margonelli, A.; Segre, A. L. *J. Am. Chem. Soc.* **1996**, *118*, 2105; (d) Resconi, L.; Fait, A.; Piemontesi, F.; Colonnesi, M.; Rychlicki, H.; Ziegler, R. *Macromolecules* **1995**, *28*, 6667.
5. (a) Eshuis, J. J. W.; Tan, Y. Y.; Meetsma, A.; Teuben, J. G. *Organometallics* **1992**, *11*, 362; (b) Horton, A. D. *Organometallics* **1996**, *15*, 2675; (c) van der Heijden, H.; Hessen, B.; Orpen, A. G. *J. Am. Chem. Soc.* **1998**, *120*, 1112; (d) Watson, P. L. *J. Am. Chem. Soc.* **1982**, *104*, 337; (e) Watson, P. L.; Roe, D. C. *J. Am. Chem. Soc.* **1982**, *104*, 6471; (f) Watson, P. L.; Parshall, G. W. *Acc. Chem. Res.* **1985**, *18*, 51; (g) Evans, W. J.; Ulibarri, T. A.; Ziller, J. W. *J. Am. Chem. Soc.* **1990**, *112*, 2314; (h) Evans, W. J.; Gonzales, S. L.; Ziller, J. W. *J. Am. Chem. Soc.* **1994**, *116*, 2600; (i) Jeske, G.; Lauke, H.; Mauerman, H.; Swepston, P. N.; Schumann, H.; Marks, T. J. *J. Am. Chem. Soc.* **1985**, *107*, 8091; (j) Jeske, G.; Schock. L. E.; Swepston, P. N.; Schumann, H.; Marks, T. J. *J. Am. Chem. Soc.* **1985**, *107*, 8103; (k) Nolan, S. P.; Stern, D.; Marks, T. J. *J. Am. Chem. Soc.* **1989**, *111*, 7844.
6. Thompson, M. E.; Baxter, S. M.; Bulls, A. R.; Burger, B. J.; Nolan, M. C.; Santarsiero, B. D.; Schaefer, W. P.; Bercaw, J. W. *J. Am. Chem. Soc.* **1987**, *109*, 203.
7. Bunel, E. E. Ph.D. Thesis, California Institute of Technology, 1989.
8. (a) Richardson, D. E.; Alameddin, N. G.; Ryan, M. F.; Hayes, T.; Eyler, J. R.; Siedle, A. R. *J. Am. Chem. Soc.* **1996**, *118*, 11244; (b) Christ, C. S.; Eyler, J. R.; Richardson, D. E. *J. Am. Chem. Soc.* **1990**, *112*, 596; (c) Christ, C. S.; Eyler, J.

R.; Richardson, D. E. *J. Am. Chem. Soc.* **1988**, *110*, 4038; (d) Alameddin, N. G.; Ryan, M. F.; Eyler, J. R.; Siedle, A. R.; Richardson, D. E. *Organometallics* **1995**, *14*, 5005; (e) Huang, Y. Q.; Hill Y. D.; Sodupe, M.; Bauschlicher, C. W.; Freiser, B. S. *J. Am. Chem. Soc.* **1992**, *114*, 9106; (f) Huang, Y.; Hill, Y. D.; Freiser, B. S. *J. Am. Chem. Soc.* **1991**, *113*, 840; (g) Feichtinger, D.; Plattner, D. A.; Chen, P. *J. Am. Chem. Soc.* **1998**, *120*, 7125.

9. Lieber, S.; Prosenc, M.-H.; Brintzinger, H.-H. *Organometallics* **2000**, *19*, 377.
10. (a) Margl, P. M.; Woo, T. K.; Blöchl, P. E.; Ziegler, T. *J. Am. Chem. Soc.* **1998**, *120*, 2174; (b) Margl, P. M.; Woo, T. K.; Ziegler, T. *Organometallics* **1998**, *17*, 4997.
11. Piers, W. E.; Shapiro, P. J.; Bunel, E. E.; Bercaw, J. E *Synlett* **1990**, 74 and references therein.
12. Thompson, M. E. Ph.D. Thesis, California Institute of Technology, 1985.
13. Burger, B. J; Thompson, M. E.; Cotter, W. D.; Bercaw, J. E. *J. Am. Chem. Soc.* **1990**, *112*, 1566.
14. McDade, C.; Bercaw, J. E. *J. Organomet. Chem.* **1985**, *279*, 281.
15. (a) Schaefer, W. P.; Köhn, R.; Bercaw, J. E. *Acta Crystallogr.* **1992**, *C48*, 251; (b) St. Clair, M.; Schaefer, W. P.; Bercaw, J. E. *Organometallics* **1991**, *10*, 525; (c) Hajela, S.; Schaefer, W. P.; Bercaw, J. E. *Acta Crystallogr.* **1992**, *C48*, 1771; (d) Yoder, J. C.; Day, M. W.; Bercaw, J. E. *Organometallics* **1998**, *17*, 4946; (e) Campion, B.K.; Heyn, R. H.; Tilley, T. D. *Organometallics* **1993**, *12*, 2584; (f) Lappert, M. F.; Singh, A.; Atwood, J. L.; Hunter, W. E. *J. Chem. Soc., Chem. Comm.* **1983**, 206; (g) Atwood, J. L.; Smith, K. D. *J. Chem. Soc., Dalton Trans.* **1973**, 2487; (h) Atwood, J. L.; Smith, K. D. *J. Am. Chem. Soc.* **1973**, *95*, 1488.
16. Hajela, S.; Bercaw, J. E. *Organometallics* **1994**, *13*, 1147.
17. (a) Bercaw, J. E. *Adv. Chem. Ser.* **1978**, *167*, 136; (b) Chirik, P. J.; Day, M. W.; Bercaw, J. E. *Organometallics* **1999**, *18*, 1873.
18. Lauher, J. W.; Hoffmann, R. *J. Am. Chem. Soc.* **1976**, *98*, 1729.
19. Lee, H.; Bonanno, J. B.; Hascall, T.; Cordaro, J.; Hahn, J. M.; Parkin, G. *J. Chem. Soc., Dalton Trans.* **1999**, 1365.
20. Evans, W. J.; Seibel, C. A.; Ziller, J. W.; Doedens, R. J. *Organometallics* **1998**, *17*, 2103.
21. Horton, A. D. *Organometallics* **1992**, *11*, 3271.
22. Ref. 2 and also Chapter 1, this work.

23. Burger, B. J.; Bercaw, J. E., *New Developments in the Synthesis, Manipulation, and Characterization of Organometallic Compounds*; Wayda, A., Darensbourg, M. Y., Eds.; American Chemical Society: Washington, DC, 1987; Vol. 357.
24. Marvich, R. H.; Brintzinger, H. H. *J. Am. Chem. Soc.* **1971**, *93*, 2046.

Chapter 3

A Study of the Mechanism of Chain Epimerization Using a Doubly Labeled Propylene

Abstract

An isotopically labeled propylene, $CH_2CD^{13}CH_3$, was synthesized and its polymerization was carried out at low concentration in toluene solution. Polymerization reactions were performed at both 50 °C and 75 °C using the isospecific metallocene catalysts *rac*-(EBTHI)$ZrCl_2$ and *rac*-(EBI)$ZrCl_2$ activated with MAO. Analysis of the NMR spectra (^{13}C, ^{1}H, and ^{2}H) of the resultant polymers revealed that the production of stereoerrors through chain epimerization proceeds exclusively through tertiary alkyl intermediates. It was also found that enantiofacial inversion of the geminally disubstituted olefin resulting from β-D (or H) elimination occurs *via* a non-dissociative process. The implications of these results on the mechanism of olefin polymerization with isospecific metallocene catalysts are discussed.

Table of Contents, Chapter 3

I. Introduction 92

II. Results and Discussion 97

A. Synthesis of the Doubly Labeled Propylene Monomer 97

B. Polymerization Experiments Using the Doubly Labeled Monomer 100

III. Conclusions 108

IV. Experimental Section 109

V. Acknowledgment 112

VI. References and Notes 112

VII. Appendix. Summary of the Processes Proposed to Occur During Chain Epimerization of the Doubly Labeled Propylene 114

Introduction

It has been generally observed that the isotacticity of polypropylene samples obtained from C_2-symmetric metallocene catalysts is greatly decreased when the polymerization reactions are carried out with low propylene concentration.[1] Homogeneous, isospecific, non-metallocene catalysts can also display this behavior.[2] Busico first ascribed this phenomenon to a competition between bimolecular insertion and a unimolecular process of epimerization of the stereochemistry at the β-carbon of the growing polymer (later termed "chain epimerization") (Scheme 1).[1b] It should be noted that a dependence of tacticity on monomer concentration has not been described for isospecific, heterogeneous Ziegler-Natta catalysts.

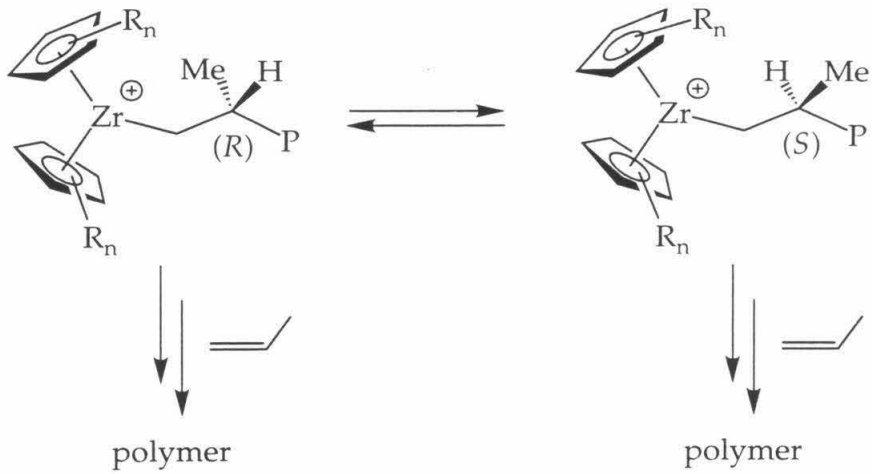

Scheme 1. Competition between insertion and chain epimerization for metallocene catalysts.

Polymerization studies using isotopically labeled propylene monomers have been performed in an attempt to elucidate the mechanism of this process. For isolated stereoerrors in a polymerization which conforms to the enantiomorphic site control statistical model the *mmmr*, *mmrr*, and *mrrm* pentads are expected in a 2:2:1 ratio.[3] Examination of the ^{13}C NMR spectra of polypropylene samples obtained from either (*E*)- or (*Z*)-[1-D]propylene revealed a reduction in the expected intensity for the *mrrm* methyl group pentad;[4] in addition, a 1:1:1 triplet was observed slightly upfield of the *mrrm* resonance. The multiplicity and the slight upfield shift of this latter signal are indicative of a deuterium-bound carbon; therefore, this resonance was assigned to a deuterium

labeled methyl group in an *mrrm* stereochemical arrangement (J_{CD} = 19 Hz). If the integrations of both the triplet and singlet *mrrm* resonances are summed, the expected ratio of intensities is realized.

It was proposed that the triplet *mrrm* signal reflects stereoerrors arising from chain epimerization (labeled (a) in Eqn 1) and that the singlet *mrrm* signal

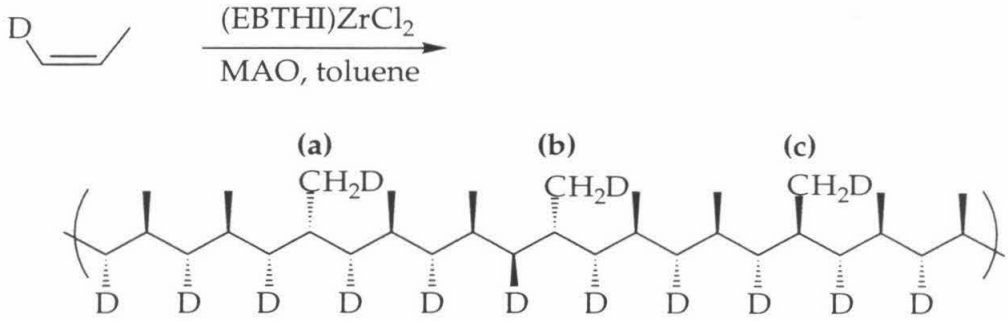

(1)

reflects stereoerrors derived from simple enantiofacial misinsertion (labeled (b) in Eqn 1). Consistent with this proposal, for polymerization runs performed at varying monomer concentrations, the intensity of the unlabeled *mrrm* signal was independent of the propylene concentration, while the intensity of the triplet resonance was reduced when the polymerizations were carried out at higher monomer concentration.[4b] An additional feature of these studies was that a 1:1:1 triplet was also observed (in a DEPT experiment) slightly upfield of the *mmmm* methyl group pentad, indicating the presence of deuterium in methyl groups of correct stereochemistry (labeled (c) in Eqn 1). The signals corresponding to the deuterium labeled *mmmm* and *mrrm* methyl group pentads were estimated to be of similar intensity.

Polymerization of [2-D]propylene yielded similar results, in that deuterium incorporation was observed into methyl groups of both correct and inverted stereochemistry.[4b,5] However, both the isotacticity and molecular weight of the resultant poly-[2-D]propylene were higher than would have been expected had unlabeled propylene been subjected to identical polymerization conditions. This indicates that chain epimerization involves β-H (or D) elimination as the rate determining step. Based on the differences in molecular weight and stereochemistry between poly-[2-D]propylene and unlabeled polypropylene, the value for k_H/k_D for β-elimination was estimated to be approximately 3 at 50 °C.[4b,6]

Two mechanisms have been put forward to explain these observations; the first, offered by Busico, enlists metallocene tertiary alkyl complexes as intermediates (Scheme 2).[1b,c] In this mechanism, β-hydrogen elimination is followed initially by a 180° rotation of the geminally disubstituted olefin. Secondary insertion then affords a tertiary alkyl complex containing two α-methyl groups. A 120° rotation about the M–C bond of this tertiary alkyl followed by β-H elimination from the methyl group labeled with an asterisk (Scheme 2) yields a new metal hydride-*gem*-olefin complex. Subsequent olefin rotation and primary insertion affords a polymer chain in which the stereochemistry at the β-carbon has been inverted. An additional consequence of this mechanism is interchange of the methylene and methyl carbons of the last inserted monomer unit, providing a rationale for the observation of deuterium atoms in the methyl groups of stereoerrors when labeled monomers were used.

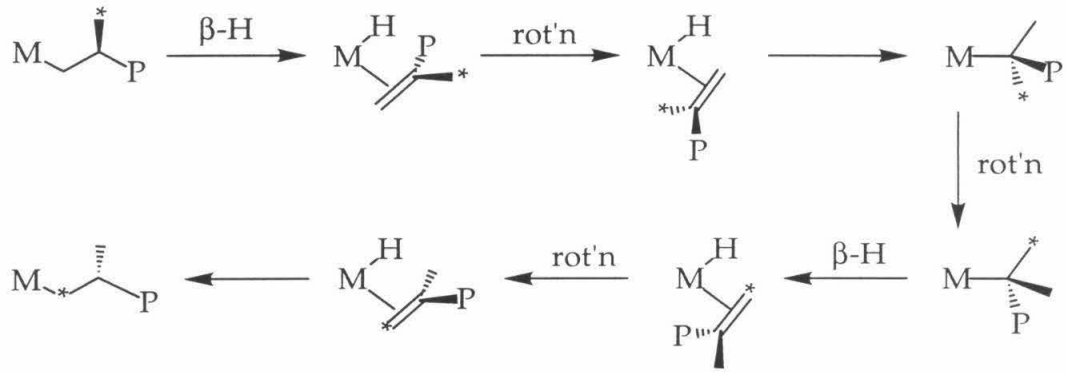

Scheme 2. Illustration of the chain epimerization process following the tertiary-alkyl mechanism.

It is important to note that, for polymerization of both [1-D]propylene and [2-D]propylene, in order to explain the presence of deuterium atoms in methyl groups of correct stereochemistry, the geminally disubstituted olefin resulting from β-H (or D) elimination must invert to the opposite enantioface during the chain epimerization process. This additional step is not easily accommodated by Busico's mechanism, but two pathways have been envisioned for its occurrence. The first is dissociative (pathway (a), Scheme 3) and the second is non-dissociative (pathway (b), Scheme 3), analogous to Gladysz' observations for a rhenium system.[7] A *gem*-olefin, upon dissociation, is not expected to be able to compete for insertion with the large excess of propylene in

these polymerization reactions, thus the non-dissociative pathway has been favored in the literature,[6,8] and computational studies support this assertion.[9]

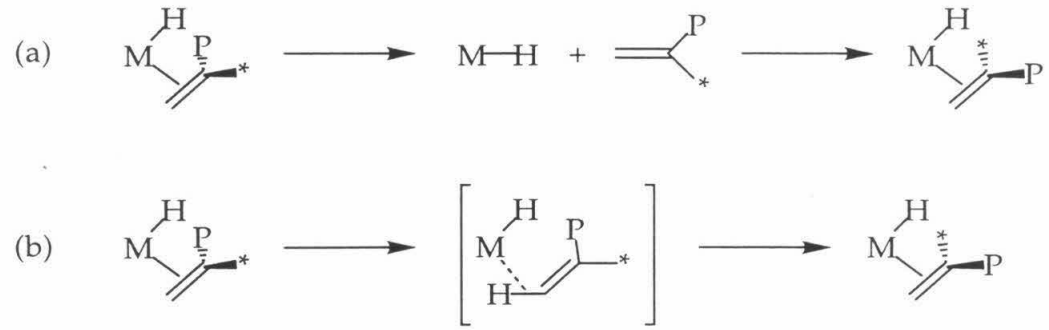

Scheme 3. Illustration of the mechanisms proposed to account for *gem*-olefin enantiofacial inversion during chain epimerization.

The second mechanistic proposal was put forward by Resconi and involves, as intermediates, metallocene dihydrogen-η^3-allyl complexes (Scheme 4).[10] The intermediacy of this type of species has also been implicated in the

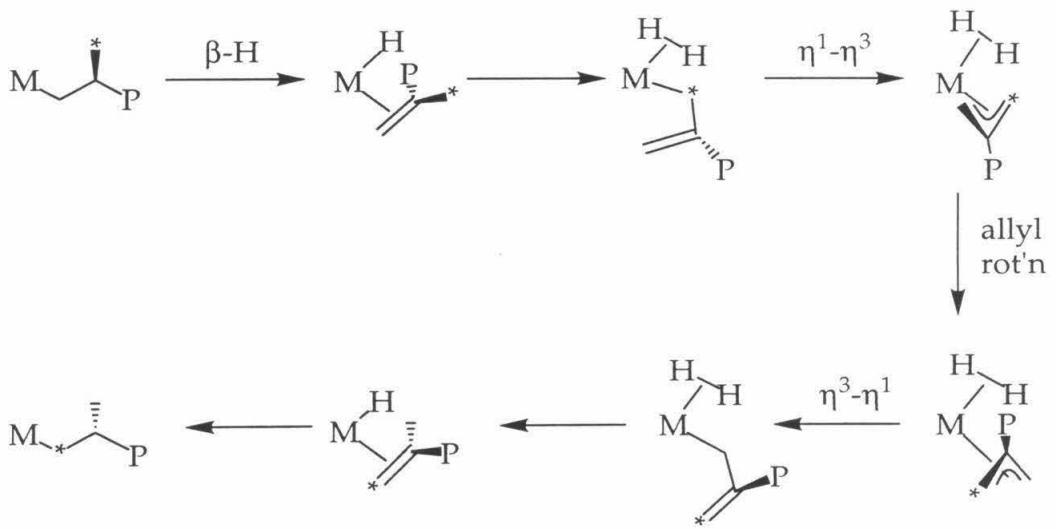

Scheme 4. Illustration of the chain epimerization process following the allyl mechanism.

production of internal unsaturation in polypropylene chains.[11] In Resconi's proposal, β-H elimination is followed by a σ-bond metathesis reaction between the hydride and the allylic C–H bonds of the coordinated olefin. This affords an

allyl-dihydrogen complex in which rotation of both the dihydrogen ligand[12] and the trihapto coordinated allyl ligand[13] should be facile. A second σ-bond metathesis reaction can then take place to yield a new olefin hydride complex. From this complex, primary insertion yields a polymer chain with inverted β-carbon stereochemistry and interchange of the methyl and methylene carbons of the last inserted monomer unit. Importantly, this mechanism can easily account for the observation of deuterium atoms in methyl groups of correct stereochemistry, as C–C bond rotation in the η^1-allyl intermediate should be facile (Eqn 2).[13] Computational studies of both this overall mechanism[14] and the details of allyl formation[15] have been performed and support the feasibility of this reaction scheme.

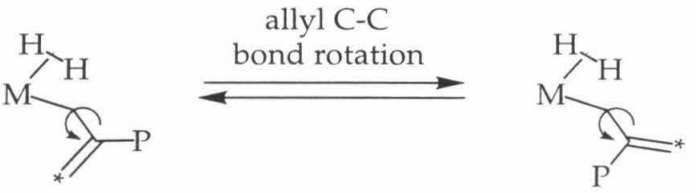

(2)

We were interested in devising an experiment that would distinguish between these two mechanistic proposals, and surmised that polymerization of a selectively labeled monomer, $CH_2CD^{13}CH_3$, would allow this. A summary of the structures expected for the stereoerrors arising from chain epimerization of this monomer are shown in Figure 1. The tertiary alkyl mechanism predicts the presence of ^{13}C-labeled methylene carbons associated with methyl groups of both inverted and correct stereochemistry (structures **A** and **C**). Also expected are ^{13}C labeled methyl groups adjacent to C–H methine carbons (structures **B** and **D**). Structures **A** and **B** result from the normal course of chain epimerization, and structures **C** and **D** result from chain epimerization with non-dissociative *gem*-olefin enantiofacial inversion. Among the products expected for chain epimerization following the allyl mechanism is structure **G** in which methyl groups containing both ^{13}C and D labels are present. This structure will be easily characterized as a 1:1:1 triplet slightly upfield of the expected location in the ^{13}C NMR. It should be noted that doubly labeled methyl groups can also arise from chain epimerization following the tertiary alkyl mechanism; this requires a crossover process involving dissociation and recoordination of the terminally unsaturated polymer chain that results from β-H elimination. Thus, the absence of such a signal in the ^{13}C NMR spectrum of the polymer would rule out either

process. Schemes outlining the detailed mechanisms predicting the formation of structures **A – G** can be found in the Appendix at the end of this chapter.

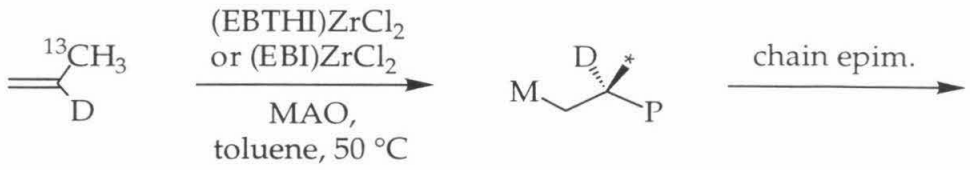

(a) Tertiary-alkyl mechanism with non-dissociative olefin enantiofacial inversion

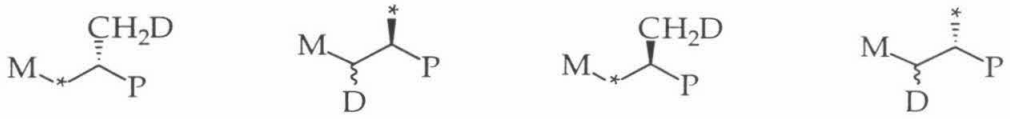

A **B** **C** **D**

(b) Allyl mechanism

E **F** **G**

Figure 1. Metal-bound products of chain epimerization for the doubly labeled propylene.

Results and Discussion

Synthesis of the Doubly Labeled Propylene Monomer

The monomer was synthesized according to Scheme 5. Several test runs of this reaction scheme carried out using unlabeled methyl iodide revealed that deuterated ethylene (C_2H_3D) was produced along with the desired propylene product. The sodium acetylide suspension was evidently contaminated with acetylene, as the amount of ethylene observed was significantly reduced if the suspension was subjected to dynamic vacuum prior to use.

Thus, after degassing the sodium acetylide suspension *in vacuo*, reaction with ^{13}C labeled methyl iodide proceeded over ~ 10 hours to afford ^{13}C-labeled propyne. Upon completion of this reaction, the volatiles were transferred onto

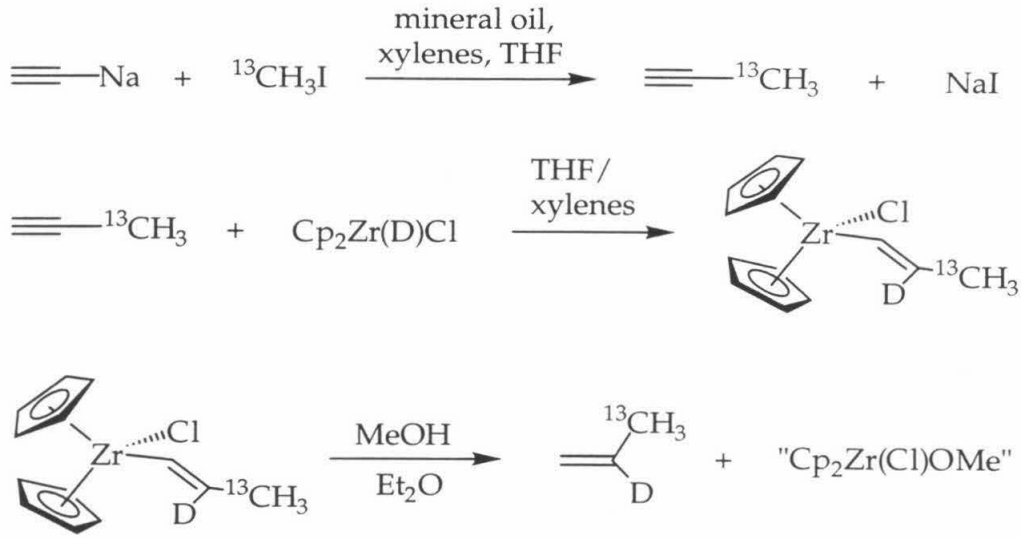

Scheme 5. Synthesis of the doubly labeled propylene monomer.

one equivalent (based on maximum theoretical yield) of deuterated Schwarz' reagent; the resulting dark green alkenyl zirconocene product was then purified by dissolution in diethyl ether followed by filtration. Addition of methanol to $Cp_2Zr(Cl)[C(H)=CD^{13}CH_3]$ at 0 °C liberated the desired doubly labeled propylene, and the volatiles from this reaction were vacuum transferred into a thick walled glass vessel for storage at reduced temperature.

Diethyl ether and the higher boiling fractions were removed from the crude product mixture by repeated trap-to-trap distillation at –95 °C. At this point, ^1H NMR analysis of the crude product mixture revealed the presence of a small amount of deuterium-labeled ethylene. As the suspension of sodium acetylide was purified by evacuation prior to beginning the synthesis, this small amount of ethylene presumably arose from a different source. It is likely that a small amount of acetylene was produced in the first reaction step by deprotonation of propyne by the starting sodium acetylide (Eqn 3).

(3)

Nonetheless, this deuterated ethylene was removed from the product by trap-to-trap distillation at –145 °C; by ^1H NMR analysis, the fraction which was volatile at this temperature was a 1:1 azeotrope of propylene and ethylene. After this step, although the only vinyl resonances visible in the ^1H NMR of the

crude product mixture were those of the desired product, features due to a second ^{13}C- and ^{2}H-labeled species were evident. This species could not be separated from the product by distillation. Using GC-MS, this second product was found to be ^{13}C- and multiply ^{2}H-labeled propane, which presumably arises from over-reduction of propyne by the deuterated Schwarz reagent. The absence of ethylene (as well as other heavier olefins) in the purified sample was also confirmed by GC-MS. Shown in Figure 2 is the ^{1}H NMR spectrum of the purified propylene/propane mixture. By integration, the isotopic purity of the propylene is estimated to be 97% for both deuterium in the 2-position and ^{13}C in the methyl group.

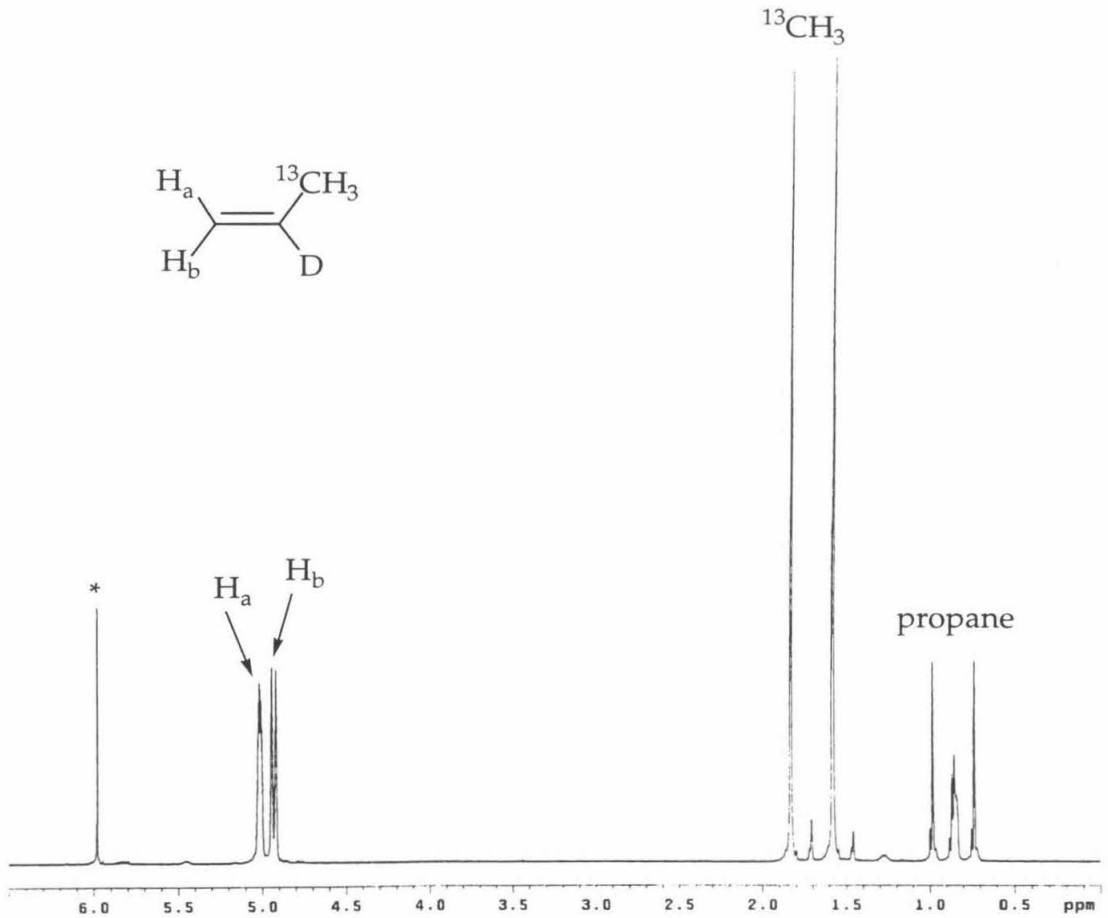

Figure 2. ^{1}H NMR spectrum of the doubly labeled propylene monomer (the * label indicates 1,1,2,2-tetrachloroethane-d_2 solvent).

Polymerization Experiments Using the Doubly Labeled Monomer

Polymerization experiments were carried out using both *rac*-(EBTHI)$ZrCl_2$ and *rac*-(EBI)$ZrCl_2$ as catalysts (with MAO activation). The polymerization apparatus was made entirely of thick-walled glass and consisted of two chambers joined by glass tubing with a needle valve and ground glass joint for connection to a vacuum line. Toluene solutions of the catalyst and MAO were loaded separately into the reaction chambers. After addition of the desired amount of monomer, the apparatus was placed in an oil bath at the appropriate temperature, and the individual solutions of catalyst and MAO were then mixed, resulting in activation of the catalyst and initiation of polymerization. As no pressure regulation was possible in these experiments, the reactions were only allowed to proceed for one minute to ensure minimal pressure drop. Five test reactions using 1 atm of unlabeled propylene with *rac*-(EBTHI)$ZrCl_2$ as catalyst at 50 °C were carried out. The intensities of the resonances in the ^{13}C NMR spectra of the polymers produced in these five test reactions were identical, with [*mmmm*] ≈ 56%. Shown in Figure 3 is a representative ^{13}C NMR spectrum of poly-[2-D-3-^{13}C]propylene produced by the method described above; the peaks in this spectrum are assigned in Table 1.

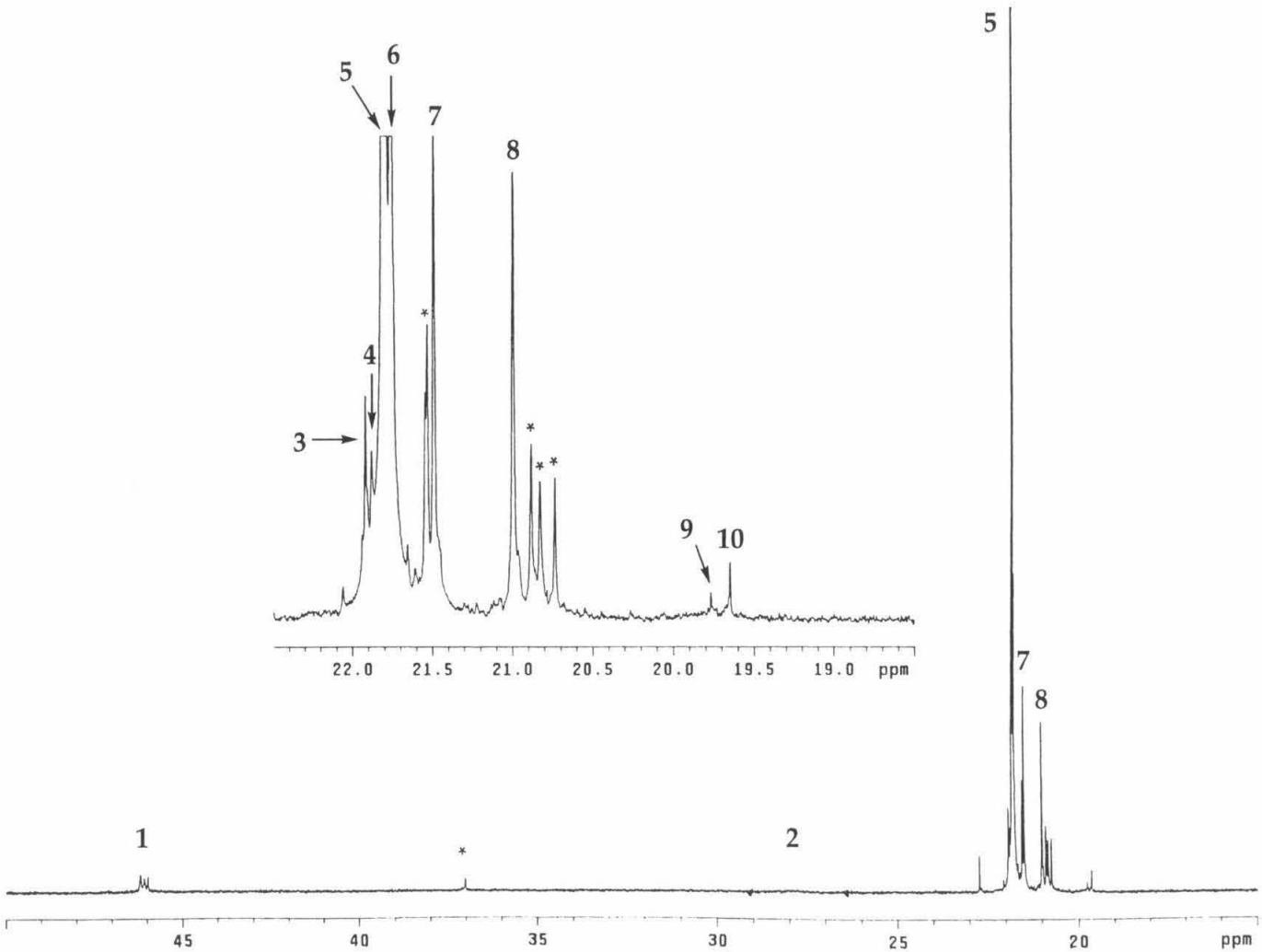

Figure 3. ^{13}C NMR spectrum of poly-[2-D-3-^{13}C]propylene made using *rac*-(EBTHI)$ZrCl_2$ with 1 atm monomer, in toluene solution at 50 °C. The * symbol denotes resonances due to chain ends and 3,1-misinsertions.

Table 1. Assignment of the Resonances in the ^{13}C NMR Spectrum of Poly-[2-D-3-^{13}C]Propylene as Shown in Figure 3[a,b]

Peak Number	δ (ppm)[c]	Structure	Stereochemical Structure	Intensity[d]
1	46.2 - 45.9	-**C**H_2-	NA[e]	4.15
2	28.5 - 27.5	-**C**H(CH_3)-	NA[e]	1.28
3	21.92	-CH(**C**H_3)-	*mmmmmm*	2.96
4	21.88	-CH(**C**H_3)-	*mmmmmr*	2.34
5	21.82	-CD(**C**H_3)-	*mmmmmm*	63.69
6	21.76	-CD(**C**H_3)-	*mmmmmr*	15.52
7	21.49	-CD(**C**H_3)-	*mmmr*	7.24
8	21.00	-CD(**C**H_3)-	*mmrr*	7.11
9	19.77	-CH(**C**H_3)-	*mrrm*	0.44
10	19.65	-CD(**C**H_3)-	*mrrm*	0.70

[a]Polymerization conditions: 0.25 mg *rac*-(EBTHI)$ZrCl_2$, 1500 equiv. MAO, 1 atm monomer, 7.5 mL toluene, 50 °C, spectrum acquired in $C_2D_2Cl_4$ at 85 °C; [b]assignments made according to reference 5; [c]downfield from TMS; [d]total intensity of methyl groups set to 100, other resonances scaled accordingly; [e]NA = not assigned.

Due to the low natural abundance of the ^{13}C isotope (*ca.* 1%) the resonances which appear in the spectra for the labeled polymers reflect incorporation of the isotopic label. From the assignments in Table 1, it is apparent that the intensity of the *mrrm* methyl group resonance is reduced from the value predicted by enantiomorphic site control statistics and that the integration of the methylene resonance is larger than expected. Furthermore, for both the *mmmm* and *mrrm* methyl group resonances, isotopomers are resolved which differ only in the substitution of hydrogen isotopes on the adjacent methine position. Also of note is the absence of a 1:1:1 triplet anywhere in the spectrum, indicating that no doubly labeled positions are present in the polymer. The peak assignments given in Table 1 are consistent with DEPT experiments carried out on the same sample, and the DEPT spectra also confirm the lack of $^{13}CH_2D$ methyl groups.

Shown in Figure 4 are the structures expected for the stereoerrors produced using the tertiary alkyl mechanism. Inspection of the ^{13}C NMR spectrum of the polymer (Figure 3) and the peak assignments in Table 1 reveals

that resonances for all of these structures (**A** – **D**, **H**) can be assigned. As such, the "extra" intensity in the methylene position and all of the methyl group resonances assigned to structures with a hydrogen atom on the methine carbon (peaks 3, 4, and 9) correspond to structures derived through chain epimerization (structures **A** – **D**). Peak 10 (Structure **H**) corresponds to stereoerrors arising from enantiofacial misinsertion. Although some of these spectral features are also consistent with the allyl mechanism, the lack of 1:1:1 triplets is not.

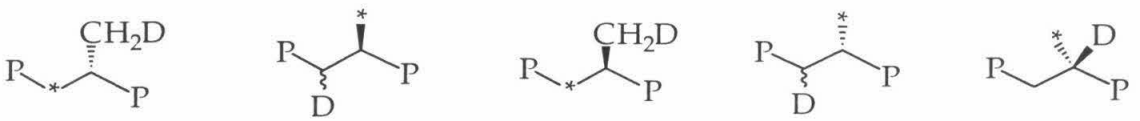

A (peak 1) **B** (peaks 3 + 4) **C** (peak 1) **D** (peak 9) **H** (peak 10)

Figure 4. Structures expected for both the products of the tertiary-alkyl mechanism of chain epimerization (**A** - **D**) and stereoerrors due to enantiofacial misinsertion (**H**) and their assignments in the ^{13}C NMR.

Before analysis of the data, the natural abundance of ^{13}C in the methylene position and ^{1}H in the methine position of the polymer needs to be accounted for. Due to the isotopic composition of the monomer, neither of these positions should be ^{13}C labeled in the absence of chain epimerization; in addition, neither chain epimerization mechanism predicts incorporation of ^{13}C into the methine position. The expected natural abundance of ^{13}C in the methylene position is then easily measured as the intensity of the methine resonance at δ 28. Integration of the residual ^{1}H in the 2-position of the monomer estimated the isotopic purity of ^{2}H in this position at 97%. Thus, to correct for this, for the *mmmm* and *mrrm* resonances, approximately 3% of the intensity of the -CD(CH_3)- resonances (peaks 5 + 6 and peak 10) was subtracted from the -CH(CH_3)- resonances (peaks 3 + 4 and peak 9, respectively), and the same number added to the intensity of the -CD(CH_3)- resonances.

The conditions used and results of the polymerization experiments are shown in Table 2. The peak intensities reported in the table have been corrected for natural abundance as discussed above. In these experiments, the actual pressure during the polymerizations was unknown, and so the numbers reported in Table 2 refer to the pressure of monomer to which the apparatus was filled at room temperature. Entry 3 refers to a reaction in which a small

amount of monomer was initially added (*ca.* 500 torr) and the polymerization allowed to proceed for 3 minutes instead of the usual 1, resulting in depletion of a substantial amount of the monomer; consistent with this assertion, a higher than normal yield (by mass) of polymer was isolated from this reaction.

Table 2. Intensity of Resonances in the ^{13}C NMR Spectra for Poly-[2-D-3-^{13}C]Propylene[a,b,c]

Entry	Monomer Pressure[d]	Temp. (°C)	Peak 1[e] (CH_2)	Peaks 3 + 4[e] *mmmm* (CH-CH_3)	Peaks 5 + 6[e] *mmmm* (CD-CH_3)	Peak 7 *mmmr*	Peak 8 *mmrr*	Peak 9[e] *mrrm* (CH-CH_3)	Peak 10[e] *mrrm* (CD-CH_3)
1[f]	1 atm	50	2.87	2.85	81.66	7.24	7.11	0.42	0.72
2[f]	≈ 500 torr	50	4.70	4.00	74.24	10.03	10.39	0.71	0.63
3[f]	starved	50	10.12	4.75	63.77	14.75	14.64	1.29	0.80
4[f]	1 atm	75	15.69	3.96	52.16	19.19	21.59	1.93	1.18
5[g]	1 atm	50	0.52	2.90	83.27	5.45	5.92	0.23	2.23
6[g]	1 atm	75	4.78	4.43	68.53	11.24	12.51	0.91	2.39

[a]Peak Numbers Refer to Figure 3 and Table 1; [b]standard conditions: 0.25 mg catalyst, 1500 equiv. MAO, 7.5 mL toluene, spectra acquired in $C_2D_2Cl_4$; [c]total integration of methyl resonances set to 100 and other peaks scaled accordingly; [d]see text; [e]intensity corrected for natural abundance as discussed in the text; [f]catalyst = *rac*-(EBTHI)$ZrCl_2$; [g]catalyst = *rac*-(EBI)$ZrCl_2$.

Comparison of the ^{13}C NMR data for the test polymerizations carried out with unlabeled monomer (*vide supra*) and for the labeled polymer listed in entry 1 (carried out under the same conditions) with literature data reveal that the monomer concentration for these standard polymerization conditions is approximately 0.3 M – 0.4 M, corresponding to a propylene pressure of about 1 atm, as expected. Resconi reported[1d] [*mmmm*] = 54% for unlabeled polypropylene, and Brintzinger reported[4b] [*mmmm*] = 84%, [*mmrr*] = 6.4%, [*mrrm* (CH_3)] = 1.0%, and [*mrrm* (CH_2D)] = 2.2% for poly-[2D]propylene under these conditions. Additionally, comparison of the ^{13}C NMR data for the sample given in entry 3 with data from Busico's laboratory[5] reveals that the propylene pressure in this experiment is less than 0.6 bar, as desired.

As previously discussed, for an isospecific polymerization which follows the enantiomorphic site control mechanism, isolated stereoerrors should result in a 2:2:1 ratio of the *mmmr*:*mmrr*:*mrrm* methyl group resonances.[3] For polymer sample 1, if the "extra" intensity in the methylene resonance (peak 1) is added to that for the *mrrm* methyl groups (peaks 9 and 10), the expected ratio is approximately realized. However, this operation will always overestimate the integration of the *mrrm* methyl groups because structure **C**, which contains a methyl group of correct stereochemistry, contributes to the intensity of peak 1. Unfortunately, resonances in the region of the spectrum where peak 1 resides have not been assigned in detail.[16] The 2:2:1 ratio of *mmmr*:*mmrr*:*mrrm* resonances dictated by the statistical model can be used, however, to provide an estimate for the relative amounts of structures **A** and **C**. If the sum of the intensities of peaks 9 and 10 is subtracted from half of the averaged intensities of peaks 7 and 8, the result is an approximation of the integration due to structure **A**. The approximate amount of structure **C** is then simply the difference between this number and the integration of peak 1 (after correction for natural abundance). The intensities estimated in this way are shown in Table 3 together with the intensities of resonances measured for structures **B**, **D**, and **H**.

Table 3. Estimated Amounts of Structures **A** - **D** and **H**

Entry[a]	**A**[b]	**B**	**C**[b]	**D**	**H**
1	2.45	2.85	0.42	0.42	0.72
2	3.77	4.00	0.93	0.71	0.63
3	5.26	4.75	4.86	1.29	0.80
4	7.09	3.96	8.60	1.93	1.18
5	0.38	2.90	0.14	0.23	2.23
6	2.64	4.43	2.14	0.91	2.39

[a]Entry numbers correspond to those in Table 2; [b]derived as discussed in the text.

Consistent with its assignment to stereoerrors derived through enantiofacial misinsertion (structure **H**), the intensity of peak 10 remains essentially constant as the polymerization pressure (and hence, monomer concentration) is lowered (entries 1 - 3). Also consistent with their assignments, the intensities of resonances due to structures **A** – **D** increase in intensity as the polymerization pressure is lowered (entries 1 - 3) and as the polymerization

temperature is raised (entry 1 vs. 4 and 5 vs. 6), conditions known to increase the favorability of chain epimerization.[1] The ^1H and ^2H NMR spectra of the polymers support these data. The intensity of the methine resonance in the ^1H NMR (δ 1.6) increases with the relative amount of chain epimerization as does the intensity of the methyl/methylene resonance in the ^2H NMR (δ 0.9). Curiously, as the overall amount of products due to chain epimerization increases, the calculated amounts of structures **A** and, especially, **C** increase much more dramatically than do the measured amounts of **B** and **D**. Although this is difficult to rationalize, it seems a minor point and the overall picture is only consistent with chain epimerization occurring through the tertiary alkyl mechanism.

A comparison of the two catalyst systems used in this study reveals that the favorability of chain epimerization is lower for the *rac*-(EBI)$ZrCl_2$ system as compared to *rac*-(EBTHI)$ZrCl_2$ (entry 1 vs. 5 and 4 vs. 6), consistent with earlier results.[1c] We also find that the more selective catalyst, *rac*-(EBI)$ZrCl_2$, gives a smaller proportion of chain epimerization structures derived from enantiofacial inversion of the terminally unsaturated polymer chain (compare **A** + **B** vs. **C** + **D** for the entries in Table 3). In addition, for both catalyst systems, the relative amount of chain epimerization which proceeds with *gem*-olefin enantiofacial inversion is increased under conditions which favor chain epimerization (*i.e.*, higher temperature, lower monomer concentration). The unimolecular step of *gem*-olefin enantiofacial inversion must therefore have a barrier which is comparable in energy to that of the bimolecular olefin insertion under the conditions examined herein. The rate of a unimolecular process is expected to respond more quickly to changes in temperature than that of a bimolecular process; in addition, reducing the olefin concentration will raise the energy barrier for olefin insertion. Both of these changes in reaction conditions, therefore, are expected to favor the unimolecular process of *gem*-olefin enantiofacial inversion relative to the bimolecular process of olefin insertion. The non-dissociative olefin enantiofacial inversions described for a rhenium system required hours to reach completion at approximately 100 °C.[7] The much faster rate which is required herein is consistent with the much lower strength of d^0-metal olefin interactions as compared to their late metal analogues.

For a sample of poly-[2-D]propylene prepared analogously to the sample of entry 1,[4b] Brintzinger had estimated an equal proportion of chain epimerization structures derived with and without enantiofacial inversion of the

terminally unsaturated polymer chain. For the polymerization outlined in entry 1, this is clearly not the case, as a *ca.* 4:1 ratio is observed for **A** + **B** : **C** + **D**. The previous evidence for *gem*-olefin enantiofacial inversion was the observation of an inverted 1:1:1 triplet which barely emerged from the *mmmm* pentad in a DEPT experiment carried out on the poly-[2-D]propylene sample.[4b] While the qualitative conclusion reached from this NMR experiment, enantiofacial inversion of the terminally unsaturated polymer chain, is certainly correct, establishing an accurate intensity for the triplet signal seems a difficult proposition, and thus the results presented herein should be deemed more reliable.

Observation of a 1:1:1 triplet in the ^{13}C NMR spectra of the poly-[2-D-3-^{13}C]propylene samples described herein would have required either operation of the allyl mechanism or operation of the tertiary alkyl mechanism with dissociation and crossover of the terminally unsaturated polymer chain. The results of Brintzinger and Busico require enantiofacial inversion of this *gem*-olefin, but not necessarily its dissociation and recoordination.[4-6] While olefin crossover may seem a rather unlikely scenario, if it is assumed that olefin dissociation occurs following every β-H (or D) elimination event, a sufficient concentration of *gem*-olefin and three-coordinate-metal centers would build up. Thus, as no triplets were observed in the ^{13}C NMR spectra of any of the labeled polymers, it must be assumed that olefin dissociation does not occur following every β-H (or D) elimination. It can therefore be stated that, following dissociation of the terminally unsaturated polymer chain, its recoordination and insertion is highly unlikely. This result might have been anticipated, and is consistent with the dogma in the polymerization field.

Although not consistent with the allyl mechanism as a contributor to chain epimerization, the results presented herein do not preclude the formation of allylic intermediates in the production of polymer internal unsaturation.[11] Chain epimerization using the allyl mechanism requires two σ-bond metathesis reactions to take place, and it may be that the strength of the metal-dihydrogen interaction is not sufficient to prevent dihydrogen ligand dissociation before the second σ-bond metathesis can occur. Upon dissociation, H_2 simply cannot compete for binding with the large excess of propylene in solution and insertion of propylene into the metallocene allyl complex that results yields formation of an internal unsaturation (Scheme 6).

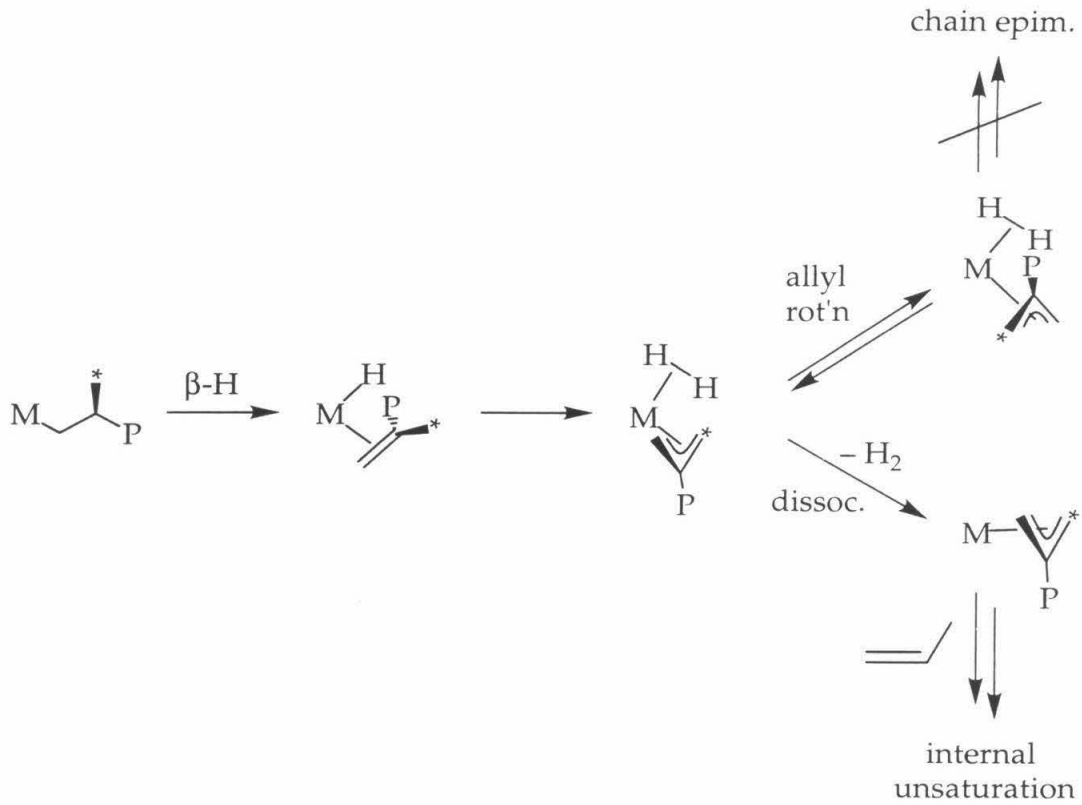

Scheme 6. Branching between chain epimerization and production of internal unsaturation in metallocene-catalyzed polymerization.

Conclusions

A doubly labeled olefin was synthesized and polymerizations were carried out at low concentration using isospecific metallocene catalysts. Resonances corresponding to all of the structures expected from operation of the tertiary alkyl mechanism of chain epimerization were located in the ^{13}C NMR spectra of the resultant polymers. Additional NMR data (DEPT, ^{1}H, and ^{2}H experiments) confirmed the assignments. Furthermore, the processes of dissociation and crossover of the terminally unsaturated polymer chain were ruled out, leading to the conclusion that the *gem*-olefin enantiofacial inversion occurs through a non-dissociative mechanism. These results are only consistent with chain epimerization occurring through the tertiary alkyl mechanism.

Experimental Section

General Considerations

All air and/or moisture sensitive compounds were manipulated using standard high-vacuum line, Schlenk, or cannula techniques, or in a glove box under a nitrogen atmosphere, as described previously.[17] Argon gas was purified and dried by passage through columns of MnO on vermiculite and activated 4 Å molecular sieves. Solvents were stored under vacuum over titanocene[18] or sodium benzophenone ketyl. The synthesis of (η^5-C_5H_5)ZrD(Cl) was carried out as previously reported.[19] Methanol (EM Science), propylene (Aldrich), sodium acetylide (Strem), *rac*-ethylene-*bis*-indenylzirconium dichloride (Aldrich), and *rac*-ethylene-*bis*-(4,5,6,7-tetrahydroindenyl)zirconium dichloride (Strem) were purchased and used as received. ^{13}C-labeled methyl iodide was purchased (Cambridge Isotopes), purified by passage through a plug of silica, and distilled from CaH_2 before use. MAO was purchased (Albemarle) and dried in vacuo to remove free trimethylaluminum before use. NMR spectra were recorded on a Varian ^{UNITY}INOVA 500 (499.853 MHz for ^{1}H) spectrometer. Analysis by GC-MS was carried out on an HP 5890 Series II gas chromatograph connected to an HP 5972 mass spectrometric detector. A 60 m x 0.32 μm internal diameter column was used which was coated with a 5 μm thick 100% methylsiloxane film.

Synthesis of (η^5-C_5H_5)$_2$Zr(Cl)[C(H)=CD(^{13}CH$_3$)]. In an inert atmosphere glove box, a suspension of sodium acetylide (17.3 wt%) in a mixture of mineral oil and xylenes (85.0 g suspension = 14.7 g NaC_2H, 0.306 mol) was weighed into a 500 mL 3-neck-round bottom flask. A large condenser designed for the use of dry ice/acetone as coolant and fitted with a gas inlet adapter was attached to the flask, as were a glass stopper and a rubber septum. The assembly was evacuated for 90 minutes, and THF (300 mL) was then added by cannula. The condenser was cooled to -78 °C, and $^{13}CH_3I$ (approx. 36 g, 0.25 mol) was injected using a syringe. The reaction was allowed to proceed for 9 hours after which time the apparatus was evacuated and the volatiles transferred under dynamic vacuum into a trap cooled to 77 K. In an inert atmosphere glove box, $Cp_2ZrD(Cl)$ (67.0 g, 0.259 mol) was weighed into a 500 mL round bottom flask. This flask was attached to a swivel frit assembly and the apparatus was evacuated. The trap containing the crude reaction mixture was then isolated from dynamic vacuum and the contents were transferred into the apparatus containing the Schwarz

reagent. The reaction was allowed to proceed for 3 hours at room temperature, after which time the solution was dark green/black. The solvent was then removed *in vacuo* and diethyl ether (200 mL) was added by vacuum transfer. An orange/red precipitate was separated from the product by filtration. This precipitate was washed 4 times with diethyl ether and the solvent was then removed from the filtrate *in vacuo* leaving the desired product as a sticky, dark green tar. ^{1}H NMR (THF-d_8): δ 7.48 (d, ZrC(H)=CD^{13}CH$_3$, 1H, $^{3}J_{CH}$ = 12 Hz), 6.98 (s, C$_5H_5$, 10H), 1.54 (d, ZrC(H)=CD^{13}CH$_3$, 3H, $^{1}J_{CH}$ = 124 Hz). ^{2}H NMR (THF): δ 5.72 (s (br), ZrC(H)=CD^{13}CH$_3$).

Synthesis of CH$_2$=CD^{13}CH$_3$. The dark green product of the previous reaction was dissolved in diethyl ether (200 mL) and the solution was transferred to a 500 mL 3-neck-round bottom flask. A large condenser designed for the use of dry ice/acetone as coolant and fitted with a gas inlet adapter was attached to the flask, as were a glass stopper and a rubber septum. The condenser was cooled to - 78 °C and the reaction flask was cooled to 0 °C. Methanol (10.0 mL, 7.91 g, 0.247 mol) was then added dropwise using a syringe. The reaction was allowed to proceed for 1 hour at 0 °C after which time the mixture was dark red and a tan solid had precipitated from solution. The apparatus was then evacuated and the volatiles were transferred, under dynamic vacuum, into a trap cooled to 77 K. When finished, the trap was isolated from dynamic vacuum and the contents of the trap were transferred to a thick walled glass vessel. The vessel was cooled to –95 °C using a toluene/dry ice slush and the portion which was volatile at this temperature was transferred, under dynamic vacuum, through one –95 °C trap into a trap cooled to 77 K. The contents of the 77 K trap were then transferred into a thick walled glass vessel and this process was repeated twice. After this time, all diethyl ether had been removed from the sample, as characterized by ^{1}H NMR. The reaction vessel containing the propylene was then cooled to -145 °C using a slush composed of a mixture of *n*-pentane and isopentane cooled with liquid nitrogen. The contents of the trap which were volatile at this temperature were then transferred, under dynamic vacuum, through one –145 °C trap into a trap cooled to 77 K. After this procedure, the thick walled reaction vessel contained a mixture of CH$_2$=CD^{13}CH$_3$ and ^{13}C and ^{2}H labeled propane. This mixture was stored at –78 °C in a thick walled glass vessel. **CAUTION: Extreme care should be taken with the storage of propylene in a closed container as its vapor pressure at room temperature exceeds 12 atm.** ^{1}H NMR (C$_6$D$_6$): δ 4.99 (m,

cis-CH(*H*)$CD^{13}CH_3$, 1H), 4.94 (d, trans-C*H*(H)$CD^{13}CH_3$, 1H, $^3J_{CH}$ = 12 Hz), 1.53 (dm, $CH_2CD^{13}CH_3$, 3H, $^1J_{CH}$ = 126 Hz). ^{13}C {^1H} NMR (C_6D_6): δ 133.3 (d(1:1:1 t), $CH_2CD^{13}CH_3$, $^2J_{CC}$ = 42 Hz, $^1J_{CD}$ = 42 Hz), 115.7 (s, $CH_2CD^{13}CH_3$), 19.2 (1:1:1 t, $CH_2CD^{13}CH_3$, $^2J_{CD}$ = 0.7 Hz). ^2H {^1H} NMR ($C_2H_2Cl_4$): d 5.88 (s (br), $CH_2C\mathit{D}^{13}CH_3$)

Polymerization Experiments. The polymerization apparatus consisted of two separate reaction chambers connected, at a 135° angle, by glass tubing with an O-ring joint. A needle valve with a ground glass joint was also present for connection to a vacuum line, and the entire apparatus was made out of thick-walled glass. The general procedure followed for the polymerization experiments is as follows. In an inert atmosphere glove box, toluene solutions of the catalyst (0.25 mg in 0.25 mL) and MAO (50 mg in 7.5 mL) were loaded separately into the reaction chambers; a magnetic stir bar was also placed in the chamber containing the MAO solution. The apparatus was then assembled and subsequently evacuated on a high vacuum line. The gas manifold of the vacuum line was filled with 1 atm of the monomer, the needle valve to the vessel containing the monomer was closed, and the needle valve to the polymerization apparatus was opened. Dissolution of the monomer was monitored by the pressure drop in the manifold, and this procedure was then repeated until no further pressure decrease was observed. Four iterations of this process sufficed to completely saturate the solutions; thus, low pressure polymerizations were carried out using only one iteration. After addition of the desired amount of monomer, the apparatus was placed in an oil bath at the appropriate temperature, and allowed to equilibrate for 15 minutes. The individual solutions of catalyst and MAO were then mixed, resulting in activation of the catalyst and initiation of polymerization; as no pressure regulation was possible in these experiments, the polymerizations were allowed to proceed for only one minute to ensure minimal pressure drop over the course of the reaction. After this time, a 4:1 mixture of methanol and concentrated aqueous HCl was added to quench the reaction, and the polymer was then precipitated from the reaction mixture by the addition of approximately 100 – 200 mL of the methanol/HCl solution. Approximately 100 mg of polymer were typically isolated.

NMR Experiments. The NMR spectra were acquired on a Varian UNITY$_{INOVA}$ 500 MHz spectrometer operating at 125.699 MHz for ^{13}C, 499.853

MHz for ^{1}H and 76.730 MHz for ^{2}H. ^{13}C and ^{1}H NMR spectra were obtained at 85 °C using dilute solutions of polymer in 1,1,2,2-tetrachloroethane-d_2 (~ 5 mg in 0.7 mL). ^{2}H spectra were acquired at 85 °C using samples of the same concentration in 1,1,2,2-tetrachloroethane with no solvent lock. For ^{13}C, a calibrated 90° pulse width was used with 4 – 10 sec recycle delay, 2 – 3 sec acquisition time, inverse gated ^{1}H decoupling, and 800 – 1000 transients. For ^{2}H, a calibrated 90° pulse width was used with 5 sec recycle delay, 1 sec acquisition time and 64 transients.

Acknowledgment

I gratefully acknowledge Peter Green and Nathan Daleska for kind and expert assistance with the GC-MS experiments.

References and Notes

1. (a) Resconi, L.; Camurati, I.; Sudmeijer, O. *Top. Catal.* **1999**, *7*, 145; (b) Busico, V.; Cipullo, R. *J. Am. Chem. Soc.* **1994**, *116*, 9329; (c) Busico, V.; Cipullo, R. *J. Organomet. Chem.* **1995**, *497*, 113; (d) Resconi, L.; Fait, A.; Piemontesi, F.; Colonnesi, M.; Rychlicki, H.; Zeigler, R. *Macromolecules*, **1995**, *28*, 6667; (e) Jüngling, S.; Mülhaupt, R.; Stehling, U.; Brintzinger, H.-H.; Fischer, D.; Langhauser, F. *J. Polymer Sci., Part A: Polymer Chem.* **1995**, *33*, 1305; (f) Schneider, M. J.; Kaji, E.; Uozumi, T.; Soga, K. *Macromol. Chem. Phys.* **1997**, *198*, 2899.
2. (a) Shmulinson, M.; Galan-Fereres, M.; Lisovskii, A.; Nelkenbaum, E.; Semiat, R.; Eisen, M. S. *Organometallics* **2000**, *19*, 1208; (b) Volkis, V.; Shmulinson, M.; Averbuj, C.; Lisovskii, A.; Edelmann, F. T.; Eisen, M. S. *Organometallics* **1998**, *17*, 3155.
3. Ewen, J. A. *J. Am. Chem. Soc.* **1984**, *106*, 6355.
4. (a) Leclerc, M. K.; Brintzinger, H.-H. *J. Am. Chem. Soc.* **1995**, *117*, 1651; (b) Leclerc, M. K.; Brintzinger, H.-H. *J. Am. Chem. Soc.* **1996**, *118*, 9024.
5. Busico, V.; Caporaso, L.; Cipullo, R.; Landriani, L.; Angelini, G.; Margonelli, A.; Segre, A. L. *J. Am. Chem. Soc.* **1996**, *118*, 2105.
6. Busico, V.; Brita, D.; Caporaso, L.; Cipullo, R.; Vacatello, M. *Macromolecules*, **1997**, *30*, 3971.
7. Peng, T.-S.; Gladysz, J. A. *J. Am. Chem. Soc.* **1992**, *114*, 4174.

8. Busico, V.; Cipullo, R.; Caporaso, L.; Angelini, G.; Segre, A. L. *J. Mol. Catal. A* **1998**, *128*, 53.
9. Prosenc, M.-H.; Brintzinger, H.-H. *Organometallics* **1997**, *16*, 3889.
10. Resconi, L. *J. Mol. Catal. A: Chem* **1999**, *146*, 167.
11. (a) Karol, F. J.; Kao, S.-C.; Wasserman, E. P.; Brady, R. C. *New J. Chem.* **1997**, *21*, 797; (b) Wasserman, E.; Hsi, E.; Young, W.-T. *Polymer Preprints* **1998**, *39* (2), 45; (c) Chapter 2, this work.
12. Kubas, G. J. *Acc. Chem. Res.* **1988**, *21*, 120.
13. (a) Abrams, M. B.; Yoder, J. C.; Loeber, C.; Day, M. W.; Bercaw, J. E. *Organometallics*, **1999**, *18*, 1389; (b) Chapter 1, this work.
14. Lieber, S.; Prosenc, M.-H.; Brintzinger, H.-H. *Organometallics* **2000**, *19*, 377.
15. (a) Margl, P. M.; Woo, T. K.; Blöchl, P. E.; Ziegler, T. *J. Am. Chem. Soc.* **1998**, *120*, 2174; (b) Margl, P. M.; Woo, T. K.; Ziegler, T. *Organometallics* **1998**, *17*, 4997.
16. Busico, V.; Cipullo, R.; Monaco, G.; Vacatello, M.; Segre, A. L. *Macromolecules* **1997**, *30*, 6251.
17. Burger, B. J.; Bercaw, J. E. *New Developments in the Synthesis, Manipulation, and Characterization of Organometallic Compounds*; Wayda, A.; Darensbourg, M. Y., Eds.; American Chemical Society: Washington, DC, 1987; Vol. 357.
18. Marvich, R. H.; Brintzinger, H. H. *J. Am. Chem. Soc.* **1971**, *93*, 2046.
19 Buchwald S. L.; Lamaire, S. J.; Nielsen, R. B.; Watson, B. T.; King, S. M. *Tetrahedron Lett.* **1987**, *28*, 3895.

Appendix. Summary of the Processes Proposed to Occur During Chain Epimerization of the Doubly Labeled Propylene.

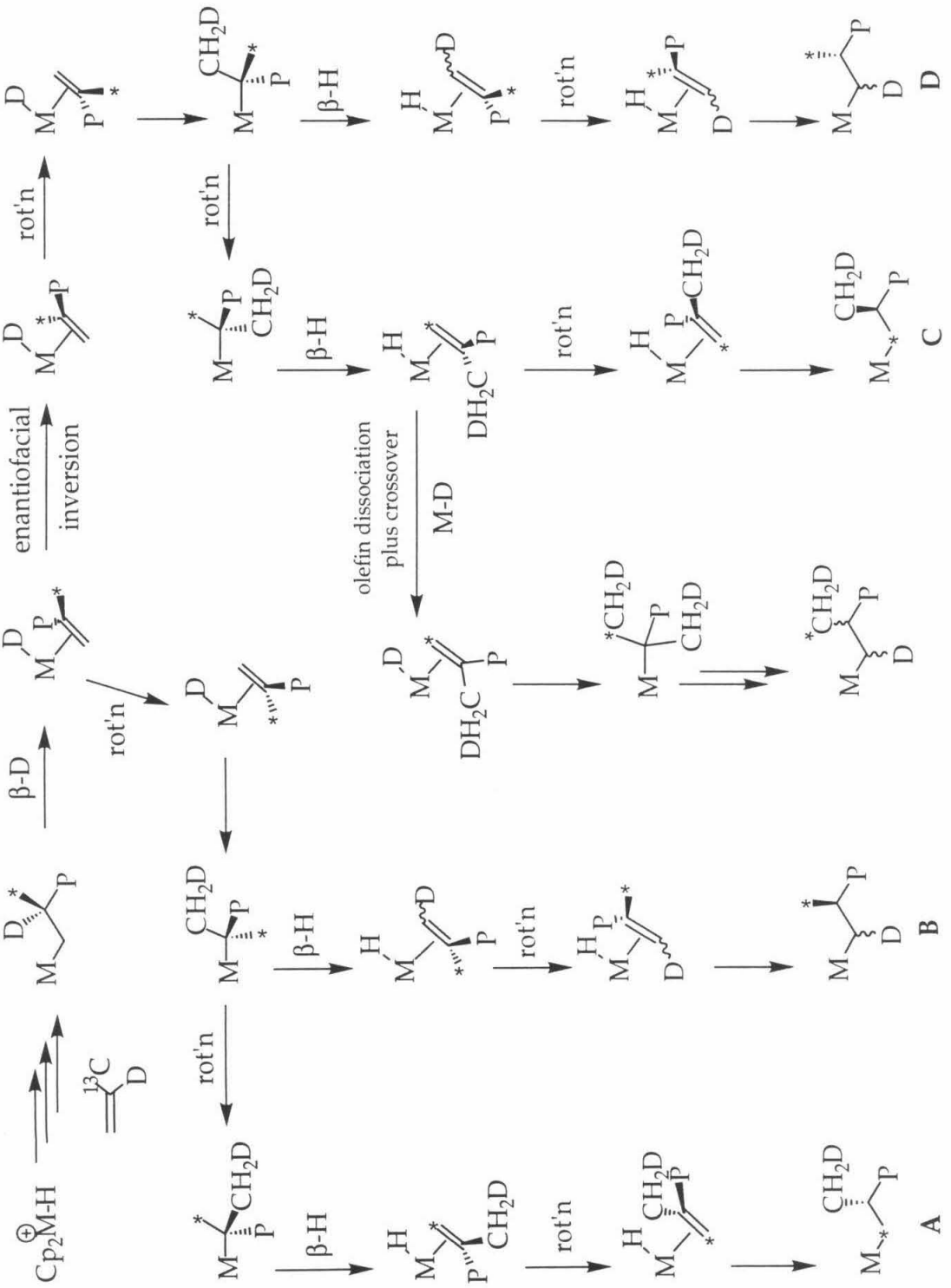

Scheme 1. Summary of proposed steps for chain epimerization using the tertiary-alkyl mechanism.

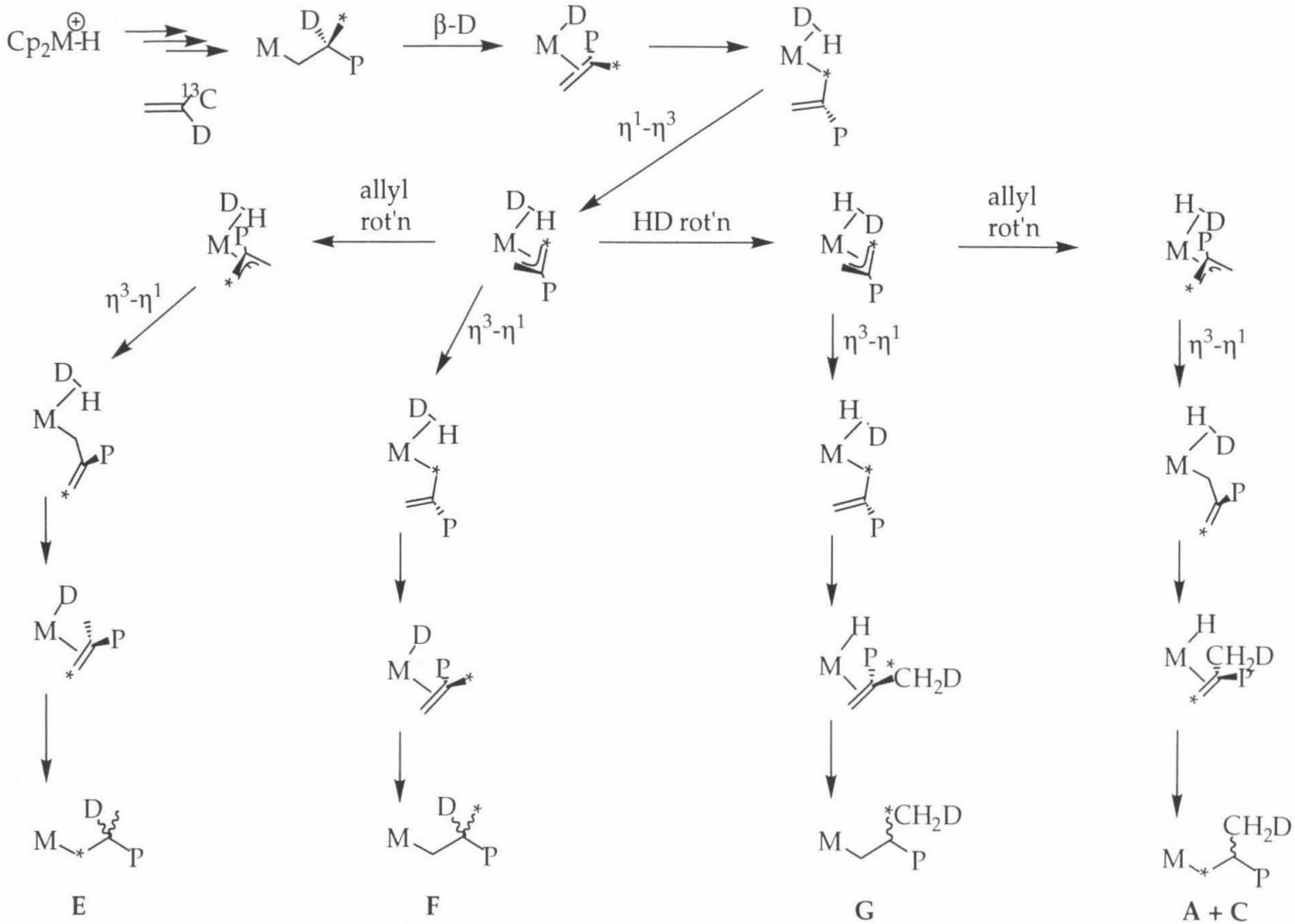

Scheme 2. Summary of proposed steps for chain epimerization using the allyl mechanism.

Appendices

Appendix 1. Numbering Scheme for Compounds Referred to in the Text 116

Appendix 2. Additional Data for the X-Ray Structure Determinations 120

Appendix 1. Numbering Scheme for Compounds Referred to in the Text

1 *rac*-IpScCl·LiCl(THF)$_2$

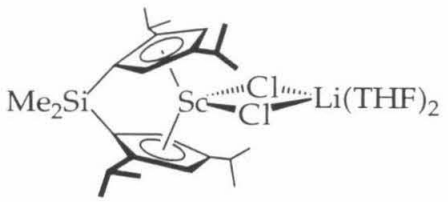

2 *meso*-[IpScCl]$_2$

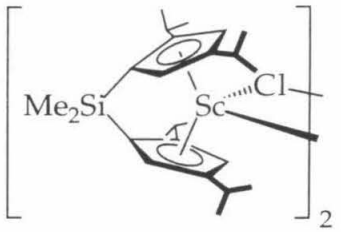

3 *rac*-IpYCl·LiCl(THF)$_2$

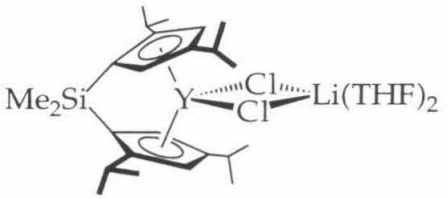

4 *meso*-[IpYCl]$_2$

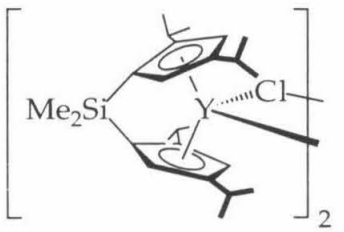

5 *rac*-IpSc(η^3-C_3H_5)

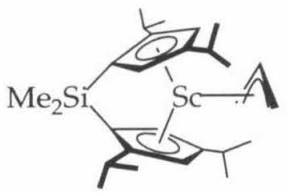

6 *meso*-IpSc(η^3-C_3H_5)

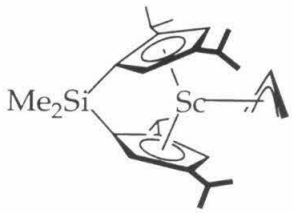

7 *rac*-IpSc(η^3-1-Me-C_3H_4)

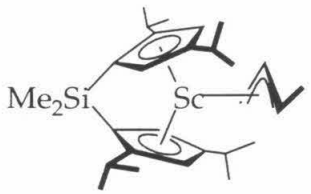

8 *meso*-IpSc(η^3-1-Me-C_3H_4)

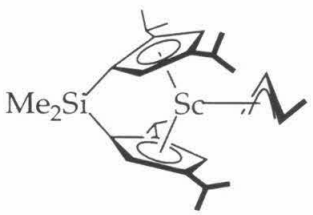

9 *meso*-IpZr(NMe_2)$_2$

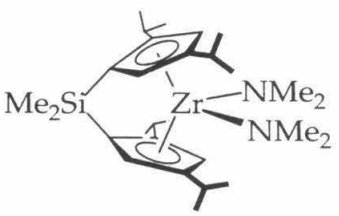

10 $Cp^*_2ScC(H)=CMe_2$

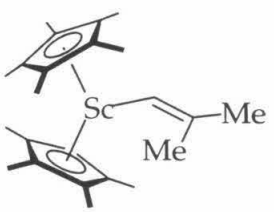

11 $Cp^*_2ScC(Me)=CMe_2$

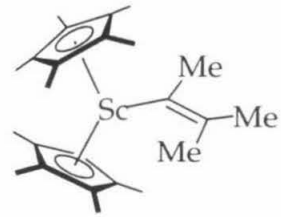

12 $OpScC(Me)=CH(Me)$

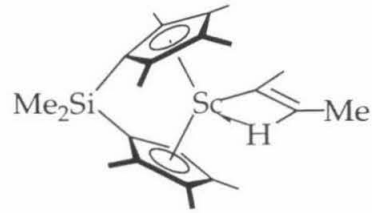

13 $OpScC(Me)=CH(CHMe_2)$

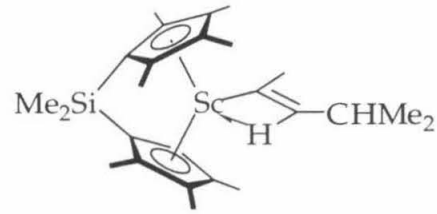

14 $[Cp^*(C_5Me_4\text{-}\mu\text{-}CH_2)Sc]_2$

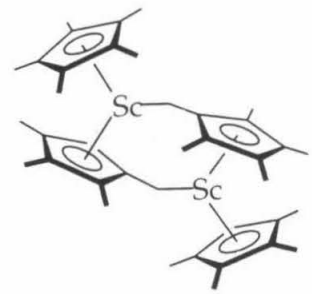

15 $OpSc(\eta^3\text{-}1\text{-}Me\text{-}C_3H_4)$

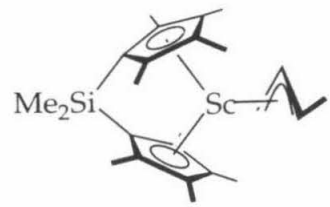

16 OpSc(η^3-1-CHMe$_2$-C$_3$H$_4$)

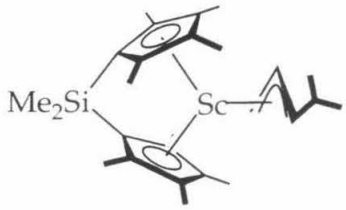

17 OpScPh

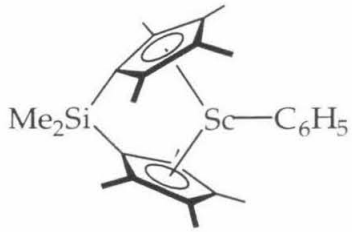

Appendix 2. Additional Data for the X-Ray Structure Determinations

A. *rac*-IpScCl·LiCl(THF)$_2$ (**1**)

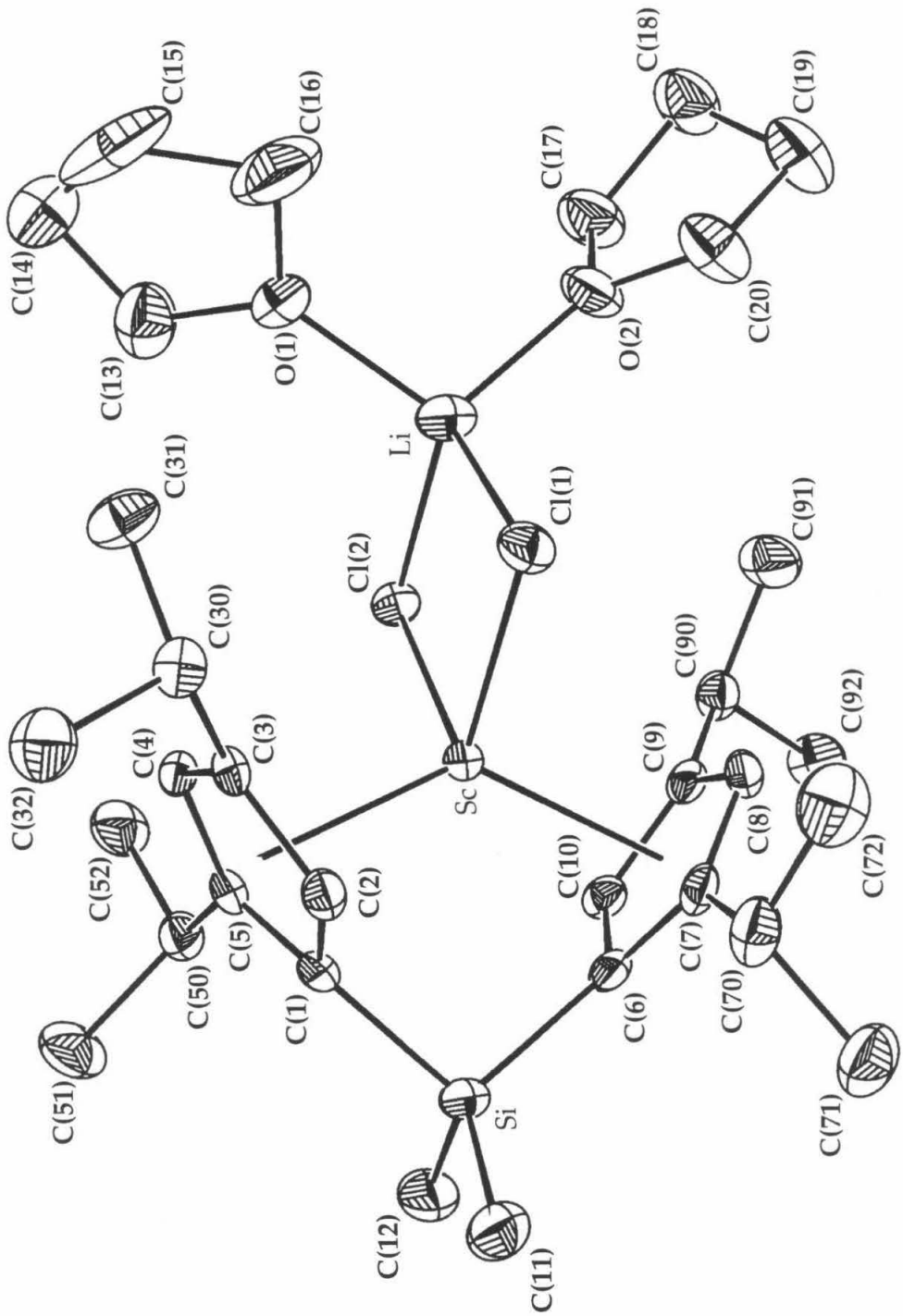

Figure 1. ORTEP representation of the molecular structure of **1** showing the complete atom labeling scheme (50% probability ellipsoids, hydrogens omitted for clarity).

Table 1. X-ray Diffraction Data Collection Parameters for **1**[a]

Feature	Value
Empirical formula	$C_{32}H_{54}Cl_2LiO_2ScSi$
Formula weight (g/mol)	621.64
Crystal size (mm)	0.4 x 0.3 x 0.3
Temp. (K)	160
Space Group	$P2_1/n$
Cell Constants	a = 12.547 (3) Å b = 19.314 (4) Å c = 14.893 (3) Å β = 96.47 (3)°
Volume (Å^3)	3586.1 (13)
Z	4
Density (calculated) (g/mL)	1.151
2θ range (°)	3.5 to 46.0
Index ranges	$0 \le h \le 13$, $-21 \le k \le 21$, $-16 \le l \le 16$
Reflections collected	10918
Independent reflections	4965
R (merge)	0.028
GOF (merge)[b]	1.11
Data / restraints / parameters	4961 / 0 / 568
GOF (F^2)[b]	1.514
R indices (all data)[c, d]	R1 = 0.0464, wR2 = 0.0691

[a]Structure was obtained on an Enraf-Nonius CAD-4 using MoKα radiation (λ = 0.71073 Å); [b]$GOF = \{\Sigma w(F_o^2 - F_c^2)^2 / n - p\}^{1/2}$ (n = number of data, p = number of variables); [c]$R1 = \Sigma | |F_o| - |F_c| | / \Sigma |F_o|$; [d]$wR2 = \{\Sigma(w(F_o^2 - F_c^2)^2) / \Sigma(wF_o^4)\}^{1/2}$.

Table 2. Special Refinement Details for **1**

Weights w are calculated as $1/\sigma^2(F_o^2)$. The variances ($\sigma^2(Fo^2)$) were derived from counting statistics plus an additional term, $(0.014I)^2$, and the variances of the merged data were obtained by propagation of error plus the addition of another term, $(0.014<I>)2$.

All esd's (except the esd in the dihedral angle between two l.s. planes) are estimated using the full covariance matrix. The cell esd's are taken into account individually in the estimation of esd's in distances, angles and torsion angles; correlations between esd's in cell parameters are only used when they are defined by crystal symmetry. An approximate (isotropic) treatment of cell esd's is used for estimating esd's involving l.s. planes.

Table 3. Atomic Coordinates (x 10^4) and Equivalent Isotropic Displacement Parameters ($Å^2$ x 10^3) for **1**[a]

	x	y	z	U_{eq}
Sc	2424(1)	2779(1)	4811(1)	17(1)
Si	2345(1)	1091(1)	4566(1)	26(1)
Cl(1)	3748(1)	3723(1)	5218(1)	28(1)
Cl(2)	983(1)	3685(1)	4633(1)	24(1)
Li	2300(4)	4514(2)	5073(3)	33(1)
O(1)	1908(2)	5018(1)	6090(1)	42(1)
O(2)	2672(1)	5247(1)	4316(1)	34(1)
C(1)	2195(2)	1661(1)	5559(2)	20(1)
C(2)	3114(2)	1985(1)	6028(2)	21(1)
C(3)	2803(2)	2543(1)	6549(1)	20(1)
C(4)	1684(2)	2589(1)	6370(2)	19(1)
C(5)	1295(2)	2055(1)	5774(1)	20(1)
C(6)	2628(2)	1799(1)	3768(1)	21(1)
C(7)	3588(2)	2196(1)	3744(1)	21(1)
C(8)	3295(2)	2828(1)	3308(2)	22(1)
C(9)	2187(2)	2851(1)	3054(1)	20(1)
C(10)	1776(2)	2222(1)	3357(2)	20(1)
C(11)	3432(3)	448(2)	4863(2)	42(1)
C(12)	1119(3)	602(2)	4110(2)	41(1)
C(13)	978(3)	4946(2)	6570(2)	47(1)
C(14)	1179(5)	5373(2)	7407(3)	78(1)
C(15)	2344(4)	5550(2)	7477(3)	81(2)
C(16)	2575(4)	5550(2)	6520(3)	79(1)
C(17)	1936(2)	5780(2)	3955(2)	42(1)
C(18)	2628(3)	6370(2)	3712(2)	44(1)
C(19)	3593(3)	6002(2)	3431(2)	46(1)
C(20)	3727(2)	5394(2)	4072(2)	42(1)
C(30)	3522(2)	2930(1)	7264(2)	25(1)
C(31)	3077(3)	3631(2)	7503(2)	36(1)
C(32)	3708(3)	2477(2)	8112(2)	34(1)
C(50)	129(2)	1866(1)	5527(2)	25(1)
C(51)	-148(3)	1230(2)	6074(2)	41(1)
C(52)	-650(2)	2444(2)	5676(2)	34(1)
C(70)	4721(2)	1949(1)	4028(2)	31(1)
C(71)	5022(3)	1382(2)	3386(2)	42(1)
C(72)	5550(2)	2524(2)	4088(2)	44(1)
C(90)	1558(2)	3397(1)	2492(2)	24(1)
C(91)	2128(3)	4091(1)	2511(2)	36(1)
C(92)	1303(3)	3148(2)	1513(2)	32(1)

[a] $U(eq)$ is defined as the trace of the orthogonalized U^{ij} tensor.

Table 4. Complete List of Bond Lengths (Å) and Angles (°) for **1**

Feature	Length (Å) or angle (°)	Feature	Length (Å) or angle (°)
Sc-Cl(1)	2.4964(8)	C(12)-H(12B)	0.93(3)
Sc-Cl(2)	2.5089(8)	C(12)-H(12C)	0.95(3)
Sc-X(1A)	2.2385(5)	C(13)-C(14)	1.491(5)
Sc-X(1B)	2.2356(6)	C(13)-H(13A)	0.98(3)
Pln1-Sc	2.228(2)	C(13)-H(13B)	0.96(3)
Pln2-Sc	2.229(2)	C(14)-C(15)	1.495(6)
Sc-C(2)	2.456(2)	C(14)-H(14A)	0.94(4)
Sc-C(1)	2.461(2)	C(14)-H(14B)	0.91(5)
Sc-C(10)	2.471(2)	C(15)-C(16)	1.486(6)
Sc-C(6)	2.479(2)	C(15)-H(15A)	0.88(3)
Sc-C(7)	2.539(2)	C(15)-H(15B)	0.98(4)
Sc-C(5)	2.544(2)	C(16)-H(16A)	0.96(3)
Sc-C(8)	2.601(2)	C(16)-H(16B)	0.94(4)
Sc-C(9)	2.604(2)	C(17)-C(18)	1.503(4)
Sc-C(3)	2.618(2)	C(17)-H(17A)	1.01(3)
Sc-C(4)	2.622(2)	C(17)-H(17B)	0.98(3)
Si-C(11)	1.862(3)	C(18)-C(19)	1.503(4)
Si-C(12)	1.865(3)	C(18)-H(18A)	1.04(3)
Si-C(1)	1.870(2)	C(18)-H(18B)	0.93(3)
Si-C(6)	1.873(2)	C(19)-C(20)	1.509(4)
Cl(1)-Li	2.364(4)	C(19)-H(19A)	0.97(3)
Cl(2)-Li	2.341(4)	C(19)-H(19B)	0.91(3)
Li-O(2)	1.900(4)	C(20)-H(20A)	0.96(3)
Li-O(1)	1.911(4)	C(20)-H(20A)	0.99(3)
O(1)-C(16)	1.430(4)	C(30)-C(31)	1.523(4)
O(1)-C(13)	1.442(3)	C(30)-C(32)	1.532(4)
O(2)-C(20)	1.440(3)	C(30)-H(30)	0.96(2)
O(2)-C(17)	1.446(3)	C(31)-H(31A)	1.02(3)
C(1)-C(2)	1.424(3)	C(31)-H(31B)	0.98(3)
C(1)-C(5)	1.428(3)	C(31)-H(31C)	0.97(3)
C(2)-C(3)	1.408(3)	C(32)-H(32A)	0.99(3)
C(2)-H(2)	0.90(2)	C(32)-H(32B)	0.94(2)
C(3)-C(4)	1.402(3)	C(32)-H(32C)	1.00(3)
C(3)-C(30)	1.513(3)	C(50)-C(52)	1.518(4)
C(4)-C(5)	1.412(3)	C(50)-C(51)	1.537(4)
C(4)-H(4)	0.89(2)	C(50)-H(50)	0.93(2)
C(5)-C(50)	1.512(3)	C(51)-H(51A)	0.93(3)
C(6)-C(10)	1.426(3)	C(51)-H(51B)	1.02(3)
C(6)-C(7)	1.430(3)	C(51)-H(51C)	0.97(3)
C(7)-C(8)	1.412(3)	C(52)-H(52A)	1.00(3)
C(7)-C(70)	1.514(3)	C(52)-H(52B)	0.92(3)
C(8)-C(9)	1.400(3)	C(52)-H(52C)	0.99(2)
C(8)-H(8)	0.88(2)	C(70)-C(72)	1.518(4)
C(9)-C(10)	1.413(3)	C(70)-C(71)	1.530(4)
C(9)-C(90)	1.512(3)	C(70)-H(70)	0.93(2)
C(10)-H(10)	0.91(2)	C(71)-H(71A)	0.99(3)
C(11)-H(11A)	0.91(3)	C(71)-H(71B)	0.99(3)
C(11)-H(11B)	0.96(3)	C(71)-H(71C)	0.92(3)
C(11)-H(11C)	0.95(3)	C(72)-H(72A)	0.93(3)
C(12)-H(12A)	0.93(3)	C(72)-H(72B)	0.95(3)

C(72)-H(72C)	0.96(3)
C(90)-C(91)	1.517(4)
C(90)-C(92)	1.534(3)
C(90)-H(90)	0.92(2)
C(91)-H(91A)	0.99(3)
C(91)-H(91B)	0.99(3)
C(91)-H(91C)	0.95(3)
C(92)-H(92A)	0.98(2)
C(92)-H(92B)	0.99(3)
C(92)-H(92C)	0.96(3)
X(1A)-Sc-X(1B)	127.91(2)
Pln1-Sc-Pln2	118.42(7)
Cl(1)-Sc-Cl(2)	88.14(3)
C(2)-Sc-C(1)	33.66(8)
C(2)-Sc-C(10)	115.39(8)
C(1)-Sc-C(10)	88.36(8)
C(2)-Sc-C(6)	86.21(8)
C(1)-Sc-C(6)	68.92(7)
C(10)-Sc-C(6)	33.48(7)
C(2)-Sc-Cl(1)	96.15(6)
C(1)-Sc-Cl(1)	129.75(6)
C(10)-Sc-Cl(1)	132.47(6)
C(6)-Sc-Cl(1)	126.64(6)
C(2)-Sc-Cl(2)	134.69(6)
C(1)-Sc-Cl(2)	122.72(6)
C(10)-Sc-Cl(2)	92.84(6)
C(6)-Sc-Cl(2)	126.18(6)
C(2)-Sc-C(7)	90.31(8)
C(1)-Sc-C(7)	89.95(8)
C(10)-Sc-C(7)	54.15(8)
C(6)-Sc-C(7)	33.09(7)
Cl(1)-Sc-C(7)	93.56(6)
Cl(2)-Sc-C(7)	134.56(6)
C(2)-Sc-C(5)	54.09(8)
C(1)-Sc-C(5)	33.09(7)
C(10)-Sc-C(5)	96.07(8)
C(6)-Sc-C(5)	92.16(8)
Cl(1)-Sc-C(5)	131.47(6)
Cl(2)-Sc-C(5)	90.15(6)
C(7)-Sc-C(5)	120.34(8)
C(2)-Sc-C(8)	120.71(8)
C(1)-Sc-C(8)	120.25(8)
C(10)-Sc-C(8)	52.48(8)
C(6)-Sc-C(8)	53.54(8)
Cl(1)-Sc-C(8)	81.32(6)
Cl(2)-Sc-C(8)	104.55(6)
C(7)-Sc-C(8)	31.87(7)
C(5)-Sc-C(8)	145.08(8)
C(2)-Sc-C(9)	139.99(8)
C(1)-Sc-C(9)	119.73(7)
C(10)-Sc-C(9)	32.20(7)
C(6)-Sc-C(9)	54.48(7)
Cl(1)-Sc-C(9)	101.69(6)
Cl(2)-Sc-C(9)	81.80(6)
C(7)-Sc-C(9)	53.37(7)
C(5)-Sc-C(9)	126.01(7)
C(8)-Sc-C(9)	31.22(7)
C(2)-Sc-C(3)	32.03(7)
C(1)-Sc-C(3)	54.37(7)
C(10)-Sc-C(3)	142.72(8)
C(6)-Sc-C(3)	117.84(7)
Cl(1)-Sc-C(3)	81.07(6)
Cl(2)-Sc-C(3)	105.91(6)
C(7)-Sc-C(3)	119.23(7)
C(5)-Sc-C(3)	53.00(7)
C(8)-Sc-C(3)	144.07(8)
C(9)-Sc-C(3)	171.98(7)
C(2)-Sc-C(4)	52.37(8)
C(1)-Sc-C(4)	53.51(7)
C(10)-Sc-C(4)	126.93(8)
C(6)-Sc-C(4)	121.35(7)
Cl(1)-Sc-C(4)	100.33(6)
Cl(2)-Sc-C(4)	82.44(6)
C(7)-Sc-C(4)	141.09(8)
C(5)-Sc-C(4)	31.67(7)
C(8)-Sc-C(4)	172.91(8)
C(9)-Sc-C(4)	152.36(8)
C(3)-Sc-C(4)	31.04(7)
C(11)-Si-C(12)	107.5(2)
C(11)-Si-C(1)	109.92(13)
C(12)-Si-C(1)	115.69(13)
C(11)-Si-C(6)	116.85(14)
C(12)-Si-C(6)	110.28(13)
C(1)-Si-C(6)	96.65(10)
C(11)-Si-Sc	128.64(12)
C(12)-Si-Sc	123.84(12)
C(1)-Si-Sc	48.08(7)
C(6)-Si-Sc	48.64(7)
Li-Cl(1)-Sc	88.07(10)
Li-Cl(2)-Sc	88.29(11)
O(2)-Li-O(1)	101.1(2)
O(2)-Li-Cl(2)	123.8(2)
O(1)-Li-Cl(2)	109.5(2)
O(2)-Li-Cl(1)	107.3(2)
O(1)-Li-Cl(1)	121.4(2)
Cl(2)-Li-Cl(1)	95.44(15)
O(2)-Li-Sc	130.7(2)
O(1)-Li-Sc	128.0(2)
Cl(2)-Li-Sc	47.90(7)
Cl(1)-Li-Sc	47.57(7)
C(16)-O(1)-C(13)	108.2(2)
C(16)-O(1)-Li	122.1(2)
C(13)-O(1)-Li	129.7(2)
C(20)-O(2)-C(17)	109.4(2)
C(20)-O(2)-Li	126.3(2)
C(17)-O(2)-Li	124.1(2)
C(2)-C(1)-C(5)	105.8(2)

C(2)-C(1)-Si	119.9(2)
C(5)-C(1)-Si	130.0(2)
C(2)-C(1)-Sc	72.98(13)
C(5)-C(1)-Sc	76.64(13)
Si-C(1)-Sc	97.50(9)
C(3)-C(2)-C(1)	110.3(2)
C(3)-C(2)-Sc	80.32(14)
C(1)-C(2)-Sc	73.36(13)
C(3)-C(2)-H(2)	123.8(13)
C(1)-C(2)-H(2)	125.9(13)
Sc-C(2)-H(2)	115.2(12)
C(4)-C(3)-C(2)	106.1(2)
C(4)-C(3)-C(30)	127.4(2)
C(2)-C(3)-C(30)	125.8(2)
C(4)-C(3)-Sc	74.63(13)
C(2)-C(3)-Sc	67.65(12)
C(30)-C(3)-Sc	129.6(2)
C(3)-C(4)-C(5)	110.0(2)
C(3)-C(4)-Sc	74.33(13)
C(5)-C(4)-Sc	71.14(12)
C(3)-C(4)-H(4)	127.5(14)
C(5)-C(4)-H(4)	122.5(14)
Sc-C(4)-H(4)	120.8(13)
C(4)-C(5)-C(1)	107.7(2)
C(4)-C(5)-C(50)	125.9(2)
C(1)-C(5)-C(50)	125.8(2)
C(4)-C(5)-Sc	77.19(13)
C(1)-C(5)-Sc	70.26(12)
C(50)-C(5)-Sc	125.5(2)
C(10)-C(6)-C(7)	106.0(2)
C(10)-C(6)-Si	120.2(2)
C(7)-C(6)-Si	128.8(2)
C(10)-C(6)-Sc	72.95(13)
C(7)-C(6)-Sc	75.76(13)
Si-C(6)-Sc	96.82(9)
C(8)-C(7)-C(6)	107.4(2)
C(8)-C(7)-C(70)	126.0(2)
C(6)-C(7)-C(70)	126.2(2)
C(8)-C(7)-Sc	76.48(13)
C(6)-C(7)-Sc	71.14(12)
C(70)-C(7)-Sc	123.6(2)
C(9)-C(8)-C(7)	110.4(2)
C(9)-C(8)-Sc	74.50(13)
C(7)-C(8)-Sc	71.65(13)
C(9)-C(8)-H(8)	124.1(13)
C(7)-C(8)-H(8)	125.4(13)
Sc-C(8)-H(8)	120.6(13)
C(8)-C(9)-C(10)	105.9(2)
C(8)-C(9)-C(90)	127.7(2)
C(10)-C(9)-C(90)	126.2(2)
C(8)-C(9)-Sc	74.28(13)
C(10)-C(9)-Sc	68.72(12)
C(90)-C(9)-Sc	125.92(15)
C(9)-C(10)-C(6)	110.2(2)
C(9)-C(10)-Sc	79.07(13)
C(6)-C(10)-Sc	73.56(13)
C(9)-C(10)-H(10)	124.7(14)
C(6)-C(10)-H(10)	125.1(14)
Sc-C(10)-H(10)	115.4(14)
Si-C(11)-H(11A)	110.2(19)
Si-C(11)-H(11B)	110.6(16)
H(11A)-C(11)-H(11B)	110.0(24)
Si-C(11)-H(11C)	114.0(17)
H(11A)-C(11)-H(11C)	108.7(25)
H(11B)-C(11)-H(11C)	103.1(23)
Si-C(12)-H(12A)	106.6(19)
Si-C(12)-H(12B)	107.6(18)
H(12A)-C(12)-H(12B)	108.0(24)
Si-C(12)-H(12C)	113.7(17)
H(12A)-C(12)-H(12C)	108.8(24)
H(12B)-C(12)-H(12C)	111.8(25)
O(1)-C(13)-C(14)	106.9(3)
O(1)-C(13)-H(13A)	104.4(18)
C(14)-C(13)-H(13A)	113.6(17)
O(1)-C(13)-H(13B)	107.7(19)
C(14)-C(13)-H(13B)	117.3(19)
H(13A)-C(13)-H(13B)	106.1(26)
C(13)-C(14)-C(15)	104.9(3)
C(13)-C(14)-H(14A)	106.4(28)
C(15)-C(14)-H(14A)	102.3(28)
C(13)-C(14)-H(14B)	111.3(30)
C(15)-C(14)-H(14B)	113.6(32)
H(14A)-C(14)-H(14B)	117.1(39)
C(16)-C(15)-C(14)	103.2(4)
C(16)-C(15)-H(15A)	108.4(22)
C(14)-C(15)-H(15A)	118.6(22)
C(16)-C(15)-H(15B)	108.6(24)
C(14)-C(15)-H(15B)	110.3(25)
H(15A)-C(15)-H(15B)	107.4(30)
O(1)-C(16)-C(15)	105.2(4)
O(1)-C(16)-H(16A)	106.3(25)
C(15)-C(16)-H(16A)	115.2(24)
O(1)-C(16)-H(16B)	108.3(22)
C(15)-C(16)-H(16B)	113.8(24)
H(16A)-C(16)-H(16B)	107.5(33)
O(2)-C(17)-C(18)	105.5(2)
O(2)-C(17)-H(17A)	109.1(17)
C(18)-C(17)-H(17A)	108.6(17)
O(2)-C(17)-H(17B)	110.2(17)
C(18)-C(17)-H(17B)	114.2(18)
H(17A)-C(17)-H(17B)	109.1(25)
C(19)-C(18)-C(17)	102.3(3)
C(19)-C(18)-H(18A)	111.8(18)
C(17)-C(18)-H(18A)	105.8(18)
C(19)-C(18)-H(18B)	113.1(17)
C(17)-C(18)-H(18B)	110.6(17)
H(18A)-C(18)-H(18B)	112.4(24)
C(18)-C(19)-C(20)	103.2(3)

C(18)-C(19)-H(19A)	108.1(19)
C(20)-C(19)-H(19A)	108.4(19)
C(18)-C(19)-H(19B)	111.3(19)
C(20)-C(19)-H(19B)	110.1(19)
H(19A)-C(19)-H(19B)	115.1(27)
O(2)-C(20)-C(19)	105.8(2)
O(2)-C(20)-H(20A)	109.7(17)
C(19)-C(20)-H(20A)	114.6(17)
O(2)-C(20)-H(20A)	105.8(17)
C(19)-C(20)-H(20A)	113.4(17)
H(20A)-C(20)-H(20A)	107.2(23)
C(3)-C(30)-C(31)	113.5(2)
C(3)-C(30)-C(32)	108.8(2)
C(31)-C(30)-C(32)	109.9(2)
C(3)-C(30)-H(30)	106.4(13)
C(31)-C(30)-H(30)	111.3(13)
C(32)-C(30)-H(30)	106.7(13)
C(30)-C(31)-H(31A)	111.1(16)
C(30)-C(31)-H(31B)	110.2(15)
H(31A)-C(31)-H(31B)	108.8(22)
C(30)-C(31)-H(31C)	109.5(15)
H(31A)-C(31)-H(31C)	108.0(22)
H(31B)-C(31)-H(31C)	109.3(21)
C(30)-C(32)-H(32A)	109.0(15)
C(30)-C(32)-H(32B)	112.9(15)
H(32A)-C(32)-H(32B)	106.5(21)
C(30)-C(32)-H(32C)	110.2(14)
H(32A)-C(32)-H(32C)	111.7(20)
H(32B)-C(32)-H(32C)	106.6(20)
C(5)-C(50)-C(52)	114.1(2)
C(5)-C(50)-C(51)	109.6(2)
C(52)-C(50)-C(51)	108.8(2)
C(5)-C(50)-H(50)	109.5(14)
C(52)-C(50)-H(50)	107.0(13)
C(51)-C(50)-H(50)	107.7(13)
C(50)-C(51)-H(51A)	110.6(17)
C(50)-C(51)-H(51B)	108.6(15)
H(51A)-C(51)-H(51B)	108.3(22)
C(50)-C(51)-H(51C)	109.7(17)
H(51A)-C(51)-H(51C)	105.7(24)
H(51B)-C(51)-H(51C)	113.8(23)
C(50)-C(52)-H(52A)	109.8(15)
C(50)-C(52)-H(52B)	112.3(16)
H(52A)-C(52)-H(52B)	110.0(21)
C(50)-C(52)-H(52C)	110.8(14)
H(52A)-C(52)-H(52C)	107.5(20)
H(52B)-C(52)-H(52C)	106.3(21)
C(7)-C(70)-C(72)	113.7(2)
C(7)-C(70)-C(71)	110.0(2)
C(72)-C(70)-C(71)	110.2(2)
C(7)-C(70)-H(70)	109.0(14)
C(72)-C(70)-H(70)	107.3(14)
C(71)-C(70)-H(70)	106.4(14)
C(70)-C(71)-H(71A)	108.8(16)
C(70)-C(71)-H(71B)	110.1(16)
H(71A)-C(71)-H(71B)	112.0(22)
C(70)-C(71)-H(71C)	110.8(16)
H(71A)-C(71)-H(71C)	109.3(23)
H(71B)-C(71)-H(71C)	105.8(23)
C(70)-C(72)-H(72A)	112.4(19)
C(70)-C(72)-H(72B)	108.7(17)
H(72A)-C(72)-H(72B)	108.9(25)
C(70)-C(72)-H(72C)	109.5(15)
H(72A)-C(72)-H(72C)	109.9(24)
H(72B)-C(72)-H(72C)	107.4(22)
C(9)-C(90)-C(91)	113.0(2)
C(9)-C(90)-C(92)	110.4(2)
C(91)-C(90)-C(92)	110.0(2)
C(9)-C(90)-H(90)	107.4(14)
C(91)-C(90)-H(90)	111.9(14)
C(92)-C(90)-H(90)	103.8(14)
C(90)-C(91)-H(91A)	109.8(15)
C(90)-C(91)-H(91B)	111.3(15)
H(91A)-C(91)-H(91B)	108.4(21)
C(90)-C(91)-H(91C)	113.2(16)
H(91A)-C(91)-H(91C)	108.3(21)
H(91B)-C(91)-H(91C)	105.6(22)
C(90)-C(92)-H(92A)	113.3(14)
C(90)-C(92)-H(92B)	112.1(14)
H(92A)-C(92)-H(92B)	105.5(19)
C(90)-C(92)-H(92C)	107.6(15)
H(92A)-C(92)-H(92C)	110.0(20)
H(92B)-C(92)-H(92C)	108.2(20)

Table 5. Anisotropic Displacement Parameters ($Å^2 \times 10^4$) for **1**[a]

	U^{11}	U^{22}	U^{33}	U^{23}	U^{13}	U^{12}
Sc	210(3)	156(2)	159(2)	-2(2)	52(2)	-11(2)
Si	389(4)	165(4)	229(4)	-7(3)	80(3)	16(3)
Cl(1)	290(4)	263(3)	292(3)	-15(3)	47(3)	-88(3)
Cl(2)	279(3)	195(3)	264(3)	1(3)	68(3)	31(3)
Li	440(30)	220(20)	330(30)	-30(20)	70(20)	-20(20)
O(1)	552(13)	352(11)	401(11)	-149(9)	199(10)	-101(10)
O(2)	355(11)	231(10)	454(11)	78(8)	102(9)	-29(8)
C(1)	300(14)	147(12)	169(13)	38(10)	65(11)	-5(11)
C(2)	216(15)	221(13)	207(14)	57(11)	72(11)	53(12)
C(3)	251(14)	209(13)	134(12)	44(10)	58(10)	-6(11)
C(4)	235(14)	189(13)	166(13)	8(10)	83(11)	25(11)
C(5)	264(14)	191(13)	156(12)	50(10)	68(10)	-17(11)
C(6)	310(15)	179(13)	156(13)	-25(10)	74(11)	44(11)
C(7)	255(14)	264(14)	133(12)	-24(10)	73(10)	36(11)
C(8)	255(15)	238(14)	181(13)	-9(11)	95(11)	-63(12)
C(9)	252(14)	215(13)	126(12)	-29(10)	42(10)	11(11)
C(10)	228(15)	208(13)	174(13)	-47(10)	30(11)	-13(12)
C(11)	650(20)	310(20)	320(20)	33(15)	150(20)	150(20)
C(12)	620(20)	290(20)	350(20)	-64(15)	120(20)	-130(20)
C(13)	480(20)	540(20)	420(20)	70(20)	150(20)	130(20)
C(14)	1270(40)	530(30)	610(30)	-140(20)	460(30)	-50(30)
C(15)	1110(40)	650(30)	600(30)	-440(20)	-150(30)	260(30)
C(16)	790(30)	750(30)	880(30)	-550(30)	320(30)	-310(30)
C(17)	410(20)	300(20)	580(20)	100(20)	130(20)	34(15)
C(18)	500(20)	360(20)	480(20)	170(20)	100(20)	20(20)
C(19)	370(20)	490(20)	520(20)	230(20)	60(20)	-30(20)
C(20)	300(20)	410(20)	560(20)	160(20)	50(20)	-38(15)
C(30)	230(14)	310(20)	216(14)	-3(11)	35(11)	0(12)
C(31)	420(20)	350(20)	300(20)	-112(14)	-10(20)	-8(15)
C(32)	340(20)	440(20)	240(20)	-3(13)	-20(14)	0(20)
C(50)	277(15)	260(14)	231(15)	-18(11)	77(12)	-67(12)
C(51)	360(20)	330(20)	560(20)	60(20)	140(20)	-100(20)
C(52)	250(20)	350(20)	430(20)	18(15)	96(14)	-57(14)
C(70)	280(20)	420(20)	240(20)	56(13)	84(12)	119(13)
C(71)	400(20)	490(20)	390(20)	10(20)	150(20)	160(20)
C(72)	200(20)	600(20)	510(20)	-20(20)	50(20)	50(20)
C(90)	257(15)	269(14)	196(14)	22(11)	53(12)	34(12)
C(91)	530(20)	290(20)	250(20)	61(13)	0(20)	-10(15)
C(92)	370(20)	340(20)	240(20)	39(13)	-35(14)	30(20)

[a]The anisotropic displacement factor exponent takes the form: $-2p^2 (h^2 a^{*2} U^{11} + ... + 2 h k a^* b^* U^{12})$

Table 6. Hydrogen Coordinates (x 10^4) and Isotropic Displacement Parameters ($Å^2$ x 10^3) for **1**

	x	y	z	U_{iso}
H(2)	3797(17)	1850(10)	6017(13)	7(5)
H(4)	1255(17)	2899(10)	6584(13)	13(6)
H(8)	3740(17)	3165(10)	3208(13)	11(6)
H(10)	1067(18)	2101(11)	3289(14)	19(6)
H(11A)	3219(24)	128(15)	5256(20)	60(10)
H(11B)	3624(21)	223(14)	4332(18)	51(9)
H(11C)	4092(23)	647(14)	5118(18)	49(9)
H(12A)	1326(23)	302(15)	3677(20)	61(10)
H(12B)	903(23)	339(15)	4580(19)	60(10)
H(12C)	556(23)	889(15)	3840(19)	58(10)
H(13A)	935(24)	4448(16)	6688(19)	66(10)
H(13B)	359(26)	5058(16)	6158(21)	75(11)
H(14A)	849(36)	5804(23)	7272(28)	132(19)
H(14B)	988(38)	5142(24)	7895(31)	155(22)
H(15A)	2556(25)	5947(17)	7720(21)	67(11)
H(15B)	2771(32)	5187(21)	7801(26)	115(16)
H(16A)	2388(31)	5970(20)	6190(25)	100(17)
H(16B)	3294(31)	5446(18)	6446(24)	96(14)
H(17A)	1509(24)	5603(15)	3385(20)	67(10)
H(17B)	1442(25)	5899(15)	4396(20)	70(10)
H(18A)	2815(26)	6652(16)	4305(22)	81(11)
H(18B)	2269(22)	6637(14)	3249(19)	51(9)
H(19A)	3407(26)	5825(16)	2821(22)	75(12)
H(19B)	4184(25)	6275(15)	3505(19)	62(10)
H(20A)	4020(23)	4988(15)	3826(19)	57(10)
H(20A)	4174(23)	5500(14)	4644(19)	59(10)
H(30)	4205(18)	2977(11)	7035(14)	26(7)
H(31A)	2917(22)	3932(14)	6942(19)	57(9)
H(31B)	3592(22)	3872(13)	7933(18)	47(8)
H(31C)	2411(22)	3566(13)	7769(17)	42(8)
H(32A)	3007(22)	2372(13)	8327(16)	44(8)
H(32B)	4025(19)	2049(13)	8004(16)	31(7)
H(32C)	4202(20)	2716(12)	8587(17)	38(7)
H(50)	16(17)	1748(11)	4915(15)	21(6)
H(51A)	313(23)	863(15)	5987(18)	52(9)
H(51B)	-914(24)	1079(14)	5854(18)	55(9)
H(51C)	-35(22)	1335(14)	6714(20)	53(9)
H(52A)	-1398(22)	2299(13)	5450(16)	44(8)
H(52B)	-483(20)	2852(13)	5401(17)	38(8)
H(52C)	-636(19)	2550(12)	6330(17)	36(7)
H(70)	4749(18)	1747(11)	4595(16)	27(7)
H(71A)	5742(24)	1198(14)	3613(18)	55(9)
H(71B)	4467(23)	1013(14)	3331(18)	53(9)
H(71C)	5040(20)	1555(13)	2809(19)	42(8)
H(72A)	5386(24)	2880(15)	4465(20)	63(10)
H(72B)	5586(22)	2705(14)	3501(19)	49(9)
H(72C)	6240(22)	2338(12)	4294(16)	38(7)
H(90)	897(18)	3430(11)	2697(14)	21(6)
H(91A)	1660(20)	4440(13)	2172(16)	41(8)
H(91B)	2804(22)	4060(13)	2233(17)	45(8)

H(91C)	2322(20)	4260(13)	3102(18)	42(8)
H(92A)	898(19)	2715(13)	1460(15)	30(7)
H(92B)	861(20)	3486(13)	1136(17)	39(7)
H(92C)	1974(22)	3093(13)	1263(17)	40(8)

B. *meso*-[IpYCl]$_2$ (**4**)

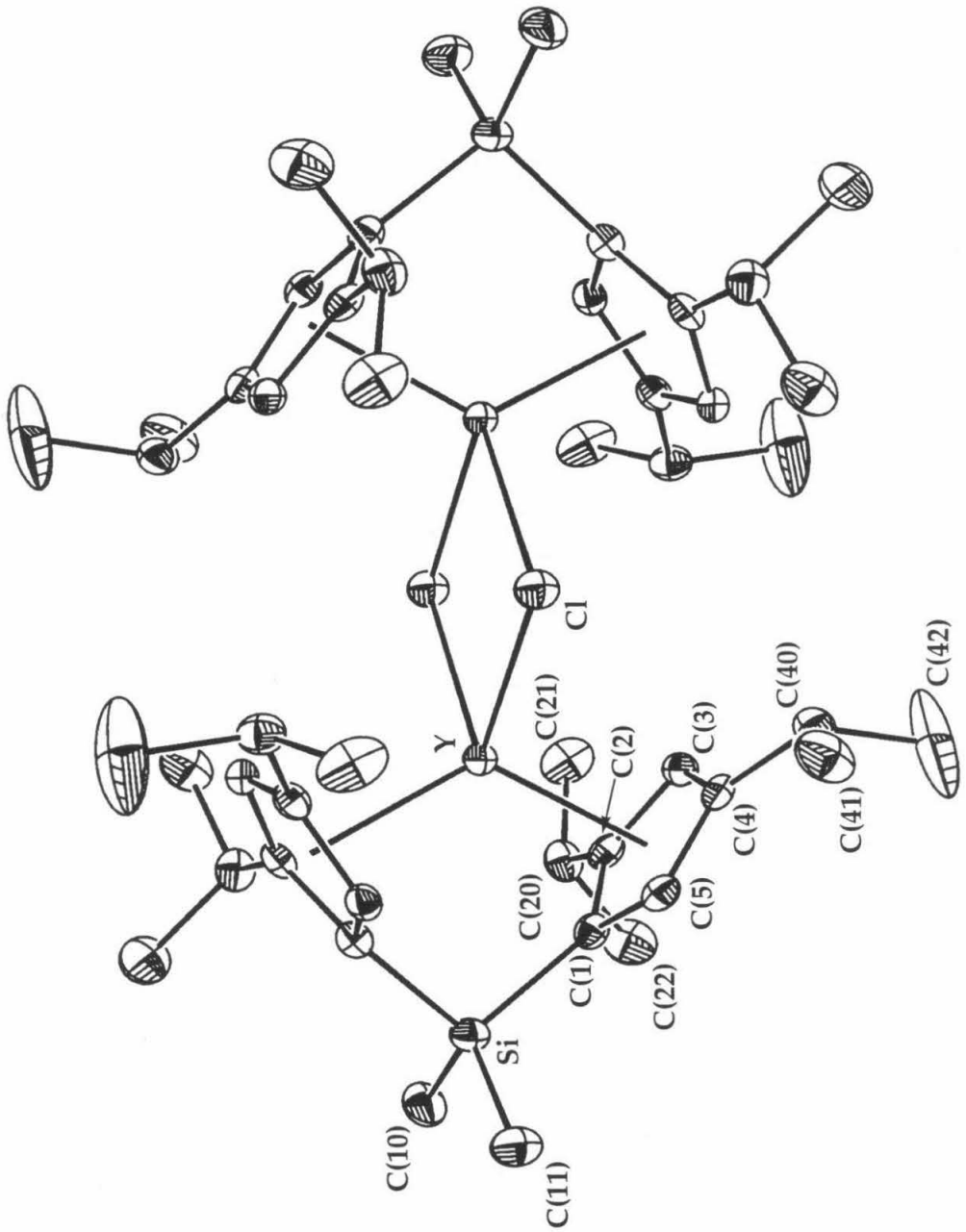

Figure 2. ORTEP representation of the molecular structure of **4** showing the complete atom labeling scheme (50% probability ellipsoids, hydrogens omitted for clarity).

Table 7. X-ray Diffraction Data Collection Parameters for **4**[a]

Feature	Value
Empirical formula	$C_{66}H_{94}Cl_2Si_2Y_2$
Formula weight (g/mol)	1192.31
Crystal size (mm)	0.4 x 0.3 x 0.3
Temp. (K)	160
Space Group	I_{bam}
Cell Constants	a = 21.060 (4) Å
	b = 14.254 (3) Å
	c = 21.754 (4) Å
Volume ($Å^3$)	6530 (2)
Z	4
Density (calculated) (g/mL)	1.213
2θ range (°)	3.5 to 55.0
Index ranges	$0 \le h \le 27, -18 \le k \le 18, 0 \le l \le 28$
Reflections collected	8421
Independent reflections	3853
R (merge)	0.046
GOF (merge)[b]	1.11
Data / restraints / parameters	3840 / 0 / 269
GOF (F^2)[b]	1.615
R indices (all data)[c, d]	R1 = 0.0951, wR2 = 0.0816

[a]Structure was obtained on an Enraf-Nonius CAD-4 using MoKα radiation (λ = 0.71073 Å); [b]$GOF = \{\Sigma w(F_o^2 - F_c^2)^2 / n - p\}^{1/2}$ (n = number of data, p = number of variables); [c]$R1 = \Sigma | |F_o| - |F_c| | / \Sigma |F_o|$; [d]$wR2 = \{\Sigma(w(F_o^2 - F_c^2)^2) / \Sigma(wF_o^4)\}^{1/2}$.

Table 9. Special Refinement Details for **4**

Weights w are calculated as $1/\sigma^2(F_o^2)$. The variances ($\sigma^2(Fo^2)$) were derived from counting statistics plus an additional term, $(0.014I)^2$, and the variances of the merged data were obtained by propagation of error plus the addition of another term, (0.014<I>)2.

All esd's (except the esd in the dihedral angle between two l.s. planes) are estimated using the full covariance matrix. The cell esd's are taken into account individually in the estimation of esd's in distances, angles and torsion angles; correlations between esd's in cell parameters are only used when they are defined by crystal symmetry. An approximate (isotropic) treatment of cell esd's is used for estimating esd's involving l.s. planes.

Table 9. Atomic Coordinates (x 10^4) and Equivalent Isotropic Displacement Parameters ($Å^2$ x 10^3) for **4**[a]

	x	y	z	U_{eq}
Y	4038(1)	-26(1)	5000	16(1)
Cl	4980(1)	1226(1)	5000	23(1)
Si	2459(1)	-322(1)	5000	20(1)
C(1)	3031(1)	-196(2)	5657(1)	17(1)
C(2)	3462(1)	-857(2)	5921(2)	18(1)
C(3)	3954(2)	-348(2)	6216(2)	18(1)
C(4)	3840(1)	623(2)	6153(1)	18(1)
C(5)	3280(2)	704(2)	5803(1)	18(1)
C(11)	1901(3)	694(4)	5000	32(1)
C(12)	1979(3)	-1418(4)	5000	31(1)
C(20)	3372(2)	-1918(2)	5948(2)	24(1)
C(21)	3972(2)	-2449(3)	6115(2)	34(1)
C(22)	2850(2)	-2158(3)	6410(2)	35(1)
C(40)	4216(2)	1391(2)	6464(2)	23(1)
C(41)	4067(2)	2363(3)	6218(2)	38(1)
C(42)	4115(5)	1368(5)	7147(2)	88(3)
C(70)	5024(3)	-4524(2)	5543(2)	50(1)
C(71)	5050(4)	-4046(4)	5000	52(2)
C(60)	1108(3)	-24(6)	7187(3)	107(2)
C(61)	1692(3)	-10(5)	6878(2)	87(2)
C(62)	2250(3)	5(5)	7198(2)	77(1)
X(1A)	3513	-15	5950	50

[a]U(eq) is defined as the trace of the orthogonalized U^{ij} tensor.

Table 10. Complete List of Bond Lengths (Å) and Angles (°) for **4**

Feature	Length (Å) or angle (°)	Feature	Length (Å) or angle (°)
Y-X(1A)#1	2.3441(4)	C(42)-H(42A)	0.88(4)
Y-X(1A)	2.3441(4)	C(42)-H(42B)	0.97(4)
Y-C(1)#1	2.570(3)	C(42)-H(42C)	0.76(5)
Y-C(1)	2.570(3)	C(70)-C(70)#3	1.361(7)
Y-C(5)#1	2.587(3)	C(70)-C(71)	1.364(5)
Y-C(5)	2.587(3)	C(70)-H(72)	0.84(3)
Y-C(2)#1	2.625(3)	C(71)-C(70)#1	1.364(5)
Y-C(2)	2.625(3)	C(71)-H(71)	0.93(5)
Y-Cl	2.6682(14)	C(60)-C(60)#4	1.361(11)
Y-Cl#2	2.6823(14)	C(60)-C(61)	1.401(7)
Y-C(3)#1	2.690(3)	C(60)-H(60)	1.10(5)
Y-C(3)	2.690(3)	C(61)-C(62)	1.367(7)
Cl-Y#2	2.6823(14)	C(61)-H(61)	1.23(7)
Si-C(12)	1.860(5)	C(62)-C(62)#4	1.313(9)
Si-C(11)	1.864(6)	C(62)-H(62)	1.12(5)
Si-C(1)	1.877(3)		
Si-C(1)#1	1.877(3)	X(1A)#1-Y-X(1A)	123.70(2)
C(1)-X(1A)	1.228(3)	X(1A)#1-Y-C(1)#1	28.48(6)
C(1)-C(5)	1.423(4)	X(1A)-Y-C(1)#1	95.80(6)
C(1)-C(2)	1.430(4)	X(1A)#1-Y-C(1)	95.80(6)
C(2)-X(1A)	1.207(3)	X(1A)-Y-C(1)	28.48(6)
C(2)-C(3)	1.418(4)	C(1)#1-Y-C(1)	67.53(13)
C(2)-C(20)	1.526(4)	X(1A)#1-Y-C(5)#1	27.14(7)
C(3)-X(1A)	1.192(3)	X(1A)-Y-C(5)#1	107.55(7)
C(3)-C(4)	1.411(4)	C(1)#1-Y-C(5)#1	32.04(9)
C(3)-H(3)	0.91(3)	C(1)-Y-C(5)#1	84.45(10)
C(4)-X(1A)	1.223(3)	X(1A)#1-Y-C(5)	107.55(7)
C(4)-C(5)	1.409(4)	X(1A)-Y-C(5)	27.14(7)
C(4)-C(40)	1.511(4)	C(1)#1-Y-C(5)	84.45(10)
C(5)-X(1A)	1.181(3)	C(1)-Y-C(5)	32.04(9)
C(5)-H(5)	0.90(3)	C(5)#1-Y-C(5)	85.01(14)
C(11)-H(11A)	0.87(6)	X(1A)#1-Y-C(2)#1	27.37(7)
C(11)-H(11B)	0.89(3)	X(1A)-Y-C(2)#1	117.28(7)
C(12)-H(12A)	0.94(4)	C(1)#1-Y-C(2)#1	31.93(8)
C(12)-H(12B)	0.95(3)	C(1)-Y-C(2)#1	90.00(9)
C(20)-C(21)	1.518(5)	C(5)#1-Y-C(2)#1	51.70(9)
C(20)-C(22)	1.528(5)	C(5)-Y-C(2)#1	114.33(11)
C(20)-H(20)	0.98(3)	X(1A)#1-Y-C(2)	117.28(7)
C(21)-H(21A)	0.96(3)	X(1A)-Y-C(2)	27.37(7)
C(21)-H(21B)	0.95(3)	C(1)#1-Y-C(2)	90.00(9)
C(21)-H(21C)	0.97(3)	C(1)-Y-C(2)	31.93(8)
C(22)-H(22A)	0.96(3)	C(5)#1-Y-C(2)	114.33(11)
C(22)-H(22B)	0.94(3)	C(5)-Y-C(2)	51.70(9)
C(22)-H(22C)	0.89(3)	C(2)#1-Y-C(2)	99.55(14)
C(40)-C(42)	1.502(6)	X(1A)#1-Y-Cl	110.24(2)
C(40)-C(41)	1.518(5)	X(1A)-Y-Cl	110.24(2)
C(40)-H(40)	0.85(3)	C(1)#1-Y-Cl	132.62(6)
C(41)-H(41A)	0.97(3)	C(1)-Y-Cl	132.62(6)
C(41)-H(41B)	1.09(4)	C(5)#1-Y-Cl	100.95(8)
C(41)-H(41C)	0.93(3)	C(5)-Y-Cl	100.95(8)

C(2)#1-Y-Cl	130.19(7)
C(2)-Y-Cl	130.19(7)
X(1A)#1-Y-Cl#2	111.59(2)
X(1A)-Y-Cl#2	111.59(2)
C(1)#1-Y-Cl#2	125.19(6)
C(1)-Y-Cl#2	125.19(6)
C(5)#1-Y-Cl#2	137.10(7)
C(5)-Y-Cl#2	137.10(7)
C(2)#1-Y-Cl#2	93.94(7)
C(2)-Y-Cl#2	93.94(7)
Cl-Y-Cl#2	81.57(4)
X(1A)#1-Y-C(3)#1	26.26(7)
X(1A)-Y-C(3)#1	146.82(7)
C(1)#1-Y-C(3)#1	51.90(9)
C(1)-Y-C(3)#1	118.42(9)
C(5)#1-Y-C(3)#1	50.48(10)
C(5)-Y-C(3)#1	133.80(10)
C(2)#1-Y-C(3)#1	30.91(9)
C(2)-Y-C(3)#1	130.04(10)
Cl-Y-C(3)#1	99.38(7)
Cl#2-Y-C(3)#1	86.69(7)
X(1A)#1-Y-C(3)	146.82(7)
X(1A)-Y-C(3)	26.26(7)
C(1)#1-Y-C(3)	118.42(9)
C(1)-Y-C(3)	51.90(9)
C(5)#1-Y-C(3)	133.80(10)
C(5)-Y-C(3)	50.48(10)
C(2)#1-Y-C(3)	130.04(10)
C(2)-Y-C(3)	30.91(9)
Cl-Y-C(3)	99.38(7)
Cl#2-Y-C(3)	86.69(7)
C(3)#1-Y-C(3)	158.95(13)
Y-Cl-Y#2	98.43(4)
C(12)-Si-C(11)	108.1(3)
C(12)-Si-C(1)	115.35(14)
C(11)-Si-C(1)	109.30(15)
C(12)-Si-C(1)#1	115.35(14)
C(11)-Si-C(1)#1	109.30(15)
C(1)-Si-C(1)#1	99.1(2)
C(12)-Si-Y	130.1(2)
C(11)-Si-Y	121.8(2)
C(1)-Si-Y	49.56(9)
C(1)#1-Si-Y	49.56(9)
X(1A)-C(1)-C(5)	52.3(2)
X(1A)-C(1)-C(2)	53.4(2)
C(5)-C(1)-C(2)	105.6(2)
X(1A)-C(1)-Si	161.3(2)
C(5)-C(1)-Si	119.6(2)
C(2)-C(1)-Si	130.7(2)
X(1A)-C(1)-Y	65.51(11)
C(5)-C(1)-Y	74.6(2)
C(2)-C(1)-Y	76.2(2)
Si-C(1)-Y	96.67(12)
X(1A)-C(2)-C(3)	53.3(2)
X(1A)-C(2)-C(1)	54.7(2)
C(3)-C(2)-C(1)	108.0(3)
X(1A)-C(2)-C(20)	174.5(3)
C(3)-C(2)-C(20)	125.6(3)
C(1)-C(2)-C(20)	126.1(3)
X(1A)-C(2)-Y	63.23(13)
C(3)-C(2)-Y	77.0(2)
C(1)-C(2)-Y	71.9(2)
C(20)-C(2)-Y	122.3(2)
X(1A)-C(3)-C(4)	55.3(2)
X(1A)-C(3)-C(2)	54.3(2)
C(4)-C(3)-C(2)	109.5(3)
X(1A)-C(3)-Y	60.47(13)
C(4)-C(3)-Y	75.5(2)
C(2)-C(3)-Y	72.0(2)
X(1A)-C(3)-H(3)	174.2(19)
C(4)-C(3)-H(3)	123.7(18)
C(2)-C(3)-H(3)	126.3(18)
Y-C(3)-H(3)	125.3(18)
X(1A)-C(4)-C(5)	52.7(2)
X(1A)-C(4)-C(3)	53.2(2)
C(5)-C(4)-C(3)	106.0(3)
X(1A)-C(4)-C(40)	174.5(3)
C(5)-C(4)-C(40)	128.4(3)
C(3)-C(4)-C(40)	125.3(3)
X(1A)-C(4)-Y	59.83(12)
C(5)-C(4)-Y	69.9(2)
C(3)-C(4)-Y	74.2(2)
C(40)-C(4)-Y	125.5(2)
X(1A)-C(5)-C(4)	55.5(2)
X(1A)-C(5)-C(1)	55.3(2)
C(4)-C(5)-C(1)	110.9(3)
X(1A)-C(5)-Y	64.90(14)
C(4)-C(5)-Y	79.3(2)
C(1)-C(5)-Y	73.3(2)
X(1A)-C(5)-H(5)	179.1(18)
C(4)-C(5)-H(5)	124.5(17)
C(1)-C(5)-H(5)	124.6(17)
Y-C(5)-H(5)	114.2(17)
Si-C(11)-H(11A)	113.9(41)
Si-C(11)-H(11B)	108.3(24)
H(11A)-C(11)-H(11B)	110.1(32)
Si-C(12)-H(12A)	116.1(26)
Si-C(12)-H(12B)	105.2(18)
H(12A)-C(12)-H(12B)	106.3(22)
C(21)-C(20)-C(2)	113.5(3)
C(21)-C(20)-C(22)	109.3(3)
C(2)-C(20)-C(22)	109.7(3)
C(21)-C(20)-H(20)	106.9(17)
C(2)-C(20)-H(20)	107.9(17)
C(22)-C(20)-H(20)	109.4(17)
C(20)-C(21)-H(21A)	111.1(21)
C(20)-C(21)-H(21B)	110.8(23)
H(21A)-C(21)-H(21B)	110.2(30)

C(20)-C(21)-H(21C)	109.0(19)	C(71)-C(70)-H(72)	120.7(24)
H(21A)-C(21)-H(21C)	104.5(26)	C(70)#1-C(71)-C(70)	119.8(5)
H(21B)-C(21)-H(21C)	111.0(28)	C(70)#1-C(71)-H(71)	120.1(3)
C(20)-C(22)-H(22A)	110.0(20)	C(70)-C(71)-H(71)	120.1(3)
C(20)-C(22)-H(22B)	108.3(19)	C(60)#4-C(60)-C(61)	118.6(3)
H(22A)-C(22)-H(22B)	108.5(27)	C(60)#4-C(60)-H(60)	99.7(27)
C(20)-C(22)-H(22C)	110.6(20)	C(61)-C(60)-H(60)	137.0(27)
H(22A)-C(22)-H(22C)	113.5(28)	C(62)-C(61)-C(60)	120.7(5)
H(22B)-C(22)-H(22C)	105.7(28)	C(62)-C(61)-H(61)	129.0(32)
C(42)-C(40)-C(4)	110.6(3)	C(60)-C(61)-H(61)	109.9(32)
C(42)-C(40)-C(41)	109.8(5)	C(62)#4-C(62)-C(61)	120.6(3)
C(4)-C(40)-C(41)	113.3(3)	C(62)#4-C(62)-H(62)	116.0(23)
C(42)-C(40)-H(40)	110.5(21)	C(61)-C(62)-H(62)	123.5(24)
C(4)-C(40)-H(40)	104.8(20)	C(5)-X(1A)-C(3)	143.2(2)
C(41)-C(40)-H(40)	107.8(20)	C(5)-X(1A)-C(2)	144.3(2)
C(40)-C(41)-H(41A)	107.9(19)	C(3)-X(1A)-C(2)	72.4(2)
C(40)-C(41)-H(41B)	115.1(21)	C(5)-X(1A)-C(4)	71.7(2)
H(41A)-C(41)-H(41B)	111.2(28)	C(3)-X(1A)-C(4)	71.5(2)
C(40)-C(41)-H(41C)	108.0(21)	C(2)-X(1A)-C(4)	143.9(2)
H(41A)-C(41)-H(41C)	104.9(27)	C(5)-X(1A)-C(1)	72.4(2)
H(41B)-C(41)-H(41C)	109.3(30)	C(3)-X(1A)-C(1)	144.4(2)
C(40)-C(42)-H(42A)	116.5(36)	C(2)-X(1A)-C(1)	71.9(2)
C(40)-C(42)-H(42B)	108.7(24)	C(4)-X(1A)-C(1)	144.1(2)
H(42A)-C(42)-H(42B)	101.6(39)	C(5)-X(1A)-Y	87.96(15)
C(40)-C(42)-H(42C)	114.0(45)	C(3)-X(1A)-Y	93.27(15)
H(42A)-C(42)-H(42C)	95.3(49)	C(2)-X(1A)-Y	89.40(14)
H(42B)-C(42)-H(42C)	119.9(51)	C(4)-X(1A)-Y	93.37(14)
C(70)#3-C(70)-C(71)	120.1(3)	C(1)-X(1A)-Y	86.01(13)
C(70)#3-C(70)-H(72)	119.2(24)		

Symmetry transformations used to generate equivalent atoms:
#1 x,y,-z+1; #2 -x+1,-y,-z+1; #3 -x+1,-y-1,z; #4 x+0,-y+0,-z+3/2.

Table 11. Anisotropic Displacement Parameters ($Å^2 \times 10^4$) for **4**[a]

	U^{11}	U^{22}	U^{33}	U^{23}	U^{13}	U^{12}
Y	154(2)	162(2)	151(2)	0	0	0(2)
Cl	207(5)	222(5)	249(5)	0	0	3(6)
Si	158(6)	231(6)	217(6)	0	0	-16(5)
C(1)	189(14)	140(20)	178(15)	-11(12)	26(11)	-1(12)
C(2)	200(20)	170(20)	180(20)	19(13)	69(14)	-2(13)
C(3)	180(20)	220(20)	140(20)	32(12)	0(13)	-1(13)
C(4)	190(20)	200(20)	150(20)	-26(14)	48(13)	15(13)
C(5)	190(20)	180(20)	180(20)	24(14)	36(14)	43(14)
C(11)	230(30)	410(40)	330(30)	0	0	50(30)
C(12)	280(30)	380(30)	260(30)	0	0	-150(30)
C(20)	290(20)	200(20)	220(20)	3(15)	-16(14)	-49(14)
C(21)	380(30)	200(20)	440(30)	50(20)	90(20)	-20(20)
C(22)	340(20)	300(20)	420(30)	80(20)	10(20)	-100(20)
C(40)	210(20)	230(20)	260(20)	-36(15)	-13(14)	-12(14)
C(41)	370(30)	230(20)	530(30)	-80(20)	-130(20)	10(20)
C(42)	1730(80)	660(40)	250(30)	-50(20)	-100(40)	-710(50)
C(70)	630(20)	380(20)	500(20)	-110(20)	-20(30)	-40(30)
C(71)	680(40)	260(30)	620(40)	0	0	30(40)
C(60)	990(40)	1320(50)	890(40)	-190(60)	-210(30)	270(60)
C(61)	1290(50)	840(40)	490(30)	30(40)	-40(30)	210(50)
C(62)	1050(40)	640(30)	610(30)	60(40)	110(30)	120(40)

[a]The anisotropic displacement factor exponent takes the form: $-2p^2 [h^2 a^{*2} U^{11} + ... + 2 h k a^* b^* U^{12}]$

Table 12. Hydrogen Coordinates (x 10^4) and Isotropic Displacement Parameters ($Å^2$ x 10^3) for **4**

	x	y	z	U_{iso}
H(3)	4268(13)	-593(20)	6455(13)	18(8)
H(5)	3105(12)	1251(18)	5686(12)	11(8)
H(11A)	2089(29)	1236(42)	5000	79(26)
H(11B)	1648(16)	644(25)	5326(16)	58(13)
H(12A)	2210(20)	-1984(31)	5000	29(14)
H(12B)	1748(14)	-1406(20)	5375(13)	25(9)
H(20)	3244(13)	-2132(20)	5537(12)	22(8)
H(21A)	4299(16)	-2345(22)	5818(15)	36(11)
H(21B)	4116(16)	-2276(25)	6513(17)	48(13)
H(21C)	3888(14)	-3119(23)	6093(13)	30(9)
H(22A)	2462(16)	-1846(23)	6299(14)	37(10)
H(22B)	2779(14)	-2811(23)	6397(15)	36(10)
H(22C)	2977(14)	-2035(22)	6791(15)	28(10)
H(40)	4600(14)	1270(20)	6378(13)	19(9)
H(41A)	4328(14)	2808(23)	6439(14)	29(9)
H(41B)	4123(18)	2445(27)	5722(19)	71(15)
H(41C)	3652(16)	2510(22)	6329(16)	42(12)
H(42A)	4231(24)	851(32)	7339(23)	85(19)
H(42B)	4389(17)	1830(28)	7336(18)	72(14)
H(42C)	3770(24)	1338(44)	7241(24)	93(27)
H(71)	5079(29)	-3397(38)	5000	72(19)
H(72)	5050(21)	-4237(23)	5881(15)	52(12)
H(60)	617(25)	200(41)	7095(22)	153(25)
H(61)	1605(31)	-95(46)	6320(35)	229(32)
H(62)	2729(23)	17(38)	6973(20)	118(18)

Symmetry transformations used to generate equivalent atoms:
#1 x,y,-z+1; #2 -x+1,-y,-z+1; #3 -x+1,-y-1,z; #4 x+0,-y+0,-z+3/2.

C. *rac*-IpSc(η^3-C_3H_5) (**4**)

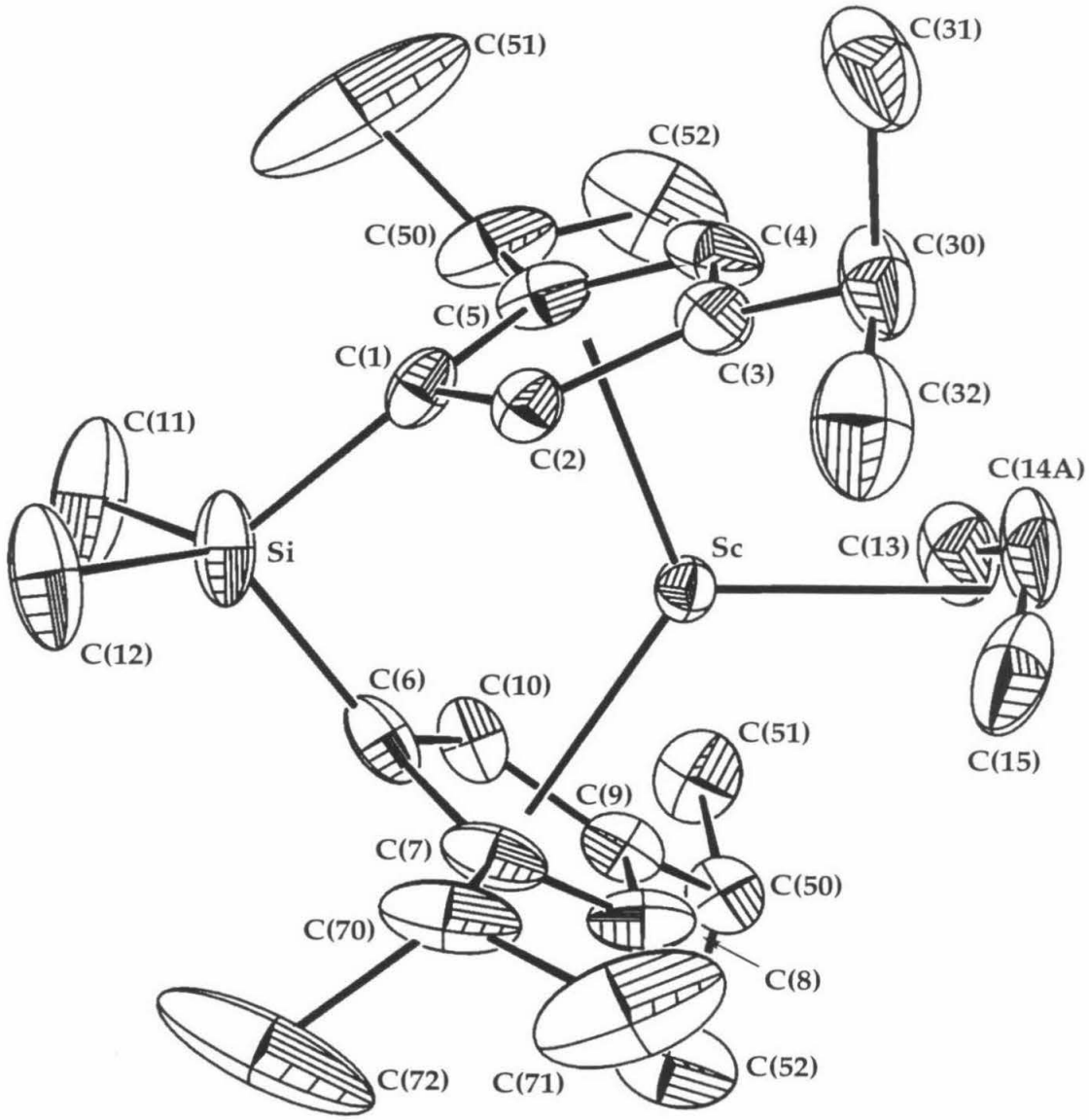

Figure 3. ORTEP representation of the molecular structure of **5** showing the complete atom labeling scheme (50% probability ellopsoids, hydrogens omitted for clarity).

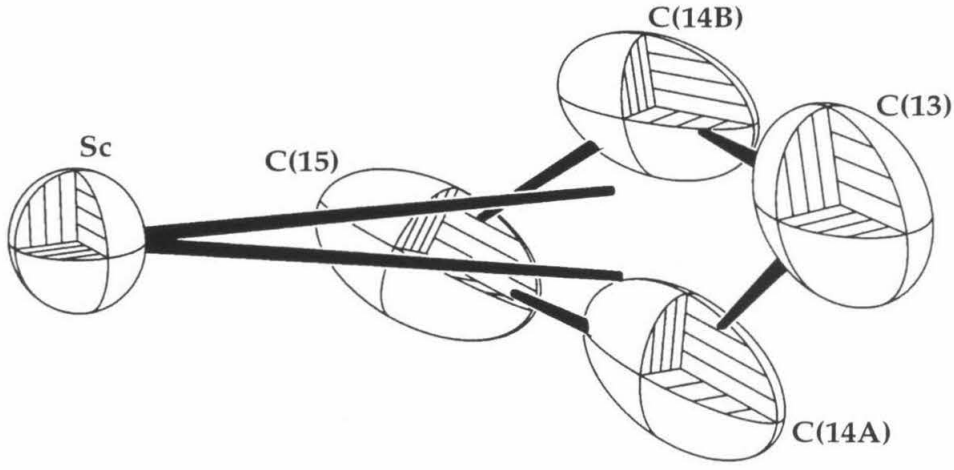

Figure 4. ORTEP representation of the molecular structure of the allyl ligand of **5** showing the disorder (50% probability ellipsoids, hydrogens omitted for clarity).

Table 13. X-ray Diffraction Data Collection Parameters for 5[a]

Feature	Value
Empirical formula	$C_{27}H_{43}ScSi$
Formula weight (g/mol)	440.66
Crystal size (mm)	0.3 x 0.2 x 0.2
Temp. (K)	160
Space Group	$P2_1/c$
Cell Constants	a = 13.669 (3) Å b = 10.601 (2) Å c = 18.057 (4) Å β = 92.90 (3)°
Volume (Å^3)	2613.2 (10)
Z	4
Density (calculated) (g/mL)	1.120
2θ range (°)	4.5 to 50
Index ranges	$-16 \le h \le 16$, $-12 \le k \le 12$, $0 \le l \le 21$
Reflections collected	10116
Independent reflections	4588
R (merge)	0.0285
GOF (merge)[b]	1.08
Data / restraints / parameters	4583 / 0 / 364
GOF (F^2)[b]	2.153
R indices (all data)[c, d]	R1 = 0.0643, wR2 = 0.0950

[a]Structure was obtained on an Enraf-Nonius CAD-4 using MoKα radiation (λ = 0.71073 Å); [b]$GOF = \{\Sigma w(F_o^2 - F_c^2)^2 / n - p\}^{1/2}$ (n = number of data, p = number of variables); [c]$R1 = \Sigma | |F_o| - |F_c| | / \Sigma |F_o|$; [d]$wR2 = \{\Sigma(w(F_o^2 - F_c^2)^2) / \Sigma(wF_o^4)\}^{1/2}$.

Table 14. Special Refinement Details for **5**

Weights w are calculated as $1/\sigma^2(F_o^2)$. The variances ($\sigma^2(Fo^2)$) were derived from counting statistics plus an additional term, $(0.014I)^2$, and the variances of the merged data were obtained by propagation of error plus the addition of another term, (0.014<I>)2.

All esd's (except the esd in the dihedral angle between two l.s. planes) are estimated using the full covariance matrix. The cell esd's are taken into account individually in the estimation of esd's in distances, angles and torsion angles; correlations between esd's in cell parameters are only used when they are defined by crystal symmetry. An approximate (isotropic) treatment of cell esd's is used for estimating esd's involving l.s. planes.

Table 15. Atomic Coordinates (x 10^4) and Equivalent Isotropic Displacement Parameters ($Å^2$ x 10^3) for **5**[a]

	x	y	z	U_{eq}
Sc	7151(1)	1417(1)	8442(1)	23(1)
Si	9380(1)	655(1)	8041(1)	39(1)
C(1)	8803(2)	2200(2)	8244(1)	28(1)
C(2)	8175(2)	2765(2)	7681(1)	25(1)
C(3)	7548(2)	3646(2)	7995(1)	30(1)
C(4)	7775(2)	3608(3)	8766(2)	38(1)
C(5)	8526(2)	2738(2)	8927(1)	33(1)
C(6)	8245(2)	-297(2)	8104(1)	32(1)
C(7)	7397(2)	-377(2)	7609(1)	35(1)
C(8)	6594(2)	-754(2)	8015(1)	38(1)
C(9)	6900(2)	-926(2)	8767(1)	31(1)
C(10)	7901(2)	-626(2)	8817(1)	32(1)
C(11)	10333(2)	71(4)	8737(2)	74(1)
C(12)	9935(2)	703(3)	7120(2)	56(1)
C(13)	5970(2)	1799(4)	9421(2)	57(1)
C(14A)	5640(4)	2449(9)	8822(5)	66(3)
C(14B)	5452(6)	1515(13)	8786(6)	53(4)
C(15)	5439(2)	2014(4)	8110(3)	63(1)
C(30)	6861(2)	4550(3)	7578(2)	47(1)
C(31)	7308(2)	5859(3)	7549(2)	68(1)
C(32)	6580(2)	4099(3)	6797(2)	62(1)
C(50)	8998(2)	2465(3)	9689(2)	52(1)
C(51)	10009(3)	3033(6)	9771(2)	150(3)
C(52)	8375(4)	2851(4)	10316(2)	83(1)
C(70)	7382(3)	-170(3)	6774(1)	48(1)
C(71)	7899(5)	-1281(3)	6411(2)	113(3)
C(72)	6375(3)	34(4)	6427(2)	89(2)
C(90)	6305(2)	-1485(3)	9370(1)	35(1)
C(91)	6136(3)	-2888(3)	9238(2)	63(1)
C(92)	6778(2)	-1273(3)	10138(1)	48(1)
X(1A)	8166	2991	8323	50
X(1B)	7407	-596	8262	50

[a] $U(eq)$ is defined as the trace of the orthogonalized U^{ij} tensor.

Table 16. Complete List of Bond Lengths (Å) and Angles (°) for **5**

Feature	Length (Å) or angle (°)	Feature	Length (Å) or angle (°)
Sc-X(1A)	2.1875(5)	C(12)-H(12B)	0.951(15)
Sc-X(1B)	2.1894(6)	C(12)-H(12C)	0.951(15)
Sc-Pln(A)	2.184(2)	C(13)-C(14A)	1.340(8)
Sc-Pln(B)	2.184(2)	C(13)-C(14B)	1.349(11)
Sc-C(14B)	2.436(7)	C(13)-H(13A)	0.961(4)
Sc-C(6)	2.450(2)	C(13)-H(13B)	0.958(4)
Sc-C(1)	2.450(2)	C(13)-H(13C)	0.963(4)
Sc-C(7)	2.457(2)	C(13)-H(13D)	0.958(4)
Sc-C(14A)	2.465(5)	C(14A)-C(15)	1.381(9)
Sc-C(2)	2.465(2)	C(14A)-H(14A)	0.906(10)
Sc-C(15)	2.469(3)	C(14A)-H(13C)	1.431(9)
Sc-C(5)	2.469(2)	C(14A)-H(15C)	1.483(8)
Sc-C(10)	2.476(3)	C(14B)-C(15)	1.331(12)
Sc-C(13)	2.487(3)	C(14B)-H(14B)	0.868(13)
Si-C(1)	1.862(3)	C(30)-C(31)	1.518(4)
Si-C(12)	1.864(3)	C(30)-C(32)	1.519(4)
Si-C(6)	1.859(3)	C(30)-H(30)	0.98(2)
Si-C(11)	1.869(3)	C(31)-H(31A)	0.985(15)
C(1)-X(1A)	1.223(2)	C(31)-H(31B)	0.985(15)
C(1)-C(2)	1.428(3)	C(31)-H(31C)	0.985(15)
C(1)-C(5)	1.428(3)	C(32)-H(32A)	0.972(15)
C(2)-X(1A)	1.183(2)	C(32)-H(32B)	0.972(15)
C(2)-C(3)	1.406(3)	C(32)-H(32C)	0.972(15)
C(2)-H(2)	0.96(2)	C(50)-C(52)	1.507(4)
C(3)-X(1A)	1.222(3)	C(50)-C(51)	1.509(4)
C(3)-C(4)	1.412(4)	C(50)-H(50)	0.99(2)
C(3)-C(30)	1.515(4)	C(51)-H(51A)	1.03(2)
C(4)-X(1A)	1.182(3)	C(51)-H(51B)	1.03(2)
C(4)-C(5)	1.400(4)	C(51)-H(51C)	1.03(2)
C(4)-H(4)	0.87(3)	C(52)-H(52A)	0.95(2)
C(5)-X(1A)	1.205(2)	C(52)-H(52B)	0.95(2)
C(5)-C(50)	1.518(4)	C(52)-H(52C)	0.95(2)
C(6)-X(1B)	1.236(3)	C(70)-C(72)	1.499(5)
C(6)-C(7)	1.429(4)	C(70)-C(71)	1.537(5)
C(6)-C(10)	1.436(3)	C(70)-H(70)	0.97(2)
C(7)-X(1B)	1.201(2)	C(71)-H(71A)	0.89(2)
C(7)-C(8)	1.408(4)	C(71)-H(71B)	0.89(2)
C(7)-C(70)	1.523(3)	C(71)-H(71C)	0.89(2)
C(8)-X(1B)	1.189(3)	C(72)-H(72A)	0.95(2)
C(8)-C(9)	1.412(3)	C(72)-H(72B)	0.95(2)
C(8)-H(8)	0.91(3)	C(72)-H(72C)	0.95(2)
C(9)-X(1B)	1.223(2)	C(90)-C(92)	1.518(4)
C(9)-C(10)	1.403(4)	C(90)-C(91)	1.522(4)
C(9)-C(90)	1.513(3)	C(90)-H(90)	0.91(2)
C(10)-X(1B)	1.180(3)	C(91)-H(91A)	0.952(15)
C(10)-H(10)	0.94(2)	C(91)-H(91B)	0.952(15)
C(11)-H(11A)	0.90(2)	C(91)-H(91C)	0.952(15)
C(11)-H(11B)	0.90(2)	C(92)-H(92A)	0.983(13)
C(11)-H(11C)	0.90(2)	C(92)-H(92B)	0.983(13)
C(12)-H(12A)	0.951(15)	C(92)-H(92C)	0.983(13)

X(1A)-Sc-X(1B)	128.49(2)
Pln(A)-Sc-Pln(B)	121.48(9)
X(1A)-Sc-C(14B)	127.6(3)
X(1B)-Sc-C(14B)	103.9(3)
X(1A)-Sc-C(6)	98.25(7)
X(1B)-Sc-C(6)	30.23(6)
C(14B)-Sc-C(6)	134.2(3)
X(1A)-Sc-C(1)	29.92(6)
X(1B)-Sc-C(1)	98.82(6)
C(14B)-Sc-C(1)	157.0(3)
C(6)-Sc-C(1)	68.66(9)
X(1A)-Sc-C(7)	115.05(7)
X(1B)-Sc-C(7)	29.23(6)
C(14B)-Sc-C(7)	110.5(3)
C(6)-Sc-C(7)	33.87(9)
C(1)-Sc-C(7)	90.99(9)
X(1A)-Sc-C(14A)	103.5(2)
X(1B)-Sc-C(14A)	128.1(2)
C(6)-Sc-C(14A)	158.3(2)
C(1)-Sc-C(14A)	133.0(2)
C(7)-Sc-C(14A)	131.0(2)
X(1A)-Sc-C(2)	28.67(6)
X(1B)-Sc-C(2)	112.53(6)
C(14B)-Sc-C(2)	133.8(3)
C(6)-Sc-C(2)	85.45(8)
C(1)-Sc-C(2)	33.78(8)
C(7)-Sc-C(2)	90.52(8)
C(14A)-Sc-C(2)	113.9(2)
X(1A)-Sc-C(15)	112.24(9)
X(1B)-Sc-C(15)	111.76(11)
C(14B)-Sc-C(15)	31.5(3)
C(6)-Sc-C(15)	135.47(14)
C(1)-Sc-C(15)	138.37(10)
C(7)-Sc-C(15)	101.97(14)
C(14A)-Sc-C(15)	32.5(2)
C(2)-Sc-C(15)	105.91(10)
X(1A)-Sc-C(5)	29.19(6)
X(1B)-Sc-C(5)	118.74(7)
C(14B)-Sc-C(5)	127.1(3)
C(6)-Sc-C(5)	92.62(9)
C(1)-Sc-C(5)	33.75(8)
C(7)-Sc-C(5)	122.05(9)
C(14A)-Sc-C(5)	106.4(2)
C(2)-Sc-C(5)	54.94(8)
C(15)-Sc-C(5)	129.50(12)
X(1A)-Sc-C(10)	116.00(7)
X(1B)-Sc-C(10)	28.45(6)
C(14B)-Sc-C(10)	110.7(3)
C(6)-Sc-C(10)	33.89(8)
C(1)-Sc-C(10)	87.95(9)
C(7)-Sc-C(10)	54.75(8)
C(14A)-Sc-C(10)	130.8(2)
C(2)-Sc-C(10)	114.87(8)
C(15)-Sc-C(10)	131.68(11)
C(5)-Sc-C(10)	95.83(9)
X(1A)-Sc-C(13)	112.52(9)
X(1B)-Sc-C(13)	112.23(9)
C(14B)-Sc-C(13)	31.8(3)
C(6)-Sc-C(13)	136.39(10)
C(1)-Sc-C(13)	133.25(12)
C(7)-Sc-C(13)	132.42(11)
C(14A)-Sc-C(13)	31.4(2)
C(2)-Sc-C(13)	135.11(10)
C(15)-Sc-C(13)	59.28(14)
C(5)-Sc-C(13)	99.51(11)
C(10)-Sc-C(13)	102.86(10)
C(1)-Si-C(12)	110.26(13)
C(1)-Si-C(6)	95.92(10)
C(12)-Si-C(6)	116.6(2)
C(1)-Si-C(11)	116.5(2)
C(12)-Si-C(11)	107.93(14)
C(6)-Si-C(11)	109.5(2)
C(1)-Si-Sc	47.99(7)
C(12)-Si-Sc	128.09(10)
C(6)-Si-Sc	47.98(7)
C(11)-Si-Sc	123.98(11)
X(1A)-C(1)-C(2)	52.31(13)
X(1A)-C(1)-C(5)	53.38(14)
C(2)-C(1)-C(5)	105.7(2)
X(1A)-C(1)-Si	159.6(2)
C(2)-C(1)-Si	118.4(2)
C(5)-C(1)-Si	130.9(2)
X(1A)-C(1)-Sc	63.09(9)
C(2)-C(1)-Sc	73.71(13)
C(5)-C(1)-Sc	73.89(13)
Si-C(1)-Sc	97.63(10)
X(1A)-C(2)-C(3)	55.55(14)
X(1A)-C(2)-C(1)	54.92(14)
C(3)-C(2)-C(1)	110.5(2)
X(1A)-C(2)-Sc	62.52(10)
C(3)-C(2)-Sc	77.68(14)
C(1)-C(2)-Sc	72.52(13)
X(1A)-C(2)-H(2)	178.6(14)
C(3)-C(2)-H(2)	125.8(14)
C(1)-C(2)-H(2)	123.7(14)
Sc-C(2)-H(2)	117.8(14)
X(1A)-C(3)-C(2)	52.96(14)
X(1A)-C(3)-C(4)	52.7(2)
C(2)-C(3)-C(4)	105.7(2)
X(1A)-C(3)-C(30)	174.4(2)
C(2)-C(3)-C(30)	126.5(2)
C(4)-C(3)-C(30)	127.5(2)
X(1A)-C(3)-Sc	58.42(10)
C(2)-C(3)-Sc	69.94(13)
C(4)-C(3)-Sc	72.72(15)
C(30)-C(3)-Sc	127.1(2)
X(1A)-C(4)-C(5)	54.8(2)

X(1A)-C(4)-C(3)	55.36(15)
C(5)-C(4)-C(3)	110.2(2)
X(1A)-C(4)-Sc	59.61(11)
C(5)-C(4)-Sc	71.26(15)
C(3)-C(4)-Sc	75.12(15)
X(1A)-C(4)-H(4)	177.5(18)
C(5)-C(4)-H(4)	125.6(18)
C(3)-C(4)-H(4)	124.1(18)
Sc-C(4)-H(4)	122.9(18)
X(1A)-C(5)-C(4)	53.3(2)
X(1A)-C(5)-C(1)	54.58(13)
C(4)-C(5)-C(1)	107.9(2)
X(1A)-C(5)-C(50)	178.0(2)
C(4)-C(5)-C(50)	125.9(2)
C(1)-C(5)-C(50)	126.1(3)
X(1A)-C(5)-Sc	62.32(10)
C(4)-C(5)-Sc	76.3(2)
C(1)-C(5)-Sc	72.37(13)
C(50)-C(5)-Sc	119.6(2)
X(1B)-C(6)-C(7)	52.96(15)
X(1B)-C(6)-C(10)	51.76(15)
C(7)-C(6)-C(10)	104.7(2)
X(1B)-C(6)-Si	160.0(2)
C(7)-C(6)-Si	130.3(2)
C(10)-C(6)-Si	119.9(2)
X(1B)-C(6)-Sc	63.15(10)
C(7)-C(6)-Sc	73.37(14)
C(10)-C(6)-Sc	74.06(14)
Si-C(6)-Sc	97.71(11)
X(1B)-C(7)-C(8)	53.5(2)
X(1B)-C(7)-C(6)	55.22(14)
C(8)-C(7)-C(6)	108.7(2)
X(1B)-C(7)-C(70)	177.1(2)
C(8)-C(7)-C(70)	125.7(3)
C(6)-C(7)-C(70)	125.5(3)
X(1B)-C(7)-Sc	62.91(10)
C(8)-C(7)-Sc	76.6(2)
C(6)-C(7)-Sc	72.77(13)
C(70)-C(7)-Sc	119.9(2)
X(1B)-C(8)-C(9)	55.3(2)
X(1B)-C(8)-C(7)	54.3(2)
C(9)-C(8)-C(7)	109.6(2)
X(1B)-C(8)-Sc	59.74(11)
C(9)-C(8)-Sc	75.78(15)
C(7)-C(8)-Sc	70.69(14)
X(1B)-C(8)-H(8)	178.3(18)
C(9)-C(8)-H(8)	126.2(18)
C(7)-C(8)-H(8)	124.2(17)
Sc-C(8)-H(8)	121.0(17)
X(1B)-C(9)-C(10)	52.84(15)
X(1B)-C(9)-C(8)	53.1(2)
C(10)-C(9)-C(8)	105.9(2)
X(1B)-C(9)-C(90)	173.5(2)
C(10)-C(9)-C(90)	126.9(2)
C(8)-C(9)-C(90)	126.7(2)
X(1B)-C(9)-Sc	57.88(9)
C(10)-C(9)-Sc	69.87(14)
C(8)-C(9)-Sc	72.16(14)
C(90)-C(9)-Sc	128.6(2)
X(1B)-C(10)-C(9)	55.7(2)
X(1B)-C(10)-C(6)	55.35(15)
C(9)-C(10)-C(6)	111.1(2)
X(1B)-C(10)-Sc	62.16(11)
C(9)-C(10)-Sc	77.97(14)
C(6)-C(10)-Sc	72.05(14)
X(1B)-C(10)-H(10)	178.6(15)
C(9)-C(10)-H(10)	125.7(15)
C(6)-C(10)-H(10)	123.3(15)
Sc-C(10)-H(10)	118.1(15)
Si-C(11)-H(11A)	109.47(10)
Si-C(11)-H(11B)	109.47(14)
H(11A)-C(11)-H(11B)	109.5
Si-C(11)-H(11C)	109.47(14)
H(11A)-C(11)-H(11C)	109.5
H(11B)-C(11)-H(11C)	109.5
Si-C(12)-H(12A)	109.47(10)
Si-C(12)-H(12B)	109.47(10)
H(12A)-C(12)-H(12B)	109.5
Si-C(12)-H(12C)	109.47(12)
H(12A)-C(12)-H(12C)	109.5
H(12B)-C(12)-H(12C)	109.5
C(14A)-C(13)-Sc	73.4(2)
C(14B)-C(13)-Sc	72.1(3)
C(14A)-C(13)-H(13A)	115.1(5)
Sc-C(13)-H(13A)	116.2(2)
C(14A)-C(13)-H(13B)	117.0(5)
Sc-C(13)-H(13B)	116.4(3)
H(13A)-C(13)-H(13B)	113.2(4)
C(14B)-C(13)-H(13C)	115.4(6)
Sc-C(13)-H(13C)	116.3(2)
C(14B)-C(13)-H(13D)	117.4(7)
Sc-C(13)-H(13D)	116.5(2)
H(13C)-C(13)-H(13D)	113.2(4)
C(13)-C(14A)-C(15)	128.5(7)
C(13)-C(14A)-Sc	75.2(3)
C(15)-C(14A)-Sc	73.9(3)
C(13)-C(14A)-H(14A)	106.2(8)
C(15)-C(14A)-H(14A)	121.6(7)
Sc-C(14A)-H(14A)	106.4(4)
C(13)-C(14A)-H(13C)	40.5(3)
C(15)-C(14A)-H(13C)	168.9(7)
Sc-C(14A)-H(13C)	99.0(3)
C(13)-C(14A)-H(15C)	160.8(6)
C(15)-C(14A)-H(15C)	35.5(3)
Sc-C(14A)-H(15C)	87.6(3)
H(13C)-C(14A)-H(15C)	154.7(7)
C(15)-C(14B)-C(13)	132.3(10)
C(15)-C(14B)-Sc	75.6(4)

C(13)-C(14B)-Sc	76.2(4)
C(15)-C(14B)-H(13B)	171.6(10)
C(13)-C(14B)-H(13B)	39.4(4)
Sc-C(14B)-H(13B)	98.9(4)
C(15)-C(14B)-H(15A)	41.6(4)
C(13)-C(14B)-H(15A)	161.4(6)
Sc-C(14B)-H(15A)	85.4(4)
H(13B)-C(14B)-H(15A)	145.4(10)
C(15)-C(14B)-H(14B)	117.8(12)
C(13)-C(14B)-H(14B)	108.2(11)
Sc-C(14B)-H(14B)	112.3(7)
C(14B)-C(15)-Sc	72.9(3)
C(14A)-C(15)-Sc	73.6(2)
C(14A)-C(15)-H(15B)	132.3(6)
Sc-C(15)-H(15B)	121.7(3)
C(14A)-C(15)-H(15A)	121.6(5)
Sc-C(15)-H(15A)	95.1(2)
H(15B)-C(15)-H(15A)	102.9(5)
C(14B)-C(15)-H(15C)	122.1(8)
Sc-C(15)-H(15C)	104.7(2)
C(14B)-C(15)-H(15D)	116.8(7)
Sc-C(15)-H(15D)	115.8(3)
H(15C)-C(15)-H(15D)	115.5(4)
C(31)-C(30)-C(32)	109.8(3)
C(31)-C(30)-C(3)	110.8(3)
C(32)-C(30)-C(3)	112.6(2)
C(31)-C(30)-H(30)	107.7(14)
C(32)-C(30)-H(30)	107.0(15)
C(3)-C(30)-H(30)	108.8(14)
C(30)-C(31)-H(31A)	109.5(2)
C(30)-C(31)-H(31B)	109.5(2)
H(31A)-C(31)-H(31B)	109.5
C(30)-C(31)-H(31C)	109.5(2)
H(31A)-C(31)-H(31C)	109.5
H(31B)-C(31)-H(31C)	109.5
C(30)-C(32)-H(32A)	109.5(2)
C(30)-C(32)-H(32B)	109.5(2)
H(32A)-C(32)-H(32B)	109.5
C(30)-C(32)-H(32C)	109.5(2)
H(32A)-C(32)-H(32C)	109.5
H(32B)-C(32)-H(32C)	109.5
C(52)-C(50)-C(5)	113.5(3)
C(52)-C(50)-C(51)	111.6(4)
C(5)-C(50)-C(51)	110.9(3)
C(52)-C(50)-H(50)	106.7(16)
C(5)-C(50)-H(50)	110.5(16)
C(51)-C(50)-H(50)	102.9(16)
C(50)-C(51)-H(51A)	109.5(2)
C(50)-C(51)-H(51B)	109.5(3)
H(51A)-C(51)-H(51B)	109.5
C(50)-C(51)-H(51C)	109.5(3)
H(51A)-C(51)-H(51C)	109.5
H(51B)-C(51)-H(51C)	109.5
C(50)-C(52)-H(52A)	109.5(2)
C(50)-C(52)-H(52B)	109.5(2)
H(52A)-C(52)-H(52B)	109.5
C(50)-C(52)-H(52C)	109.5(2)
H(52A)-C(52)-H(52C)	109.5
H(52B)-C(52)-H(52C)	109.5
C(72)-C(70)-C(7)	113.7(3)
C(72)-C(70)-C(71)	111.4(4)
C(7)-C(70)-C(71)	109.2(3)
C(72)-C(70)-H(70)	107.8(13)
C(7)-C(70)-H(70)	108.6(13)
C(71)-C(70)-H(70)	105.8(13)
C(70)-C(71)-H(71A)	109.5(2)
C(70)-C(71)-H(71B)	109.5(3)
H(71A)-C(71)-H(71B)	109.5
C(70)-C(71)-H(71C)	109.5(2)
H(71A)-C(71)-H(71C)	109.5
H(71B)-C(71)-H(71C)	109.5
C(70)-C(72)-H(72A)	109.5(2)
C(70)-C(72)-H(72B)	109.5(2)
H(72A)-C(72)-H(72B)	109.5
C(70)-C(72)-H(72C)	109.5(2)
H(72A)-C(72)-H(72C)	109.5
H(72B)-C(72)-H(72C)	109.5
C(92)-C(90)-C(9)	112.3(2)
C(92)-C(90)-C(91)	110.0(2)
C(9)-C(90)-C(91)	110.7(2)
C(92)-C(90)-H(90)	106.7(16)
C(9)-C(90)-H(90)	107.5(16)
C(91)-C(90)-H(90)	109.5(16)
C(90)-C(91)-H(91A)	109.5(2)
C(90)-C(91)-H(91B)	109.5(2)
H(91A)-C(91)-H(91B)	109.5
C(90)-C(91)-H(91C)	109.5(2)
H(91A)-C(91)-H(91C)	109.5
H(91B)-C(91)-H(91C)	109.5
C(90)-C(92)-H(92A)	109.5(2)
C(90)-C(92)-H(92B)	109.47(14)
H(92A)-C(92)-H(92B)	109.5
C(90)-C(92)-H(92C)	109.5(2)
H(92A)-C(92)-H(92C)	109.5
H(92B)-C(92)-H(92C)	109.5
C(4)-X(1A)-C(2)	143.4(2)
C(4)-X(1A)-C(5)	71.8(2)
C(2)-X(1A)-C(5)	144.8(2)
C(4)-X(1A)-C(1)	143.8(2)
C(2)-X(1A)-C(1)	72.8(2)
C(5)-X(1A)-C(1)	72.0(2)
C(4)-X(1A)-C(3)	71.9(2)
C(2)-X(1A)-C(3)	71.5(2)
C(5)-X(1A)-C(3)	143.7(2)
C(1)-X(1A)-C(3)	144.3(2)
C(4)-X(1A)-Sc	92.60(13)
C(2)-X(1A)-Sc	88.81(11)
C(5)-X(1A)-Sc	88.49(11)

C(1)-X(1A)-Sc	86.99(11)
C(3)-X(1A)-Sc	93.16(11)
C(10)-X(1B)-C(8)	143.1(2)
C(10)-X(1B)-C(7)	144.7(2)
C(8)-X(1B)-C(7)	72.2(2)
C(10)-X(1B)-C(9)	71.4(2)
C(8)-X(1B)-C(9)	71.6(2)
C(7)-X(1B)-C(9)	143.8(2)
C(10)-X(1B)-C(6)	72.9(2)
C(8)-X(1B)-C(6)	144.0(2)
C(7)-X(1B)-C(6)	71.8(2)
C(9)-X(1B)-C(6)	144.3(2)
C(10)-X(1B)-Sc	89.39(12)
C(8)-X(1B)-Sc	92.28(13)
C(7)-X(1B)-Sc	87.86(12)
C(9)-X(1B)-Sc	93.88(11)
C(6)-X(1B)-Sc	86.62(11)

Table 17. Anisotropic Displacement Parameters ($Å^2 \times 10^4$) for **5**[a]

	U^{11}	U^{22}	U^{33}	U^{23}	U^{13}	U^{12}
Sc	201(2)	255(2)	250(2)	-2(2)	37(2)	8(2)
Si	308(4)	609(5)	252(4)	177(4)	119(3)	211(4)
C(1)	199(12)	430(20)	203(12)	36(11)	30(10)	-44(11)
C(2)	237(12)	312(14)	201(13)	4(11)	34(10)	-15(11)
C(3)	320(14)	255(13)	343(14)	16(12)	134(11)	-26(11)
C(4)	570(20)	262(14)	321(15)	-85(13)	235(14)	-114(14)
C(5)	386(15)	410(20)	203(13)	-18(12)	47(11)	-169(13)
C(6)	480(20)	287(14)	212(13)	39(11)	99(12)	161(12)
C(7)	630(20)	243(14)	191(13)	-23(11)	43(13)	-50(13)
C(8)	550(20)	298(15)	263(14)	3(12)	-79(13)	-120(14)
C(9)	430(20)	255(13)	232(13)	38(11)	9(11)	27(11)
C(10)	380(20)	360(20)	217(13)	63(12)	55(12)	123(12)
C(11)	410(20)	1320(40)	500(20)	500(20)	140(20)	380(30)
C(12)	540(20)	770(20)	400(20)	240(20)	260(20)	360(20)
C(13)	480(20)	540(20)	740(30)	40(20)	380(20)	30(20)
C(14A)	350(30)	480(70)	1220(70)	250(40)	480(40)	150(30)
C(14B)	190(40)	390(90)	1040(90)	130(60)	270(50)	10(40)
C(15)	270(20)	570(20)	1060(30)	380(30)	50(20)	70(20)
C(30)	410(20)	380(20)	650(20)	186(15)	300(20)	134(13)
C(31)	650(20)	380(20)	1040(30)	220(20)	440(20)	160(20)
C(32)	530(20)	720(30)	600(20)	330(20)	80(20)	240(20)
C(50)	620(20)	720(20)	202(14)	-3(15)	-47(13)	-330(20)
C(51)	1430(50)	2560(80)	470(30)	480(30)	-480(30)	-1450(50)
C(52)	1490(50)	820(30)	190(20)	-10(20)	80(20)	50(30)
C(70)	930(30)	320(20)	177(14)	-1(12)	3(15)	-180(20)
C(71)	2800(80)	380(20)	250(20)	-60(20)	430(30)	-30(30)
C(72)	1130(30)	1230(40)	280(20)	190(20)	-230(20)	-590(30)
C(90)	410(20)	350(20)	289(14)	59(12)	57(12)	20(13)
C(91)	1010(30)	470(20)	420(20)	70(20)	210(20)	-180(20)
C(92)	510(20)	670(20)	269(15)	98(15)	116(13)	-30(20)

[a]The anisotropic displacement factor exponent takes the form: $-2p^2 [h^2 a^{*2} U^{11} + ... + 2 h k a^* b^* U^{12}]$

Table 18. Hydrogen Coordinates ($\times 10^4$) and Isotropic Displacement Parameters ($Å^2 \times 10^3$) for **5**

	x	y	z	U_{iso}
H(11A)	10064(7)	-32(21)	9179(9)	70(10)
H(11B)	10824(12)	636(14)	8784(9)	101(16)
H(11C)	10569(12)	-674(17)	8585(7)	99(15)
H(12A)	9438(8)	865(18)	6745(6)	61(10)
H(12B)	10237(13)	-85(14)	7027(5)	67(10)
H(12C)	10413(12)	1354(15)	7119(4)	98(15)
H(13A)	6203	2305	9834	103(25)
H(13B)	5588	1089	9562	106(23)
H(14A)	5797	3267	8914	64(19)
H(15B)	5270	2418	7676	64(17)
H(15A)	5207	1124	8011	53(15)
H(13C)	5913	2657	9588	230(83)
H(13D)	5968	1195	9815	85(34)
H(14B)	5197	772	8835	24(20)
H(15C)	5458	2833	8037	10(15)
H(15D)	5115	1529	7713	565(234)
H(31A)	7861(12)	5849(5)	7220(9)	76(11)
H(31B)	7542(12)	6115(8)	8051(8)	48(10)
H(31C)	6809(9)	6462(10)	7356(10)	75(10)
H(32A)	6296(13)	3260(15)	6819(2)	83(12)
H(32B)	7160(9)	4072(17)	6507(6)	67(10)
H(32C)	6104(13)	4676(13)	6565(6)	71(10)
H(51A)	10328(10)	2798(21)	10283(11)	112(13)
H(51B)	9960(4)	4003(18)	9726(13)	148(21)
H(51C)	10433(10)	2687(18)	9359(11)	77(12)
H(52A)	8290(14)	3743(17)	10310(8)	111(16)
H(52B)	8689(10)	2604(19)	10776(9)	67(10)
H(52C)	7752(13)	2450(18)	10259(7)	131(21)
H(71A)	7547(14)	-1981(18)	6459(13)	102(15)
H(71B)	8492(16)	-1387(16)	6632(11)	186(32)
H(71C)	7960(18)	-1118(12)	5931(13)	83(11)
H(72A)	5989(8)	-699(14)	6493(10)	128(17)
H(72B)	6419(3)	194(19)	5911(9)	91(12)
H(72C)	6079(8)	735(16)	6655(8)	34(9)
H(91A)	6749(10)	-3315(8)	9259(10)	88(14)
H(91B)	5817(13)	-3011(4)	8763(9)	65(10)
H(91C)	5737(13)	-3214(7)	9610(8)	62(9)
H(92A)	7404(10)	-1730(13)	10184(3)	57(9)
H(92B)	6340(8)	-1585(14)	10513(5)	43(7)
H(92C)	6896(11)	-367(13)	10215(4)	47(8)
H(2)	8197(16)	2572(21)	7164(13)	31(7)
H(4)	7504(19)	4090(24)	9087(15)	44(8)
H(8)	5976(19)	-882(25)	7811(15)	48(8)
H(10)	8308(17)	-648(23)	9252(14)	38(7)
H(30)	6254(18)	4616(22)	7841(14)	40(7)
H(50)	9126(19)	1554(25)	9749(14)	42(8)
H(70)	7770(16)	568(21)	6675(12)	23(6)
H(90)	5716(19)	-1075(23)	9356(14)	37(8)

D. *meso*-IpSc(η^3-1-Me-C_3H_4) (**8**)

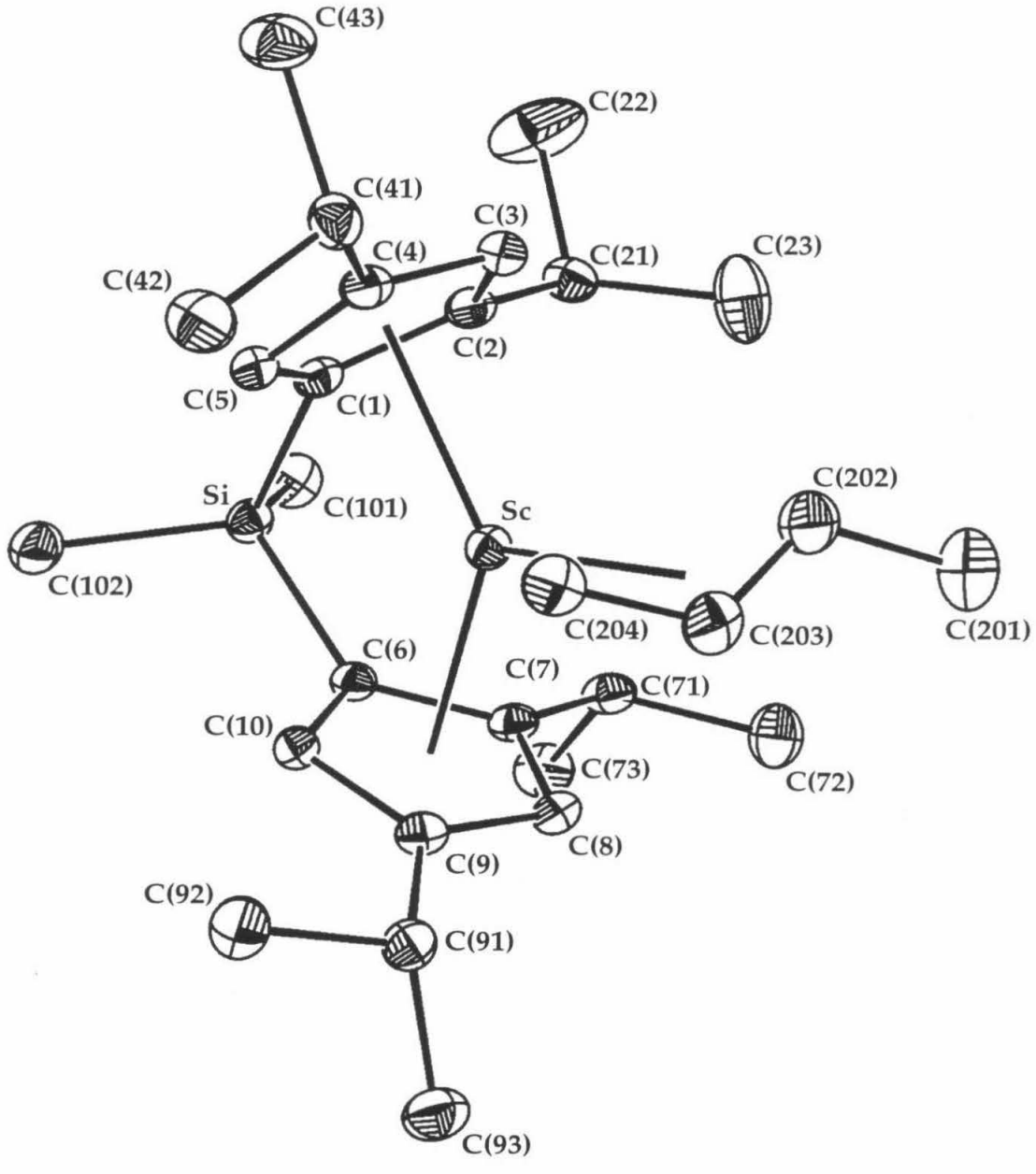

Figure 5. ORTEP representation of the molecular structure of **8** showing the complete atom labeling scheme (50% probability ellipsoids, hydrogens omitted for clarity).

Table 19. X-ray Diffraction Data Collection Parameters for **8**[a]

Feature	Value
Empirical formula	$C_{28}H_{45}ScSi$
Formula weight (g/mol)	454.69
Crystal size (mm)	0.4 x 0.2 x 0.2
Temp. (K)	160
Space Group	$P2_1/n$
Cell Constants	a = 9.259 (2) Å
	b = 23.948 (6) Å
	c = 12.352 (3) Å
	β = 102.68 (2)°
Volume (Å^3)	2672 (1)
Z	4
Density (calculated) (g/mL)	1.130
2θ range (°)	3.4 to 55.0
Index ranges	$-12 \le h \le 11$, $-31 \le k \le 31$, $-16 \le l \le 16$
Reflections collected	12493
Independent reflections	6108
R (merge)	0.03
GOF (merge)[b]	1.13
Data / restraints / parameters	6105 / 0 / 463
GOF (F^2)[b]	1.579
R indices (all data)[c, d]	R1 = 0.0448, wR2 = 0.0803

[a]Structure was obtained on an Enraf-Nonius CAD-4 using MoKα radiation (λ = 0.71073 Å); [b]$GOF = \{\Sigma w(F_o^2 - F_c^2)^2 / n - p\}^{1/2}$ (n = number of data, p = number of variables); [c]$R1 = \Sigma | |F_o| - |F_c| | / \Sigma |F_o|$; [d]$wR2 = \{\Sigma(w(F_o^2 - F_c^2)^2) / \Sigma(wF_o^4)\}^{1/2}$.

Table 20. Special Refinement Details for **8**

Weights w are calculated as $1/\sigma^2(F_o^2)$. The variances ($\sigma^2(Fo^2)$) were derived from counting statistics plus an additional term, $(0.014I)^2$, and the variances of the merged data were obtained by propagation of error plus the addition of another term, (0.014<I>)2.

All esd's (except the esd in the dihedral angle between two l.s. planes) are estimated using the full covariance matrix. The cell esd's are taken into account individually in the estimation of esd's in distances, angles and torsion angles; correlations between esd's in cell parameters are only used when they are defined by crystal symmetry. An approximate (isotropic) treatment of cell esd's is used for estimating esd's involving l.s. planes.

Table 21. Atomic Coordinates (x 10^4) and Equivalent Isotropic Displacement Parameters ($Å^2$ x 10^3) for **8**[a]

	x	y	z	U_{eq}
Sc	2119(1)	6149(1)	2858(1)	15(1)
Si	-861(1)	6008(1)	905(1)	17(1)
C(1)	-524(2)	6388(1)	2260(2)	16(1)
C(2)	216(2)	6909(1)	2545(2)	18(1)
C(3)	786(2)	6913(1)	3707(2)	18(1)
C(4)	413(2)	6411(1)	4172(2)	18(1)
C(5)	-363(2)	6084(1)	3279(2)	17(1)
C(6)	1060(2)	5731(1)	1042(1)	15(1)
C(7)	2374(2)	6005(1)	892(1)	16(1)
C(8)	3602(2)	5723(1)	1551(2)	18(1)
C(9)	3099(2)	5270(1)	2107(2)	17(1)
C(10)	1538(2)	5283(1)	1802(2)	16(1)
C(21)	245(2)	7397(1)	1772(2)	20(1)
C(22)	-1008(4)	7797(1)	1830(3)	52(1)
C(23)	1714(3)	7702(1)	1993(2)	41(1)
C(41)	594(2)	6294(1)	5396(2)	21(1)
C(42)	582(3)	5674(1)	5675(2)	27(1)
C(43)	-618(3)	6600(1)	5822(2)	29(1)
C(71)	2443(2)	6467(1)	66(2)	20(1)
C(72)	3990(3)	6714(1)	191(2)	30(1)
C(73)	1893(3)	6251(1)	-1119(2)	27(1)
C(91)	4055(2)	4828(1)	2796(2)	20(1)
C(92)	3148(2)	4438(1)	3358(2)	24(1)
C(93)	4923(3)	4497(1)	2093(2)	29(1)
C(101)	-1596(3)	6452(1)	-334(2)	25(1)
C(102)	-2167(2)	5417(1)	912(2)	24(1)
C(201)	5665(3)	7080(1)	3289(2)	39(1)
C(202)	4580(2)	6765(1)	3798(2)	28(1)
C(203)	4693(2)	6210(1)	4036(2)	25(1)
C(204)	3696(2)	5888(1)	4508(2)	23(1)

[a]U(eq) is defined as the trace of the orthogonalized U^{ij} tensor.

Table 22. Complete List of Bond Lengths (Å) and Angles (°) for **8**

Feature	Length (Å) or angle (°)	Feature	Length (Å) or angle (°)
Sc-X(1B)	2.1923(4)	C(43)-H(43A)	0.93(2)
Sc-X(1A)	2.2054(5)	C(43)-H(43C)	0.97(2)
Sc-X(1C)	2.3002(9)	C(71)-C(72)	1.525(3)
Sc-C(204)	2.317(2)	C(71)-C(73)	1.531(3)
Sc-C(10)	2.446(2)	C(71)-H(71)	0.96(2)
Sc-C(6)	2.456(2)	C(72)-H(72A)	0.97(2)
Sc-C(1)	2.463(2)	C(72)-H(72B)	0.98(2)
Sc-C(5)	2.470(2)	C(72)-H(72C)	1.00(2)
Sc-C(2)	2.503(2)	C(73)-H(73A)	0.97(2)
Sc-C(203)	2.509(2)	C(73)-H(73B)	0.98(2)
Sc-C(7)	2.514(2)	C(73)-H(73C)	0.96(2)
Sc-C(9)	2.547(2)	C(91)-C(92)	1.521(3)
Si-C(102)	1.863(2)	C(91)-C(93)	1.527(3)
Si-C(101)	1.866(2)	C(91)-H(91)	0.99(2)
Si-C(1)	1.870(2)	C(92)-H(92A)	1.03(2)
Si-C(6)	1.871(2)	C(92)-H(92B)	0.97(2)
C(1)-C(2)	1.430(2)	C(92)-H(92C)	0.96(2)
C(1)-C(5)	1.433(3)	C(93)-H(93A)	0.97(2)
C(2)-C(3)	1.418(3)	C(93)-H(93B)	0.97(2)
C(2)-C(21)	1.512(3)	C(93)-H(93C)	0.94(2)
C(3)-C(4)	1.408(3)	C(101)-H(101)	0.95(2)
C(3)-H(3)	0.97(2)	C(101)-H(101)	0.96(2)
C(4)-C(5)	1.413(3)	C(101)-H(101)	0.90(2)
C(4)-C(41)	1.511(3)	C(102)-H(102)	0.94(2)
C(5)-H(5)	0.94(2)	C(102)-H(102)	0.94(2)
C(6)-C(7)	1.429(2)	C(102)-H(102)	0.97(2)
C(6)-C(10)	1.431(2)	C(201)-C(202)	1.501(3)
C(7)-C(8)	1.415(3)	C(201)-H(201)	0.99(2)
C(7)-C(71)	1.518(3)	C(201)-H(201)	0.96(3)
C(8)-C(9)	1.417(3)	C(201)-H(201)	1.00(2)
C(8)-H(8)	0.95(2)	C(202)-C(203)	1.361(3)
C(9)-C(10)	1.412(3)	C(202)-H(202)	0.93(2)
C(9)-C(91)	1.515(3)	C(203)-C(204)	1.422(3)
C(10)-H(10)	0.97(2)	C(203)-H(203)	1.01(2)
C(21)-C(23)	1.515(3)	C(204)-H(204)	0.95(2)
C(21)-C(22)	1.519(3)	C(204)-H(204)	0.96(2)
C(21)-H(21)	0.95(2)		
C(22)-H(22A)	0.97(2)	X(1B)-Sc-X(1A)	128.66(3)
C(22)-H(22B)	1.03(3)	X(1B)-Sc-X(1C)	113.05(2)
C(22)-H(22C)	0.95(3)	X(1A)-Sc-X(1C)	118.26(2)
C(23)-H(23A)	1.00(3)	C(204)-Sc-C(10)	105.23(7)
C(23)-H(23B)	0.95(2)	C(204)-Sc-C(6)	137.87(7)
C(23)-H(23C)	0.93(2)	C(10)-Sc-C(6)	33.93(6)
C(41)-C(42)	1.524(3)	C(204)-Sc-C(1)	135.97(7)
C(41)-C(43)	1.527(3)	C(10)-Sc-C(1)	87.08(6)
C(41)-H(41)	0.91(2)	C(6)-Sc-C(1)	69.49(6)
C(42)-H(42A)	0.98(2)	C(204)-Sc-C(5)	103.51(7)
C(42)-H(42B)	0.95(2)	C(10)-Sc-C(5)	87.31(6)
C(42)-H(42C)	0.97(2)	C(6)-Sc-C(5)	87.91(7)
C(43)-H(43A)	0.97(2)	C(1)-Sc-C(5)	33.76(6)

C(204)-Sc-C(2)	128.19(7)	C(3)-C(4)-C(5)	106.4(2)
C(10)-Sc-C(2)	117.96(7)	C(3)-C(4)-C(41)	125.7(2)
C(6)-Sc-C(2)	91.65(6)	C(5)-C(4)-C(41)	127.2(2)
C(1)-Sc-C(2)	33.45(6)	C(3)-C(4)-Sc	73.27(11)
C(5)-Sc-C(2)	54.70(6)	C(5)-C(4)-Sc	69.58(10)
C(204)-Sc-C(203)	33.97(7)	C(41)-C(4)-Sc	129.56(13)
C(10)-Sc-C(203)	115.34(7)	C(4)-C(5)-C(1)	110.0(2)
C(6)-Sc-C(203)	133.72(7)	C(4)-C(5)-Sc	78.00(11)
C(1)-Sc-C(203)	156.23(7)	C(1)-C(5)-Sc	72.85(11)
C(5)-Sc-C(203)	133.68(7)	C(4)-C(5)-H(5)	125.2(12)
C(2)-Sc-C(203)	126.48(7)	C(1)-C(5)-H(5)	124.8(12)
C(204)-Sc-C(7)	129.61(7)	Sc-C(5)-H(5)	115.2(12)
C(10)-Sc-C(7)	54.88(6)	C(7)-C(6)-C(10)	106.2(2)
C(6)-Sc-C(7)	33.38(6)	C(7)-C(6)-Si	130.21(14)
C(1)-Sc-C(7)	92.30(7)	C(10)-C(6)-Si	118.39(14)
C(5)-Sc-C(7)	118.93(7)	C(7)-C(6)-Sc	75.55(10)
C(2)-Sc-C(7)	99.38(6)	C(10)-C(6)-Sc	72.67(10)
C(203)-Sc-C(7)	106.82(7)	Si-C(6)-Sc	96.83(8)
C(204)-Sc-C(9)	83.76(7)	C(8)-C(7)-C(6)	107.9(2)
C(10)-Sc-C(9)	32.76(6)	C(8)-C(7)-C(71)	126.0(2)
C(6)-Sc-C(9)	55.45(6)	C(6)-C(7)-C(71)	125.8(2)
C(1)-Sc-C(9)	119.50(6)	C(8)-C(7)-Sc	75.20(11)
C(5)-Sc-C(9)	116.55(6)	C(6)-C(7)-Sc	71.07(10)
C(2)-Sc-C(9)	147.09(6)	C(71)-C(7)-Sc	125.12(12)
C(203)-Sc-C(9)	83.69(7)	C(7)-C(8)-C(9)	109.6(2)
C(7)-Sc-C(9)	54.41(6)	C(7)-C(8)-Sc	72.36(10)
C(102)-Si-C(101)	108.51(11)	C(9)-C(8)-Sc	73.71(11)
C(102)-Si-C(1)	110.24(9)	C(7)-C(8)-H(8)	125.3(12)
C(101)-Si-C(1)	114.54(10)	C(9)-C(8)-H(8)	125.1(12)
C(102)-Si-C(6)	109.63(9)	Sc-C(8)-H(8)	121.4(12)
C(101)-Si-C(6)	116.40(10)	C(10)-C(9)-C(8)	106.2(2)
C(1)-Si-C(6)	97.07(8)	C(10)-C(9)-C(91)	127.1(2)
C(102)-Si-Sc	121.33(7)	C(8)-C(9)-C(91)	126.4(2)
C(101)-Si-Sc	130.15(8)	C(10)-C(9)-Sc	69.69(10)
C(1)-Si-Sc	48.64(6)	C(8)-C(9)-Sc	74.01(10)
C(6)-Si-Sc	48.43(6)	C(91)-C(9)-Sc	125.73(12)
C(2)-C(1)-C(5)	105.9(2)	C(9)-C(10)-C(6)	110.0(2)
C(2)-C(1)-Si	128.44(14)	C(9)-C(10)-Sc	77.55(11)
C(5)-C(1)-Si	120.29(14)	C(6)-C(10)-Sc	73.40(10)
C(2)-C(1)-Sc	74.81(11)	C(9)-C(10)-H(10)	125.1(10)
C(5)-C(1)-Sc	73.39(11)	C(6)-C(10)-H(10)	124.9(11)
Si-C(1)-Sc	96.61(8)	Sc-C(10)-H(10)	115.6(10)
C(3)-C(2)-C(1)	107.9(2)	C(2)-C(21)-C(23)	113.5(2)
C(3)-C(2)-C(21)	125.4(2)	C(2)-C(21)-C(22)	109.8(2)
C(1)-C(2)-C(21)	126.4(2)	C(23)-C(21)-C(22)	110.6(2)
C(3)-C(2)-Sc	75.84(11)	C(2)-C(21)-H(21)	109.1(11)
C(1)-C(2)-Sc	71.74(10)	C(23)-C(21)-H(21)	106.1(12)
C(21)-C(2)-Sc	123.35(13)	C(22)-C(21)-H(21)	107.5(12)
C(4)-C(3)-C(2)	109.7(2)	C(21)-C(22)-H(22A)	111.2(14)
C(4)-C(3)-Sc	74.91(11)	C(21)-C(22)-H(22B)	109.2(14)
C(2)-C(3)-Sc	71.64(10)	H(22A)-C(22)-H(22B)	106.4(19)
C(4)-C(3)-H(3)	125.4(11)	C(21)-C(22)-H(22C)	109.8(18)
C(2)-C(3)-H(3)	124.8(11)	H(22A)-C(22)-H(22C)	111.7(22)
Sc-C(3)-H(3)	121.4(11)	H(22B)-C(22)-H(22C)	108.5(22)

C(21)-C(23)-H(23A)	111.9(18)
C(21)-C(23)-H(23B)	112.6(14)
H(23A)-C(23)-H(23B)	111.5(23)
C(21)-C(23)-H(23C)	106.9(16)
H(23A)-C(23)-H(23C)	108.9(24)
H(23B)-C(23)-H(23C)	104.5(20)
C(4)-C(41)-C(42)	113.7(2)
C(4)-C(41)-C(43)	109.1(2)
C(42)-C(41)-C(43)	110.4(2)
C(4)-C(41)-H(41)	109.5(12)
C(42)-C(41)-H(41)	108.5(12)
C(43)-C(41)-H(41)	105.4(12)
C(41)-C(42)-H(42A)	112.2(12)
C(41)-C(42)-H(42B)	111.1(14)
H(42A)-C(42)-H(42B)	111.2(19)
C(41)-C(42)-H(42C)	111.2(12)
H(42A)-C(42)-H(42C)	105.9(17)
H(42B)-C(42)-H(42C)	105.0(18)
C(41)-C(43)-H(43A)	110.2(13)
C(41)-C(43)-H(43A)	109.9(14)
H(43A)-C(43)-H(43A)	107.9(19)
C(41)-C(43)-H(43C)	111.0(12)
H(43A)-C(43)-H(43C)	108.3(17)
H(43A)-C(43)-H(43C)	109.4(18)
C(7)-C(71)-C(72)	113.1(2)
C(7)-C(71)-C(73)	110.0(2)
C(72)-C(71)-C(73)	109.6(2)
C(7)-C(71)-H(71)	108.4(11)
C(72)-C(71)-H(71)	108.1(12)
C(73)-C(71)-H(71)	107.6(12)
C(71)-C(72)-H(72A)	108.5(14)
C(71)-C(72)-H(72B)	110.7(13)
H(72A)-C(72)-H(72B)	109.4(18)
C(71)-C(72)-H(72C)	111.5(12)
H(72A)-C(72)-H(72C)	109.2(18)
H(72B)-C(72)-H(72C)	107.5(17)
C(71)-C(73)-H(73A)	111.9(12)
C(71)-C(73)-H(73B)	110.0(12)
H(73A)-C(73)-H(73B)	105.3(17)
C(71)-C(73)-H(73C)	114.0(13)
H(73A)-C(73)-H(73C)	111.2(18)
H(73B)-C(73)-H(73C)	103.8(17)
C(9)-C(91)-C(92)	111.8(2)
C(9)-C(91)-C(93)	111.0(2)
C(92)-C(91)-C(93)	110.7(2)
C(9)-C(91)-H(91)	106.3(10)
C(92)-C(91)-H(91)	108.7(10)
C(93)-C(91)-H(91)	108.2(11)
C(91)-C(92)-H(92A)	111.6(11)
C(91)-C(92)-H(92B)	110.2(12)
H(92A)-C(92)-H(92B)	108.7(16)
C(91)-C(92)-H(92C)	112.8(13)
H(92A)-C(92)-H(92C)	105.7(16)
H(92B)-C(92)-H(92C)	107.6(17)
C(91)-C(93)-H(93A)	112.5(13)
C(91)-C(93)-H(93B)	111.9(12)
H(93A)-C(93)-H(93B)	106.3(17)
C(91)-C(93)-H(93C)	112.0(14)
H(93A)-C(93)-H(93C)	107.2(18)
H(93B)-C(93)-H(93C)	106.5(18)
Si-C(101)-H(101)	117.2(13)
Si-C(101)-H(101)	109.5(13)
H(101)-C(101)-H(101)	106.1(18)
Si-C(101)-H(101)	108.1(14)
H(101)-C(101)-H(101)	107.3(18)
H(101)-C(101)-H(101)	108.2(19)
Si-C(102)-H(102)	111.5(13)
Si-C(102)-H(102)	110.9(13)
H(102)-C(102)-H(102)	108.0(18)
Si-C(102)-H(102)	108.4(14)
H(102)-C(102)-H(102)	108.7(18)
H(102)-C(102)-H(102)	109.4(19)
C(202)-C(201)-H(201)	111.9(15)
C(202)-C(201)-H(201)	110.3(14)
H(201)-C(201)-H(201)	103.5(19)
C(202)-C(201)-H(201)	113.7(14)
H(201)-C(201)-H(201)	108.9(19)
H(201)-C(201)-H(201)	107.9(20)
C(203)-C(202)-C(201)	123.7(2)
C(203)-C(202)-Sc	65.46(12)
C(201)-C(202)-Sc	131.5(2)
C(203)-C(202)-H(202)	118.7(12)
C(201)-C(202)-H(202)	115.7(12)
Sc-C(202)-H(202)	86.8(12)
C(202)-C(203)-C(204)	126.3(2)
C(202)-C(203)-Sc	84.99(13)
C(204)-C(203)-Sc	65.61(11)
C(202)-C(203)-H(203)	114.8(13)
C(204)-C(203)-H(203)	117.2(13)
Sc-C(203)-H(203)	110.2(13)
C(203)-C(204)-Sc	80.43(12)
C(203)-C(204)-H(204)	114.4(12)
Sc-C(204)-H(204)	103.4(12)
C(203)-C(204)-H(204)	116.8(12)
Sc-C(204)-H(204)	119.6(11)
H(204)-C(204)-H(204)	116.5(16)

Table 5. Anisotropic Displacement Parameters ($Å^2 \times 10^4$) for **8**[a]

	U^{11}	U^{22}	U^{33}	U^{23}	U^{13}	U^{12}
Sc	138(2)	169(2)	150(2)	-3(1)	30(1)	-2(2)
Si	138(3)	192(3)	164(3)	-4(2)	20(2)	7(2)
C(1)	130(9)	183(9)	186(9)	-5(8)	47(7)	28(8)
C(2)	172(10)	175(10)	196(9)	-8(8)	66(8)	22(8)
C(3)	174(10)	167(10)	196(10)	-29(8)	55(8)	-4(8)
C(4)	177(10)	177(9)	199(9)	-9(8)	70(8)	20(8)
C(5)	156(10)	158(10)	214(10)	-7(8)	61(8)	8(8)
C(6)	155(9)	159(9)	151(9)	-31(7)	42(7)	3(8)
C(7)	180(9)	176(9)	151(9)	-19(7)	70(7)	20(8)
C(8)	151(10)	191(10)	208(10)	-7(8)	66(8)	13(8)
C(9)	177(10)	180(9)	167(9)	-13(8)	51(8)	20(8)
C(10)	158(9)	163(9)	168(9)	-14(7)	55(8)	-10(8)
C(21)	256(11)	168(10)	187(10)	6(8)	69(9)	19(8)
C(22)	590(20)	450(20)	630(20)	320(20)	350(20)	320(20)
C(23)	460(20)	368(15)	381(15)	120(12)	32(13)	-179(13)
C(41)	231(11)	213(11)	182(10)	-27(8)	56(8)	-48(9)
C(42)	371(14)	245(11)	226(11)	14(9)	119(10)	-10(10)
C(43)	398(15)	287(13)	230(12)	-11(10)	154(11)	30(11)
C(71)	220(10)	194(10)	203(10)	13(8)	91(8)	38(9)
C(72)	309(13)	291(12)	307(12)	62(10)	100(10)	-60(10)
C(73)	329(13)	298(12)	195(10)	37(9)	95(10)	10(10)
C(91)	158(10)	203(10)	224(10)	7(8)	17(8)	13(8)
C(92)	219(11)	241(11)	259(11)	65(9)	31(9)	12(9)
C(93)	249(12)	258(12)	384(13)	35(10)	114(11)	64(10)
C(101)	214(11)	295(12)	224(11)	20(9)	4(9)	14(10)
C(102)	184(11)	268(12)	261(11)	-20(10)	40(9)	-10(9)
C(201)	321(14)	401(15)	408(15)	11(12)	28(12)	-115(12)
C(202)	222(11)	314(12)	280(12)	-43(10)	13(9)	-22(10)
C(203)	170(10)	333(12)	193(10)	-37(9)	-46(8)	-11(9)
C(204)	222(11)	262(12)	192(10)	1(9)	-10(9)	15(9)

[a]The anisotropic displacement factor exponent takes the form: $-2p^2 [h^2 a^{*2} U^{11} + ... + 2 h k a^* b^* U^{12}]$

Table 23. Hydrogen Coordinates (x 10^4) and Isotropic Displacement Parameters ($Å^2$ x 10^3) for **8**

	x	y	z	U_{iso}
H(3)	1325(21)	7221(8)	4120(15)	20(5)
H(5)	-710(22)	5720(8)	3340(15)	22(5)
H(8)	4615(23)	5819(8)	1601(16)	25(6)
H(10)	882(20)	5027(7)	2072(14)	12(5)
H(21)	88(21)	7263(8)	1030(15)	18(5)
H(22A)	-1016(25)	8112(10)	1335(19)	41(7)
H(22B)	-844(28)	7961(10)	2622(22)	53(8)
H(22C)	-1923(34)	7604(11)	1674(23)	67(10)
H(23A)	2555(37)	7445(13)	1976(26)	94(12)
H(23B)	1710(26)	8014(10)	1511(19)	42(7)
H(23C)	1846(28)	7857(10)	2696(21)	50(8)
H(41)	1465(22)	6444(7)	5778(15)	15(5)
H(42A)	1331(25)	5464(9)	5390(18)	35(6)
H(42B)	691(27)	5619(10)	6446(21)	49(7)
H(42C)	-365(24)	5504(8)	5339(17)	27(6)
H(43A)	-568(25)	6997(9)	5687(17)	36(6)
H(43A)	-1545(26)	6474(9)	5448(18)	34(7)
H(43C)	-512(22)	6542(8)	6617(18)	27(6)
H(71)	1789(22)	6762(8)	182(15)	22(5)
H(72A)	3935(26)	7024(9)	-325(19)	43(7)
H(72B)	4368(25)	6848(9)	949(19)	36(6)
H(72C)	4707(24)	6430(9)	28(17)	31(6)
H(73A)	1905(24)	6541(9)	-1667(18)	32(6)
H(73B)	2559(23)	5960(8)	-1279(16)	25(6)
H(73C)	944(26)	6069(9)	-1244(18)	35(6)
H(91)	4771(20)	5030(7)	3374(15)	14(5)
H(92A)	2638(23)	4650(8)	3894(16)	28(6)
H(92B)	2396(24)	4251(9)	2805(17)	31(6)
H(92C)	3738(24)	4156(9)	3796(17)	33(6)
H(93A)	5526(24)	4734(9)	1736(17)	33(6)
H(93B)	5594(23)	4230(9)	2536(17)	28(6)
H(93C)	4294(25)	4290(9)	1529(18)	36(7)
H(101)	-968(24)	6737(9)	-500(17)	31(6)
H(101)	-1841(24)	6221(9)	-984(18)	32(6)
H(101)	-2434(26)	6619(9)	-237(18)	35(7)
H(102)	-1895(24)	5202(8)	1567(18)	31(6)
H(102)	-2186(24)	5179(9)	306(18)	35(6)
H(102)	-3152(27)	5569(10)	870(18)	45(7)
H(201)	5173(27)	7362(10)	2753(20)	45(7)
H(201)	6320(28)	7298(10)	3846(20)	49(7)
H(201)	6286(27)	6836(10)	2921(19)	45(7)
H(202)	3954(22)	6982(8)	4118(15)	16(5)
H(203)	5406(26)	5999(9)	3676(18)	40(7)
H(204)	3304(22)	6080(8)	5058(16)	24(6)
H(204)	3936(22)	5501(8)	4648(15)	23(5)

E. *meso*-IpZr(NMe_2)$_2$ (**9**)

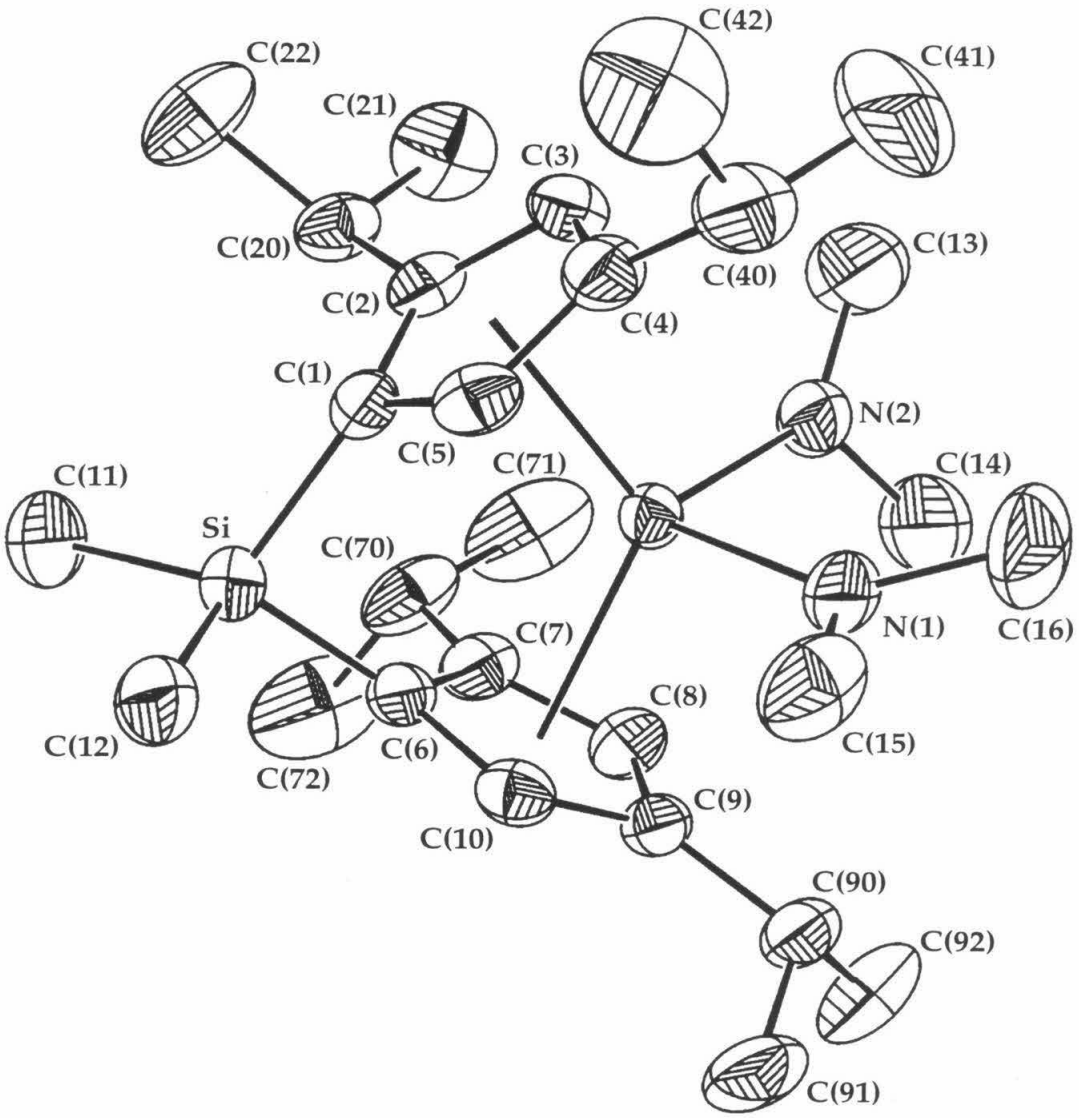

Figure 6. ORTEP representation of the molecular structure of **9** showing the complete atom labeling scheme (50% probability ellipsoids, hydrogens omitted for clarity).

Table 25. X-ray Diffraction Data Collection Parameters for **9**[a]

Feature	Value
Empirical formula	$C_{28}H_{50}N_2SiZr$
Formula weight (g/mol)	534.01
Crystal size (mm)	0.5 x 0.3 x 0.3
Temp. (K)	293
Space Group	$P2_1/n$
Cell Constants	a = 17.354 (3) Å b = 10.179 (2) Å c = 17.628 (4) Å β = 107.43 (3)°
Volume ($Å^3$)	26970.9 (10)
Z	4
Density (calculated) (g/mL)	1.194
2θ range (°)	4 to 50.0
Index ranges	$-20 \le h \le 20$, $-12 \le k \le 5$, $-21 \le l \le 21$
Reflections collected	16710
Independent reflections	5211
R (merge)	0.053
GOF (merge)[b]	1.04
Data / restraints / parameters	5207 / 0 / 339
GOF (F^2)[b]	1.403
R indices (all data)[c, d]	R1 = 0.0939, wR2 = 0.0716

[a]Structure was obtained on an Enraf-Nonius CAD-4 using MoKα radiation (λ = 0.71073 Å); [b]$GOF = \{\Sigma w(F_o^2 - F_c^2)^2 / n - p\}^{1/2}$ (n = number of data, p = number of variables); [c]$R1 = \Sigma | |F_o| - |F_c| | / \Sigma |F_o|$; [d]$wR2 = \{\Sigma(w(F_o^2 - F_c^2)^2) / \Sigma(wF_o^4)\}^{1/2}$.

Table 26. Special Refinement Details for **9**

Weights w are calculated as $1/\sigma^2(F_o^2)$. The variances ($\sigma^2(Fo^2)$) were derived from counting statistics plus an additional term, $(0.014I)^2$, and the variances of the merged data were obtained by propagation of error plus the addition of another term, (0.014<I>)2.

All esd's (except the esd in the dihedral angle between two l.s. planes) are estimated using the full covariance matrix. The cell esd's are taken into account individually in the estimation of esd's in distances, angles and torsion angles; correlations between esd's in cell parameters are only used when they are defined by crystal symmetry. An approximate (isotropic) treatment of cell esd's is used for estimating esd's involving l.s. planes.

Table 27. Atomic Coordinates (x 10^4) and Equivalent Isotropic Displacement Parameters ($Å^2$ x 10^3) for **9**[a]

	x	y	z	U_{eq}
Zr	5276(1)	7477(1)	2571(1)	31(1)
Si	3834(1)	9211(1)	3048(1)	43(1)
N(1)	5281(2)	5408(3)	2524(2)	47(1)
N(2)	6316(2)	7718(3)	2244(2)	47(1)
C(1)	3929(2)	8725(4)	2071(2)	36(1)
C(2)	4397(2)	9253(4)	1609(2)	42(1)
C(3)	4491(2)	8263(4)	1075(2)	41(1)
C(4)	4098(2)	7120(3)	1173(2)	35(1)
C(5)	3766(2)	7404(5)	1799(2)	38(1)
C(6)	4848(2)	8643(4)	3662(2)	33(1)
C(7)	5617(2)	9226(4)	3739(2)	36(1)
C(8)	6208(2)	8239(4)	4012(2)	38(1)
C(9)	5848(2)	7064(4)	4116(2)	42(1)
C(10)	5016(2)	7303(4)	3885(2)	40(1)
C(11)	3604(3)	10979(4)	3169(3)	73(1)
C(12)	3035(2)	8192(5)	3267(2)	62(1)
C(13)	7142(3)	8138(6)	2613(3)	89(2)
C(14)	6287(3)	7282(7)	1442(3)	91(2)
C(15)	4677(3)	4562(4)	2681(3)	69(1)
C(16)	5939(4)	4614(6)	2429(3)	87(2)
C(20)	4640(3)	10673(4)	1563(2)	58(1)
C(22)	3939(4)	11416(5)	1003(3)	108(2)
C(21)	5400(3)	10832(5)	1310(3)	89(2)
C(40)	4009(2)	5871(4)	696(2)	44(1)
C(41)	3228(3)	5163(4)	643(3)	64(1)
C(42)	4072(3)	6132(5)	-136(2)	77(2)
C(70)	5779(2)	10686(4)	3721(2)	42(1)
C(72)	5785(4)	11289(5)	4521(3)	78(2)
C(71)	6557(3)	11034(5)	3546(3)	71(1)
C(90)	6272(3)	5816(5)	4480(2)	60(1)
C(91)	7119(3)	5693(6)	4425(4)	110(2)
C(92)	6280(4)	5723(6)	5344(3)	109(2)

[a]U(eq) is defined as the trace of the orthogonalized U^{ij} tensor.

Table 28. Complete List of Bond Lengths (Å) and Angles (°) for **9**

Feature	Length (Å) or angle (°)	Feature	Length (Å) or angle (°)
Zr-N(2)	2.067(3)	N(1)-Zr-C(5)	88.02(14)
Zr-N(1)	2.107(3)	C(10)-Zr-C(5)	92.91(11)
Zr-C(10)	2.496(3)	C(6)-Zr-C(5)	86.09(11)
Zr-C(6)	2.552(3)	N(2)-Zr-C(1)	128.70(12)
Zr-C(5)	2.567(3)	N(1)-Zr-C(1)	119.58(12)
Zr-C(1)	2.573(3)	C(10)-Zr-C(1)	87.42(12)
Zr-C(2)	2.631(4)	C(6)-Zr-C(1)	65.73(11)
Zr-C(9)	2.638(4)	C(5)-Zr-C(1)	32.25(11)
Zr-C(7)	2.651(3)	N(2)-Zr-C(2)	97.21(12)
Zr-C(8)	2.684(4)	N(1)-Zr-C(2)	132.03(12)
Zr-C(3)	2.701(4)	C(10)-Zr-C(2)	114.56(12)
Zr-C(4)	2.714(3)	C(6)-Zr-C(2)	85.54(12)
Si-C(1)	1.847(4)	C(5)-Zr-C(2)	51.32(13)
Si-C(12)	1.863(4)	C(1)-Zr-C(2)	31.53(10)
Si-C(6)	1.860(4)	N(2)-Zr-C(9)	102.54(12)
Si-C(11)	1.870(4)	N(1)-Zr-C(9)	82.91(12)
N(1)-C(15)	1.446(5)	C(10)-Zr-C(9)	31.44(10)
N(1)-C(16)	1.450(5)	C(6)-Zr-C(9)	53.17(11)
N(2)-C(13)	1.450(4)	C(5)-Zr-C(9)	123.45(11)
N(2)-C(14)	1.468(5)	C(1)-Zr-C(9)	117.03(11)
C(1)-C(2)	1.415(5)	C(2)-Zr-C(9)	137.80(11)
C(1)-C(5)	1.428(5)	N(2)-Zr-C(7)	97.27(12)
C(2)-C(3)	1.421(5)	N(1)-Zr-C(7)	134.33(12)
C(2)-C(20)	1.515(5)	C(10)-Zr-C(7)	52.19(12)
C(3)-C(4)	1.386(5)	C(6)-Zr-C(7)	31.80(10)
C(4)-C(5)	1.418(4)	C(5)-Zr-C(7)	112.71(12)
C(4)-C(40)	1.506(4)	C(1)-Zr-C(7)	84.42(11)
C(6)-C(10)	1.426(5)	C(2)-Zr-C(7)	89.44(11)
C(6)-C(7)	1.429(4)	C(9)-Zr-C(7)	51.53(11)
C(7)-C(8)	1.413(5)	N(2)-Zr-C(8)	84.31(11)
C(7)-C(70)	1.515(5)	N(1)-Zr-C(8)	108.51(12)
C(8)-C(9)	1.387(5)	C(10)-Zr-C(8)	50.74(11)
C(9)-C(10)	1.398(4)	C(6)-Zr-C(8)	51.79(11)
C(9)-C(90)	1.511(5)	C(5)-Zr-C(8)	137.73(11)
C(20)-C(21)	1.522(5)	C(1)-Zr-C(8)	114.16(11)
C(20)-C(22)	1.519(5)	C(2)-Zr-C(8)	118.68(11)
C(40)-C(41)	1.513(5)	C(9)-Zr-C(8)	30.19(10)
C(40)-C(42)	1.526(5)	C(7)-Zr-C(8)	30.71(10)
C(70)-C(71)	1.516(5)	N(2)-Zr-C(3)	85.42(12)
C(70)-C(72)	1.534(5)	N(1)-Zr-C(3)	105.34(12)
C(90)-C(91)	1.508(6)	C(10)-Zr-C(3)	138.46(12)
C(90)-C(92)	1.520(5)	C(6)-Zr-C(3)	114.96(12)
		C(5)-Zr-C(3)	49.80(11)
N(2)-Zr-N(1)	95.38(14)	C(1)-Zr-C(3)	51.56(11)
N(2)-Zr-C(10)	133.06(11)	C(2)-Zr-C(3)	30.88(10)
N(1)-Zr-C(10)	88.24(14)	C(9)-Zr-C(3)	168.12(11)
N(2)-Zr-C(6)	129.08(12)	C(7)-Zr-C(3)	119.26(11)
N(1)-Zr-C(6)	119.97(13)	C(8)-Zr-C(3)	145.35(11)
C(10)-Zr-C(6)	32.78(11)	N(2)-Zr-C(4)	104.26(11)
N(2)-Zr-C(5)	133.91(11)	N(1)-Zr-C(4)	80.86(11)

C(10)-Zr-C(4)	122.46(11)
C(6)-Zr-C(4)	115.85(10)
C(5)-Zr-C(4)	30.98(9)
C(1)-Zr-C(4)	52.77(10)
C(2)-Zr-C(4)	51.18(11)
C(9)-Zr-C(4)	149.74(12)
C(7)-Zr-C(4)	136.63(11)
C(8)-Zr-C(4)	166.92(10)
C(3)-Zr-C(4)	29.66(10)
C(1)-Si-C(12)	108.9(2)
C(1)-Si-C(6)	97.23(15)
C(12)-Si-C(6)	109.8(2)
C(1)-Si-C(11)	116.5(2)
C(12)-Si-C(11)	108.3(2)
C(6)-Si-C(11)	115.5(2)
C(15)-N(1)-C(16)	109.3(4)
C(15)-N(1)-Zr	125.2(3)
C(16)-N(1)-Zr	125.0(3)
C(13)-N(2)-C(14)	105.4(3)
C(13)-N(2)-Zr	137.6(3)
C(14)-N(2)-Zr	116.8(3)
C(2)-C(1)-C(5)	104.7(3)
C(2)-C(1)-Si	131.4(3)
C(5)-C(1)-Si	120.1(3)
C(2)-C(1)-Zr	76.5(2)
C(5)-C(1)-Zr	73.6(2)
Si-C(1)-Zr	97.94(13)
C(1)-C(2)-C(3)	108.2(3)
C(1)-C(2)-C(20)	127.6(4)
C(3)-C(2)-C(20)	123.4(4)
C(1)-C(2)-Zr	72.0(2)
C(3)-C(2)-Zr	77.3(2)
C(20)-C(2)-Zr	125.0(2)
C(4)-C(3)-C(2)	110.7(3)
C(4)-C(3)-Zr	75.7(2)
C(2)-C(3)-Zr	71.8(2)
C(3)-C(4)-C(5)	104.8(3)
C(3)-C(4)-C(40)	127.6(3)
C(5)-C(4)-C(40)	127.5(4)
C(3)-C(4)-Zr	74.6(2)
C(5)-C(4)-Zr	68.8(2)
C(40)-C(4)-Zr	122.9(2)
C(4)-C(5)-C(1)	111.6(3)
C(4)-C(5)-Zr	80.3(2)
C(1)-C(5)-Zr	74.1(2)
C(10)-C(6)-C(7)	105.3(3)
C(10)-C(6)-Si	122.6(3)
C(7)-C(6)-Si	128.3(3)
C(10)-C(6)-Zr	71.5(2)
C(7)-C(6)-Zr	77.9(2)
Si-C(6)-Zr	98.33(13)
C(8)-C(7)-C(6)	107.4(3)
C(8)-C(7)-C(70)	125.8(3)
C(6)-C(7)-C(70)	125.4(3)
C(8)-C(7)-Zr	75.9(2)
C(6)-C(7)-Zr	70.3(2)
C(70)-C(7)-Zr	130.0(2)
C(9)-C(8)-C(7)	110.4(3)
C(9)-C(8)-Zr	73.1(2)
C(7)-C(8)-Zr	73.3(2)
C(8)-C(9)-C(10)	106.1(3)
C(8)-C(9)-C(90)	126.9(4)
C(10)-C(9)-C(90)	126.8(4)
C(8)-C(9)-Zr	76.7(2)
C(10)-C(9)-Zr	68.7(2)
C(90)-C(9)-Zr	123.9(3)
C(9)-C(10)-C(6)	110.8(4)
C(9)-C(10)-Zr	79.9(2)
C(6)-C(10)-Zr	75.8(2)
C(21)-C(20)-C(2)	113.4(4)
C(21)-C(20)-C(22)	110.7(5)
C(2)-C(20)-C(22)	109.1(4)
C(4)-C(40)-C(41)	112.1(3)
C(4)-C(40)-C(42)	111.4(3)
C(41)-C(40)-C(42)	110.1(4)
C(71)-C(70)-C(7)	114.6(3)
C(71)-C(70)-C(72)	109.4(4)
C(7)-C(70)-C(72)	108.9(3)
C(9)-C(90)-C(91)	113.7(4)
C(9)-C(90)-C(92)	109.6(4)
C(91)-C(90)-C(92)	110.0(5)

Table 29. Anisotropic Displacement Parameters ($Å^2 \times 10^4$) for 9[a]

	U^{11}	U^{22}	U^{33}	U^{23}	U^{13}	U^{12}
Zr	305(2)	269(2)	345(2)	-19(3)	100(1)	9(2)
Si	375(6)	429(8)	493(7)	-127(6)	122(5)	62(6)
N(1)	540(20)	270(20)	560(20)	-40(20)	70(20)	80(20)
N(2)	400(20)	510(30)	540(20)	-120(20)	194(14)	-30(20)
C(1)	350(20)	270(20)	390(20)	-10(20)	10(20)	60(20)
C(2)	500(20)	320(30)	360(20)	10(20)	20(20)	30(20)
C(3)	490(20)	390(30)	340(20)	-10(20)	150(20)	-40(20)
C(4)	360(20)	320(30)	330(20)	-30(20)	40(20)	20(20)
C(5)	310(20)	420(30)	420(20)	0(30)	106(15)	-60(30)
C(6)	370(20)	320(20)	330(20)	-60(20)	130(20)	-20(20)
C(7)	460(20)	340(20)	260(20)	-40(20)	80(20)	-40(20)
C(8)	310(20)	390(30)	410(20)	10(20)	40(20)	-20(20)
C(9)	470(20)	380(30)	360(20)	10(20)	60(20)	40(20)
C(10)	440(20)	400(30)	360(20)	-40(20)	110(20)	-110(20)
C(11)	670(30)	580(40)	870(40)	-170(30)	140(30)	260(30)
C(12)	480(30)	810(40)	650(30)	-260(20)	280(30)	-60(30)
C(13)	510(30)	1280(60)	960(40)	-440(40)	330(30)	-180(30)
C(14)	600(30)	1340(60)	860(30)	-340(40)	340(30)	100(40)
C(15)	980(40)	340(30)	690(40)	10(30)	160(30)	20(30)
C(16)	1080(40)	490(40)	990(50)	-70(40)	260(40)	350(40)
C(20)	950(40)	300(30)	400(30)	0(20)	70(20)	-50(30)
C(22)	1650(70)	320(40)	940(50)	170(30)	-110(50)	60(40)
C(21)	1450(50)	450(40)	770(40)	90(30)	320(40)	-380(40)
C(40)	510(20)	350(30)	400(20)	-70(20)	50(20)	-10(20)
C(41)	700(30)	400(30)	690(30)	-170(30)	30(30)	-150(30)
C(42)	1220(50)	550(40)	560(30)	-230(30)	310(30)	-140(40)
C(70)	510(20)	300(30)	400(20)	-20(20)	50(20)	-60(20)
C(72)	1240(50)	410(40)	690(40)	-230(30)	290(40)	-220(30)
C(71)	770(40)	510(40)	850(40)	60(30)	270(30)	-160(30)
C(90)	720(30)	370(30)	560(30)	70(30)	-30(20)	110(30)
C(91)	960(50)	850(60)	1280(60)	240(50)	20(40)	500(40)
C(92)	1560(70)	830(50)	800(40)	490(40)	250(40)	400(50)

[a]The anisotropic displacement factor exponent takes the form: $-2p^2 [h^2 a^{*2} U^{11} + ... + 2 h k a^* b^* U^{12}]$

Table 30. Hydrogen Coordinates (x 10^4) and Isotropic Displacement Parameters ($Å^2$ x 10^3) for **9**

	x	y	z	U_{iso}
H(3)	4778(2)	8369(4)	710(2)	23(9)
H(5)	3479(2)	6804(5)	2006(2)	17(9)
H(8)	6760(2)	8360(4)	4108(2)	22(8)
H(10)	4626(2)	6673(4)	3879(2)	26(10)
H(11A)	3568(3)	11121(4)	3696(3)	103(19)
H(11B)	3099(3)	11207(4)	2787(3)	165(26)
H(11C)	4026(3)	11518(4)	3087(3)	139(25)
H(12A)	2982(2)	8438(5)	3775(2)	71(13)
H(12B)	3181(2)	7281(5)	3277(2)	82(19)
H(12C)	2530(2)	8331(5)	2863(2)	74(14)
H(13A)	7200(3)	8446(6)	3142(3)	92(17)
H(13B)	7272(3)	8836(6)	2306(3)	119(23)
H(13C)	7501(3)	7412(6)	2636(3)	142(24)
H(14A)	5752(3)	6982(7)	1166(3)	131(22)
H(14B)	6664(3)	6577(7)	1480(3)	82(16)
H(14C)	6426(3)	8002(7)	1156(3)	161(30)
H(15A)	4241(3)	5086(4)	2744(3)	62(14)
H(15B)	4914(3)	4070(4)	3159(3)	111(20)
H(15C)	4475(3)	3967(4)	2244(3)	91(17)
H(16A)	6340(4)	5174(6)	2323(3)	185(35)
H(16B)	5736(4)	4017(6)	1992(3)	140(25)
H(16C)	6176(4)	4124(6)	2907(3)	160(28)
H(20)	4746(3)	11058(4)	2094(2)	46(11)
H(22A)	3465(4)	11303(5)	1171(3)	102(23)
H(22B)	3837(4)	11081(5)	473(3)	106(20)
H(22C)	4071(4)	12333(5)	1011(3)	117(18)
H(21A)	5521(3)	11749(5)	1290(3)	97(17)
H(21B)	5315(3)	10449(5)	793(3)	98(18)
H(21C)	5843(3)	10398(5)	1687(3)	116(23)
H(40)	4456(2)	5288(4)	969(2)	35(10)
H(41A)	3195(3)	4376(4)	335(3)	75(14)
H(41B)	2779(3)	5724(4)	392(3)	76(15)
H(41C)	3214(3)	4941(4)	1168(3)	129(23)
H(42A)	4013(3)	5320(5)	-425(2)	89(16)
H(42B)	4589(3)	6511(5)	-96(2)	76(16)
H(42C)	3653(3)	6729(5)	-410(2)	66(15)
H(70)	5331(2)	11081(4)	3306(2)	30(9)
H(72A)	5290(4)	11076(5)	4630(3)	84(17)
H(72B)	5836(4)	12226(5)	4497(3)	100(16)
H(72C)	6232(4)	10942(5)	4935(3)	121(22)
H(71A)	6615(3)	11972(5)	3545(3)	93(17)
H(71B)	6544(3)	10691(5)	3035(3)	54(13)
H(71C)	7006(3)	10661(5)	3948(3)	95(18)
H(90)	5958(3)	5073(5)	4194(2)	88(17)
H(91A)	7353(3)	4885(6)	4668(4)	104(18)
H(91B)	7438(3)	6419(6)	4696(4)	104(23)
H(91C)	7105(3)	5698(6)	3877(4)	147(29)
H(92A)	6551(4)	4930(6)	5574(3)	94(17)
H(92B)	5735(4)	5711(6)	5369(3)	88(20)
H(92C)	6560(4)	6467(6)	5633(3)	164(33)

F. $Cp^*_2ScC(H)=CMe_2$ (**10**)

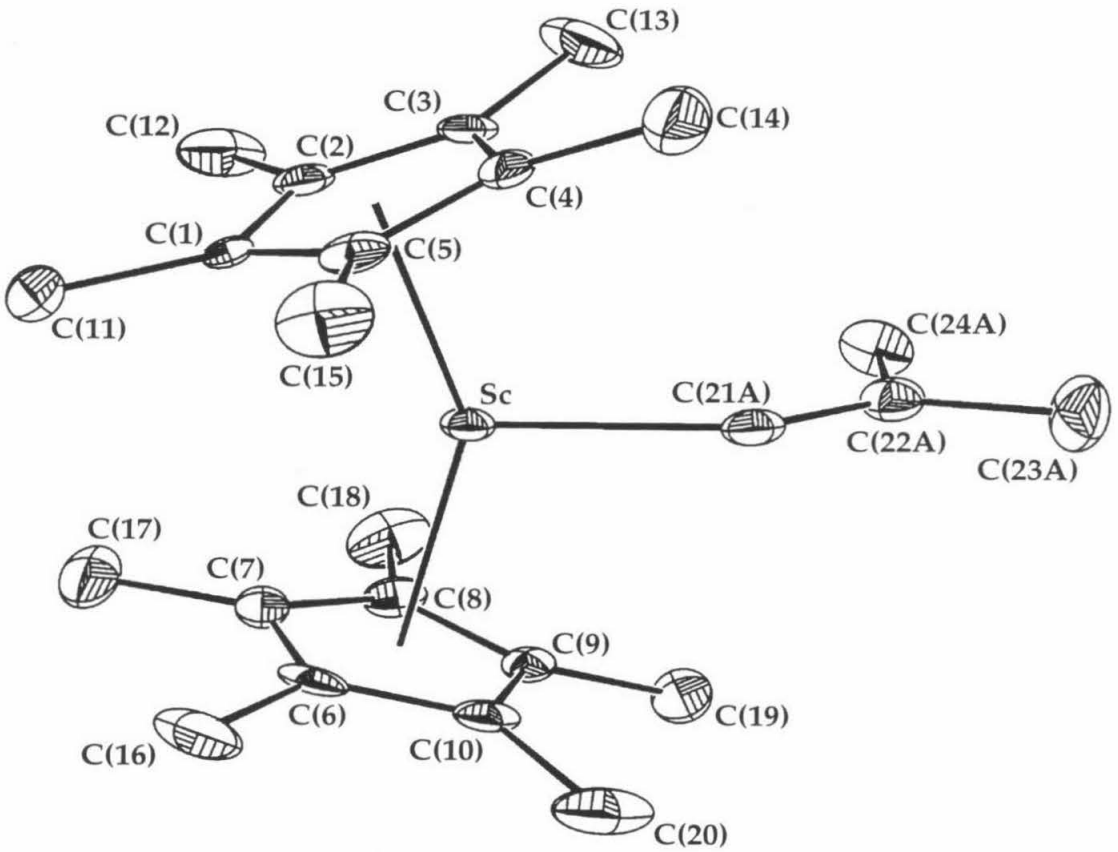

Figure 7. ORTEP representation of the molecular structure of **10** showing the complete atom labeling scheme (50% probability ellipsoids, hydrogens omitted for clarity).

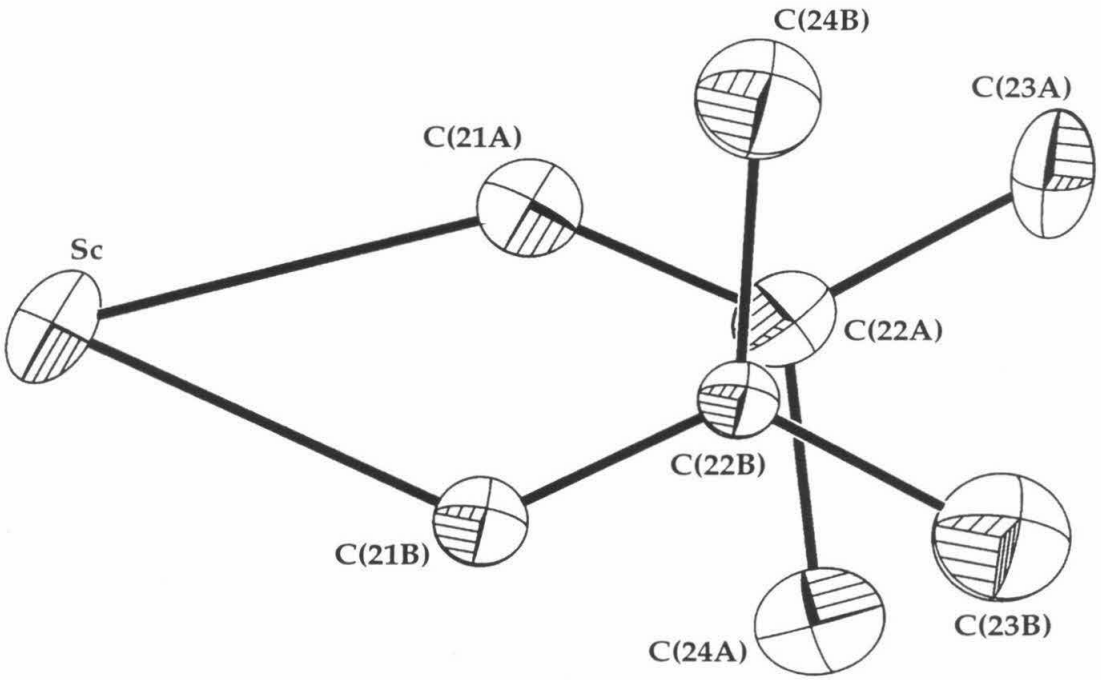

Figure 8. ORTEP representation of the molecular structure of the isobutenyl ligand of **10** showing the modeling of the disorder (50% probability ellipsoids, hydrogens omitted for clarity).

Table 31. X-ray Diffraction Data Collection Parameters for **10**[a]

Parameter	Value
Empirical formula	$C_{24}H_{37}Sc$
Formula weight (g/mol)	370.50
Crystal size (mm)	0.15 x 0.22 x 0.27
Temp. (K)	84
Space group	$P2_1/c$
Cell Constants	a = 14.490 (5) Å b = 10.935 (5) Å c = 14.604 (8) Å β = 107.15 (3)°
Volume (Å^3)	2211.1 (18)
Z	4
Density (calculated) (g/mL)	1.113
2θ range (°)	3.0 to 50.00
Index ranges	$-17 \le h \le 16$, $-12 \le k \le 12$, $-14 \le l \le 17$
Reflections collected	12788
Independent reflections	3879
R (merge)	0.0791
GOF (merge)	1.07
Data / restraints / parameters	3879 / 0 / 354
GOF (F^2)[b]	1.562
R indices (all data)[c,d]	R1 = 0.0875, wR2 = 0.0881

[a]Structure was obtained on an Enraf-Nonius CAD-4 using MoKα radiation (λ = 0.71073 Å); [b]$GOF = \{\Sigma w(F_o^2 - F_c^2)^2 / n - p\}^{1/2}$ (n = number of data, p = number of variables); [c]$R1 = \Sigma | |F_o| - |F_c| | / \Sigma |F_o|$; [d]$wR2 = \{\Sigma(w(F_o^2 - F_c^2)^2) / \Sigma(wF_o^4)\}^{1/2}$.

Table 32. Special Refinement Details for **10**

One outlying reflection (-1 0 6) was rejected from the refinement.

The isobutenyl ligand is disordered and was modeled as two separate groups. The minor component was modeled with isotropic carbon atoms and calculated hydrogen atoms. The coordinates of all other hydrogen atoms were refined. The displacement parameters for all hydrogen atoms were fixed at 1.2 times the U_{eq} of the attached carbon.

Weights w are calculated as $1/\sigma^2(F_o^2)$. The variances ($\sigma^2(Fo^2)$) were derived from counting statistics plus an additional term, $(0.014I)^2$, and the variances of the merged data were obtained by propagation of error plus the addition of another term, (0.014<I>)2.

All esd's (except the esd in the dihedral angle between two l.s. planes) are estimated using the full covariance matrix. The cell esd's are taken into account individually in the estimation of esd's in distances, angles and torsion angles; correlations between esd's in cell parameters are only used when they are defined by crystal symmetry. An approximate (isotropic) treatment of cell esd's is used for estimating esd's involving l.s. planes.

Table 33. Atomic Coordinates (x 10^4) and Equivalent Isotropic Displacement Parameters ($Å^2$ x 10^3) for **10**[a]

	x	y	z	U_{eq}
Sc	7413(1)	5553(1)	8205(1)	20(1)
C1	7412(2)	7211(2)	7041(2)	18(1)
C2	6653(2)	6398(3)	6592(2)	20(1)
C3	7075(2)	5277(2)	6454(2)	20(1)
C4	8079(2)	5376(3)	6828(2)	20(1)
C5	8295(2)	6572(3)	7214(2)	19(1)
C6	7710(2)	6949(3)	9595(2)	23(1)
C7	6713(2)	7009(3)	9130(2)	24(1)
C8	6301(2)	5849(3)	9194(2)	23(1)
C9	7048(2)	5079(2)	9726(2)	18(1)
C10	7924(2)	5746(3)	9963(2)	21(1)
C11	7297(3)	8567(3)	7132(2)	32(1)
C12	5601(2)	6720(4)	6244(2)	38(1)
C13	6554(3)	4161(3)	5950(2)	39(1)
C14	8818(2)	4441(3)	6756(2)	36(1)
C15	9283(2)	7110(3)	7632(2)	36(1)
C16	8425(3)	7989(3)	9778(2)	41(1)
C17	6139(3)	8161(3)	8789(2)	41(1)
C18	5256(2)	5532(4)	8808(2)	39(1)
C19	6936(3)	3817(3)	10084(2)	31(1)
C20	8882(2)	5289(4)	10569(2)	40(1)
C21A[b]	8154(3)	3690(4)	8470(2)	21(1)
C22A[b]	7937(5)	2503(6)	8415(4)	21(1)
C23A[b]	8662(4)	1479(4)	8665(3)	34(1)
C24A[b]	6887(3)	2065(5)	8054(3)	32(1)
C21B[c]	7017(7)	3603(9)	8072(7)	21(3)[d]
C22B[c]	7614(12)	2633(18)	8362(14)	15(5)[d]
C23B[c]	7302(10)	1390(12)	8290(10)	43(4)[d]
C24B[c]	8664(9)	2858(11)	8878(9)	36(3)[d]

[a]U(eq) is defined as the trace of the orthogonalized U_{ij} tensor. [b]Population 0.728(5); [c]Population 0.272(5); [d]U_{iso}

Table 34. Complete List of Bond Lengths (Å) and Angles (°) for **10**

Feature	Length (Å) or angle (°)	Feature	Length (Å) or angle (°)
Sc-CpA	2.164	C15-H15C	0.96(3)
Sc-CpB	2.167	C16-H16A	0.94(3)
Sc-C21A	2.282(4)	C16-H16B	0.99(3)
Sc-C21B	2.202(10)	C16-H16C	0.96(3)
Sc-PlnA	2.164(2	C17-H17A	0.90(3)
Sc-PlnB	2.167(2)	C17-H17B	0.95(3)
Sc-C10	2.462(3)	C17-H17C	1.03(3)
Sc-C5	2.463(3)	C18-H18A	0.93(3)
Sc-C2	2.467(3)	C18-H18B	0.94(3)
Sc-C6	2.474(3)	C18-H18C	0.95(3)
Sc-C3	2.476(3)	C19-H19A	0.95(3)
Sc-C8	2.481(3)	C19-H19B	1.02(3)
Sc-C4	2.482(3)	C19-H19C	1.01(3)
Sc-C9	2.484(3)	C20-H20A	0.89(3)
Sc-C1	2.485(3)	C20-H20B	0.93(3)
Sc-C7	2.489(3)	C20-H20C	1.00(3)
C1-C5	1.415(4)	C21A-C22A	1.332(7)
C1-C2	1.415(4)	C21A-H21A	1.08(3)
C1-C11	1.503(4)	C22A-C23A	1.505(8)
C2-C3	1.410(4)	C22A-C24A	1.533(7)
C2-C12	1.499(4)	C23A-H23A	1.09(4)
C3-C4	1.400(3)	C23A-H23B	0.92(4)
C3-C13	1.508(4)	C23A-H23C	1.04(4)
C4-C5	1.422(4)	C24A-H24A	1.08(4)
C4-C14	1.506(4)	C24A-H24B	1.02(4)
C5-C15	1.500(4)	C24A-H24C	1.02(4)
C6-C7	1.406(4)	C21B-C22B	1.356(18)
C6-C10	1.420(4)	C21B-H21B	0.9500
C6-C16	1.508(4)	C22B-C23B	1.43(2)
C7-C8	1.416(4)	C22B-C24B	1.506(18)
C7-C17	1.511(4)	C23B-H23D	0.9800
C8-C9	1.410(4)	C23B-H23E	0.9800
C8-C18	1.492(4)	C23B-H23F	0.9800
C9-C10	1.414(4)	C24B-H24D	0.9800
C9-C19	1.502(4)	C24B-H24E	0.9800
C10-C20	1.496(4)	C24B-H24F	0.9800
C11-H11A	0.95(3)		
C11-H11B	1.03(3)	CpA-Sc-CpB	144.4
C11-H11C	0.96(3)	CpA-Sc-C21A	106.3
C12-H12A	0.95(3)	CpB-Sc-C21A	107.9
C12-H12B	0.98(3)	CpA-Sc-C21B	107.7
C12-H12C	1.06(3)	CpB-Sc-C21B	104.3
C13-H13A	0.96(3)	PlnA-PlnB	35.48(9)
C13-H13B	1.02(3)	C5-C1-C2	108.1(2)
C13-H13C	1.01(3)	C5-C1-C11	126.1(3)
C14-H14A	0.99(3)	C2-C1-C11	124.7(3)
C14-H14B	0.99(3)	C3-C2-C1	107.5(2)
C14-H14C	0.98(3)	C3-C2-C12	126.6(3)
C15-H15A	0.94(3)	C1-C2-C12	125.6(3)
C15-H15B	1.01(3)	C4-C3-C2	108.8(2)

C4-C3-C13	124.5(3)
C2-C3-C13	126.7(3)
C3-C4-C5	107.9(2)
C3-C4-C14	126.8(3)
C5-C4-C14	125.0(3)
C1-C5-C4	107.6(2)
C1-C5-C15	125.7(3)
C4-C5-C15	126.5(3)
C7-C6-C10	107.7(2)
C7-C6-C16	127.3(3)
C10-C6-C16	124.7(3)
C6-C7-C8	108.7(2)
C6-C7-C17	125.8(3)
C8-C7-C17	124.5(3)
C9-C8-C7	107.5(2)
C9-C8-C18	126.7(3)
C7-C8-C18	125.7(3)
C8-C9-C10	108.3(2)
C8-C9-C19	126.6(3)
C10-C9-C19	124.7(3)
C9-C10-C6	107.8(2)
C9-C10-C20	125.6(3)
C6-C10-C20	126.4(3)
H11A-C11-H11B	102(2)
H11A-C11-H11C	103(2)
H11B-C11-H11C	121(2)
H12A-C12-H12B	102(2)
H12A-C12-H12C	103(2)
H12B-C12-H12C	109(2)
H13A-C13-H13B	108(2)
H13A-C13-H13C	112(2)
H13B-C13-H13C	109(2)
H14A-C14-H14B	104(2)
H14A-C14-H14C	107(2)
H14B-C14-H14C	112(3)
H15A-C15-H15B	101(2)
H15A-C15-H15C	107(2)
H15B-C15-H15C	108(2)
H16A-C16-H16B	109(3)
H16A-C16-H16C	96(3)
H16B-C16-H16C	117(3)
H17A-C17-H17B	108(3)
H17A-C17-H17C	100(3)
H17B-C17-H17C	118(3)
H18A-C18-H18B	102(2)
H18A-C18-H18C	108(3)
H18B-C18-H18C	105(3)
H19A-C19-H19B	106(2)
H19A-C19-H19C	109(2)
H19B-C19-H19C	112(2)
H20A-C20-H20B	108(3)
H20A-C20-H20C	107(3)
H20B-C20-H20C	101(3)
C22A-C21A-Sc	140.2(4)
C22A-C21A-H21A	112.1(19)
Sc-C21A-H21A	107.8(19)
C21A-C22A-C23A	125.1(5)
C21A-C22A-C24A	121.3(6)
C23A-C22A-C24A	113.6(5)
C22A-C23A-H23A	113(2)
C22A-C23A-H23B	111(3)
H23A-C23A-H23B	113(3)
C22A-C23A-H23C	111(2)
H23A-C23A-H23C	110(3)
H23B-C23A-H23C	98(3)
C22A-C24A-H24A	119(2)
C22A-C24A-H24B	107(2)
H24A-C24A-H24B	114(3)
C22A-C24A-H24C	116(2)
H24A-C24A-H24C	99(3)
H24B-C24A-H24C	101(3)
C22B-C21B-Sc	127.2(11)
C22B-C21B-H21B	116.4
Sc-C21B-H21B	116.4
C21B-C22B-C23B	124.2(16)
C21B-C22B-C24B	119.1(16)
C23B-C22B-C24B	116.4(14)
C22B-C23B-H23D	109.5
C22B-C23B-H23E	109.5
C22B-C23B-H23F	109.5
H23D-C23B-H23E	109.5
H23D-C23B-H23F	109.5
H23E-C23B-H23F	109.5
C22B-C24B-H24D	109.5
C22B-C24B-H24E	109.5
C22B-C24B-H24F	109.5
H24D-C24B-H24E	109.5
H24D-C24B-H24F	109.5
H24E-C24B-H24F	109.5

Table 35. Anisotropic Displacement Parameters ($Å^2 \times 10^4$) for **10**[a]

	U^{11}	U^{22}	U^{33}	U^{23}	U^{13}	U^{12}
Sc	354(3)	155(3)	90(2)	-14(3)	88(2)	-61(3)
C1	327(17)	168(15)	77(13)	41(11)	108(12)	19(13)
C2	253(17)	284(17)	75(13)	26(12)	62(12)	41(14)
C3	316(17)	228(17)	70(13)	-20(12)	71(12)	-26(13)
C4	278(16)	228(16)	108(13)	48(12)	101(12)	60(13)
C5	223(16)	264(16)	110(14)	32(12)	84(12)	-85(13)
C6	396(18)	243(16)	99(14)	-87(12)	145(13)	-142(14)
C7	408(19)	219(16)	135(14)	12(13)	159(14)	55(14)
C8	249(16)	314(19)	131(14)	11(13)	85(12)	-10(14)
C9	290(16)	182(15)	98(13)	6(12)	98(12)	-49(13)
C10	235(16)	313(18)	86(13)	-58(13)	61(12)	24(14)
C11	570(20)	206(17)	231(18)	51(14)	190(17)	21(17)
C12	290(19)	630(30)	185(16)	-58(17)	37(15)	109(18)
C13	540(20)	400(20)	246(18)	-179(16)	149(17)	-100(18)
C14	460(20)	366(19)	305(18)	80(18)	171(16)	161(19)
C15	302(19)	470(20)	330(20)	16(17)	116(16)	-114(17)
C16	720(30)	340(20)	207(17)	-133(15)	203(19)	-250(20)
C17	700(30)	350(20)	300(19)	112(17)	329(19)	221(19)
C18	270(18)	620(20)	306(18)	80(20)	110(15)	20(20)
C19	470(20)	272(18)	234(17)	62(15)	202(16)	15(16)
C20	324(19)	700(30)	167(16)	-113(19)	60(15)	44(19)
C21A	260(20)	260(30)	96(19)	-5(17)	51(17)	-4(19)
C22A	260(40)	250(30)	150(30)	4(19)	90(30)	-40(30)
C23A	460(30)	190(20)	400(30)	90(20)	160(20)	20(20)
C24A	320(30)	370(30)	280(30)	-60(20)	120(20)	-40(30)

[a]The anisotropic displacement factor exponent takes the form: $-2p^2 (h^2 a^{*2} U^{11} + ... + 2 h k a^* b^* U^{12})$

Table 36. Hydrogen Coordinates (x 10^4) and Isotropic Displacement Parameters ($Å^2$ x 10^3) for **10**

	x	y	z	U_{iso}
H11A	7321(19)	8950(30)	6560(20)	39
H11B	6610(20)	8780(30)	7150(20)	39
H11C	7850(20)	8900(30)	7600(20)	39
H12A	5460(20)	7190(30)	5670(20)	45
H12B	5170(20)	6010(30)	6050(20)	45
H12C	5349(19)	7270(30)	6720(20)	45
H13A	6580(20)	4190(30)	5300(20)	46
H13B	6910(20)	3400(30)	6260(20)	46
H13C	5870(20)	4110(30)	5980(20)	46
H14A	8941(19)	4450(30)	6120(20)	44
H14B	9470(20)	4550(30)	7230(20)	44
H14C	8550(20)	3630(30)	6820(20)	44
H15A	9560(20)	7400(30)	7170(20)	43
H15B	9280(20)	7880(30)	8020(20)	43
H15C	9730(20)	6550(30)	8030(20)	43
H16A	8480(20)	8420(30)	10350(20)	49
H16B	9080(20)	7710(30)	9770(20)	49
H16C	8140(20)	8650(30)	9350(20)	49
H17A	5830(20)	8380(30)	9220(20)	49
H17B	6560(20)	8810(30)	8750(20)	49
H17C	5550(20)	8000(30)	8200(20)	49
H18A	4860(20)	5900(30)	9130(20)	47
H18B	4970(20)	5800(30)	8180(20)	47
H18C	5140(20)	4680(30)	8790(20)	47
H19A	6874(19)	3860(20)	10710(20)	37
H19B	6310(20)	3430(30)	9670(20)	37
H19C	7520(20)	3300(30)	10100(20)	37
H20A	8960(20)	5390(30)	11190(20)	48
H20B	9010(20)	4470(30)	10470(20)	48
H20C	9440(20)	5710(30)	10430(20)	48
H21A	8920(30)	3840(30)	8740(30)	25
H23A	9400(30)	1800(40)	8910(30)	41
H23B	8510(30)	940(40)	9090(30)	41
H23C	8570(30)	890(40)	8080(30)	41
H24A	6310(30)	2730(40)	7930(30)	38
H24B	6840(30)	1510(40)	7480(30)	38
H24C	6670(30)	1480(40)	8500(30)	38
H21B	6354	3421	7780	25
H23D	6612	1351	7939	52
H23E	7409	1050	8933	52
H23F	7669	917	7947	52
H24D	8797	3738	8891	43
H24E	9066	2434	8543	43
H24F	8815	2549	9536	43

G. OpSc(η^3-1-Me-C_3H_4) (**6**)

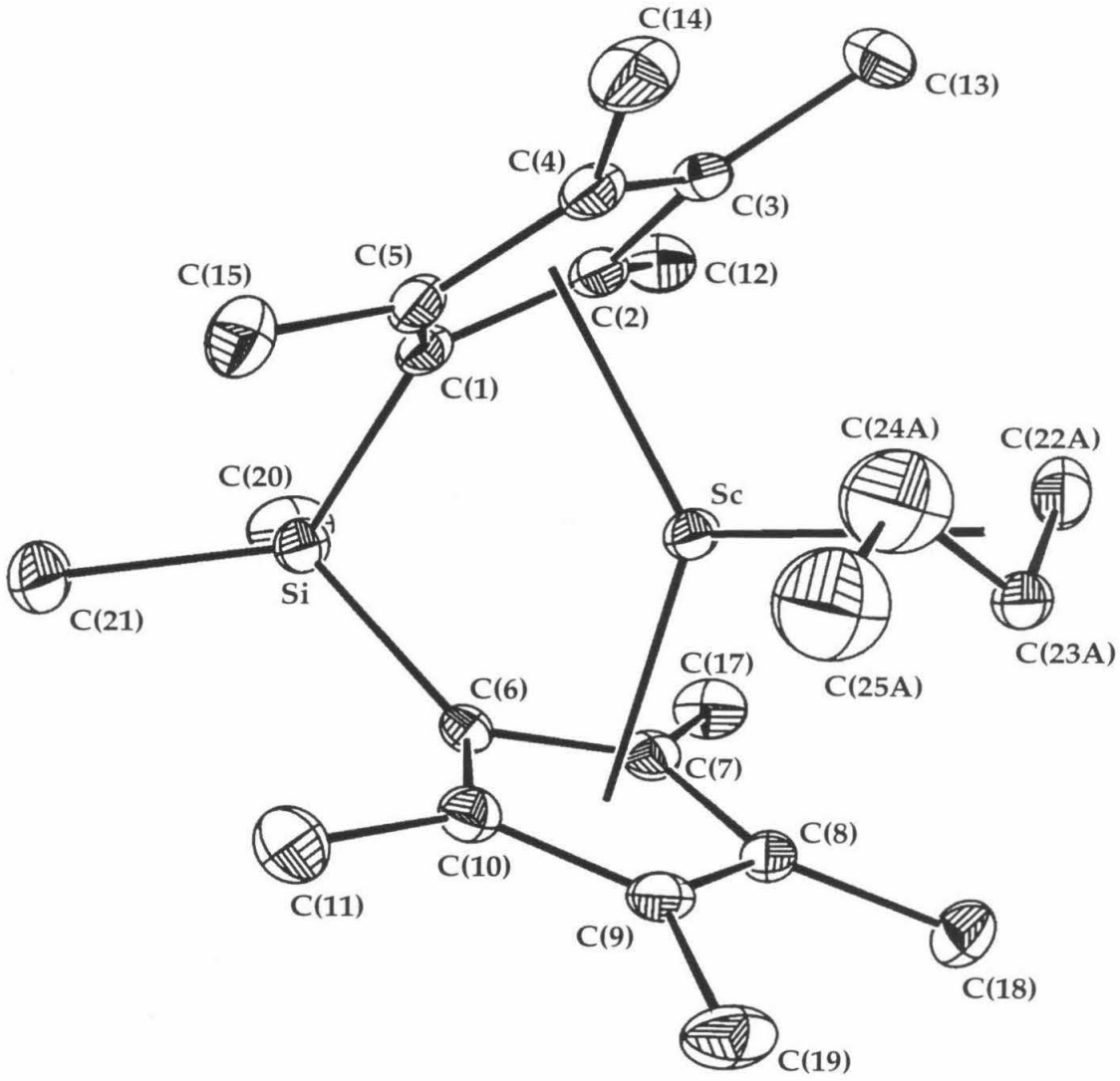

Figure 9. ORTEP representation of the molecular structure of **15** showing the complete atom labeling scheme (50% probability ellipsoids, hydrogens omitted for clarity).

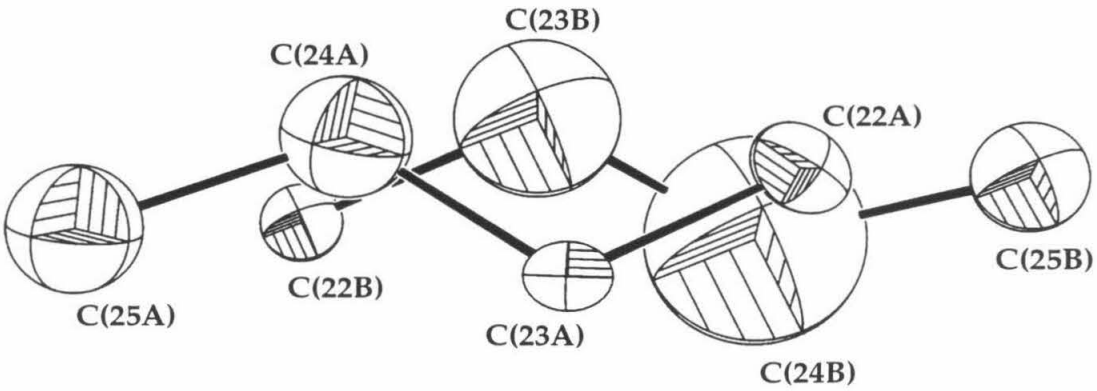

Figure 10. ORTEP representation of the molecular structure of the crotyl ligand of **15** showing the modeling of the disorder (50% probability ellipsoids, hydrogens omitted for clarity).

Table 37. X-Ray Diffraction Data Collection Parameters for **15**[a]

Parameter	Value
Empirical formula	$C_{24}H_{37}ScSi$
Formula weight (g/mol)	398.59
Crystal size (mm)	0.37 x 0.35 x 0.26
Temp. (K)	84
Space group	$P2_1/c$
Cell Constants	a = 15.174 (8) Å b = 10.086 (3) Å c = 15.174 (8) Å β = 109.80 (3)°
Volume (Å^3)	2185.0 (18)
Z	4
Density (calculated) (g/mL)	1.212
2θ range (°)	5.0 to 55.00
Index ranges	$-19 \le h \le 0$, $-13 \le k \le 13$, $-19 \le l \le 19$
Reflections collected	11037
Independent reflections	5010
R (merge)	0.026
GOF (merge)	1.01
Data / restraints / parameters	5010 / 32 / 374
GOF (F^2)[b]	2.579
R indices (all data)[c,d]	R1 = 0.0691, wR2 = 0.1174

[a]Structure was obtained on an Enraf-Nonius CAD-4 using MoKα radiation (λ = 0.71073 Å); [b]$GOF = \{\Sigma w(F_o^2 - F_c^2)^2 / n - p\}^{1/2}$ (n = number of data, p = number of variables); [c]$R1 = \Sigma | |F_o| - |F_c| | / \Sigma |F_o|$; [d]$wR2 = \{\Sigma(w(F_o^2 - F_c^2)^2) / \Sigma(wF_o^4)\}^{1/2}$.

Table 38. Special Refinement Details for **15**

The crotyl ligand in this structure is disordered. This disorder appears as a two-fold rotation about the C_2-axis defined by the cyclopentadienyl ligand set. The disorder ratio is 65:35. The major component was refined anisotropically with bond distances restrained to reasonable values and the anisotropic displacement parameters restrained to approximate isotropic behavior. The minor component was refined isotropically with distances and angles restrained to be similar to those of the major component.

All of the hydrogen atoms except those on the crotyl ligand were found in the difference Fourier map and were refined without restraints. The hydrogen atoms of the crotyl ligand were constrained to calculated geometry and their displacement parameters set equal to 1.2 times those of the appropriate carbon atom.

The unit cell used in data collection was C-centered orthorhombic. This cell was transformed to a monoclinic cell by the following matrix as shown below.

Orthorhombic cell		Transformation matrix		Monoclinic cell
a=17.4492(42)Å b=24.8291(50)Å c=10.0862(31)Å	→	$\begin{bmatrix} 0.5 & -0.5 & 0 \\ 0 & 0 & -1 \\ 0.5 & 0.5 & 0 \end{bmatrix}$	→	a=15.174(8)Å b=10.086(3)Å c=15.174(8)Å β=109.80°

It is interesting to note that this same compound, $C_{24}H_{37}ScSi$ (structure ID JCY8), crystallizes from benzene in an orthorhombic unit cell (shown below), space group P_{bca}, with dimensions that appear to be a composite of the two cells for as solved **15**. The crystal structure of JCY8 shows the same disorder as is observed here. The following cell is the orthorhombic cell of JCY8; the relationship between the lattices of **15** and JCY8 (if indeed there is one) is not known at this time.

a = 10.0784 (57) Å
b = 15.1151 (79) Å
c = 28.6873 (136) Å

The variances ($\sigma^2(Fo^2)$) were derived from counting statistics plus an additional term, $(0.014I)^2$, and the variances of the merged data were obtained by propagation of error plus the addition of another term, $(0.014\langle I\rangle)^2$.

All esd's (except the esd in the dihedral angle between two l.s. planes) are estimated using the full covariance matrix. The cell esd's are taken into account individually in the estimation of esd's in distances, angles and torsion angles; correlations between esd's in cell parameters are only used when they are defined by crystal symmetry. An approximate (isotropic) treatment of cell esd's is used for estimating esd's involving l.s. planes.

Table 39. Atomic Coordinates (x 10^4) and Equivalent Isotropic Displacement Parameters ($Å^2$ x 10^3) for **15**[a]

	x	y	z	U_{eq}
Sc	2746(1)	948(1)	1687(1)	16(1)
Si	2139(1)	-2146(1)	1493(1)	18(1)
C(1)	1416(2)	-590(2)	1222(2)	16(1)
C(2)	1291(2)	224(3)	410(2)	18(1)
C(3)	1065(2)	1528(3)	600(2)	20(1)
C(4)	1044(2)	1557(3)	1526(2)	21(1)
C(5)	1269(2)	274(3)	1915(2)	18(1)
C(6)	3318(2)	-1327(2)	1920(2)	15(1)
C(7)	3761(2)	-716(2)	1323(2)	17(1)
C(8)	4422(2)	218(3)	1850(2)	18(1)
C(9)	4393(2)	228(3)	2770(2)	18(1)
C(10)	3717(2)	-705(3)	2816(2)	18(1)
C(11)	3565(2)	-1058(3)	3717(2)	27(1)
C(12)	1265(2)	-179(3)	-552(2)	25(1)
C(13)	760(2)	2617(3)	-115(3)	30(1)
C(14)	691(2)	2677(3)	1966(3)	31(1)
C(15)	1218(2)	-71(3)	2862(2)	26(1)
C(17)	3648(2)	-1057(3)	324(2)	24(1)
C(18)	5121(2)	955(3)	1534(2)	29(1)
C(19)	5070(2)	951(3)	3583(2)	30(1)
C(21)	1884(3)	-3266(3)	2363(3)	32(1)
C(20)	1972(2)	-3300(3)	478(3)	31(1)
C(22A)	3125(3)	2952(5)	965(2)	27(1)
C(23A)	3546(2)	3117(4)	1955(2)	17(1)
C(24A)	2923(4)	3150(7)	2478(3)	50(2)
C(25A)	3269(4)	3312(6)	3527(3)	52(2)
C(22B)	3198(6)	2858(8)	2751(5)	20(2)
C(23B)	2956(8)	3377(12)	1823(6)	80(5)
C(24B)	3363(16)	2736(13)	1217(8)	149(10)
C(25B)	3314(7)	3320(10)	288(5)	39(3)

[a]U(eq) is defined as the trace of the orthogonalized U_{ij} tensor.

Table 40. Complete List of Bond Lengths (Å) and Angles (°) for **15**

Feature	Length (Å) or angle (°)	Feature	Length (Å) or angle (°)
Sc-C(1)	2.451(3)	C(17)-H(17B)	0.92(4)
Sc-C(2)	2.502(3)	C(17)-H(17C)	0.91(5)
Sc-C(5)	2.475(3)	C(18)-H(18A)	0.97(4)
Sc-C(6)	2.436(2)	C(18)-H(18B)	0.97(4)
Sc-C(7)	2.464(3)	C(18)-H(18C)	1.01(3)
Sc-C(10)	2.485(3)	C(19)-H(19A)	0.96(3)
Sc-C(24A)	2.496(6)	C(19)-H(19B)	0.88(4)
Sc-C(23A)	2.469(4)	C(19)-H(19C)	0.94(3)
Sc-C(22A)	2.459(5)	C(21)-H(21A)	0.92(4)
Sc-C(22B)	2.458(8)	C(21)-H(21B)	0.78(4)
Sc-C(23B)	2.471(13)	C(21)-H(21C)	1.09(3)
Sc-C(24B)	2.256(17)	C(20)-H(20A)	1.01(4)
Si-C(21)	1.874(3)	C(20)-H(20B)	0.94(4)
Si-C(6)	1.876(3)	C(20)-H(20C)	0.90(4)
Si-C(1)	1.879(3)	C(22A)-C(23A)	1.4295(13)
Si-C(20)	1.877(3)	C(22A)-H(22A)	0.9500
C(1)-C(2)	1.439(4)	C(22A)-H(22B)	0.9500
C(1)-C(5)	1.440(4)	C(23A)-C(24A)	1.4259(12)
C(2)-C(3)	1.414(4)	C(23A)-H(23A)	0.9500
C(2)-C(12)	1.502(4)	C(24A)-C(25A)	1.5072(13)
C(3)-C(4)	1.418(4)	C(24A)-H(24A)	0.9500
C(3)-C(13)	1.503(4)	C(25A)-H(25A)	0.9800
C(4)-C(5)	1.415(4)	C(25A)-H(25B)	0.9800
C(4)-C(14)	1.500(4)	C(25A)-H(25C)	0.9800
C(5)-C(15)	1.506(4)	C(22B)-C(23B)	1.4293(16)
C(6)-C(10)	1.432(4)	C(22B)-H(22C)	0.9500
C(6)-C(7)	1.438(3)	C(22B)-H(22D)	0.9500
C(7)-C(8)	1.411(4)	C(23B)-C(24B)	1.4247(16)
C(7)-C(17)	1.505(4)	C(23B)-H(23B)	0.9500
C(8)-C(9)	1.411(4)	C(24B)-C(25B)	1.5067(16)
C(8)-C(18)	1.501(4)	C(24B)-H(24B)	0.9500
C(9)-C(10)	1.411(4)	C(25B)-H(25D)	0.9800
C(9)-C(19)	1.501(4)	C(25B)-H(25E)	0.9800
C(10)-C(11)	1.504(4)	C(25B)-H(25F)	0.9800
C(11)-H(11A)	0.92(4)		
C(11)-H(11B)	0.95(4)	C(6)-Sc-C(24A)	142.49(15)
C(11)-H(11C)	0.97(4)	C(6)-Sc-C(1)	70.37(9)
C(12)-H(12A)	1.00(3)	C(24A)-Sc-C(1)	130.21(12)
C(12)-H(12B)	0.96(3)	C(6)-Sc-C(24B)	129.3(3)
C(12)-H(12C)	0.99(3)	C(24A)-Sc-C(24B)	56.8(2)
C(13)-H(13A)	0.93(4)	C(1)-Sc-C(24B)	143.5(5)
C(13)-H(13B)	0.91(4)	C(6)-Sc-C(22B)	129.5(2)
C(13)-H(13C)	0.97(3)	C(24A)-Sc-C(22B)	13.01(19)
C(14)-H(14A)	0.95(3)	C(1)-Sc-C(22B)	134.81(18)
C(14)-H(14B)	0.90(4)	C(24B)-Sc-C(22B)	61.8(3)
C(14)-H(14C)	0.95(3)	C(6)-Sc-C(7)	34.13(8)
C(15)-H(15A)	0.94(3)	C(24A)-Sc-C(7)	137.76(13)
C(15)-H(15B)	1.02(3)	C(1)-Sc-C(7)	91.19(9)
C(15)-H(15C)	0.96(3)	C(24B)-Sc-C(7)	96.6(3)
C(17)-H(17A)	1.01(5)	C(22B)-Sc-C(7)	128.6(2)

C(6)-Sc-C(22A)	135.51(13)
C(24A)-Sc-C(22A)	58.60(13)
C(1)-Sc-C(22A)	133.32(11)
C(24B)-Sc-C(22A)	10.6(5)
C(22B)-Sc-C(22A)	65.95(19)
C(7)-Sc-C(22A)	101.62(13)
C(6)-Sc-C(23B)	153.2(3)
C(24A)-Sc-C(23B)	24.11(17)
C(1)-Sc-C(23B)	136.2(3)
C(24B)-Sc-C(23B)	34.71(16)
C(22B)-Sc-C(23B)	33.71(12)
C(7)-Sc-C(23B)	128.4(2)
C(22A)-Sc-C(23B)	34.78(19)
C(6)-Sc-C(23A)	132.81(11)
C(24A)-Sc-C(23A)	33.38(6)
C(1)-Sc-C(23A)	156.82(10)
C(24B)-Sc-C(23A)	27.1(4)
C(22B)-Sc-C(23A)	35.34(18)
C(7)-Sc-C(23A)	109.30(10)
C(22A)-Sc-C(23A)	33.73(5)
C(23B)-Sc-C(23A)	20.7(3)
C(6)-Sc-C(5)	90.92(9)
C(24A)-Sc-C(5)	97.59(11)
C(1)-Sc-C(5)	33.99(8)
C(24B)-Sc-C(5)	139.1(4)
C(22B)-Sc-C(5)	100.85(18)
C(7)-Sc-C(5)	120.59(9)
C(22A)-Sc-C(5)	130.36(13)
C(23B)-Sc-C(5)	111.0(2)
C(23A)-Sc-C(5)	129.67(10)
C(6)-Sc-C(10)	33.81(8)
C(24A)-Sc-C(10)	108.87(16)
C(1)-Sc-C(10)	90.70(9)
C(24B)-Sc-C(10)	122.8(5)
C(22B)-Sc-C(10)	96.0(2)
C(7)-Sc-C(10)	55.12(9)
C(22A)-Sc-C(10)	133.23(13)
C(23B)-Sc-C(10)	125.3(2)
C(23A)-Sc-C(10)	109.69(11)
C(5)-Sc-C(10)	94.19(9)
C(6)-Sc-C(2)	90.88(9)
C(24A)-Sc-C(2)	123.72(15)
C(1)-Sc-C(2)	33.75(8)
C(24B)-Sc-C(2)	109.9(5)
C(22B)-Sc-C(2)	135.6(2)
C(7)-Sc-C(2)	94.71(9)
C(22A)-Sc-C(2)	99.97(11)
C(23B)-Sc-C(2)	114.1(2)
C(23A)-Sc-C(2)	129.94(10)
C(5)-Sc-C(2)	54.93(9)
C(10)-Sc-C(2)	119.98(9)
C(21)-Si-C(6)	114.95(15)
C(21)-Si-C(1)	114.43(14)
C(6)-Si-C(1)	97.19(11)
C(21)-Si-C(20)	101.65(17)
C(6)-Si-C(20)	113.83(14)
C(1)-Si-C(20)	115.58(14)
C(21)-Si-Sc	129.53(12)
C(6)-Si-Sc	48.35(7)
C(1)-Si-Sc	48.84(8)
C(20)-Si-Sc	128.81(12)
C(2)-C(1)-C(5)	105.8(2)
C(2)-C(1)-Si	124.21(19)
C(5)-C(1)-Si	124.7(2)
C(2)-C(1)-Sc	75.06(14)
C(5)-C(1)-Sc	73.92(14)
Si-C(1)-Sc	95.93(11)
C(3)-C(2)-C(1)	109.1(2)
C(3)-C(2)-C(12)	121.4(2)
C(1)-C(2)-C(12)	129.1(2)
C(3)-C(2)-Sc	77.38(15)
C(1)-C(2)-Sc	71.19(14)
C(12)-C(2)-Sc	123.89(18)
C(4)-C(3)-C(2)	108.1(2)
C(4)-C(3)-C(13)	126.6(3)
C(2)-C(3)-C(13)	124.7(3)
C(4)-C(3)-Sc	73.83(15)
C(2)-C(3)-Sc	70.45(15)
C(13)-C(3)-Sc	128.37(19)
C(5)-C(4)-C(3)	108.1(2)
C(5)-C(4)-C(14)	125.2(3)
C(3)-C(4)-C(14)	126.0(3)
C(5)-C(4)-Sc	69.57(14)
C(3)-C(4)-Sc	74.38(15)
C(14)-C(4)-Sc	129.3(2)
C(4)-C(5)-C(1)	109.0(2)
C(4)-C(5)-C(15)	121.7(2)
C(1)-C(5)-C(15)	128.9(2)
C(4)-C(5)-Sc	78.04(15)
C(1)-C(5)-Sc	72.09(14)
C(15)-C(5)-Sc	122.55(19)
C(10)-C(6)-C(7)	105.9(2)
C(10)-C(6)-Si	124.62(19)
C(7)-C(6)-Si	124.47(19)
C(10)-C(6)-Sc	74.99(14)
C(7)-C(6)-Sc	74.02(14)
Si-C(6)-Sc	96.51(10)
C(8)-C(7)-C(6)	108.8(2)
C(8)-C(7)-C(17)	122.7(2)
C(6)-C(7)-C(17)	128.2(2)
C(8)-C(7)-Sc	78.24(15)
C(6)-C(7)-Sc	71.85(14)
C(17)-C(7)-Sc	120.97(18)
C(9)-C(8)-C(7)	108.2(2)
C(9)-C(8)-C(18)	125.1(3)
C(7)-C(8)-C(18)	126.3(3)
C(9)-C(8)-Sc	74.47(14)
C(7)-C(8)-Sc	69.37(14)

C(18)-C(8)-Sc	127.54(19)
C(8)-C(9)-C(10)	108.1(2)
C(8)-C(9)-C(19)	125.1(3)
C(10)-C(9)-C(19)	126.1(3)
C(8)-C(9)-Sc	73.82(15)
C(10)-C(9)-Sc	69.94(14)
C(19)-C(9)-Sc	129.2(2)
C(9)-C(10)-C(6)	109.0(2)
C(9)-C(10)-C(11)	122.7(2)
C(6)-C(10)-C(11)	127.9(2)
C(9)-C(10)-Sc	77.82(15)
C(6)-C(10)-Sc	71.20(14)
C(11)-C(10)-Sc	123.19(19)
C(10)-C(11)-H(11A)	112(3)
C(10)-C(11)-H(11B)	114(2)
H(11A)-C(11)-H(11B)	95(3)
C(10)-C(11)-H(11C)	110(2)
H(11A)-C(11)-H(11C)	107(3)
H(11B)-C(11)-H(11C)	117(3)
C(2)-C(12)-H(12A)	109.6(19)
C(2)-C(12)-H(12B)	113.7(19)
H(12A)-C(12)-H(12B)	108(3)
C(2)-C(12)-H(12C)	110.1(17)
H(12A)-C(12)-H(12C)	105(2)
H(12B)-C(12)-H(12C)	109(3)
C(3)-C(13)-H(13A)	106(2)
C(3)-C(13)-H(13B)	111(2)
H(13A)-C(13)-H(13B)	111(3)
C(3)-C(13)-H(13C)	114(2)
H(13A)-C(13)-H(13C)	104(3)
H(13B)-C(13)-H(13C)	110(3)
C(4)-C(14)-H(14A)	112(2)
C(4)-C(14)-H(14B)	111(2)
H(14A)-C(14)-H(14B)	109(3)
C(4)-C(14)-H(14C)	117(2)
H(14A)-C(14)-H(14C)	103(3)
H(14B)-C(14)-H(14C)	103(3)
C(5)-C(15)-H(15A)	114.4(19)
C(5)-C(15)-H(15B)	109.0(17)
H(15A)-C(15)-H(15B)	106(3)
C(5)-C(15)-H(15C)	111(2)
H(15A)-C(15)-H(15C)	104(3)
H(15B)-C(15)-H(15C)	112(3)
C(7)-C(17)-H(17A)	111(3)
C(7)-C(17)-H(17B)	114(2)
H(17A)-C(17)-H(17B)	114(3)
C(7)-C(17)-H(17C)	119(3)
H(17A)-C(17)-H(17C)	91(3)
H(17B)-C(17)-H(17C)	106(3)
C(8)-C(18)-H(18A)	113(2)
C(8)-C(18)-H(18B)	113(2)
H(18A)-C(18)-H(18B)	108(3)
C(8)-C(18)-H(18C)	112.4(18)
H(18A)-C(18)-H(18C)	106(3)
H(18B)-C(18)-H(18C)	104(3)
C(9)-C(19)-H(19A)	108.2(18)
C(9)-C(19)-H(19B)	108(3)
H(19A)-C(19)-H(19B)	115(3)
C(9)-C(19)-H(19C)	109(2)
H(19A)-C(19)-H(19C)	107(3)
H(19B)-C(19)-H(19C)	109(3)
H(21A)-C(21)-H(21B)	111(3)
H(21A)-C(21)-H(21C)	111(3)
H(21B)-C(21)-H(21C)	102(3)
H(20A)-C(20)-H(20B)	105(3)
H(20A)-C(20)-H(20C)	105(3)
H(20B)-C(20)-H(20C)	116(3)
C(23A)-C(22A)-H(22A)	120.0
C(23A)-C(22A)-H(22B)	120.0
H(22A)-C(22A)-H(22B)	120.0
C(24A)-C(23A)-C(22A)	116.3(3)
C(24A)-C(23A)-H(23A)	121.9
C(22A)-C(23A)-H(23A)	121.9
C(23A)-C(24A)-C(25A)	122.0(4)
C(23A)-C(24A)-H(24A)	119.0
C(25A)-C(24A)-H(24A)	119.0
C(24A)-C(25A)-H(25A)	109.5
C(24A)-C(25A)-H(25B)	109.5
H(25A)-C(25A)-H(25B)	109.5
C(24A)-C(25A)-H(25C)	109.5
H(25A)-C(25A)-H(25C)	109.5
H(25B)-C(25A)-H(25C)	109.5
C(23B)-C(22B)-H(22C)	120.0
C(23B)-C(22B)-H(22D)	120.0
H(22C)-C(22B)-H(22D)	120.0
C(24B)-C(23B)-C(22B)	116.5(4)
C(24B)-C(23B)-H(23B)	121.8
C(22B)-C(23B)-H(23B)	121.8
C(23B)-C(24B)-C(25B)	122.1(5)
C(23B)-C(24B)-H(24B)	118.9
C(25B)-C(24B)-H(24B)	118.9
C(24B)-C(25B)-H(25D)	109.5
C(24B)-C(25B)-H(25E)	109.5
H(25D)-C(25B)-H(25E)	109.5
C(24B)-C(25B)-H(25F)	109.5
H(25D)-C(25B)-H(25F)	109.5
H(25E)-C(25B)-H(25F)	109.5

Table 41. Anisotropic Displacement Parameters ($Å^2 \times 10^4$) for **15**[a]

	U^{11}	U^{22}	U^{33}	U^{23}	U^{13}	U^{12}
Sc	128(2)	111(2)	250(3)	-3(2)	58(2)	-3(2)
Si	170(4)	111(3)	239(4)	-8(3)	62(3)	-11(3)
C(1)	114(12)	141(12)	224(14)	-19(10)	57(10)	-20(9)
C(2)	124(12)	176(13)	227(14)	-4(11)	48(10)	-4(10)
C(3)	115(12)	170(13)	302(16)	37(11)	53(11)	8(10)
C(4)	140(13)	149(13)	337(16)	-26(12)	91(12)	-12(10)
C(5)	141(12)	164(13)	254(14)	-4(11)	90(11)	-24(10)
C(6)	153(12)	95(12)	205(13)	15(10)	64(10)	33(10)
C(7)	156(12)	166(13)	184(13)	5(10)	71(10)	32(10)
C(8)	136(12)	161(13)	248(14)	33(11)	83(11)	29(10)
C(9)	140(12)	166(13)	204(14)	-6(11)	8(10)	18(10)
C(10)	175(13)	183(13)	190(13)	19(10)	62(11)	23(10)
C(11)	305(17)	333(17)	170(14)	33(13)	78(13)	-2(15)
C(12)	209(15)	283(16)	235(15)	-6(13)	43(12)	12(13)
C(13)	215(16)	232(16)	397(19)	89(14)	17(15)	28(13)
C(14)	255(17)	211(16)	530(20)	-72(15)	211(16)	23(13)
C(15)	278(16)	246(16)	289(17)	-22(13)	160(13)	-37(13)
C(17)	240(15)	312(16)	193(14)	-24(13)	102(12)	35(13)
C(18)	197(15)	284(17)	420(20)	68(15)	151(14)	-11(13)
C(19)	217(15)	282(17)	300(17)	-80(15)	-25(13)	-6(14)
C(21)	283(18)	185(16)	520(20)	111(15)	151(16)	-7(14)
C(20)	268(17)	202(16)	420(20)	-130(14)	51(15)	3(13)
C(22A)	257(14)	242(14)	280(14)	82(9)	51(9)	-67(9)
C(23A)	153(12)	120(12)	219(13)	-11(9)	41(9)	-10(9)
C(24A)	496(19)	471(19)	496(19)	-28(10)	140(11)	-2(10)
C(25A)	525(19)	514(19)	517(19)	-10(10)	175(11)	-8(10)

[a]The anisotropic displacement factor exponent takes the form: $-2p^2 (h^2 a^{*2} U^{11} + ... + 2 h k a^* b^* U^{12})$

Table 42. Hydrogen Coordinates ($\times 10^4$) and Isotropic Displacement Parameters ($Å^2 \times 10^3$) for **15**

	x	y	z	U_{iso}
H(11A)	3350(30)	-340(40)	3970(30)	69(13)
H(11B)	3030(30)	-1600(40)	3640(30)	76(14)
H(11C)	4150(30)	-1340(40)	4180(30)	54(11)
H(12A)	630(20)	10(30)	-1020(20)	43(10)
H(12B)	1410(20)	-1100(30)	-600(20)	36(9)
H(12C)	1700(20)	370(30)	-750(19)	25(8)
H(13A)	850(20)	3400(40)	220(20)	51(11)
H(13B)	150(30)	2520(40)	-480(20)	49(11)
H(13C)	1150(20)	2700(40)	-510(20)	48(11)
H(14A)	800(20)	3520(40)	1740(20)	38(9)
H(14B)	70(30)	2590(40)	1860(20)	49(11)
H(14C)	960(20)	2760(30)	2630(20)	37(10)
H(15A)	1380(20)	-950(30)	3050(20)	34(9)
H(15B)	550(20)	50(30)	2850(20)	33(8)
H(15C)	1650(20)	450(30)	3340(20)	43(10)
H(17A)	3500(30)	-250(50)	-90(30)	96(16)
H(17B)	4130(30)	-1560(40)	270(30)	64(12)
H(17C)	3110(30)	-1450(40)	-40(30)	77(14)
H(18A)	5270(30)	1830(40)	1810(20)	55(11)
H(18B)	5710(30)	480(40)	1660(30)	59(12)
H(18C)	4900(20)	1090(30)	830(20)	35(9)
H(19A)	5190(20)	1800(30)	3370(20)	30(9)
H(19B)	5570(30)	450(40)	3820(30)	60(12)
H(19C)	4790(20)	1100(30)	4040(20)	42(10)
H(20A)	2110(20)	-2980(40)	-100(30)	53(11)
H(20B)	1340(30)	-3560(40)	260(30)	56(11)
H(20C)	2390(20)	-3950(40)	720(20)	49(11)
H(21A)	1270(30)	-3520(40)	2080(20)	49(11)
H(21B)	2220(30)	-3870(40)	2450(30)	49(12)
H(21C)	2010(20)	-2900(30)	3070(20)	35(9)
H(22A)	2465	2871	691	32
H(22B)	3506	2923	581	32
H(23A)	4205	3201	2249	20
H(24A)	2269	3067	2154	59
H(25A)	3908	2966	3789	62
H(25B)	2858	2821	3790	62
H(25C)	3264	4254	3684	62
H(22C)	3612	2123	2935	24
H(22D)	2947	3249	3184	24
H(23B)	2544	4112	1620	96
H(24B)	3675	1913	1405	179
H(25D)	2657	3456	-99	46
H(25E)	3609	2711	-32	46
H(25F)	3644	4171	391	46